Tropospheric nitrogen chemistry

- measurements and modelling

Research Notes from NERI No. 120

Ministry of Environment and Energy
National Environmental Research Institute

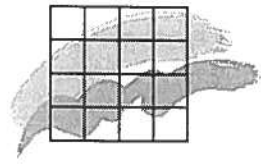

Tropospheric nitrogen chemistry

- measurements and modelling

Research Notes from NERI No. 120

Anne-Birte Storm
Atmospheric Environment

Data sheet

Title:	Tropospheric nitrogen chemistry
Subtitle:	- measurement and modelling
Author:	Anne-Birte Storm
Department:	Department of Atmospheric Environment
Serial title and No.:	Research Notes from NERI No. 120
Publisher:	Ministry of Environment and Energy National Environmental Research Institute ©
URL:	http://www.dmu.dk
Date of publication:	February 2000
Referees:	Torben Stoyer Hansen, Department of Chemistry, University of Odense, Flemming M. Nicolaisen
Layout:	Anne-Birte Storm
Drawings:	Anne-Birte Storm
Please cite as: from	Storm, A.B (2000): Tropospheric nitrogen chemistry - measurements and modelling. National Environmental Research Institute, 164 pp. - Research Notes NERI No. 120
	Reproduction is permitted, provided the source is explicitly acknowledged.
Editing complete:	August 1999
ISSN:	1395-5675
Paper quality:	Cyclus Offset, 100% recycled paper
Printed by:	Print: Information Service Department, Risø, 2000
Number of pages:	178
Circulation:	50
Price:	DKK 80,00- (incl. 25% VAT, excl. freight)

For sale at:

National Environmental Research Institute
P.O. Box 358
DK-4000 Roskilde
Denmark
Tel.: +45 46 30 12 00
Fax.: +45 46 30 12 14

Miljøbutikken
Information and Books
Læderstræde 1
DK-1201 Copenhagen K
Denmark
Tel.: +45 33 95 40 00
Fax: +45 33 92 76 90
E-mail: butik@mem.dk
URL: www.mem.dk/butik

Contents

1 Introduction

The troposphere

The troposphere encloses the earth with an approximately 10 kilometer thick layer of gases and water vapor. Despite the high degree of mixing among gases in the tropospheric layer, the capacity of the layer is far from infinite, as earlier has been assumed. The volume of the tropospheric layer is only 0.5 % of the volume of the earth.

Chemical composition of the troposphere

The overall chemical composition of the troposphere is fairly constant with N_2 making up for 78.1% of the volume, O_2 20.9 %, Argon 0.93 % leaving less than 0.1 % of other gases. Although N_2 constitutes more than 78% of the atmosphere it is not relevant in tropospheric chemistry due to its great inertness.

Growing environmental concern

Thus, although the chemical composition of the troposphere is fairly constant with N_2, O_2 and the noble gases taking up more than 99.9 % it is the changes in the remaining 0.1 % of the tropospheric gases that has led to increasing concern among chemists, environmentalists, politicians and ordinary people throughout the twentieth century. The concern about the effect of human activities on the environment, that emerged in the late seventies, has encouraged a growing interest and knowledge about the chemical composition of the troposphere, the interactions between chemical species and their role in various environmental threats.

The need for improved measurement techniques

As many of the tropospheric species involved in air pollution phenomena are present only in very small concentrations a need for new and improved measurement techniques developed. Thus, a technique that would facilitate the measurement of species present in concentrations in the range of ppt to ppm was needed.

The DOAS technique

The technique of Differential Optical Absorption Spectroscopy (DOAS) was developed in the late seventies to fill the need for reliable, accurate and specific measurements of tropospheric species [F.-Pitts and Pitts, 1986].

The nitrate radical

In the late seventies the nitrate radical (NO_3) was identified and measured in the troposphere for the first time by Platt *et al.*, using long path Differential Optical Absorption Spectroscopy - DOAS [Platt *et al.*, 1980].

The nitrate radical in tropospheric chemistry

The only important tropospheric source of the nitrate radical is the reaction of NO_2 with O_3:

$$NO_2 + O_3 \rightarrow NO_3 + O_2 \qquad (1.1)$$

Thus, the nitrate radical may be formed both during day-time and night-time. However, the nitrate radical photolyses rapidly in actinic radiation and thus, can not exist during day-light hours.

$$NO_3 + h\nu\ (\lambda < 670\ nm) \rightarrow NO + O_2 \qquad (1.2)$$
$$\rightarrow NO_2 + O\ (^3P) \qquad (1.3)$$

[F-Pitts and Pitts, 1986].

It was recognized that the nitrate radical plays an important role in the atmospheric chemical cycles involving oxides of nitrogen and ozone. The nitrate radical in addition to being an important oxidizing species in night-time tropospheric chemistry, through its equilibrium with N_2O_5, constitutes a sink for atmospheric NOx [Wayne *et al.*, 1991].

The nitrate radical in Scandinavia

Because of the long scandinavian nights it could be speculated that the nitrate radical chemistry may be of increased importance in Scandinavian countries [Ljungstrom *et al.*, 1996]. However, no measurements of the nitrate radical in Scandinavia are available in the open litterature [Ljungstrom *et al.*, 1996].

Monitoring programmes

In 1977 the European monitoring and evaluation programme (EMEP) was launched. The aim of the programme was to monitor trans-boundary air pollution. This and many other initiatives was a result of the increasing interest into the chemical species and reactions of the troposphere. In Denmark the first systematic air quality measurements was started in 1982. Today, the Danish Urban Air Quality Network (LMP) and the Background Monitoring Programme (BOP) monitors the concentration levels of several tropospheric species [Palmgren *et al.*, 1997].

DOAS in monitoring programmes

Today, measurements of NO_2 and O_3 used in the Danish monitoring programmes are performed by chemiluminescence monitors and UV absorption monitors respectively. However, if the monitor measurements could be replaced by DOAS measurements only one instrument would be needed. In addition other species could be measured as well.

Atmospheric modelling and monitoring

Currently, mathematical models are widely used in atmospheric chemistry e.g. for interpretation of ambient measurements. Furthermore, atmospheric models are powerful tools in exploring the reaction mechanisms of the troposphere and in predicting future tendencies of pollution levels. Together, monitoring programmes and atmospheric modelling, is a powerful tool for gaining new insights into the chemical reactions of the troposphere.

1.1 Aim of the thesis

Nitrate radical chemistry

The lack of nitrate radical measurements in Denmark was one of the reasons for studying the nitrate radical chemistry. In particular it was the intention to study the role of the nitrate radical in Danish night-time chemistry, the diurnal cycle, concentration levels, production rates, loss mechanisms and lifetimes. It was also the intention to work on a new measurement technique, for minimizing the effect of water interference, when measuring the nitrate radical by the DOAS technique.

DOAS measurements

In order to study the nitrate radical chemistry the production rates of the radical must be calculated. This necessitates the measurement of nitrogen dioxide and ozone. As it was the intention to study the tropospheric nitrogen chemistry at Lille Valby, the concentration of ni-

trous acid was also measured. Thus, measurements of NO_3, NO_2, O_3 and HONO were performed at Lille Valby, 1998.

Comparison of monitor and DOAS data

As most monitors can only measure one species at a time it would be desirable to replace monitors by DOAS instruments, as they are capable of measuring several species simultaneously and with great time resolution. Thus, the correlation between DOAS and monitor measurements was studied. The comparisons were done for NO_2 and O_3.

Modelling nitrate radical chemistry

Finally the experimental data on the nitrate radical was compared to model studies.

1.2 Structure of the thesis

Chapter 2

Chapter 2 gives an overview of the tropospheric nitrogen chemistry related to the nitrate radical. It also decribes some of the health implications of elevated tropospheric NOx and O_3 concentrations.

Chapter 3

In this chapter the basic features of the DOAS technique is described. Procedures for maintenance of the DOAS instrument and quality control of the DOAS measurement data are described. In particular a NO_2 calibration of the Lille Valby DOAS is presented.

Chapter 4

Chapter 4 is divided into sections that describe the Lille Valby measurements of NO_2, O_3, HONO and NO_3 respectively. The particular concerns for measuring each species by the DOAS technique is discussed as is the results of the measurements.

Chapter 5

This chapter gives an introduction to the ACDEP model (Atmospheric Chemistry and Deposition model) used at the Danish National Environmental Research Institute for calculating nitrogen deposition to the Danish waters. Results form the ACDEP model is compared with DOAS measurements from the Lille Valby DOAS.

Chapter 6

The last chapter deals with the implementation and update of a new chemical reaction scheme for future use in the ACDEP model. The new chemical reaction scheme is implemented in a simple box-model and this is used to study the effect of heterogeneous loss of N_2O_5 on the nitrate radical concentration

1.3 Abbreviations and acronyms

DOAS - Differential Optical Absorption Spectroscopy
PAN - Peroxy acetyl nitrate
UV - Ultra Violet
IR - Infra Red
ppt - parts per trillion
ppb - parts per billion
ppm - parts per million
RIMI - Risoe Integrated Environmental Project
EMEP - European Monitoring and Evaluation Programme
DS - Dansk Standard
VOC - Volatile Organic Compound
ACDEP - Atmospheric Chemistry and Deposition model
CBM IV - Carbon Bond Mechanism IV
EBI - Euler Backward Iterative
MCM - Master Chemical Mechanism
NOx = NO_2 + NO
gNOz - sum of the gaseous oxidation products of NOx
gNOy = NOx + gNOz
PCA - Photo Chemical Age
P_{NO3} - nitrate radical production rate
UiB - University of Bergen
NERI - National Environmental Research Institute
NMR - Nordisk Minister Råd

2 Tropospheric nitrogen

2.1 Tropospheric nitrogen chemistry

2.1.1 Introduction

The discussion of the tropospheric nitrogen chemistry in this chapter is focused on the chemistry related to the nitrate radical. An attempt to include all tropospheric nitrogen chemistry would be beyond the scope of this text. Three atmospheric oxidants important in tropospheric chemistry are ozone, the hydroxyl- and nitrate radical. Ozone and the hydroxyl radical are both formed during day-time due to photolysis reactions. Due to its short lifetime, the hydroxyl radical is not important in night-time chemistry. The precursors of the nitrate radical, NO_2 and O_3 allows for its formation at day- and night-time. However due to the rapid photolysis of NO_3 it can only build up at night. Thus out of the three oxidants, only ozone is present both at night and day-time. The division of this chapter into night- and day-time chemistry reflects the difference in the chemistry of the two periods of the day. All reaction rates are given at 298 K unless otherwise noted.

2.1.2 Day-time chemistry

The day-time tropospheric chemistry is strongly influenced by photolysis reactions and especially the chemistry of the OH radical. The hydroxyl radical, also called the "detergent" of the atmosphere, reacts with most gases emitted to the atmosphere, either by human activities and/or natural processes [Crutzen *et al.*, 1999]. Thus the only reactions of the hydroxyl radical with tropospheric species discussed here, are those that are relevant for discussion of the nitrate radical chemistry.

Sources of the OH radical

The O (^{1}D) formed in reaction (2.4), when reacting with water constitutes an important source of the OH radical:

$$O(^1D) + H_2O \rightarrow 2\,OH \qquad (2.1)$$

Other sources of the OH radical are photolysis of nitrous acid and hydrogen peroxide:

Photolysis of HONO

$$HONO + h\nu\ (\lambda < 400\ nm) \rightarrow OH + NO \qquad (2.2)$$

$$H_2O_2 + h\nu\ (\lambda < 360\ nm) \rightarrow 2\,OH \qquad (2.3)$$

Thus the nitrous acid concentration decreases rapidly at sunrise [F-Pitts and Pitts, 1986]. The photolysis of HONO is an important source of the OH radical and thus may contribute to initiatiation of photochemical air pollution in the early morning [Platt *et al.*, 1980]. Because of its high photolysis rate, concentrations below 1 ppb will produce OH radicals at a rate similar to that of reaction 2.1 [Perner *et al.*, 1979].

Photolysis of Ozone

The photolysis of ozone produces molecular oxygen and atomic oxygen either or both of which may be in an excited state. At wavelengths below 340 nm the primary photochemical process of ozone is:

$$O_3 + h\nu\ (\lambda \leq 340\ nm) \rightarrow O_2 + O\ (^1D) \qquad (2.4)$$

Although most of the excited oxygen atoms are collisionally deactivated to the ground state, some of the O (^1D) atoms reacts with water vapor to produce OH radicals as in reaction (2.1). The deactivated oxygen atoms O (^3P) on the other hand may react with molecular oxygen and form ozone, reaction (2.24) [Crutzen et al., 1999].

Day-time sources of HONO

Nitrous acid can be produced by the reaction of OH radical with NO:

$$OH + NO \overset{M}{\rightleftarrows} HONO \qquad (2.5)$$

In the day-time, nitrous acid is in photochemical equilibrium with OH and NO due to the rapid photolysis of HONO. Thus a net production of OH must come from sources of HONO other than reaction (2.5).

Another possible day-time source of HONO is:

$$RCH_2O^{\bullet} + NO_2 \rightarrow RCHO + HONO \qquad (2.6)$$

[Platt et al., 1980].

Day-time production of HNO_3

The OH formed as a direct or indirect product of photolysis can react with NO_2 to form nitric acid:

$$OH + NO_2 \overset{M}{\rightarrow} HNO_3 \qquad (2.7)$$

[F.-Pitts and Pitts, 1986].

Source of NO_3

The only important source of nitrate radicals in the troposphere is the reaction of NO_2 with ozone:

$$NO_2 + O_3 \rightarrow NO_3 + O_2 \qquad (2.8)$$

; $k_{2.8} = (3.2 \pm 0.06) \times 10^{-17}$ cm^3 molecule^{-1} s^{-1}, at 298 K [Atkinson, R. *et al.*, 1997].

Photolysis of NO_3

However the nitrate radical photolyzes rapidly in actinic radiation.

$$NO_3 + h\nu\ (\lambda < 670\ nm) \rightarrow NO + O_2 \qquad (2.9)$$

$$\rightarrow NO_2 + O\ (^3P) \qquad (2.10)$$

Due to this reaction the nitrate radical can not build up during day-time [F-Pitts and Pitts, 1986].

Reaction with OH

The fast reaction between the NO_3 radical and the OH radical:

$$OH + NO_3 \rightarrow HO_2 + NO_2 \qquad (2.11)$$

; $k_{2.11} = 2.0\ 10^{-11}$ cm^{3}molecule^{-1}s^{-1} [Atkinson, R. *et al.*, 1997]

is an example of a feasible tropospheric reaction of little practical importance since the two species do not co-exist.

2.1.3 Night-time chemistry

At night however, the nitrate radical may exist in concentrations of a few ppt to hundreds of ppt. Especially during photochemical smog episodes, with high O_3 concentrations and a low [NO]/[NO_2] ratio, the NO_3 concentration may reach several hundred ppt [Wayne *et al.*, 1991].

Nitrate radical tropospheric chemistry

The mechanism for production of nitrate radicals at night-time is the same as that for the day-time, reaction (2.8).

Night-time sinks for NO_3

At night when there is no photolysis, considerable concentration levels of nitrate radicals may build up. The nitrate radical reacts with numerous organic species, either via hydrogen abstraction or by addition reactions. This opens for further loss mechanisms of the nitrate radical.

Reaction with NO

The nitrate radical reacts rapidly with NO:

$$NO_3 + NO \rightarrow 2\ NO_2 \qquad (2.12)$$

; $k_{2.12} = 2.6 \times 10^{-11} cm^3 molecule^{-1} s^{-1}$ [Atkinson, R. *et al.*, 1997].

Therefore NO and NO_3 can not co-exist. However the NO levels are usually low at night as the NO sources are predominantly day-time sources, thus, permitting elevated levels of NO_3.

Reaction with alkanes

Reactions of the nitrate radical with alkanes are slow. The reaction is through hydrogen abstraction by NO_3:

$$RH + NO_3 \rightarrow R^\bullet + HNO_3 \qquad (2.13)$$

The rate constants are in the range (3 - 10) * 10^{-17} for n-butane to n-octane. However the rate constant increases with increasing branching of the alkane [F.-Pitts & Pitts, 1986].

Reaction with aldehydes

The reaction of nitrate radicals with aldehydes are through hydrogen abstraction by NO_3:

$$NO_3 + RCHO \rightarrow RCO^\bullet + HNO_3 \qquad (2.14)$$

The reaction rates for the reaction of nitrate radical with formaldehyde and acetaldehyde are relatively slow, 5.8 * 10^{-16} and 2.7 * $10^{-15} cm^3 molecule^{-1} s^{-1}$ respectively [Atkinson, R. *et al.*, 1997].

Reaction with DMS

The reaction between the nitrate radical and dimethylsulphide (DMS, CH_3SCH_3) is fast with a reaction rate of 1.1 * 10^{-12} $cm^3 molecule^{-1} s^{-1}$ [Atkinson, R. *et al.*, 1997]. The reaction proceeds through hydrogen abstraction by NO_3.

$$CH_3SCH_3 + NO_3 \rightarrow CH_3SCH_2^\bullet + HNO_3 \qquad (2.15)$$

[N.R. Jensen et al., 1991]. Thus in the marine troposphere the nitrate radical may lead to the formation of HNO_3 and the removal of NOx by deposition.

Reaction with alkenes

Nitrate radicals react rapidly with alkenes. The reaction rates are found to increase with increasing substitution of the double bond [F-Pitts & Pitts, 1986]. Akimoto and co-workers proposed that the reaction mechanism for reaction between nitrate radicals and propene proceeds via addition of the radical to the double bond.

$$CH_3CH=CH_2 + NO_3 \rightarrow CH_3\dot{C}HCH_2ONO_2 \qquad (2.16)$$

thus forming a secondary alkyl radical. Further reactions can then lead to the formation of 1,2-propanediol dinitrate (PDDN) and α-(nitrooxy)acetone [F-Pitts & Pitts, 1986]. These reaction products are very hazardous to human health as described in section 2.2.

Reactions with naturally emitted hydrocarbons

The nitrate radical reacts rapidly with naturally emitted unsaturated hydrocarbons such as isoprene, α-pinene and other terpenes. The rate constants for the reactions of NO_3 with isoprene and α-pinene are $0.58 * 10^{-12}$ and $6.1 * 10^{-12}$ $cm^3molecule^{-1}s^{-1}$ respectively, at 295 K [F-Pitts & Pitts, 1986].

Night-time production of HNO_3

The nitric acid formed in the NO_3 hydrogen abstraction reactions (2.13 - 2.15) supplement the day-time source of nitric acid, reaction (2.7). F-Pitts and Pitts estimates that the nitric acid formed in the NO_3 hydrogen abstraction reactions can attribute with 15% of the overall HNO_3 production, but this is only a very rough estimate [F-Pitts & Pitts, 1986]. Another night-time source of nitric acid is the hydrolysis of N_2O_5 as shown in reaction (2.18).

N_2O_5 equilibrium

As the nitrate radical is in fast equilibrium with NO_2 and N_2O_5, any loss process for N_2O_5 is also a loss process for NO_3 and *vice versa*. However, due to the rapid photolysis of NO_3 in the day-time, loss processes through the equilibrium of N_2O_5 will only be important at night-time.

$$NO_2 + NO_3 \underset{\rightarrow}{\overset{M}{\leftarrow}} N_2O_5 \qquad (2.17)$$

; $k_{eq,\ 2.17} = 3.35 * 10^{-11}$ $cm^3molecule^{-1}s^{-1}$ [F-Pitts & Pitts, 1986]. Hence a strong coupling exists between these species. Therefore any loss process for N_2O_5 other than 2.17 will also constitute a loss process for NO_2 and NO_3. At low temperatures the equilibrium is shifted to the right. Thus at low temperatures N_2O_5 can serve as a reservoir for NO_2 and NO_3.

Hydrolysis of N_2O_5

N_2O_5 in the gas phase can react with H_2O to produce nitric acid.

$$N_2O_5\ (g) + H_2O\ (l/g) \rightarrow 2\ HNO_3\ (aq) \qquad (2.18)$$

The reaction rate for the reaction with H_2O in the gas phase is $< 2 * 10^{-21}$ [Atkinson *et al.*, 1997]. Thus this reaction is of limited importance in tropospheric chemistry. However studies suggest that dissolution of N_2O_5 into water droplets followed by reaction with the liquid H_2O or reaction of N_2O_5 with H_2O adsorbed on surfaces are significantly

faster than the homogeneous reaction [F-Pitts & Pitts, 1986]. This is supported by studies of NO_3 lifetimes which show that no long lifetimes of NO_3 are found for relative humidities above 50%[F-Pitts & Pitts, 1986]. Hence the heterogeneous reaction of nitric acid with H_2O in various condensed phases is an important tropospheric sink for N_2O_5 and thereby of NOx.

NO_3 in aqueous solution

The nitrate radical is itself quite water soluble and may react with anions such as chloride ions present in the solution:

$$(NO_3)_{aq} + (Cl^-)_{aq} \rightarrow (NO_3^-)_{aq} + (Cl)_{aq} \qquad (2.19)$$

Thus liberating free chlorine atoms[Platt & Heintz, 1994].

Alkyl radicals

The primary fate of the alkyl radicals formed in the above reactions, where NO_3 reacts by hydrogen abstraction, is reaction with molecular oxygen:

$$R^\bullet + O_2 \xrightarrow{M} RO_2^\bullet \qquad (2.20)$$

In the case of the acetyl radical:

$$CH_3CO + O_2 \rightarrow CH_3C(O)OO^\bullet \qquad (2.21)$$

Alkyl peroxy radicals

The acetyl peroxy radical thus formed may react with NO, yielding NO_2 and an alkoxy radical:

$$RO_2^\bullet + NO \rightarrow RO^\bullet + NO_2 \qquad (2.22)$$

Subsequent photolysis of the NO_2 (day-time) leads to the formation of tropospheric ozone:

$$NO_2 + h\nu\ (\lambda \leq 420\ nm) \rightarrow NO + O(^3P) \qquad (2.23)$$

$$O(^3P) + O_2 \xrightarrow{M} O_3 \qquad (2.24)$$

as described in section 2.2. Alternatively the alkyl peroxy radical may react with NO_2:

$$RO_2^\bullet + NO_2 \underset{}{\overset{M}{\leftrightharpoons}} RO_2NO_2 \qquad (2.25)$$

In the case of the acetyl peroxy radical from reaction (2.21):

$$CH_3C(O)OO^\bullet + NO_2 \overset{M}{\leftrightharpoons} CH_3C(O)OONO_2 \qquad (2.26)$$

PAN (Peroxy Acetyl Nitrate) is formed.

The alkyl peroxy nitrates decomposes thermally back to the reactants. Thus peroxy alkyl nitrates, including PAN, may serve as reservoirs for NO_2 at low temperatures [F-Pitts & Pitts, 1986]. The basic chemistry of the alkoxy- and peroxy radicals apply equally at day- and night-time.

Night-time reaction

At night when elevated concentrations of the nitrate radical may exist, the alkyl peroxy radicals can also react with NO_3:

$$RO_2^{\bullet} + NO_3 \rightarrow RO^{\bullet} + NO_2 + O_2 \quad (2.27)$$
$$\rightarrow \text{other products}$$

It is seen that NO_3 has the same role as NO in the day-time conversion of $RO_2^{\bullet}$ to $RO^{\bullet}$ under the production of NO_2, reaction (2.22). As reaction (2.22) can only occur at day-time or under ozone free night-time conditions the reaction of $RO_2^{\bullet}$ with NO_3 will be dominant at night-time [Platt et al., 1990].

Night-time OH radical production

Reaction (2.27) may be part of a proposed night-time chain of reactions leading to enhanced night-time peroxy radical concentrations and production of OH. The proposed mechanism is given below:

$$NO_3 + HR + O_2 \rightarrow RO_2^{\bullet} + HNO_3 \quad (2.28)$$

$$NO_3 + RO_2^{\bullet} \rightarrow RO^{\bullet} + NO_2 + O_2 \quad (2.29)$$

$$RO^{\bullet} + O_2 \rightarrow HO_2^{\bullet} + R'CHO \quad (2.30)$$

$$HO_2^{\bullet} + NO_3 \rightarrow OH + NO_2 + O_2 \quad (2.31)$$

$$2\,(NO_2 + O_3 \rightarrow NO_3 + O_2) \quad (2.32)$$

$$\text{Net: } 3\,NO_3 + HR + 2\,O_3 \rightarrow OH + 2\,O_2 + HNO_3 + R'CHO \quad (2.33)$$

As opposed to the day-time photochemically initiated oxidation of hydrocarbons this reaction mechanism results in the consumption of ozone. Likewise it offers the possibility of "day-time" OH reactions occurring at night! However this mechanism has not yet been proven correct [Wayne *et al.*, 1991].

Alkoxy radicals

Alkoxy radicals may react with either NO or NO_2:

$$RO^{\bullet} + NO \rightarrow RONO \quad (2.34)$$

$$RO^{\bullet} + NO_2 \rightarrow RONO_2 \quad (2.35)$$

Forming alkyl nitrite and alkyl nitrate respectively. Again these reactions apply equally at day- and night-time, except for the fact that NO primarily has day-time sources.

Night-time sources of HONO

At night when photolytic production of radicals do not exist, the sources of nitrous acid are:

$$NO + NO_2 + H_2O \lesssim 2\,HONO \quad (2.36)$$

$$NO + HONO_2 \rightarrow NO_2 + HONO \quad (2.37)$$

Reaction (2.36) is a heterogeneous surface catalysed reaction [F-Pitts & Pitts, 1986]. Elevated concentrations of HONO accumulated over night will then photolyse at dawn leading to the production of OH radicals.

2.1.4 Comparison of NO_3, OH and O_3 oxidation reactions

The different concentration levels and reaction rates for the reactive species NO_3, OH and O_3 with various species makes direct comparisons of their importance as tropospheric oxidants difficult. However an adequate measure of their respective oxidizing power is found in the lifetime of a species with respect to reaction with NO_3, OH and O_3.

Table 2.1 Rate constant and lifetime for reactions of selected species with ozone, the hydroxyl- and nitrate radical. The lifetimes are found as $\tau = 1/k[O_3, OH \text{ or } NO_3]$. The concentrations for O_3, OH and NO_3, used are $[O_3] = 30$ ppb $= 7.38 * 10^{11}$ molecules cm^{-3}, $[OH] = 0.04$ ppt $= 1 * 10^{6}$ molecules cm^{-3}, $[NO_3] = 10$ ppt $= 2.46 * 10^{8}$ molecules cm^{-3} respectively. Thus they are representative of a relatively unpolluted tropospheric environment.

Species	NO_3 lifetime (τ) rate constant ($cm^3 molecule^{-1} s^{-1}$)	OH lifetime (τ) rate constant ($cm^3 molecule^{-1} s^{-1}$)	O_3 lifetime (τ) rate constant ($cm^3 molecule^{-1} s^{-1}$)
n-butane	3.6 y	4.6 days	4400 y
	$3.6 * 10^{-17}$ P,R	$2.5 * 10^{-12}$ P	$\leq 9.8 * 10^{-24}$ P
Formaldehyde	81 days	30 h	21483 y
	$5.8 * 10^{-16}$ *	$9.2 * 10^{-12}$ *	$\leq 2 * 10^{-24}$ P
Propene	6.3 days	11 h	38 h
	$7.5 * 10^{-15}$ *	$2.6 * 10^{-11}$ * ◊	$1.0 * 10^{-17}$ *
2-methyl-2-butene	6.8 min	3.2 h	53 min.
	$9.9 * 10^{-12}$ P,R	$8.69 * 10^{-11}$ P	$42.3 * 10^{-17}$ P
α-pinene	11 min.	5 h	4.5 h
	$6.1 * 10^{-12}$ P,R	$5.32 * 10^{-11}$ P	$8.4 * 10^{-17}$ P
Isoprene (2-methyl-1,3-butadiene)	1.9 h	2.75 h	26 h
	$5.8 * 10^{-13}$ P,R	$10.1 * 10^{-11}$ P	$1.43 * 10^{-17}$ P

*) [Atkinson, R. *et al.*, 1997]
P) F.-Pitts and Pitts, 1986.
◊) The addition reaction
R) $k_{eq} = 3.35 * 10^{-11}$ $cm^3 molecule^{-1} s^{-1}$

It is seen from Table 2.1 that the reaction of 2-methyl-2-butene with OH is faster than that of NO_3 with 2-methyl-2-butene. The fact that NO_3 is present in much higher consentrations than OH, however, results in the lifetime of 2-methyl-2-butene with respect to the NO_3 reaction being much shorter than that for the OH reaction. Thus although the reaction rates for NO_3 with some species, such as isoprene and α-pinene, are generally less than those for OH, periods of elevated NO_3 concentrations can make the oxidation of these species by NO_3 important in tropospheric chemistry.

2.1.5 Functions of the nitrate radical in tropospheric chemistry

Important tropospheric functions

Thus the primary functions of the nitrate radical in night-time tropospheric chemistry can be summarized as:

1. Initiates oxidation of organic species at night-time. Thus the nitrate radical has the same role as the OH radical during day-time.

2. A source of HNO_3 mainly through the equilibrium with N_2O_5 but also through hydrogen abstraction reactions.

3. The nitrate radical through its coupling with N_2O_5 constitutes a night-time sink for NOx via the deposition of HNO_3.

4. The reactions of NO_3 with alkenes can lead to the formation of organic nitrate compounds such as di-nitrates, which are hazardous to human health.

5. It increases the oxidizing power of the atmosphere (compared to its precursor O_3) due to its more rapid reaction rates. Also nightly formation of OH radicals through NO_3 initiated chain reactions may be possible.

Figure 2.1 Reaction scheme of tropospheric oxidized nitrogen species related to nitrate radical chemistry.

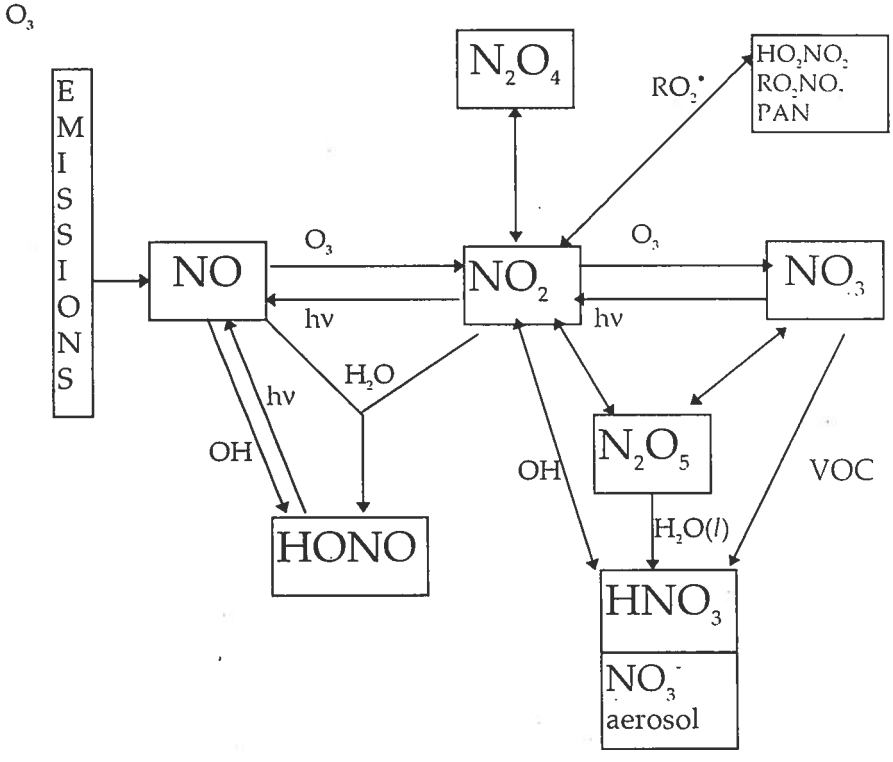

2.2 Environmental issues

2.2.1 Introduction

The odd nitrogen species in the atmosphere participate in various atmospheric pollution phenomena. Many of these phenomena are quite new and strongly coupled with the industrialization, especially in the twentieth century. Atmospheric air pollution has been acknowledged as an increasing threat not only to vegetation but also to human health, in urban as well as rural areas. The wish to investigate and understand these harmful effects, is the main reason for the vast amount of research in tropospheric chemistry and related sciences.

Nitrogen in atmospheric pollution phenomena

In the following, some of the roles of nitrogen species in atmospheric pollution phenomena are presented, along with the effects on vegetation and humans.

2.2.2 Photochemical air pollution

Stratospheric ozone production

Early in the twentieth century is was believed that the presence of ozone in the troposphere was due to intrusions from the stratosphere only. It was known that ozone was present in the stratosphere at considerable mixing ratios, and the source of the ozone was recognized to be the photodissociation of oxygen. As this reaction only takes place at wavelengths less than 242 nm, production of ozone in the troposphere was not considered possible [Graedel *et al.*, 1993].

Tropospheric ozone

However considerable damage to vegetable crops in the Los Angeles area in the mid 1940s changed the picture. By then it was known that ozone could cause extensite damage to vegetation. Likewise ozone had been found to be an important constituent of photochemical smog occurrences. Thus the search for a tropospheric mechanism for ozone creation began. It was not until the early 1970s however, that the full mechanism, proposed by Crutzen, of tropospheric ozone creation was understood [Graedel *et al.*,1993]. It took this long because it was not until 1971, that the source of the key initiator of tropospheric ozone formation, the hydroxyl radical, was recognized [Graedel *et al.*,1993].

The mechanism

The conditions needed for tropospheric ozone formation is the presence of NMHCs (Non Methane Hydro Carbons), nitric oxide and solar radiation. The mechanism is initiated by the attack of OH on the NMHC, resulting in an alkylradical. The alkylradical then reacts with oxygen giving a peroxyalkylradical. In the presence of NO this reacts to produce an alkoxy radical and NO_2. Further reactions lead to the degradation of the original hydrocarbon by one carbon atom, the production of carbonmonoxide and ozone as shown below:

$$RCH_3 + HO\cdot \rightarrow RCH_2\cdot + H_2O$$
$$RCH_2\cdot + O_2 \rightarrow RCH_2O_2\cdot$$
$$RCH_2O_2\cdot + NO \rightarrow RCH_2O\cdot + NO_2$$
$$RCH_2O\cdot + O_2 \rightarrow RCHO + HO_2\cdot$$
$$HO_2\cdot + NO \rightarrow HO\cdot + NO_2$$

$$RCHO + h\nu \rightarrow R\cdot + CHO\cdot$$
$$CHO\cdot + O_2 \rightarrow CO + HO_2\cdot$$
$$HO_2 + NO \rightarrow HO\cdot + NO_2$$
$$3\,[\,NO_2 + h\nu\ (\lambda \leq 410\ nm) \rightarrow NO + O(^3P)\,]$$
$$3\,[\,O(^3P) + O_2 + M \rightarrow O_3 + M\,]$$

Net: $RCH_3 + 6O_2 + h\nu \rightarrow R\cdot + CO + 3O_3 + H_2O$

The ozone formating steps are the photolysis of NO_2 produced from reaction of peroxyalkylradicals with NO, followed by $O(^3P)$'s reaction with molecular oxygen.

Net formation of ozone

Thus, this photochemical reaction path results in a net formation of ozone. The carbonmonoxide also formed in this reaction path can itself react with the hydroxyl radical:

$$CO + HO\cdot \rightarrow H\cdot + CO_2$$
$$H\cdot + O_2 + M \rightarrow HO_2\cdot + M$$
$$HO_2\cdot + NO \rightarrow HO\cdot + NO_2$$
$$NO_2 + h\nu\ (\lambda \leq 410\ nm) \rightarrow NO + O(^3P)$$
$$O(^3P) + O_2 + M \rightarrow O_3 + M$$

Net: $CO + 2O_2 + h\nu \rightarrow CO_2 + O_3$

leading to further production of ozone and carbondioxide.

NO as catalyst in ozone formation

Thus, in both reaction mechanisms NO has functioned as a catalyst for ozone production, as NO is regenerated in the process. However if the concentration of NO in the atmosphere is low, another reaction mechanism comes into action:

$$CO + HO\cdot \rightarrow H\cdot + CO_2$$
$$H\cdot + O_2 + M \rightarrow HO_2\cdot + M$$
$$HO_2\cdot + O_3 \rightarrow HO\cdot + 2\,O_2$$

Net: $CO + O_3 \rightarrow CO_2 + O_2$

Ozone destruction

Following this reaction path leads to the destruction of ozone rather than formation. The path taken depends on the ratio of the NO and O_3 concentrations. And because the reaction of HO_2 with NO is 4000 times faster than the reaction of HO_2 with O_3, the ratio of NO to O_3 for the former to be most important is only 1 to 4000 [Crutzen, 1994].

Critical level of NO

That is, when the NO concentration exceeds 5-10 ppt(v), as is always the case on the northern hemisphere, the ozone producing reaction path is the one taken.

2.2.3 Effects of elevated tropospheric O_3 concentrations

2.2.3.1 Effects on humans

Toxic gas

Ozone is a toxic gas that causes respiratory irritation and injury. At present, the level of knowledge on the health effects of elevated

ozone concentrations on humans and animals is high. Much of the knowledge however is related to the effects of short-term exposures in the range of minutes or hours [Mustafa, 1994]. Humans and animals are exposed to ozone through inhalation.

Symptoms

The symptoms of ozone exposure occurs within the first hours of exposure. Coughing, subternal pain, wheezing, inflammation of the skin and shortness of breath are typical symptoms. The symptoms increases with increased exposure and can last for hours or days after the exposure has ceased [Mustafa, 1994].

Effects of exposure

Exposure to ozone leads to a decrease in respiratory functions, inflammation of the lungs and an increase in the permeability of the respiratory epithelium, which can enhance the uptake of other inhaled toxic pollutants. Ozone also has a negative effect on the lungs ability to clear out particles, and is being suspected to have a carcinogen effect [Mustafa, 1994].

The mechanism

Because ozone is a powerful oxidant it can cause oxidative destruction in biological systems either by direct reactions or through the formation of free radicals and reactive intermediates. Although much is known about the effects of ozone exposure on humans and animals the underlying mechanisms are very complex and not fully understood. [Alexis et.al., 1994].

2.2.3.2 Effect of elevated ozone concentrations on vegetation

Elevated ozone concentrations has a severe impact on vegetable crops. The effect on crops exposed to ozone can be directly measured as a decrease in the harvest yields.

2.2.3.3 Effect of elevated ozone concentrations on materials

Elevated ozone concentrations also causes damage to rubber and similar materials. The effect of ozone on rubber is that it is cracked and aged upon reaction with ozone. This effect has been employed as a measurement method for ozone concentrations [Manahan, S.E., 1994].

2.2.4 Effect of elevated NO_2 concentrations on humans

Effects on humans

NO_2 is a toxic pungent red-brown gas that causes respiratory irritation and injury. It causes both short-term health effects and is suspected of long-term carcinogen effects. Like ozone it induces free radical reactions, altered membrane permeability and respiratory inflammation of the lungs. It also damages the ciliated cells, thus depressing the clearance of particles and infectious agents [Mustafa *et al.*, 1994].

2.2.5 Effect of Organic nitrates on humans

The reaction of alkenes with NO_3 may lead to the formation of organic nitrates. In particular 1,2-propane-diol-dinitrate and α-(nitrooxy)acetone may be formed in the reaction of propene with NO_3. Dinitrates causes headaches, dizziness and eye irritations. All phenomena that are observed during smog episodes [F.-Pitts & Pitts,

1986]. Also α-(nitrooxy)acetone is a mutagen in the Ames test [F.-Pitts & Pitts, 1986].

2.2.6 Nitrogen deposition to fields and oceans

The atmospheric deposition of nitrogen compounds mainly derive from emissions of nitrogen oxides (NOx) and ammonia (from agriculture) [Holten-Andersen *et al.*, 1997]. In the atmosphere NOx can be converted to nitric acid (HNO_3) in various vays. For example via reaction 2.7, 2.13 - 2.15 or 2.18. Thus the tropospheric NOx emissions causes acidification of clouds and rain due to its conversion to HNO_3. Upon deposition, HNO_3 can acidify soils and forests. Also deposition to lakes, coastal areas and oceans may lead to eutrophication of the waters [Holten-Andersen *et al.*, 1997].

2.2.7 Emission politics

In order to follow the trends in the concentration levels of various pollutants, monitoring networks such as the Danish Air Quality Monitoring Network (LMP) and the Danish Background Monitoring Network (BOP) have been established. In this section the trends in NOx emissions, NO_2 concentration levels and O_3 concentration levels are given. For NO_2 and O_3 exceedances of threshold values are described.

2.2.7.1 Trends in Danish NOx emissions

Figure 2.2 below shows the Danish emissions of NOx 1975 - 1995

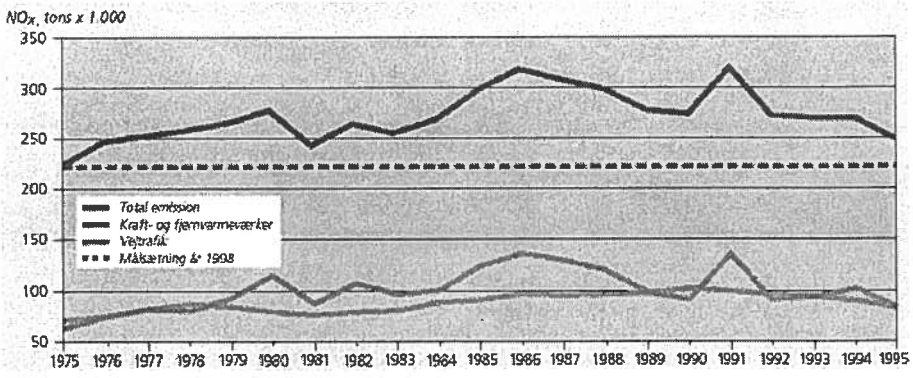

Figure 2.2 The development in the Danish NOx emissions apportioned by the main sources over the period 1975-1995. The emission target for 1998 is included for comparison (dashed line). (Source: National Environmental Research Institute and Risø National Laboratory, data from the CORINAIR database). The top line is the total emission. The bottom lines are road traffic and power and district heating stations (curved,top bottom line) respectively [Holten-Andersen *et al.*, 1997].

Sources of NOx

The Danish sources of NOx in 1995 were the following.

- 24 % from power and district heating stations
- 3 %from industrial combustion
- 2 % from residential and non-residential premises
- 23 % from road transport.
- 48 % from other mobile sources.

"Other mobile sources" include railways, national and international air and sea traffic and off-road emissions from agriculture, forestry, industry, gardens and households. (Source: National Environmental Research Institute, data from the CORINAIR database). Thus transport accounts for 71 % of the total Danish NOx emissions [Holten-Andersen *et al.*, 1997].

2.2.7.2 Trends in urban NO_2 concentration levels

Figure 2.3 below shows the development in the concentration of nitrogen oxides in Copenhagen, Odense and Aalborg over the period 1988-1996. The concentration levels at the background station, Lille Valby, is also shown for the period 1991- 1996.

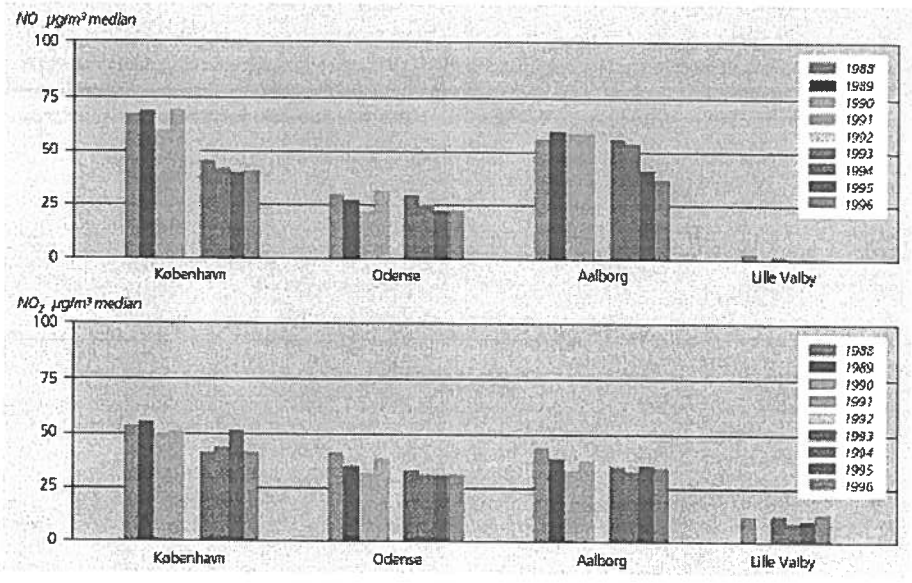

Figure 2.3 The development in the concentration of nitrogen oxides in Copenhagen, Odense and Aalborg over the period 1988-1996. The concentration levels at the background station, Lille Valby, is also shown for the period 1991- 1996 (Source: Kemp et al., 1997). [Holten-Andersen *et al.*, 1997].

Table 2.2 Current Danish (and EU) limits for atmospheric NO_2 and O_3. From Figure 2.3 and Table 2.2 it can be seen that the annual guiding NO_2 value of 50 µg/m^3 was exceeded in Copenhagen in the periods 1988 - 1991 and in 1995.

Species	Limiting value µg/m^3	Average over (Hours)	Statistics	Period	Type of regulation
NO_2	200	1	98 percentile	Year	Binding
	135	1	98 percentile	Year	Guiding
	50	1	Median	Year	Guiding
O_3	360	1	Max. 1 hour	-	Public warning
	180	1	Max. 1 hour	-	Public info.
	200	1	Max. 1 hour	Year	Threshold val.
	110	1	Max. 8 hours	Year	Threshold val.
	65	24	Max. 24 hours	Year	Threshold val.

Exceedance of threshold NO_2 values

In the Danish cities road traffic dominates the emissions of NOx completely. Currently the concentration levels of nitrogen oxides in some Danish towns are close to the levels considered as harmful by the WHO [Holten-Andersen *et al.*, 1997]. The current Danish limiting values for NO_2 and O_3 in the atmosphere is given on page 21.

2.2.7.3 Trends in O_3 concentration levels

The trends in the Danish ozone concentration levels for the years 1991- 1998 are given below.

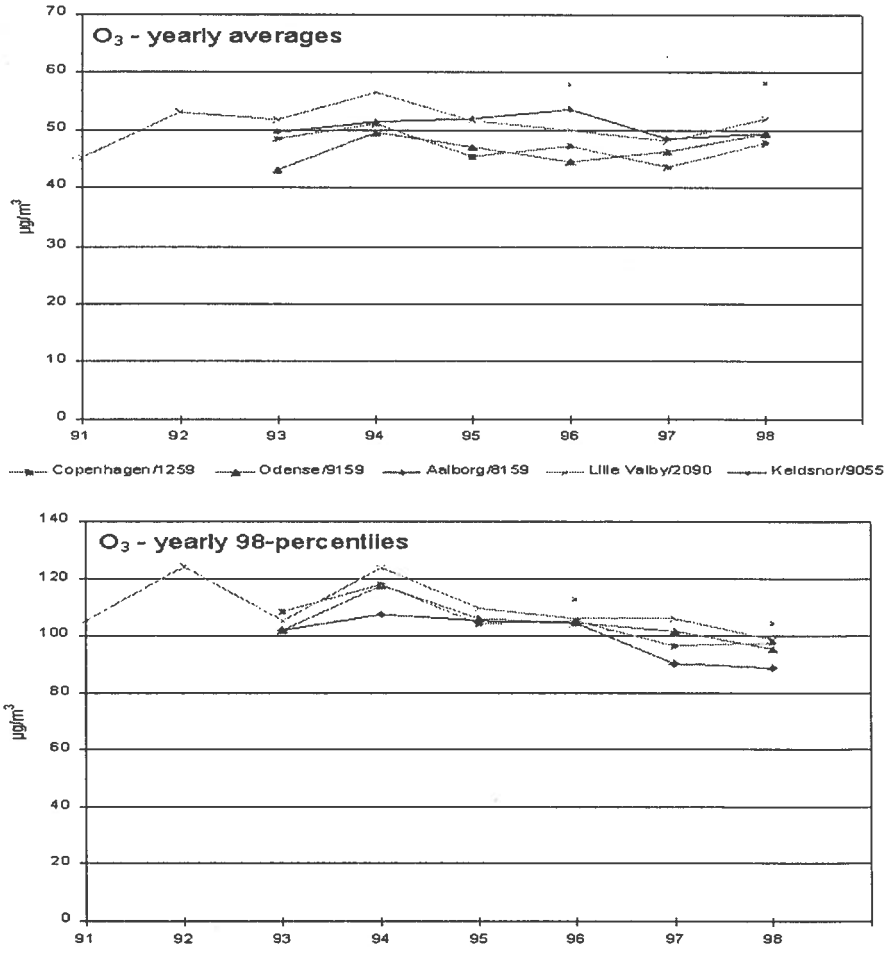

Figure 2.4 The development of Danish ozone concentrations 1991-1998. Notice the large yearly averages and yearly 98-percentiles for the background station Lille Valby. This illustrates the fact that in the cities ozone concentrations are effectively reduced by reaction with NO [Holten-Andersen *et al.*, 1997].

2.2.7.4 Danish aspects of elevated ozone concentrations

Long range transport

In Denmark, elevated concentrations of ozone are mostly encountered in connection with long range transport of photochemical pollution from central Europe. Episodes of this kind occur in the summer period under high pressure weather conditions, with little vertical mixing, much sun and little wind. During such episodes the ozone concentration level may increase to several times the background concentration level [Holten-Andersen *et al.*, 1997].

Economical effects

For Danish background ozone concentrations of 30 - 35 ppb(V) a 10% reduction of the harvest yield is to be expected [Fenger, 1997].A rough estimate based on foreign studies, suggest that the economical effect of the 10% reduction in the harvest yield is a loss in the order of 1 billion kroner per year [Fenger, 1997]. The critical ozone concentration for injury on crops is 40 ppb - AOT40. Calculations have shown that the AOT40 value, on a European scale was exceeded for 83 % of the total cultivated area in 1994 [Holten-Andersen *et al.*, 1997].

Determining the economical effects of elevated ozone concentrations on humans is not a straight forward task. However, it is beyond doubt that it does have some, not insignificant effect, economically as well as on the lives of potentially sensitive populations, such as asthmatics and people with other respiratory diseases.

Exceedence of threshold values

Studies have shown that the EU threshold values (See table 2.2) for ozone exposure are often exceeded under Danish conditions [Granby, 1997]. Granby found that the 24-hour threshold of 65 $\mu g/m^3$ (32.5 ppb) was exceeded at all times of the year, roughly every third day. The 8-hour moving average value of 110 $\mu g/m^3$ (55 ppb) was only exceeded March through September whereas hourly concentrations above 180 $\mu g/m^3$ (90 ppb), that requires information of the public, were only observed from May to August [Granby, 1997].

3 The DOAS technique

3.1 Introduction

The birth of a new technique

The DOAS technique - Differential Optical Absorption Spectroscopy - pioneered by Platt and Perner in the late 1970s [F.-Pitts & Pitts, 1986] - is a relatively new measurement technique in tropospheric chemistry, that has gone through continued improvements up to present. The basic theoretical foundation of the technique is the Lambert-Beer's law. The "absorption cell" in this case is an open light-path created by focusing light from an emitter-lamp unto a receiving unit often placed hundreds of metres or even a few kilometers apart.

Advantages of the DOAS technique

The DOAS technique, apart from being able to measure absorption in the IR (infrared) region of the spectrum also measures absorption in the UV/visible region. Many of the atmospheric pollutants that could not be measured in the IR region with the desired specificity and sensitivity can readily be measured in the UV/visible region. This is true for species such as the nitrate radical (that can be measured only by this technique at present), HONO and others. Thus a DOAS instrument enables the simultaneous and precise measurement of many key tropospheric pollutants, with great time resolution and using the same instrument. The use of path lengths of several hundred metres up to a few kilometers results in detection limits in the order of a few ppt to a few ppb depending on the species of interest. A further advantage of the DOAS technique is that the measured concentrations are averages over long distances which tends to even out local variations. Also the DOAS technique does not suffer from wall losses and the lack of specificity that some chemical methods and monitors do. Finally the ability to monitor several atmospheric species simultaneously with great time resolution is a most valuable tool in determining chemical couplings among species in atmospheric research and in monitoring programmes.

Disadvantages

One of the greatest disadvantages of using the DOAS technique is the sensitivity to meteorological phenomena such as rain and fog, where the visibility is markedly reduced. In this case the measurements are not reliable and can not be used. Also, the presence of interfering species needs to be taken properly into account. Otherwise the measurements may be in error. Likewise uncertainties in the absorption cross sections for a given species will be reflected in a corresponding uncertainty in the estimated concentrations.

3.2 Theoretical Foundations of the DOAS technique

Absorption spectroscopy in ambient studies

Absorption spectroscopy is a well known and widely used technique in analytical chemistry. However, it was not until the mid 1950s that the first long path length IR spectroscopy was applied to monitor species in ambient air [F.-Pitts. & Pitts, 1986]. Among the first species

in ambient air to be identified by this new technique was PAN (Peroxy-acetyl-nitrate) [F.-Pitts & Pitts, 1986].

Characteristic absorption peaks: "fingerprints"

The absorption spectroscopy measurement technique is based on the fact that most species possesses characteristic fine structures or "fingerprints" that can be used for their identification and measurement. By submitting the species of interest to radiation of wavelengths of its characteristic absorption peaks, the concentration can be found by applying the Lambert-Beer's law.

Lambert-Beer's law

The theoretical foundation of the absorption spectroscopy and thus of the DOAS measurement technique is the Lambert-Beer's law:

$$I = I_0 * e^{-N\sigma L} \qquad (3.1)$$

This relates the intensity of the light, before (I_0) and after (I) passage through an air sample, as a function of the concentration in number of molecules per cubic centimeter (N), the length of the path in centimeters (L) and the absorption cross section (σ). The gas phase absorption cross section is thus in units of cm^2 $molecule^{-1}$. Thus in order to apply the Lambert-Beers law for finding the unknown concentration of a species four different parameters are needed.

1. The path length (Measured in a straightforward way).

2. The absorption cross sections

3. The incident light intensity on the air-sample.

4. The intensity of light after passage through the air-sample (The absorption spectrum measured by the DOAS instrument).

Absorption cross sections

The absorption of a molecule is a measure of the ability of the molecule to absorb incident light of a particular wavelength. As a molecule does not absorb radiation equally at different wavelenghts of the spectrum, absorption cross sections depend on the wavelength of the incident light. Table 3.1 gives an example of the absorption cross sections for the nitrate radical at different wavelengths of the spectrum.

Table 3.1 Absorption cross sections (cm_2 $molecule^{-1}$, base e) averaged over each nanometer for the gaseous nitrate radical at 298 K. [F.-Pitts & Pitts, 1986]. Note the maximum absorption cross section at 662 nm.

λ (nm)	$10^{20}\sigma$ (cm^2)	λ (nm)	$10^{20}\sigma$ (cm^2)
656	122	663	1618
657	162	664	1017
658	185	665	615
659	278	666	397
660	522	667	185
661	1063	668	125
662	1756	669	92

The absorption cross sections are generally measured in the laboratory by using known concentrations of the species being measured.

$$\sigma = \{1/([N]L\} \ln (I_0 / I) \qquad (3.2)$$

Where σ, N, I_0, and I have the same meaning as above.

The incident light intensity

The incident light intensity on the air-sample (I_0) can not readily be found in ambient air measurements as absorbing species, as well as particles scattering the light, will allways be present.

Differential absorption

The solution is to look at the absorption on either side of a distinct absorption peak I_0', rather than at the true I_0. This method is illustrated in Figure 3.1 for a species with a distinct absorption peak at wavelength λ_2. At wavelengths λ_1 and λ_3, in the Figure, the absorption spectrum is not structured but some absorption is occurring so the true light intensity I_0 can not be measured. Thus it is the differential absorption (I_0'/I) rather than the absolute absorption (I_0/ I) that is used in the Lambert-Beer's law for determining the concentration of the species. Thus the name of the DOAS technique: *Differential Optical Absorption Spectroscopy.*

Differential Optical Absorption Spectroscopy.

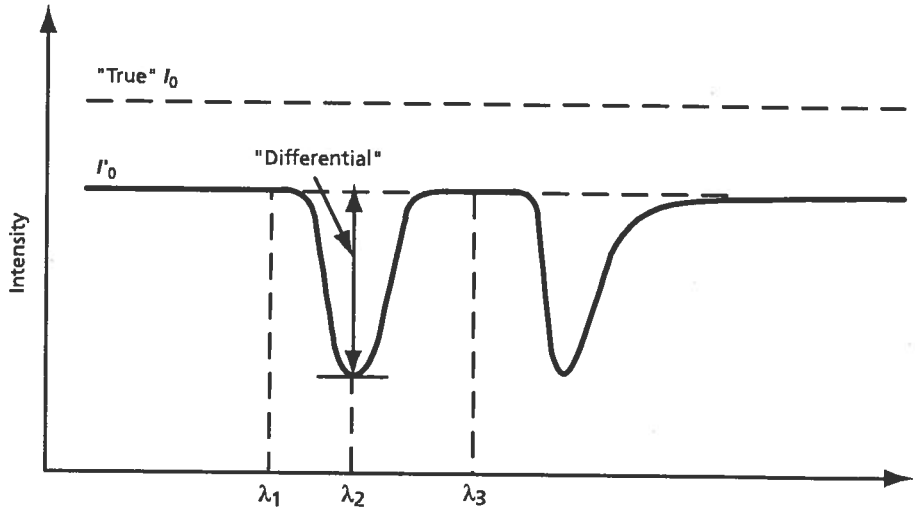

Figure 3.1. Illustration of the differential absorption concept used in the DOAS technique. [Figure from F.-Pitts & Pitts, 1986].

Absorption spectroscopy in the UV/visible region

Unfortunately absorption spectroscopy in ambient air in the IR region of the spectrum is limited due to the presence of strongly absorbing species such as H_2O, CO_2 and CH_4. Fortunately though, many of the key pollutants of interest does possess fine structure in the UV/visible region of the spectrum which allows for their detection and measurement at ambient concentrations.

Advantages of operating in the UV/visible region

An advantage of applying absorption spectroscopy to the UV/visible region of the spectrum is that the absorption cross sections are generally larger in this region than in the IR region. This allows for better detection limits and the ability to measure species that could not be measured with the required sensitivity using IR spectroscopy. The DOAS technique employs this fact in measuring NO_3 and HONO, species that can not currently be measured with the necessary sensitivity and accuracy by other measurement techniques. Table 3.2 gives

the absorption coefficients and measurement ranges for some atmospheric species that can be measured by the DOAS technique.

Table 3.2 Wavelength range and differential absorption coefficients for some atmospheric species of interest when using DOAS [F.-Pitts & Pitts, 1986].

Species	Wavelength range	Differential absorption coefficient	
	(nm)	($cm^2 molecule^{-1}$)e	at λ (nm)
SO_2	200-230, 290-310	$5.7 * 10^{-19}$	300
NO	215, 226	$2.3 * 10^{-18}$	226
NO_2	330-500	$1.0 * 10^{-19}$	363
NO_3	623, 662	$1.8 * 10^{-17}$	662
HONO	330-380	$4.2 * 10^{-19}$	354
O_3	220-330	$4.5 * 10^{-21}$	~328
HCHO	250-360	$6.8 * 10^{-20}$	339

Optimal wavelength region

In finding the optimal wavelength region for detecting and measuring a tropospheric species it is necessary to look at least 3 parameters.

1. The Differential absorption cross sections - should be maximized.
2. The atmospheric attenuation (see below) - should be minimized.
3. The interference from other species - should be eliminated.

In chapter 4.3 trade-offs between these parameters are discussed for ozone. Thus, in general, the wavelength regions used for measuring a particular species, in different implementations of the DOAS technique may vary. Some manufacturers, such as OPSIS, Sweden, do not supply information on which wavelength regions are used.

3.3 Instrument Build-up

The OPSIS AR 500 system

In this section the basic construction of a DOAS system will be described. It should be noted that allthough all DOAS systems are based on the same principles, various implementations of the overall design exist. The design described here is mainly that of the Lille Valby DOAS, the OPSIS AR 500 system, but most of the description will apply for other DOAS systems as well.

The main units

A DOAS system consists of three main units. An emitter unit that projects light unto a receiver unit. Thus, creating an open light path for ambient measurements. From the receiver, data are sent to the analyzer through a fibre optic cable.

The emitter unit

In the emitter, light is created by a spark discharge in a xenon lamp. The light from the xenon lamp covers a wide range of the spectrum - the UV, visible and IR wave length regions. Two kinds of lamps may be used. An ozone-generating type A lamp, and a non-ozone-generating type B lamp, used when ozone is one of the species being measured. At the Lille Valby DOAS, lamps of type B are used. The

xenon lamp is placed in the focal point of a spherical mirror, which collimates the light into a parallel beam before it is transmitted through the ambient air unto the receiver.

Receiver and analyzer units

At the receiver a telescope refocuses the light, whereupon it is let through a fibre optic cable to the analyzer. Here the received light enters the entrance slit of a high-performance spectrometer.

The spectrometer

In the spectrometer, the received light is split by a dispersion element into its wavelength components so that the variation of the absorption with frequency can be monitored. This is done by having a rotating disk with radial slits move across the exit focal plane of the spectrometer. In this way a 40 nm wide segment can be scanned repeatedly in a chosen region of the spectrum. Thus by using only one detector different wavelength regions can be recorded seperately. The light intensity passing through the moving slits is monitored by a photomultiplier. The signals are digitized by an A/D converter for further analysis and spectral deconvolution by the built-in computer. Having in this way split the absorption spectrum into regions for which we know the absorption cross sections the concentration can be calculated.

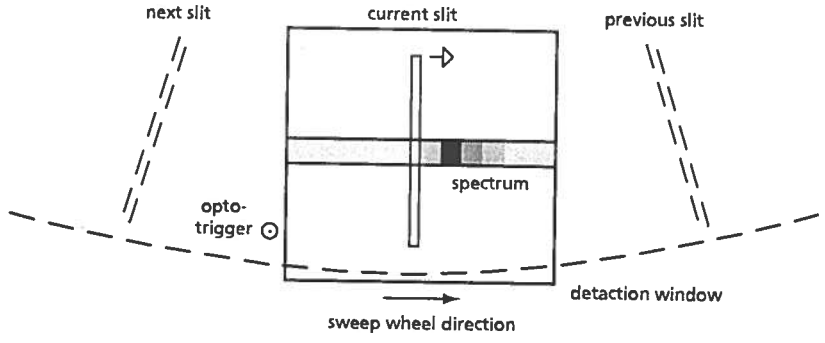

Figure 3.2 The moving slits [F.-Pitts and Pitts, 1986].

3.4 Spectral Deconvolution

As mentioned in section 3.2 the DOAS technique builds on the fact that different species possess distinct absorption peaks at different wavelengths that can serve as "fingerprints" for their identification and measurement. This "fingerprint" information is found in the fine structures of the absorption spectrum. Thus the absorption spectrum needs to be processed in a number of steps, by the build-in computer, before it can be used for determining the concentrations of the species present in the ambient air. Several corrections must be made in order to compensate for scattered light, the xenon-lamp spectrum and other interferences.

Lamp spectrum

A reference spectrum of the lamp is first subtracted, leaving a "raw" spectrum. Due to the scattering effect of the different sized particles in the ambient air some broadband absorption will also be present in the spectrum.

Polynomial fitting of broad band absorption

Making the assumption that the broadband absorption does not include any narrowband structures it can be removed by fitting a

polynomial onto the spectrum. A polynomium of degree 5 is normally used, but the degree should not be too high in order not to fit any of the fine structure. When the polynomium has been fitted to the absorption spectrum it is subtracted from the spectrum. What is left is a superimposed differential spectrum of all the absorbing species. In other words it contains the fine structures that represent the "fingerprints"of the species being measured.

The Lambert-Beer's law for more absorbing species

The total absorption of all species at any wavelength can be described by the expression:

$$A(i) = [c_1\Delta\sigma_1(i) + c_2\Delta\sigma_2(i) + ... c_j\Delta\sigma_j(i)]L \qquad (3.3)$$

; where j is the number of species, σ_j is the absorption coefficient of species j and c_j is the unknown concentration of species j. The task then, is to find the concentrations (c_1, c_2, ... c_j) of all the individually absorbing species.

Least squares fitting

A theoretical spectrum is calculated using pre-recorded cross-section spectra of all the (assumed) absorbing species. This spectrum is fitted to the differential spectrum using least squares fitting.

$$\Sigma_i\Sigma_j[\ A(i) - Lc_j\Delta\sigma_j(i)]^2 \qquad (3.4)$$

; where the double-sum is over the number of species (j) and the number of absorption cross-section intervals in the 40 nm wide region of the spectrum that is being scanned (i). This is a highly overdetermined system of equations that can be solved by least squares fitting. Thus the above expression is minimized by varying the unknown concentrations c_j. The final values of c_j are the desired concentrations of the absorbing species.

Residual absorption

The residual absorption, that is what is left when subtracting the mathematical spectrum from the differential absorption spectrum is a measure of the accuracy with which the concentrations have been determined. A large residual absorption can be an indicator that absorbing species are present, which have not been accounted for.

Accuracy of absorption cross sections

Uncertainty in the determination of the absorption cross sections will be reflected in a corresponding uncertainty in the determination of the concentration of the measured species. This is discussed for the individual species in chapter 4.

Interfering species

The presence of interfering species may be seen as residual absorption in the residual spectrum, for the wavelength region in which a tropospheric species is measured. Thus, interfering species may result in an error in the concentration determined for the measured species. In section 4.5 H_2O interference in NO_3 measurements is discussed.

3.5 The Lille Valby DOAS system

Geographical description

The measurement site is situated in a semi-rural environment at Lille Valby, Sjælland. The geographical coordinates are 12°07'07''E,

55°41'42''N with an altitude above sea level of 15 m. The variation of the terrain is less than 5 m in a radius of 1 km from the station. The site is 30 km West of Copenhagen (850.000 inhabitants) and 8 km North of Roskilde (40.000 inhabitants). A few kilometers West of the site is the Roskilde Fjord. A road with about 6000 vehicles daily, passes along the Roskilde Fjord in a North South direction about 1 km West of the station. The Lille Valby measurement site is also the Danish station in the EUROTRAC TOR (*Tro*pospheric *O*zone *Re*search) monitoring network.

The DOAS system

The central unit in the DOAS system used at Lille Valby is an OPSIS AR 500 Multi-Component Air Quality Analyzer. The analyzer, placed indoors, receives light from the outdoor receiver unit through a fibre optic cable. An open light path is created by projecting light from the emitter, placed across a field 721.2 m from the receiver, unto the receiving unit. The light is produced by a spark discharge in a xenon lamp installed in the emitter.

Figure 3.3 The emitter unit at Lille Valby, Sealand. Photo by B. Jensen, NERI, Roskilde.

The analyzer

In the analyzer, a high-performance spectrometer converts the received light into digital signals for further analysis by the built-in computer. The computer software includes the spectrographic "fingerprints" of the measured compounds. Thus, as described above, using Lambert-Beer's law, the various compounds are detected and measured through the absorption they cause in the spectrum of received light. Margins of error for each obtained value as

well as the proportion of transmitted light received by the analyzer is noted. This allows for data as well as system verification.

Detection limits at Lille Valby

The detection limits for an OPSIS AR 500 system using a measurement time of 1 min. and a path length of 500 metres are 0.1 $\mu g/m^3$ for NO_3, 1 $\mu g/m^3$ for NO_2 and 3 $\mu g/m^3$ for O_3 [OPSIS, 1995]. Thus the detection limits are improved by a factor of 1.44 (721.2m/ 500m = 1.44) relative to the 500 m path length limits, for a measurement time of 1 minute. The approximate Lille Valby detection limits for selected compounds are therefore:

NO_2 (1 $\mu g/m^3$ * 0.4869 ppb(v)/$\mu g/m^3$)/1.4424= 0.38 ppb(v)

O_3 (3 $\mu g/m^3$ * 0.4667 ppb(v)/$\mu g/m^3$)/ 1.4424= 0.97 ppb(v)

NO_3 (0.1 $\mu g/m^3$ * 0.3613 ppb(v)/$\mu g/m^3$)/ 1.4424= 25 ppt(v)

HONO(1 $\mu g/m^3$ * 0.4765 ppb(v)/$\mu g/m^3$)/1.4424= 0.33 ppb(v)

Thus the nitrate radical has a detection limit of approximately 25 ppt. The detection limits for NO_2 , O_3 and HONO are 0.38 ppb(v) , 0.97 ppb(v) and 0.33 ppb(v) respectively.

Path length and detection limits

A trade-off, when using the DOAS technique, is that of path length and detection limits. Generally, a longer path length results in a lower detection limit. However, the atmospheric attenuation (light scattering by gases and particles and light absorption by gases and particles [F.-Pitts & Pitts, 1986]) also increases with increasing path length. Thus a trade-off must be made between sufficiently low detection limits and low atmospheric attenuation.

Special conditions

To ensure the stability of the system both the receiver and the emitter units are placed on concrete fundaments. However, some instability due to solar heating of the housings did occur. In the early spring the sun is not in the sky long enough for the heating to have any disturbing effect, even over a week-long period. Later in the spring and especially during the summertime, however, the sun effectively heats up the exterior of the emitter and receiver units. This results in a need for re-alignment of the system, in order to obtain a fairly constant and acceptable light level. The effect can be quite pronounced and therefore several daily adjustments might be needed. For night time measurements, as in the case of nitrate radical measurements, the system must be re-aligned when it has "cooled off" which does not take place until some time after sunset. At summertime this is some time between 9-10 PM. The problem was solved by setting up a "shading device", which kept the heating to a minimum, that did not markedly alter the alignment. As the shading device was not set up until mid-June 1998 the data for some nights previous to this time are sparse because the light level did not exceed the minimum acceptable level of 15%. See section 3.6.1.1 for a definition of the light level.

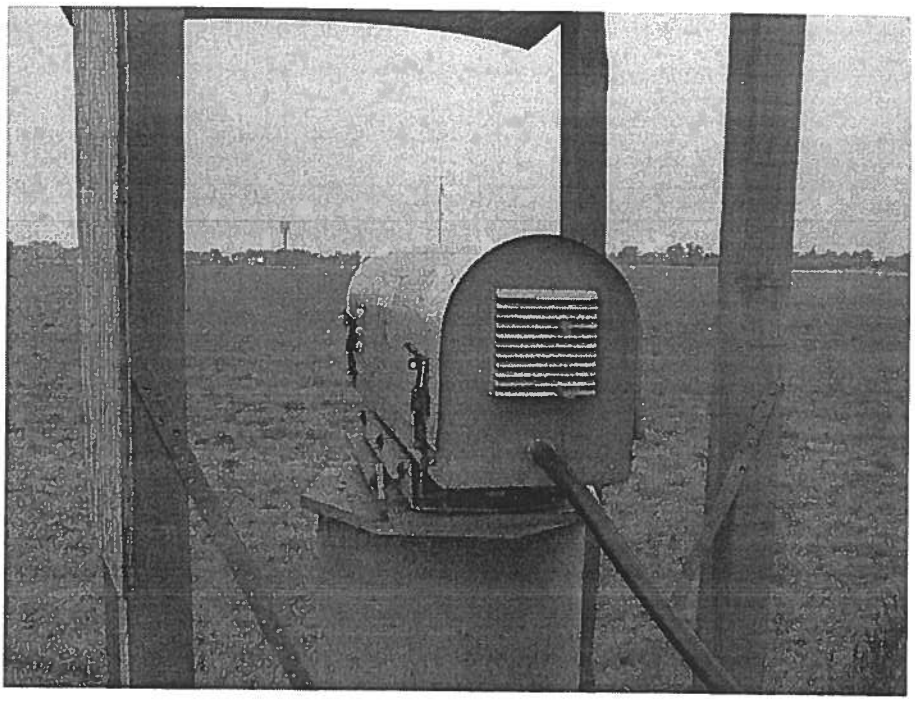

Figure 3.4 The receiver unit at the Lille Valby DOAS. Note that the light from the lamp at the emitter can be seen in the background. Also the "shading devices" mentioned in the text can be seen on the side and above the DOAS. Photo by B. Jensen, NERI, Roskilde.

Meteorological data

Along with the DOAS measurements at Lille Valby, meteorological data was supplied by the RIMI (Risoe Integrated Environmental Project) project at Risø. The available data included global radiation, temperature, wind direction and wind speed. Global radiation data was used to define the nighttime periods of interest. Nighttime was defined as global radiation less than 2 W/m^2 and in the cases of missing meteorological data as the time between 9 PM and 4 AM.

3.6 Quality control and maintenance

Optimal quality measurements

To ensure optimal quality measurement data from the DOAS instrument, it is necessary to perform regular performance checks of the instrument itself as well as quality analysis of the obtained data.

3.6.1 Data quality control

The DOAS instrument presents each measurement result in the form of three parameters:

1. Concentration ($\mu g/m^3$ or ppb)
2. Standard deviation ($\mu g/m^3$ or ppb)
3. Light level (%)

Quality control of measurement data

These parameters, besides giving the desired (if correct) concentration of the measured species, can be manipulated in order to perform quality control of the measurement data. The following sections describe how this can be done.

Measurement information

The measurement results themselves give information on the quality of the measurement.

1. Negative concentrations

A negative concentration in itself is not necessarily an indicator for error in the measurement. Negative concentrations up to two times the standard deviation falls within the uncertainty limits of the measurement and is thus accepted and stored as correct. However, large negative concentrations does indicate a serious error in the measurement [OPSIS, 1996].

2. Negative standard deviation values

This is an indicator that the evaluation has not converged properly. Thus, the measurement is uncertain or completely incorrect. It is however, stored with the negative std.dev. functioning as an indication of the error [OPSIS, 1996].

3. Negative light levels

A negative light level is an indicator that the user defined maximum standard deviation limit is exceeded for this measurement. The value is stored however [OPSIS, 1996].

3.6.1.1 The Light level

The light level is one of the main parameters in the quality control of the DOAS measurements.

The light level may vary over the cause of a day or change slowly over a longer period due to various reasons. Ideally these variations should be kept to a minimum.

Daily variations

This kind of variation can normally be explained by meteorological phenomena. Clearly the light levels may drop due to decreased visibility on a foggy or rainy day. Likewise dust phenomena, for example around harvest, will also affect the light intensity. In the case of the Lille Valby DOAS, extensive daily drifting of the light level was found to be due to solar heating of the instrument. Placing the receiver and emitter units on concrete bases did not suffice to solve this problem as described in section 3.5.

Drifting of light level

The light level may decrease slowly over time for various reasons:

1. Deterioration of the lamp. An old lamp will show a decrease in the intensity of the deep-UV part of the lamp spectrum. Thus the effect should be most pronounced for gases measured in the deep-UV region such as NO. However, if the lamp is changed as prescribed every 6 months this phenomenon should not occur (to any significant extent) [OPSIS, 1996].

2. Movements in the instrument base.

The base upon which the instrument is placed may move slowly with time. Placing the DOAS on a concrete base should eliminate this problem.

Definition of light level

The light level describes the amplification done by the photomultiplier tube in the analyzer. On the analog/digital card the photomultiplier gain is adjusted so that the output current reaches a certain value. This is done by varying the gain voltage, until the desired output current is reached. Thus a voltage of 190 V D/C corresponds to a light level of 100%(min. amplification) and a voltage of 1100 V D/C corresponds to a light level of 0%(max. amplification) [Virkkula, 1996]. The light level is calculated for the wavelength at which most light arrives at the photomultiplier. In the case of ozone measurements in the 265.7 - 304.4 nm region the light level is calculated at approximately 297 nm which has the highest intensity of the xenon lamp spectrum in that region. NO_2 is measured in the 406.2 - 444.2 nm region the light level is calculated at approximately 444 nm [Virkkula, 1996]. I have not been able to find the precise wavelength intervals used by OPSIS in the measurements of HONO and NO_3 as OPSIS do not provide their users with that kind of information. Thus an estimate of the wavelength for which the light level is given can not be made. Also it should be noted that OPSIS do not themselves provide the information about the wavelength for which the light level is reported. Without any attenuation the light level would be 100%.

3.6.1.2 Lowest acceptable light level and standard deviation

Normally the standard deviation will increase with decreasing light levels, because the signal-to-noise ratio is then decreasing. Thus one might suspect that an upper value of the standard deviation could be used for excluding bad data. However, in the case of high pollution levels the standard deviation also increases because the signal-to-noise ratio is then a constant. Thus to perform a quality analysis of the DOAS data it is necessary to look at the signal-to-noise ratio as well.

How to find lowest acceptable light level

The analysis builds on plotting the light level against the standard deviation. Examples of such plots are given in Appendix B.1 and B.2.

Now the lowest acceptable light level L and the standard deviation D_i is found in the following way:

1. A curve is drawn directly underneath the scattered points in the diagram.

2. The point on the curve, where the noise becomes dominant is found.

3. Following the curve uphill 1/4 to 1/3 of its length then defines the lowest acceptable light level L and the standard deviation D_i.

4. However, light levels below 15 % should not be accepted. In this case one should proceed uphill along the curve until it crosses the 15 % light level and a new std.dev. D_i should be found from that point.

Now the task is to exclude data of high std.dev. caused by interferences and not to exclude data of high std.dev. caused by high pollution levels. To do this the signal-to-noise ratio needs to be found.

Finding the signal-to-noise ratio

The signal-to-noise is defined as concentration divided by std.dev. (C/D). This value is estimated by plotting concentration versus std.dev. in a scatter plot as shown in Appendix B.1-B.2. Now the bad data points found in the lower right hand side of the diagram should be identified and excluded.

Data points to be excluded

The data points to be excluded lies below a straight line that goes through the previously determined value of standard deviation on the x-axis, D_i. The only problem is to find the proper slope of the curve, the signal-to-noise ratio. One way to do this is to draw a straight line along which the main part of data points are found. Using the slope of this line a straight line through D_i on the x-axis can then be drawn. The data points to be excluded are thus those that lie below this line.

Lowest acceptable concentration

In order not to accept data points of high negative values but of low std.dev. all data with a negative concentration greater than the negative of the std.dev. (- D_i) should also be excluded.

3.6.2 Corrections from datalogger data

OPSIS provides several data-logging units for automatic temperature and pressure correction of measurements. They also registrate wind speed, wind direction, and rainfall. Use of dataloggers is optional. Thus it is worth estimating the size of the errors introduced into the measurements when choosing not to use datalogger data for correction. Estimates of this kind are done below.

3.6.2.1 Temperature correction from data-logger.

The conversion factors for converting between μgm^{-3} and ppb are temperature dependent. The conversion factors and their temperature dependence can be found in the following way. The calculations are shown for NO_2.

$$P * V = n * R * T \Rightarrow \qquad V = n * R * T / P$$

Thus at T = 273 K and P = 1.00 atm.

$$V = (1\ mol * 0{,}082057\ atm * l * mol^{-1} * K^{-1} * 273K)/1atm$$
$$= 22{,}401561\ L$$

Thus, the conversion factor for converting from ppb to micrograms at 273 K and 1.00 atm. is:

$$46/22{,}401561 = 2{,}053428\ \mu gm^{-3}ppb^{-1}$$

;where 46 is the approximate molecular weight of NO_2. Thus, to convert from micrograms to ppb at 273 K and 1.00 atm. the conversion factor is:

$$1/2{,}053428 = 0.48699\ ppb\mu g^{-1}m^3$$

Likewise at T = 288 K and P = 1.00 atm.

$$V = (1\ mol * 0{,}082057\ atm * l * mol^{-1} * K^{-1} * 288K)/1atm$$
$$= 23.632416\ L$$

Thus, the conversion factor for converting from ppb to micrograms at 288 K and 1.00 atm. is:

$$46/23.632416 = 1.946479\ \mu gm^{-3}ppb^{-1}$$

Thus, to convert from micrograms to ppb at 288 K and 1.00 atm. the conversion factor is:

$$1/1.946479 = 0.51375\ ppb\mu g^{-1}m^3$$

Thus, the error introduced for a measurement of NO_2 of 10 μgm^{-3} using the conversion factor at 273 K instead of the one for 288 K at 1.00 atm is ((0.51375 - 0.48699) / 0.51375) * 100 % ≈ 5 %. Thus the DOAS measurements are underestimated by 5 % in this case. Likewise, at temperatures below zero the DOAS measurements will be overestimated.

3.6.2.2 Pressure correction from data-logger.

The conversion factors for converting between μgm^{-3} and ppb are dependent on pressure. The conversion factors and their pressure dependence can be found just as their temperature dependence. Again the calculations are made for NO_2.

$$P * V = n * R * T \Rightarrow \qquad V = n * R * T / P$$

At T = 273 K and P = 101.325 kPa = 1 atm the conversion factors are the same as calculated above. Thus, the conversion factor for converting from ppb to micrograms at 273 K and 1 atm is:

$$46/22{,}401561 = 2{,}053428\ \mu gm^{-3}ppb^{-1}$$

;where 46 is the approximate molecular weight of NO_2.

And to convert from micrograms to ppb at 273 K and 1 atm the conversion factor is:

$$1/2{,}053428 = 0.48699\ ppb\mu g^{-1}m^3$$

Now for constant temperature, T = 273 K and P = 0.97 atm

$$V = (1\ mol * 0{,}082057\ atm * l * mol^{-1} * K^{-1} * 273K)/0.97\ atm$$
$$= 23.0944\ L$$

Thus the conversion factor for converting from ppb to micrograms at 273 K and 0.97 (low pressure episodes) atm. is:

$$46/23.0944 = 1.99\ \mu gm^{-3}ppb^{-1}$$

Thus to convert from micrograms to ppb at 288 K the conversion factor is:

$1/1.99 = 0.5021\ ppb\mu g^{-1}m^3$

Thus the error introduced for a measurement of NO_2 of 10 $\mu g\ m^{-3}$ using the conversion factor at 1 atm instead of the one for 0.97 atm at 273 K is ((0.5021-0.48699) /0.5021) * 100 % ≈ 3 %.

Conversion factors used

The conversion factors used throughout this thesis for converting between ppb and μgm^{-3} are those given in the OPSIS software manual [OPSIS, 1995].

Table 3.3. Conversion factors for converting between ppb and μgm^{-3}. The conversion factors are for T_0 = 273.15 K and P_0 = 101.32 kPa. The molar volume is 22.40 m^3/kmol [OPSIS, 1995].

Species	Conversion factor 1 $\mu gm^{-3} \leftrightarrow$ n ppbV	Conversion factor 1 ppbV $\leftrightarrow$ n μgm^{-3}
NO_2	0.4869	2.054
O_3	0.4667	2.143
NO_3	0.3613	2.768
HONO	0.4765	2.099

3.6.3 Maintenance

In order to obtain quality measurement data the performance of the DOAS instrument has to be checked regularly and the results included in the data evaluation process. The performance checks can be divided into groups depending on the frequency with which they should be done. The OPSIS manual suggests the following guidelines.

1. Once a week: System check, check of light levels and standard deviations.
2. Every two weeks: Precision test (U.S. EPA requirement).
3. Once a month: Reference calibration, data backup, visual inspection of the system including the emitter, receiver, opto-fibre, etc.
4. Every third month: Span calibration
5. Once a year: - Accuracy audit (U.S. EPA requirement)
   - Examination of the complete system, including recertification of all test gases.

3.6.3.1 System check (Once a week)

The built-in automatic System Check performs a check of the spectrometer and the related electronics to ensure that the recorded spectra are reasonable.

Stability check of rotating disk

First the stability of the rotating disk is tested. This is done by testing the time between two slits in the disk during one and ten revolutions

respectively. If the deviation is below the limit of 0.1 % the test result is OK.

Checking the grating positioning

For movable grating systems the positioning of the grating needs to be performed with great accuracy. The result of the positioning check is presented in the form of the parameters P1 and P2 and both must be within the permissible limits.

Checking the detection system

The last test deals with the performance of the detection system. The grating positioning with respect to the detector is measured to ensure that the image, originating from the optic fibre, is projected onto the detector as centred as possible. Also the analogue offset in the detection system is determined. The results of these checks are given in the parameters P3, P4 and P5. These should also be within some predetermined limits.

A more thorough description can be found in the OPSIS manuals [OPSIS, 1995 and OPSIS, 1996].

Along with the System Check the light levels should be inspected for each gas (and for each path). If the light levels are dropping the cause for this should be looked into.

3.6.3.2 Precision test (U.S. EPA requirement, every two weeks).

A precision test is defined in the U.S. EPA 40 CFR Part 58 regulations. The OPSIS Quality Assurance and Quality Control Manual gives a thorough description of how to perform a precision test [OPSIS, 1996].

3.6.3.3 Reference calibration (Once a month)

In order to ensure that the raw lamp spectrum used in the deconvolution routine of the DOAS system is of optimal quality a new reference spectrum, taken at zero gas conditions, needs to be recorded on a regular basis. This will compensate for changes in the analyzer spectrometer as well as in the electronics and minimize instrument noise.

Reference spectrum

A new reference spectrum can be made by performing a reference calibration as described in the OPSIS Quality Assurance and Quality Control Manual [OPSIS, 1996]. The effect of such a calibration is to record a new reference spectrum for the wave length regions (windows) used in measuring the selected gases. If more pollutants are evaluated in the same wavelength region only one reference spectrum is necessary. A more thorough description can be found in the OPSIS manual [OPSIS, 1996].

3.6.3.4 Span calibration (Every third month)

The principles and control of a span calibration is described in the following, section 3.7.

3.6.3.5 Accuracy audit (U.S. EPA requirement, once a year)

An accuracy audit test is also defined in the U.S. EPA 40 CFR Part 58 regulations. The OPSIS Quality Assurance and Quality Control Manual gives a thorough description of how to perform a precision test [OPSIS, 1996]. Except for some modifications it is a multipoint span/offset calibration as described in section 3.7 below.

3.6.3.6 Mercury lamps for checking grating precision

Upon manufacture of the DOAS instrument, a mercury spectrum is recorded for most of the measurement components. Thus the precision of the grating can later on be checked by recording a new mercury spectrum and comparing the position of the mercury peaks with those of the post manufactory spectrum. In this way a drift in channels can be found and corrected for. To perform this check an OPSIS mercury lamp CA 004 is required.

3.6.3.6 Light attenuation test

Atmospheric attenuation may influence on the DOAS measurements and thus the analyser's sensitivity to light attenuation should be checked. A light attenuation test is carried out for each gas (and each path), since the result may depend on both the wavelength region and the path length. Special hardware, grids which simulate increasing levels of light attenuation, are needed for a light attenuation test. The grids are placed in front of the receiver entrance one at a time and the effect on the light level is observed. If a standard deviation increases when attenuating the light, this is an indication that the light level for that species is too low. The procedure is thoroughly described in the OPSIS quality control manual [OPSIS, 1996].

3.7 Calibration of the DOAS instrument

Calibration of the instrument is part of the normal operational procedure. A calibration serves to check if the analyzer is responding correctly, when measuring a given gas concentration. If not, the calibration procedures will supply you with information enabling you to make the necessary corrections for resuming correct operation.

3.7.1 The control of the calibration system

Multipoint span calibration

A multipoint span calibration, as described in this chapter, consists of at least six roughly and equally spaced calibration points, including the zero point, covering at least 80 % of the measurement range [OPSIS, 1996].

Calibration points

Calibration points are pairs of measured signals and known concentrations. Plotting the analyzer responce (Y) as a function of the theoretical/calculated concentration (X) in an ordinary x-y plot ideally gives a straight line with the equation:

$$Y = k^* X + b \qquad (3.5)$$

Analyzer responce and the Lambert-Beers law

The analyzer responce (Y), that is the concentration measured by the analyzer, is found by applying the Lambert-Beers law to the measured spectral intensities as described in section 3.2.

Instrument correction factors

The slope (k) and intercept (b) of the y-axis then defines the desired instrument correction factors:

$$\text{span factor} = 1/k \quad (3.6)$$

$$\text{offset factor} = -b \quad (3.7)$$

Ideally the span factor, which adjusts the instrument sensitivity, should be 1.000. However, the slope (k) should not deviate from 1.0 by more than +/- 20 %[OPSIS, 1996]. Likewise the offset factor, adjusting the deviation from zero, when measuring zero gas, ideally should be 0.000 [OPSIS, 1996].

Basic requirements

The span-calibration should be done within an interval of 10-80 % of the operational measurement range. That is the optical density when calibrating should be comparable to the optical density of the outdoor measurements, for each gas being calibrated. The maximum optical density of the outdoor measurements, $O_{d,max}$, is expressed as:

$$O_{d,max} = L * C_{max} \quad (3.8)$$

,where C_{max} is the maximum concentration of the species being calibrated. To achieve the same density when calibrating, a cell of length L_c is required:

$$L_c = O_d / C_{std} \quad (3.9)$$

With an outdoor-path length of 721,2 m, a measurement range for NO_2 of 0-500 ppb (instrument range), and a standard gas concentration C_{std} of 961 ppm, a cell of length:

$$L_c = (721{,}2 * 500 \text{ ppb}) / 961000 \text{ ppb} = 0{,}375 \text{ m}$$

corresponds to the maximum optical density. However for Lille Valby a range of 0-20 ppb is sufficient. Thus, a cell of length 1.5 cm is sufficient for obtaining the maximum optical density.

Obtaining the calibration points

The various calibration points for different optical densities can be obtained in two ways. Either by varying the length of the calibration cell or by varying the standard gas concentration by dilution. Variation of the calibration cell length offers no contribution from errors in the dilution system.

At least three calibration cells of lengths: L1, L2 and L3 must be used. From these a total of 7 different calibration cell lengths can be obtained by combination:

L1, L2, L3, L1 + L2, L1 + L3, L2 + L3, L1 + L2 + L3

giving 7 points on the calibration curve. Besides the calibration cells the additional hardware needed for a span calibration is described in the OPSIS Quality Control manual [OPSIS, 1996].

3.7.2 The NO_2 calibration procedure

Only a brief description of the steps in the calibration procedure will be given, along with the calculations concerning the dilution system and the correction factors.

Instrument setup

The calibration bench, calibration cells, lamp etc. was connected as instructed in the OPSIS Quality Control manual [OPSIS, 1996].

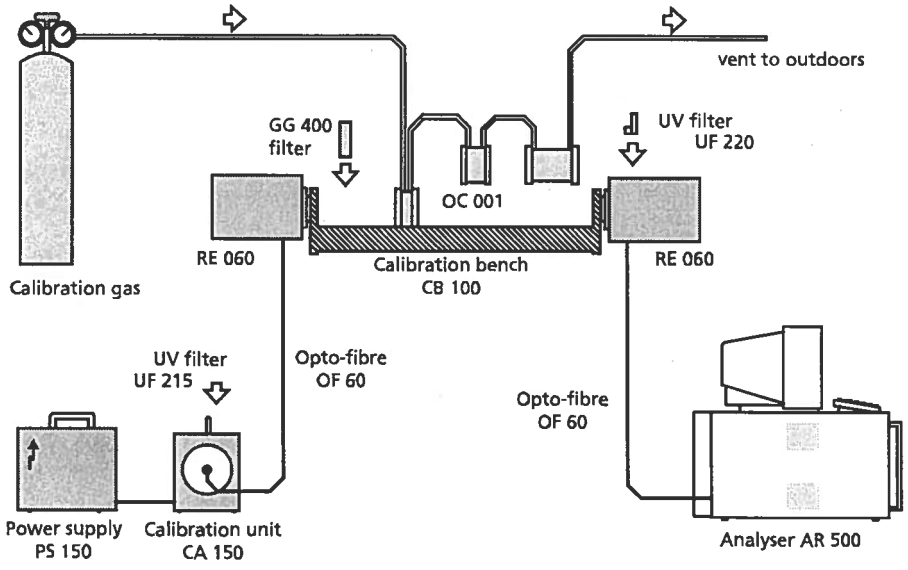

Figure 3.5 The setup for performing a dynamic, multipoint span calibration for NO_2. The GG 400 UV filter is required for NO_2 calibrations only (protects against photolysis of the NO_2).

Three calibration cells were used:

L1 = 99.24 mm, L2 = 40.02 mm, L3 = 10.18 mm.

Measurements were done on seven different cell combinations as described above, and on three different dilutions of the 961 ppm NO_2 standard gas: 50 %, 25 % and 12.5 % dilution. For cell combinations L1+L2 and L1+L2+L3 measurements were also made for 6.25 % dilution.

The dilution system

In this case a dilution of the NO_2 gas was obtained by mixing the NO_2 bottle-gas with zero-air in a mixing cell, using flowmeters to vary the dilution factor. The total flow rate was measured to be 1078 ml/min. A dilution of the NO_2 gas of 50 % then corresponds to a combined flow of zero-gas and NO_2 gas of 539 ml/min each. The calibration curves for the flow-meters are:

Flowrate = 63.35714 * (reading in %) + 10.45054
; for the Zero-air flowmeter
Flowrate = 25.65526 * (reading in %) + 48.08334
; for the NO_2 flowmeter

From these the reading for any desired flowrate can be found. For the zero-gas it was found that a flow of 539 ml/min corresponds to a reading on the flowmeter of 8.34%. Likewise is was found that for the NO_2 mass flow controller a flow of 539 ml/min corresponds to a reading of 19.14 %. A 50% dilution therefore consists of flows of

zero-gas and NO_2 at 8.34% and 19.14% respectively, for a total of 1078 ml/min.

Table 3.4 Dilution factors and corresponding flowmeter readings.

NO_2 - dilution factor	Flowmeter reading NO_2 in %	Flowmeter reading Zero air in %
50 %	19.14	8.34
25 %	8.63	12.6
12.5 %	3.38	14.72
6.25 %	0.75	15.8

The concentration of the NO_2 standard gas used was 961 ppm. The Mass Flow Controller calibration curves are given in Appendix D.

3.7.3 Results

Completing the measurements a total of 21 calibration points was obtained. The maximum concentration obtained was 359.0296 ppb and the minimum concentration was 6.114363 ppb. Thus the 21 calibration points span a range of (359.0296 - 6.114363) ppb = 352.92 ppb or sligtly above 70 % of the full instrument measurement range of 0-500 ppb. And well above the expected ambient range of 0-20 ppb. The full results of the calibration procedure is given in Appendix D.

Calculations on measurements made in ppb

The DOAS instrument allows for operation with two concentration measures: ppb or micrograms per cubicmeter. The calculated concentration ($C_{calc.}$) at 50 % dilution and for a combined cell length of 0,13926m is found from the expression:

$$C_{calc.} = C_{used} * L_{cell}/L_{path} \qquad (3.10)$$

where C_{used} is the concentration of the bottle NO_2 gas after dilution. L_{cell} is the length of the calibration cell and L_{path} is the pathlength given in the DOAS instrument. As the concentration of the bottle gas used is 961 ppm, the concentration in ppb for a dilution of 50% is:

$$C_{used} = (961*1000)/2) \text{ ppb} = 480500 \text{ ppb}$$

Thus for L_{cell} = L1+L2 = 0.1392 m and L_{path} = 200 m the calculated concentration can be found from the expression:

$$C_{50\%,(L1+L2)} = ((961*1000)/2) \text{ ppb} * 0{,}13926\text{m}/\ 200\ \text{m} = 334{,}57215 \text{ ppb}.$$

The concentration C_{used} is multiplied by the factor L_{cell}/L_{path} because the measurement path length used in the DOAS instrument measurement evaluation is set to 200 metres. Thus it sees the measured optical density as if it was obtained over a path length of 200 metres and corrects for this.

The calibration curve

The result of plotting measured against calculated values for all calibration points are seen in Figure 3.6. It shows the calibration curve for all validated calibration points as well as for each cell combina-

tion. Table 3.5 gives the slope, intercept, correlation coefficient, span factor and offset factor for each cell combination.

Table. 3.5 Results of the calibration procedure for different calibration cell combinations.

Cell length	k	b	R	Std. Dev.	Span factor: 1/k	Offset factor: -b
L1	0.9937	3.38	1	0.35333	1.0063	-3.38
L1+L2	0.9997	4.7591	1	0.395	1.0003	-4.7591
L1+L2+L3	1.017	4.4078	1	0.425	0.9833	-4.4078
L1+L3	1.0023	2.58	1	0.33333	0.9977	-2.58
L3	1.0033	0.14	0.9992	0.13333	0.9967	-0.14
L2+L3	1.0027	1.52	1	0.22	0.9973	-1.52
L2	0.9962	1.72	1	0.21333	1.0038	-1.72
All Data	1.0151	1.5343	0.9996		0.9851	-1.5343

3.7.4 Statistic analysis of calibration results

In order to test the calibration result by means of a significance test, the following null hypothesis is tested.

Null hypothesis

The null hypothesis states that the analytical method, in this case the DOAS measurements of the NO_2 concentrations, is *not* subject to systematic error [Miller, 1993]. Thus there is no difference between the observed and known (in this case the calculated values) values, other than that which can be attributed to random variation [Miller, 1993]. Assuming that the null hypothesis is true, the probability that the differences between the observed and known values are really only a result of random errors can be calculated. Normally the null hypothesis is rejected if the probability of the differences occurring by chance is less than 1 in 20 (i.e. 0.05 or 5%) [Miller, 1993]. Thus, there is a 1 in 20 chance that the null hypothesis is accepted when it was really false.

DS procedure

In order to test the null hypothesis the following procedure from DS (Dansk Standard, ISO/DIS 13752) was used.

The original datasets (x_i, y_i) were transformed into (x_i', y_i') to obtain a linear relationship with constant variance by:

$$y_i' = y_i/x_i \,,\; xi' = 1/x_i$$

Then the coefficients of the linear regression function are computed:

$$b_1' = \frac{\sum_i x_i' y_i' - \left(\sum_i x_i' \sum_i y_i'\right)/N}{\sum_i (x_i')^2 - \left(\sum_i x_i'\right)^2/N}$$

$$b_0' = \bar{y}' - b_1' \bar{x}'$$

F test

Now 5 measurements pairs on both extremes of the measurement range (N_1, N_2) is chosen. Then the statistic F is calculated:

$$F = \frac{\left(\sum_{i=1}^{N_1}\left(y_i - \hat{y}_i'\right)^2\right) / (N_1 - 1)}{\left(\sum_{j=1}^{N_2}\left(y'_j - \hat{y}_j\right)^2\right) / (N_2 - 1)}$$

;where $\hat{y}_i = b_0 + b_1 x_i$.

Critical F value

The critical F value for a two-tailed test with i = number of degrees of freedom of the numerator = 5 and j = number of degrees of freedom of the denominator = 5 was found to be 7.146 [Table A.3. Miller, 1993].

Calculated F value

The calculated value of F using 5 measurements at each end of the measurement range was 1.265. Since this value is below the critical value of 7.146 the null hypothesis is accepted. That is, we can say with 95 % certainty that it is true. Thus, there is no difference between the observed (DOAS) values and the known (Calculated) values other than random errors.

3.7.5 Conclusions

From Table 3.4, Table 3.5 and Appendix D it can be concluded that:

The slope

– The slope (k) for the calibration curves deviates from 1 by less than 2 percent in all cases. Thus, it is far below the maximum acceptable value of 20 %. Also, the acceptable deviation from 1 of 20% is far too generous.

The correlation coefficients

– The correlation coefficients (R^2) are all better than 0.99. In fact the correlation coefficient for the ALL DATA calibration curve is 0.9996.

Variations

– The variations in the five individual measurement values are - except four - less than 3 times the mean of the standard deviation for all optical densities. These measurements however, are all included in the ALL DATA Figure.

Intercept

– The intercept value (b) should be within two times the mean of the recorded standard deviation at approximately 10 % of the measurement range level. In this case 10 % of the measurement range level is best represented by the measurement at the cell combination: L1 + L2 + L3 and dilution factor: 6.25 % NO_2, with a measured optical density of 50.36 ppb. The mean standard deviation at this optical density is 0.2. Thus a b-value for all data of 1.5 clearly exceeds two times the mean standard deviation.

Statistical result

The statistical check of the NO_2 calibration showed that the DOAS system performed well. The calculated F value of 1.265 is well below the critical F value of 7.146. Thus, the DOAS is capable of reproducing, that is measuring, the true values satisfactorily using the Lambert-beers law, with no systematic errors.

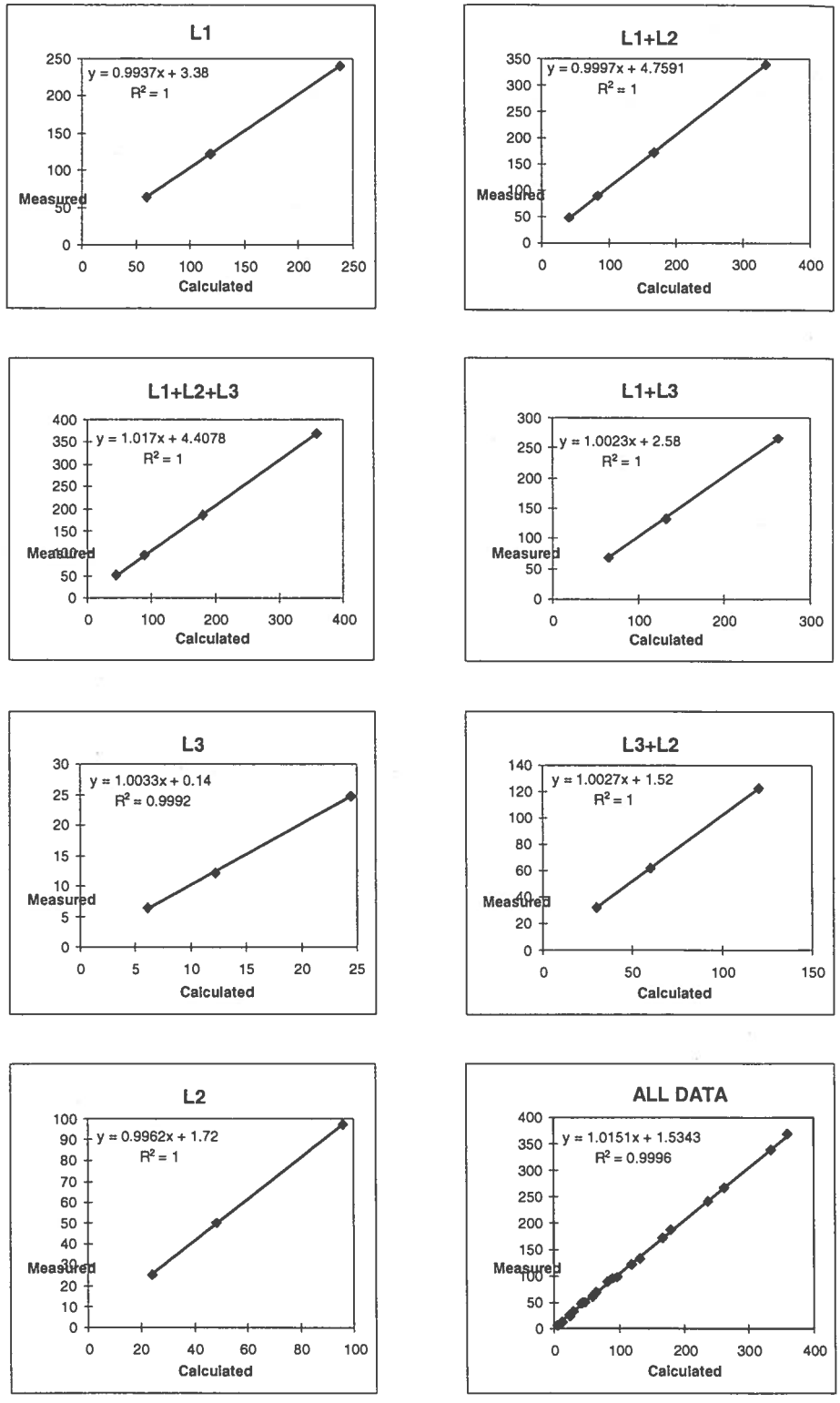

Figure 3.6 Calibration results for each combination of cell-lengths. The ALL DATA Figure gives the calibration curve for all the obtained calibration points.

4 DOAS measurements at Lille Valby, Denmark, 1998

4.1 Introduction

The DOAS technique is a very useful tool in investigating the tropospheric chemistry. Its ability to measure several tropospheric species almost simultaneously, and with great time resolution using only a single instrument, makes it a good candidate for use in monitoring networks.

DOAS in monitoring networks

Measurements of NO_2 and O_3 used in the Danish monitoring programmes are presently performed by chemiluminescence monitors and UV absorption monitors respectively. However, if the monitor measurements could be replaced by DOAS measurements only one instrument would be needed. In addition, other species could be measured as well.

Discrepancies between methods

However, before DOAS instruments can replace monitor measurements, results of the two measurement methods should be compared. If discrepancies between the methods are found, these should be investigated and understood. Prior to the installation of the DOAS technique it should be concluded that this will result in an improvement of the measurements or at least a *status quo*.

Lille Valby DOAS data, 1998

In the following sections, data from the Lille Valby DOAS is presented. It should be noted that the measurements were started on April 14.th 1998. Thus any reference to April, 1998, is a reference to the period 14-30/4 1998. Also note, that when "raw" measurement data are given in Appendix A.1-A.4, data for April is not shown. This is due to the lack of those data in the NERI database. The April DOAS data (as well as for the other months), that are referred to in the text, are taken directly from the OPSIS analyzer.

4.2 NO_2 measurements at Lille Valby, 1998

4.2.1 Introduction

Motivation

The NO_2 measurements were motivated by two purposes. First the NO_2 concentration is necessary in determining the NO_3 production rates that are crucial in exploring the NO_3 chemistry. Secondly it was the intention to compare DOAS NO_2 and chemiluminescence monitor NO_2 measurements in order to determine whether the DOAS technique could replace the monitor technique when measuring NO_2.

4.2.2 Measuring NO_2 by DOAS

Absorption peaks used by the OPSIS DOAS systems

The OPSIS DOAS system uses the absorption peak of NO_2 at 425 nm for its detection and measurement. [OPSIS, Sweden, 1995].

Absorption cross sections

The NO_2 absorption cross sections in the 400-440 nm region are in the order of 46.91 - 61.94 * 10^{-20} $cm^2molecule^{-1}$. The absorption cross section at 425 nm is 55.26 * 10^{-20} $cm^2molecule^{-1}$ [Atkinson *et al.*, 1997]. For comparison this is two orders of magnitude lower than the nitrate radical absorption cross sections at its distinct absorption peaks used in DOAS measurements.

Uncertainties in σNO_2

Some uncertainty in determining the NO_2 absorption cross sections is due to the equilibrium:

$$2\,NO_2 \rightleftarrows N_2O_4 \qquad (4.1)$$

;k_{eq} = 6.84 atm^{-1} at 298K [F.-Pitts & Pitts, 1986].

Due to this equilibrium the absorption by N_2O_4 needs to be corrected for. This is done by using data for the N_2O_4 absorption cross sections and k_{eq} for the dimerization reaction of NO_2 [Atkinson *et al.*, 1997]. Thus, uncertainties in the equilibrium constant, or incorrect compensations for the equilibrium will effect the NO_2 absorption cross section determination. Resent studies show that the recommended absorption cross sections can be taken to be independent of temperature [Atkinson *et al.*, 1997].

Interference and Spectral deconvolution

No corrections for interfering species in the OPSIS NO_2 wavelength region are made. Thus, the spectral deconvolution procedure for NO_2 is the standard procedure described in chapter 3.4.

4.2.3 DOAS NO_2 measurements at Lille Valby, 1998

Period of measurements

The measurement of NO_2 at Lille Valby was conducted April through September 1998. The DOAS instrument used is the one described in chapter 3. Meteorological data for the whole period are given in Appendix C.

Integration time

The integration time used in the NO_2 measurements was 1 minut at all times. OPSIS suggests a measurement time of 30 seconds, depending on the total time of a measurement cycle. As only 4 components are measured a measurement time of 1 minute gives a sufficient time resolution on the measurements.

4.2.4 Results

Measurement data

The "raw" DOAS NO_2 measurements from Lille Valby for the months May to September 1998 are given in Appendix A.1. From the figures it can be seen that at zero light level the concentration drops to a default value of -1000 and the standard deviation to a default value of 999. The main reason for the many sudden drops in light intensity is solar heating of the instrument as described in chapter 3.5. Thus, if the DOAS measurements are to be used for any practical purpose a sorting of the data is necessary.

4.2.3.1 Quality control

Quality control of the measurement data is performed as described in section 3.6.1

Negative standard deviations

As can be seen from the plots of light level versus standard deviation and concentration versus standard deviation for the NO_2 DOAS measurements April - september, 1998, Appendix B.1, some of the values have negative standard deviations. As mentioned in chapter 3.6.1 this is an indicator that the evaluation of the spectrum did not convert properly. Thus, these values should not be used. The amount of negative standard deviations seems to be growing from April to July. Thus, indicating that the evaluation of the spectre is not done properly.

Negative concentrations

Likewise some negative concentrations can be seen. Again the amount of negative concentrations is growing from April - July. Thus, indicating that some serious error in the evaluation of the spectres is most likely present [OPSIS, 1995].

30 minute values

In order to exclude the high negative concentrations as well as the measurements with negative standard deviations the data used in the NO_2 DOAS/monitor comparisons are 30 minute values. This means that the measurement values are averages over 30 minutes, computed directly by the OPSIS system. When this option is used the negative std.dev.'s and negative concentrations twice the standard deviation are excluded.

Light level ≥ 15 %

As the light level of a measurement decreases the standard deviation increases. Thus, low light level measurements should be excluded. The OPSIS manuals recommend that light levels below 5 % should never be used [OPSIS, 1996]. A value of 15 % for the minimum acceptable light level was chosen. Excluding measurements with a light level below 15 %also excludes the measurements with the highest standard deviations as can be seen from the figures of light versus standard deviation. Appendix A.1, besides the raw DOAS NO_2 data, gives concentration, light level and standard deviation for the NO_2 data when measurements with a corresponding light level below 15% are excluded.

Performed quality control

Using 30 minute measurement values and excluding measurements with a light level below 15 % should result in data of acceptable quality for further use. Not simply excluding data with standard deviations above a certain value ensures that measurements at high pollution levels, that have high standard deviations, are not erroneously excluded (See section 3.6.1.2). Thus, the following quality control criteria are used:

$$\text{std.dev.} \geq 0 \qquad C_{DOAS} \geq -(2*\text{std.dev.}) \qquad \text{Light level} \geq 15\ \%$$

Measurements are excluded if they do not comply with all of the above criteria.

Excluded measurements

Thus, measurements taken when the light intensity is below 15 % are excluded when using the measurements. For example in the com-

parison of chemiluminescence monitor and DOAS data described below. For the months April-September the number of measurements that are in this way excluded is given in the table below. The data used are the 1 minute measurement values and not 30 minute OPSIS averages. Also given are the average monthly concentrations calculated from the sorted data.

Table 4.1 DOAS NO_2 measurements at Lille Valby, 1998. The first column gives the total number of measurement data. Note that this is "raw" 1 minute measurements. Column two gives the number of measurements when measurements with a corresponding light level below 15 % are excluded. Numbers in parentheses are monthly average light levels. Column three gives the number of excluded measurements. The last column gives the monthly average NO_2 concentrations.

Lille Valby 1998 Month	NO_2 All Data (Average Light)	NO_2 L > 15% (Average Light)	Number of exclusions (in %)	Monthly Averages in ppb
April	5538 (33.6)	4739 (38.9)	799 (14)	6.24
May	9749 (32.3)	7986 (38.9)	1763 (18)	2.81
June	10240 (33.9)	9026 (38.1)	1214 (12)	2.94
July	10185 (33.9)	9877 (34.7)	308 (3)	2.47
August	10064 (32.9)	9766 (33.7)	298 (3)	2.38
September	9860 (33.1)	8386 (38.6)	1474 (15)	5.44

4.2.3.2 Monitor NO_2 measurements

The NOx monitor

The NOx monitor at Lille Valby, uses the chemiluminescence of NO_2 as a means of measuring NOx and NO.

Principle

When NO reacts with excess ozone it produces electronically excited nitrogen dioxide and oxygen. The electronically excited nitrogen dioxide then releases the excess energy in the form of light.

$$O_3 + NO \rightarrow NO_2 + O_2 \qquad (4.2)$$

$$NO_2^* \rightarrow NO_2 + h\nu \ (590 < \lambda < 3000nm) \qquad (4.3)$$

The intensity of the emitted light is proportional to the NO concentration. Thus, NO can be measured in this way.

NO_2 measurements

A NOx monitor measures both NO and the sum of NO + NO_2 = NOx. NOx is measured by reducing the NO_2 in a photolytical converter to NO before the chemiluminescence detection [Skov, *et al.*, 1997]. The monitor is let to cycle between two different air-inlets, one in which the air is injected directly and one in which the air passes through the NO_2 converter before it reaches the chemiluminescence detector . Thus, in this way the NO_2 concentration (C_{NO2}) can be measured as the difference:

$$C_{NO2} = C_{NOx} - C_{NO} \qquad (4.4)$$

However, other gaseous nitrogen species such as PAN, HNO_3, NH_3, N_2O_5, HONO and organic nitrates are also reduced to NO in the converter. Thus, the difference, $C_{NOx} - C_{NO}$, does not only represent C_{NO2}

but the sum of C_{NO2} and other reduced species. Thus, when the NO_2 monitor measures NOx, what it really measures is the sum of NOx and gNOz where:

$$gNOz = gNOy - NOx \quad (4.5)$$

For NO_2 therefore the selectivity of this method is poor.

4.2.4 Results

Monitor NO_2 at Lille Valby 1998

The figures below show the monitor NO_2 measurements from Lille Valby, April - June, 1998.

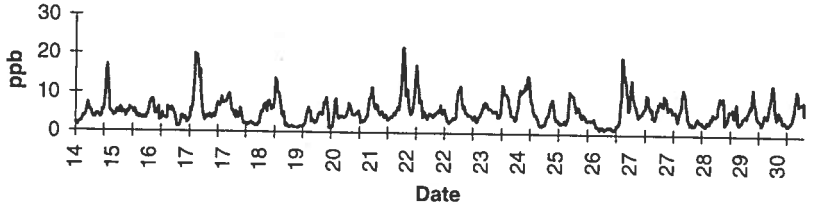

Figure 4.1 Monitor NO_2 at Lille Valby, April, 1998.

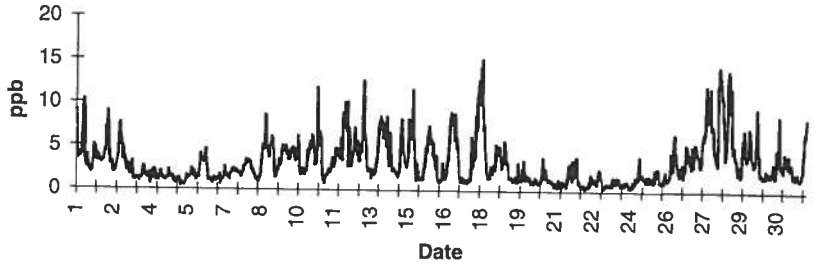

Figure 4.2 Monitor NO_2 at Lille Valby, May, 1998.

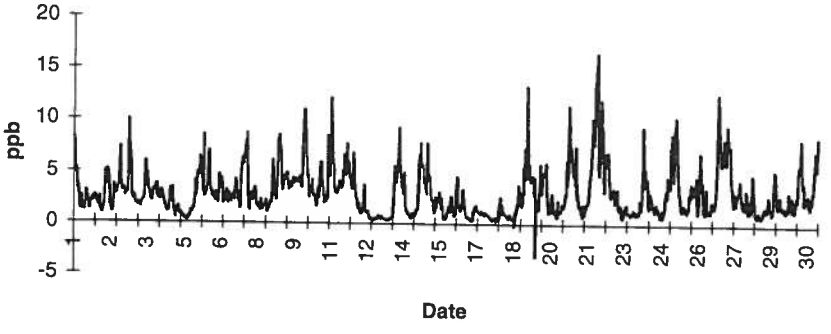

Figure 4.3 Monitor NO_2 at Lille Valby, June, 1998.

4.2.5 DOAS versus Monitor measurements

DOAS data

The DOAS data used for the DOAS/monitor comparisons are 30 minute values as described above. Measurements with light levels below 15 % are excluded. This ensures the quality of the data.

Monitor data

The monitor NO_2 measurements are averages over 30 minutes. Thus, the DOAS and monitor data have the same time resolution, when used. Table 4.2 gives the monthly average concentrations for the two measurement methods.

Table 4.2 Monthly average NO_2 concentrations for DOAS and monitor measurements at Lille Valby, 1998. Numbers in parentheses are the number of measurements used. Also given are the monthly average light levels for the DOAS measurements when light levels below 15 % are excluded.

Month	DOAS NO_2 - monthly averages (ppb)	DOAS NO_2 Average light level (%)	Monitor NO_2 - monthly averages (ppb)
April	6.23 (694)	38.6	5.6 (768)
May	2.81 (1158)	38.7	3.2 (1449)
June	2.95 (1303)	37.9	3.0 (1401)

Monitor versus DOAS data

Because the chemiluminescence monitor is expected to overestimate the NO_2 concentrations by the factor gNOz, it would be expected that the monitor NO_2 concentrations would be higher than the DOAS NO_2 concentrations. However, it can be seen that for the month of April the average DOAS concentration is appreciably higher than the monitor average concentration. This is reflected in the negative values of gNOz for April, Figure 4.4.

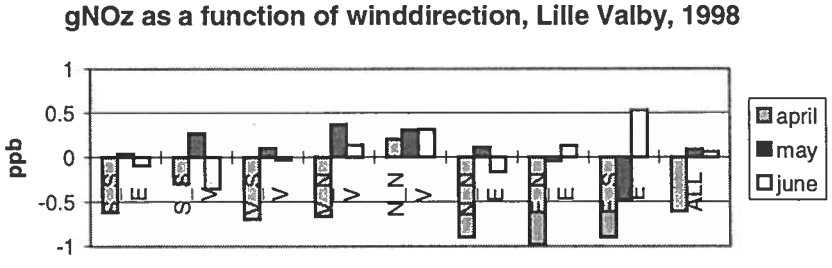

Figure 4.4 The negative gNOz values are due to the fact that the average monthly DOAS NO_2 measurements for April are higher than the corresponding monthly average monitor NO_2 measurements.

For the months of May and June the average monitor ozone levels are just above the DOAS levels as expected. Thus, the negative gNOz values may be related to meteorological phenomena such as temperature or humidity as discussed below.

Exclusion of bad data using light level

It should be noted that the above average monthly DOAS NO_2 concentrations and light levels, computed from OPSIS 30 minute averages are almost the same as those calculated directly from the 1 minute measurement values when light levels below 15 % are also excluded, Table 4.1. This should not be interpreted as the two data sets being equal. But high negative concentration values and values with high standard deviations that are excluded in the 30 minute average OPSIS data mostly coincide with very low light levels. Thus, it shows that the light level is an important parameter in the quality analysis of DOAS data.

As mentioned above, the NO_2 monitor is suspected to be in error by the amount of "gNOz". Thus, in order to analyze the correlation between the monitor and DOAS measurements it is natural to perform the analysis on the basis of parameters that are supposedly related to gNOz. Simply performing the analysis by looking at the correlation for different intervals of gNOz would not reveal anything new as the calculated gNOz values are simply the actual difference in measurement between the two methods. Parameters that can be used for analysis are ozone concentration levels, PCA (Photo Chemical Age) and the wind direction as described below. The value of gNOz itself can be found from the measurement data. How this is done is described in the following.

4.2.5.1 gNOz calculations

As mentioned the NOx monitor measures 2 things:

1. NO
2. NOx = NO + NO_2

Thus, $NO_{2\text{-monitor}}$ can be found as the difference

$$NO_{2\text{-monitor}} = NOx - NO$$

However, as mentioned when NO_2 is reduced to NO other gaseous nitrogen species are reduced as well. Thus, what is really determined in the monitor NOx measurements is:

$$\begin{aligned} NO_{x\text{-monitor}} &= NO_2 + NO + HONO + PAN + N_2O_5 + HNO_3 \ldots \\ &= NOx + gNOz \end{aligned}$$

Thus:

$$\begin{aligned} NO_{2\text{-monitor}} &= NOx\_monitor - NO \\ &= NOx + gNOz - NO = NO_2 + gNOz \end{aligned}$$

Therefore the monitor NO_2 concentrations are in error by the amount of gNOz, or equivalently the amount of reduced gaseous nitrogen species other than NO_2. As the DOAS measures NO_2 with great specificity, the magnitude of gNOz can be estimated from the equation:

$$NO_{2\text{-monitor}} - NO_{2\text{-DOAS}} \approx gNOz \qquad (4.6)$$

As gNOz is a measure of the amount of oxidized nitrous species in an airmass it would be expected that the mixing ratio of gNOz would increase with the age of the airmass. Also it would be expected that the value of gNOz would increase with increased photochemistry. Thus, it would be expected that the gNOz values would increase during warm and sunny months.

The monthly average concentrations of gNOz along with monthly maximum and minimum values are given in Table 4.3.

Table 4.3 Monthly average concentrations of gNOz along with monthly maximum and minimum values. The monthly average temperatures are calculated from Risø RIMI data (RIMI = Risoe Integrated Environmental Project).

Month 1998	Monthly averages	max. value	min. value	Monthly average temperature (°C)
April	-0.65	3.45	-9.26	6.93
May	0.07	3.77	-6.34	12.3
June	-0.08	2.61	-6.18	14.4

From Table 4.3 it is seen that there is no clear trend in the values of gNOz for the months April - June. Only the minimum values increase over the whole period. April has the lowest monthly average and although the monthly average increases in May to a positive value it decreases again in June to just below zero. The average monthly temperature increases during the course of the months as would be expected.

4.2.5.2 Correlation of monitor/ DOAS NO_2 versus O_3 concentration

Granby found that the gNOz portion of gNOy increased from 21 % at 20-30 ppb of ozone, to 67 % at 50-60 ppb of ozone [Granby, K., 1997]. Thus, an increasing discrepancy of the two measurement techniques with increasing ozone concentration would be expected as:

$$NO_{2\text{-monitor}} = NO_2 + gNOz$$
$$NO_{2\ DOAS} = NO_2$$

Thus, the correlation, R^2, between the two measurement methods were analyzed for different ozone concentration intervals of 0-10 ppb, 10-20 ppb, 20-30 ppb, 30-40 ppb and >40 ppb. Table 4.4 gives the correlation coefficients of the methods for the various months at different ozone concentration intervals. The comparison is based on half hour concentration averages for both techniques.

Table 4.4 Correlation coefficients, R^2, between DOAS and monitor NO_2 measurements for different ozone concentration intervals.

month	0-10 ppb	10-20 ppb	20-30 ppb	30-40 ppb	>40 ppb
April	0.990322	0.969839	0.931493	0.851157	0.84799
May	0.89916	0.824354	0.961427	0.900393	0.374267
June	0.876417	0.91018	0.884189	0.826304	0.752104

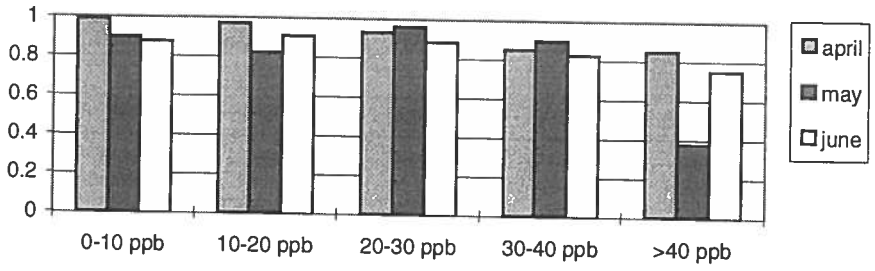

Figure 4.5 Correlation coefficients, R^2, between DOAS and monitor NO_2 measurements for different ozone concentration intervals, Lille Valby, 1998.

The greatest discrepancies between the methods are seen at the high ozone concentration levels. Likewise the best correspondance between the methods is seen at the lowest ozone concentration intervals. For April there is a continuous decrease in the correlation coefficient going from low to high ozone concentration levels.

4.2.5.3 Correlation of monitor/ DOAS NO_2 versus winddirection

As the quality of the airmasses that reaches Lille Valby depends strongly on the wind direction (and wind speed) a variation in the correlations between the different wind directions could be suspected.

Point measurements

As the monitor NO_2 values are point measurements and the DOAS NO_2 values are average concentrations over the whole path length, that in itself, might cause some discrepancy between the methods. Thus, the best correlation between the methods would be suspected for wind directions parallel to the DOAS path. The DOAS measurements would then resemble a point measurement the most. The DOAS path runs in an East/West direction with a slight South-West/North-Eastern tilt. Thus, wind directions parallel to the DOAS path are ENE and VSV. As can be seen from Figure. 4.6 below the correlation coefficient for the ESE wind direction is good, however, the VSV direction has the worst correlation coefficients. The measurements for wind directions diagonal to the measurement should be correspondingly bad. That is for NNV and SSE. This is not the case.

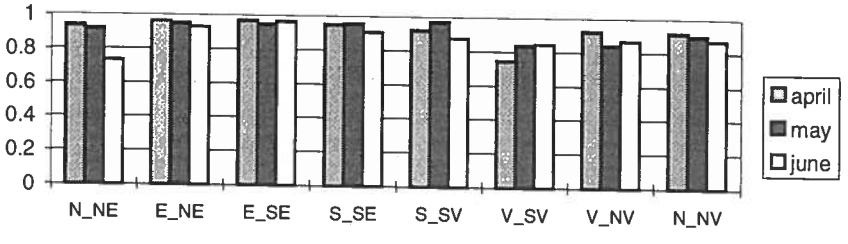

Figure 4.6 Correlation coefficients, R^2, for the DOAS/monitor NO_2 measurements at different winddirections, Lille Valby, 1998.

Expected best correlation

On the basis of the kind of airmasses that reaches Lille Valby the best correlation between monitor and DOAS data would be expected for "new" air masses where the nitrogen species have not fully been

oxidized and therefore the amount of gNOz should not be too high. Thus, the best correlations would be expected for air masses from an Eastern (Copenhagen) direction or from the S_SV (Roskilde and the highway). Combining the expected effect of comparing DOAS and monitor measurements and the expected effect of the airmasses reaching Lille Valby the best correlation should be found for the E_NE winddirection.

Best correlations

The best correlations are seen for winds from Eastern or Southern directions. The worst correlations are seen for winds from a Western direction or Northern, especially from the West-SouthWest. However, the E_NE direction does not show the best correlation, which is actually found in the E_SE direction.

4.2.5.4 Correlation versus PCA

The Photochemical Age (PCA) of an airmass is defined as:

$$PCA = 1 - (NOx/gNOy) \quad (4.7)$$

where

$$gNOy = NOx + gNOz \; ; \; NOx = NO_2 + NO \quad (4.8)$$

In young airmasses the ratio of NOx is close to that of gNOy and PCA is therefore close to zero. In old airmasses however, some of the NOx have been converted to gNOz. Thus, in this this case the value of PCA has increased [Skov, *et al.*, 1997].

PCA at Lille Valby

The monitor at Lille Valby measures

$$NOx\_monitor = NOx + gNOz = gNOy$$

Thus, gNOy in the equation for PCA can be substituted by NOx_monitor. Now to find

$$NOx = gNOy - gNOz = NO_2 + NO$$

we use again that

$$gNOy = NOx + gNOz$$

Now

$$\begin{aligned} gNOz &= gNOy - NOx \\ &= NOx\_monitor - NO\_monitor - NO2\_DOAS \\ &= NO2\_monitor - NO2\_DOAS \end{aligned}$$

Thus,

$$\begin{aligned} NOx &= gNOy - gNOz \\ &= NOx\_monitor - (NO2\_monitor - NO2\_DOAS) \end{aligned}$$

So we can find PCA = 1 - (NOx/gNOy) as

$$\begin{aligned} PCA &= 1 - (NOx / gNOy) \\ &= 1 - ((gNOy - gNOz)/gNOy) \\ &= 1 - ((NOx\_monitor - (NO2\_monitor - NO2\_DOAS)) \\ &\quad / NOx\_monitor) \end{aligned}$$

4.2.5.5 Results

The results of plotting NO2_DOAS against NO2_monitor gives the following correlation coefficients for different intervals of PCA.

Table 4.5 Correlation coefficients, R^2, between monitor and DOAS NO_2 data, for different intervals of PCA, PCA > 0.

Month	0 - 0.1	0.1 - 0.2	0.2 - 0.3	0.3 - 0.4	0.4 - 0.5	> 0.5
April	0.9864	0.9799	0.9702	0.9282	0.8921	0.881
May	0.994	0.9891	0.9784	0.956	0.8418	0.5067
June	0.9945	0.9914	0.9796	0.9306	0.8379	0.5331

At negative values of gNOz, when NO2_DOAS is greater than NO2_monitor, the PCA becomes negative. The correlation coefficients for these negative values for PCA are given below.

Table 4.6 Correlation coefficients, R^2, between monitor and DOAS NO_2 data, for different intervals of PCA, PCA < 0.

Month	< -0.5	-0.5 - (-0.4)	-0.4 -(-0.3)	-0.3-(-0.2)	-0.2 - (-0.1)	-0.1- 0
April	0.8527	0.998	0.9986	0.9948	0.9902	0.9948
May	0.9895	0.9984	0.9975	0.9944	0.988	0.9957
June	0.9172	0.9956	0.9976	0.9972	0.9963	0.9964

Figure 4.7 below shows the correlation coefficients for all the PCA intervals, negative and positive.

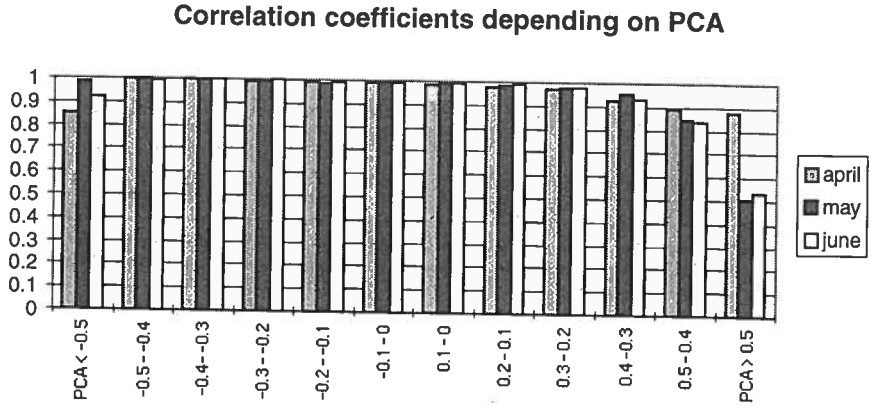

Figure 4.7 The correlation coefficients, R^2, for the DOAS and Monitor NO_2 measurements related to photochemical age, PCA, of the airmasses.

4.2.6 Discussion

Correlation coefficients for positive PCA values

The correlation coefficients for positive values of PCA follows a pattern that would be expected from a straightforward analysis. The PCA is a measure of the photochemical age of the airmass and therefore it would be expected that the amount of gNOz in the airmass would correlate to some extent with the PCA. Thus, it would be ex-

pected that the correlation of the measurement methods would decrease with increasing PCA and thereby increasing gNOz as:

$$NO_{2\text{-monitor}} - NO_{2\text{-DOAS}} \approx gNOz$$

Negative values of PCA

However, in some cases the calculated PCA is negative. This occurs for negative values of gNOz when, contrary to the expected, the DOAS NO_2 concentrations are higher than the Monitor NO_2 concentration.

The "meaning" of negative PCA values

Although it is easy to see (from the expression of PCA, and the data), that the negative values of PCA occur for times when the NO2_DOAS concentrations are greater than the NO2_monitor concentrations, the meaning of these negative values is not correspondingly clear.

Correlation coefficients for negative PCA values

Also the correlation for the negative PCA values is surprisingly good for all intervals. There seems to be no increasing or decreasing trend in either positive or negative directions.

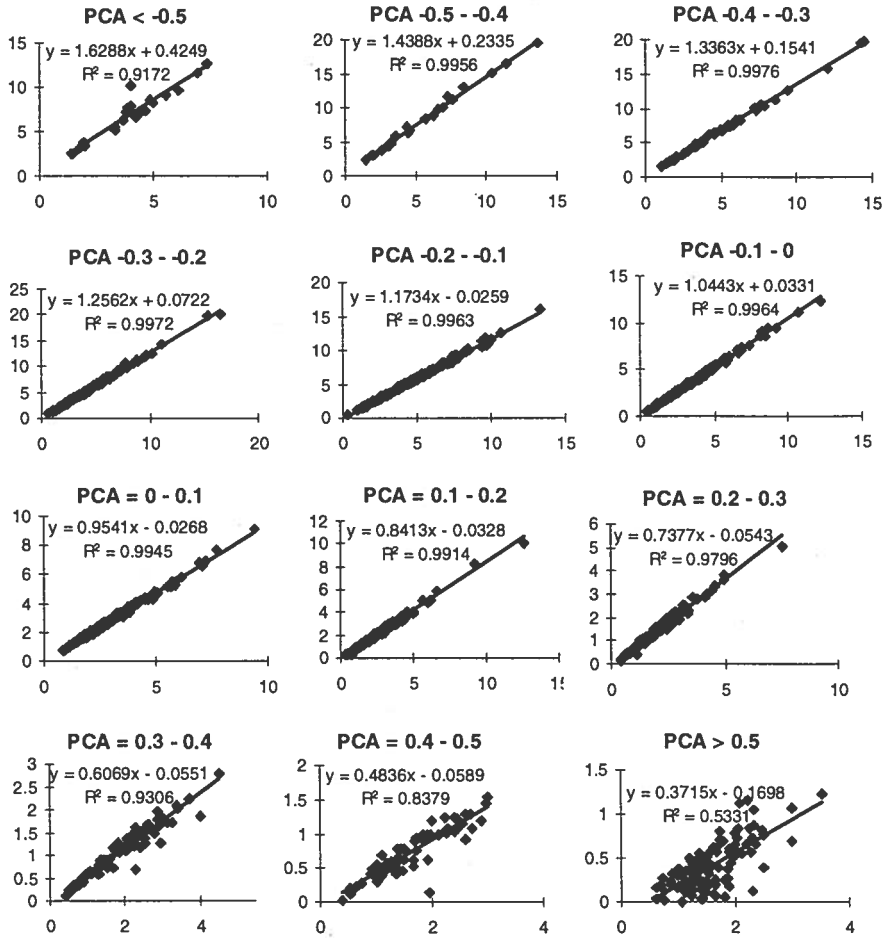

Figure 4.8 Correlation and Correlation coefficients, R^2, for DOAS/monitor NO_2 measurements at different intervals of Photo Chemical Age, PCA, June, 1998. The x-axes corresponds to DOAS NO_2 measurements and the y-axes to monitor NO_2 measurements.

Decreasing slopes

Another curiosity is that the slope of the correlation coefficients tends to decrease slowly but steadily on going from high negative PCA

values to high positive PCA values. This is the case for all months, April, May and June. Figure 4.8 above, shows this tendency for June, 1998.

Thus, 4 observations needs to be explained:

1. The interpretation of negative PCA values
2. The constant high correlation coefficients for negative PCA values
3. The behaviour, as was expected, for positive PCA values
4. The decrease in slope on going from negative PCA values to positive PCA values.

Possible explanations

Apparently there are several ways of explanation for these curiosities. One being that the negative PCA values and the decreasing slopes are indicators of some systematic error in either of the measurement methods. Another being that the negative PCA values and the decreasing slopes are indications of some real chemical phenomena. Finally one could ask if it has any meaning to analyze the dependency of the correlation coefficients upon PCA at all.

Correlation coefficients and PCA

The last question bounds in the fact that the PCA depends on both the relative humidity (from the monitor NO_2 measurements) and temperature (DOAS measurements), corrections that are not made in this calculation. Thus, the calculated PCA should not be taken as a real measure for the photochemical age of the airmass, but as a means of studying the correlation coefficients for the methods.

Effect of monitor error on measurements

Quenching of the NO_2 monitor at high absolute humidities will result in an underestimate of the NO_2 concentrations. Thus, the measured NO_2 would be lower than the actual concentration. This could explain the negative gNOz values and thus, the negative PCA values, as these occur for DOAS NO_2 concentrations higher than the corresponding monitor NO_2. However, this would not explain the high correlations for negative PCA values.

Effect of DOAS error on measurements

A possible source of error in the DOAS measurements, that would explain the episodes of higher NO_2 DOAS than monitor, could be the lack of using data-logger data in connection with the measurements, as no temperature corrections are made. Instead all measurements are treated as though they were made at 273 K. Clearly this is not satisfactory for months like May and June with average temperatures around 10 - 15 °C. The temperature dependence lies in the conversion factors for each gas, used when data measured in $\mu g/m^3$ are converted into values of ppb. An example of the error introduced in this way for DOAS NO_2 measurements at 15 °C is given in chapter 3.6. This kind of error would result in a 5 % underestimate of the DOAS values. Thus, this can not explain the occurrence of DOAS NO_2 values greater than the monitor values.

Effect of lacking temperature corrections

However, the lack of temperature corrections of the DOAS measurements does have the effect of underestimating the actual concentrations at high temperatures and of overestimating the concentrations at low temperatures. This effect grows with the difference in actual temperature from 273 K.

Effect of light level

At low light levels the concentrations are highly inaccurate and could be overestimated. However, light levels below 15 % have been excluded and the negative values of PCA does not coincide with low light levels.

PCA related to winddirection

If PCA is related to winddirection it is seen from Figure 4.9 below that the only winddirection for which there are no ocurrences of negative PCA values throughout the three months is the North-Northwest direction. That is for winds from the North and diagonal to the DOAS path. Thus, if the negative PCA values indicate some measurement error then this should depend on winddirection and be minimized for winds from the North-Northwest. This would mean that the wind would come from the Roskilde Fjord area. Thus, to the extent that the absolute humidity is affected by the winddirection this would not support the theory of monitor NO_2 error due to high absolute humidity.

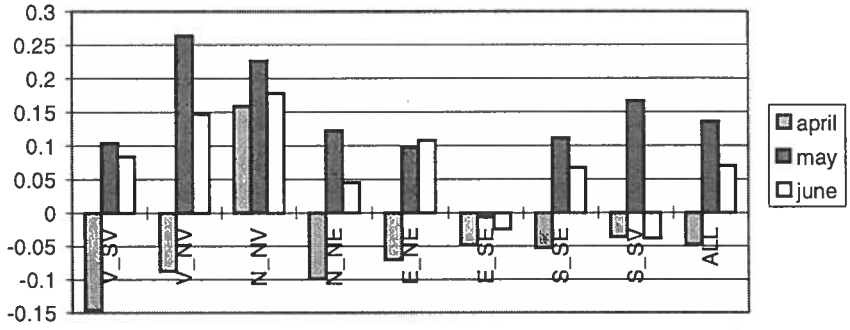

Figure 4.9 Monthly averages of PCA for different winddirections at Lille Valby, 1998.

Large values of PCA

It would be expected that the largest values of PCA should be found for the South-Southeastern direction during transport episodes of photochemical air pollution from that direction. However, the largest values of PCA are found in the North-Northwest, West-Northwest and South-Southwest directions. The spring and summer of 1998 was very cold and rainy. Thus there were no pronounced photochemical transport episodes from the South-Southeast. The bad summer is also reflected in the relatively low values of PCA most of which are below 0.2.

Comparison with other studies

Ziv and Iakovleva investigated the relationship between monitor and DOAS NO_2 measurements at the HCØ (Copenhagen) monitoring station. They found a yearly negative mean bias error, meaning that the monitor data is greater than the DOAS data, for the years 1994 - 1996 [Ziv *et al.*, 1998]. The largest negative biases are generally found in the spring and summer months. However, months of positive bias (meaning that the DOAS data is greater than the monitor data) do

occur. But only during November - March of all years [Ziv *et al.*, 1998].

Temperature dependence

This suggests that the observed discrepancies between the methods may be temperature dependent. Ziv *et al.* found that the difference (monitor - DOAS) in ppb, between the methods, were positive for temperatures above zero degrees celcius and negative for temperatures below zero[Ziv *et al.*, 1998]. This means that at temperatures above zero the monitor concentrations were higher than the DOAS data and the opposite for measurements below zero degrees celcius. From Table 4.2 it is seen that the monitor measurements were also higher than the DOAS measurements in this study. For April, however, the DOAS measurements were higher than the monitor measurements.

4.2.7 Conclusions

The DOAS NO_2 measurements

The growing amount of negative standard deviations and negative concentrations for the months April - July indicates serious evaluation errors. Thus, the level of quality control and maintenance of the Lille Valby DOAS should be highly increased. The procedures for quality control and maintenance described in chapter 3.6 and the OPSIS quality assurance manual should be followed.

Monitor/DOAS correlation

- The correlations for the two measurement methods when dividing the measurements according to ozone concentration intervals behave as expected. Thus, the correlation decreases with increasing ozone concentration.
- The behaviour of the correlation for the two measurement methods when dividing the measurements according to different winddirections can not be explained on the basis of the effects considered here.
- The correlations for the two measurement methods when dividing the measurements according to different values of PCA can not easily be explained. For positive values of PCA the correlation decreases with increasing PCA as expected. However, for negative PCA values the surprisingly good correlations for all values of PCA can not be explained. Likewise the systematic decreasing trend of the slopes of the linear regression lines can not be explained.
- The interpretation of negative gNOz values is uncertain.

Discrepancies between the methods

The analysis does reveal discrepancies between the two measurement methods. The dependence of correlation's between the DOAS and monitor measurement methods upon ozone concentration levels supports the theory that discrepancies lies partly in the amount of gaseous nitrogen species other than NO_2 that are reduced in the NO_2 monitor. This is also supported by the fact that the monitor values generally are higher than the corresponding DOAS measurements, except for April, 1998. The study of Ziv and Iakovleva shows that the discrepancy between the methods is dependent on temperature. This should be further investigated.

DOAS replacing NO_2 monitors

DOAS measurements could effectively replace monitor NO_2 measurements if the data quality control and instrument maintenance is kept at a high level and temperature and pressure corrections should be performed.

4.3 O_3 measurements at Lille Valby, 1998

4.3.1 Introduction

Motivation

First, the O_3 concentration is necessary in determining the nitrate radical production rates that are crucial in exploring the nitrate radical chemistry. Secondly, it was the intention to compare DOAS and monitor measurements in order to determine whether the DOAS technique could replace the monitor technique when measuring O_3.

4.3.2 Measuring O_3 by DOAS

Choice of wavelength region for DOAS O_3 measurements

When choosing the optimal wavelength region for DOAS measurements several parameters need to be taken into account. The magnitude of the absorption cross sections as well as interference from other species and atmospheric attenuation (light scattering by gases and particles and light absorption by gases and particles [F.-Pitts & Pitts, 1986]) needs to be evaluated in the candidate wavelength region. In the case of ozone measurements, the UV region 200 - 330 nm is of interest.

Interferences in the 200 - 270 nm region

The strongest absorption of the ozone molecule in the UV 200 - 330 nm region is around 256 nm. Here the absorption cross sections are in the order of $1.1 * 10^{-18}$ $cm^2molecule^{-1}$[Atkinson *et al.*, 1997]. However, in this region the atmospheric attenuation is also strongest. This together with the fact that the efficiency of the light transmittance decreases with shorter UV wavelengths and the strong oxygen absorption below 270 nm makes this region unfit for DOAS measurements [Axelsson, 1990].

Interferences in the 305 - 330 nm region

NO_2 and SO_2 may interfere with ozone measurements in the 300-360 nm region (the Huggins bands). SO_2 has a strong differential absorption around 300 nm and up to 325 nm where it is strongly reduced. However, NO_2 absorbs increasingly in this region. Traditionally the wavelength region around 328 nm was used for the detection of ozone by DOAS. This was a compromise between the increasing NO_2 absorption, the decreasing ozone absorption with wavelength in this region and the fade off of SO_2 absorption at 325 nm [Axelsson, 1990].

The 270 - 305 nm region

However, ozone has a strong differential absorption peak at 283 nm suitable for DOAS measurements. At this wavelength the differential absorption cross section is $10.7 * 10^{-20}$ $cm^2molecule^{-1}$. In this region the major interference stems from SO_2 absorption [Axelsson, 1990].

Spectral deconvolution

Fortunately, the SO_2 absorption is weak and can be handled by including a SO_2 reference spectrum in the deconvolution routine for ozone [Axelsson et. al, 1990]. The same procedure that is used in handling water interference, when measuring nitrate radicals by DOAS.

the sample forms a ratio I/I_0. This ratio is related through the Beer-Lambert law to the ozone concentration.

$$C_{O_3} = -\frac{10^9}{\alpha \cdot \ell} \cdot \frac{T}{273°K} \cdot \frac{29.92 inHg}{P} \cdot \ell n \frac{I}{I_0} \qquad (4.9)$$

where:

I	= Intensity of light passed through the sample
I_0	= Intensity of light through sample free of ozone
α	= absorption coefficient in $cm^2 molecule^{-1}$
ℓ	= path length in cm
C_{O3}	= concentration of ozone in ppb
P	= pressure in inches of mercury
T	= temperature in Kelvin

Temperature and pressure dependence

As can be seen from the equation the measurements need to be corrected for temperature and pressure as they influence the density of the sample. A change in density is reflected in the number of ozone molecules in the absorption tube, thereby changing the amount of light removed from the light beam by the absorbing gas. These corrections are done automatically [Advanced Pollution Instrumentation, ozone analyzer manual].

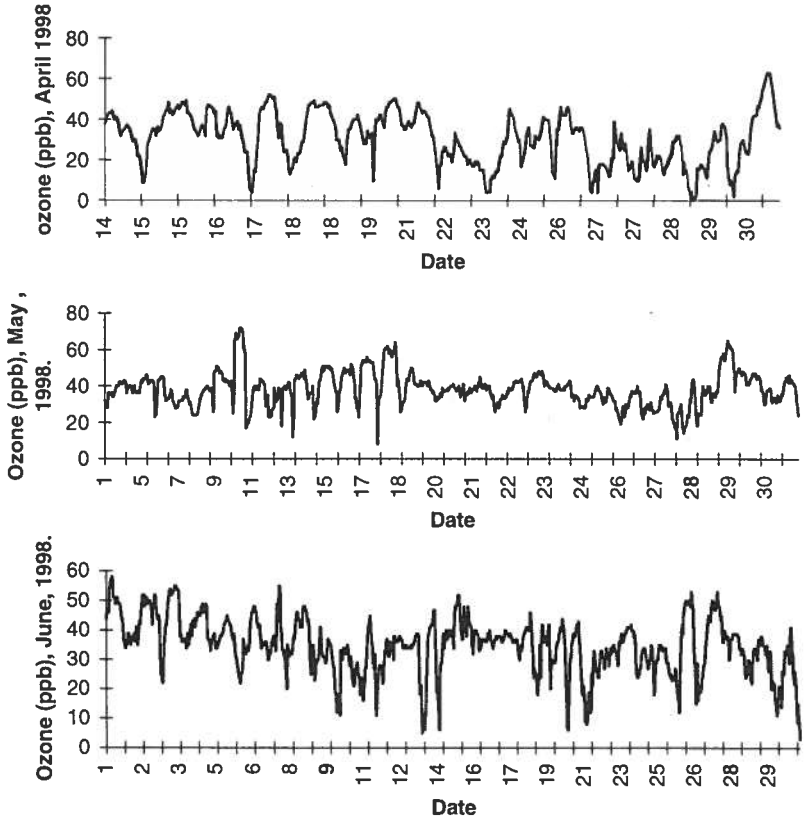

Figure 4.10 Monitor ozone concentration levels, in ppb, at Lille Valby, April - June, 1998.

Interference from other gaseous species

The method of measuring ozone by UV absorption is subject to interference from many sources. The Lille Valby monitor successfully eliminates interference from SO_2, NO_2, NO, H_2O and meta-xylene (meta-xylene was most likely chosen because it is used as a measure

OPSIS system absorption region

In the OPSIS AR 500 system the wavelength region used for detecting and measuring ozone is the 265.7 - 304.4 nm region [A. Virkkula, 1996]. Thus, this covers the region around 283 nm recommended for ozone measurements by Axelsson *et al.*

4.3.3 The measurement campaign

Period of measurements

The measurement of O_3 at Lille Valby was conducted April through September 1998. The DOAS instrument used is the one described in chapter 3. Meteorological data for the whole period are given in Appendix C.

Measurement time

The integration time used in the O_3 measurements was 1 minute at all times.

4.3.3.1.1 Results

Measurement data

DOAS data from the DMU database, concentration and light level, for the months May to September 1998 are given in Appendix A.2. Here, measurement data with a light level below 5 % are excluded. For comparison "raw" data for the month of May, 1998, including all measurements are also presented. From this figure it can be seen that at zero light level the concentration drops to a default value of -1000 (and the standard deviation to a default value of 999. The main reason for these many sudden drops in light intensity is solar heating of the instrument as described in chapter 3.5. If the DOAS ozone measurements are to be used for any practical purpose a sorting of the data, other than the 5 % minimum light level, is necessary. The quality control criteria for the DOAS data used in the DOAS/monitor data comparison is given in section 4.3.4.

4.3.3.2 Monitor O_3 measurements

The ozone monitor

The ozone monitor at Lille Valby is an M400A Ozone Analyzer. The absorption coefficients of ozone in the UV region are large enough for ozone to absorb strongly in this region. In particular the monitor uses the UV absorption of ozone at 254 nm for its detection and measurement [Advanced Pollution Instrumentation, ozone analyzer manual].

Principle of operation

The method is based on the Beer-Lambert equation [Advanced Pollution Instrumentation, ozone analyzer manual]. The monitor is equipped with a mercury lamp, that predominantly emits light in the 254 nm region. The light from the lamp shines down a hollow quarts tube that is alternately filled with sample gas, then filled with gas scrubbed to remove ozone. In this way, a measurement cycle is completed every 6 seconds. During the first 2 seconds the sample tube is flushed with sample gas, then in the next second the UV light intensity is measured and I is obtained. The sample valve is then switched to admit scrubbed (ozone free) sample gas for 2 seconds followed by a 1 second measurement of the UV light intensity to obtain I_0. The measurement of I_0 every 6 seconds minimizes instrument drift due to changing intensity of the lamp due to ageing and dirt. Thus, the ratio of the intensity of light passing through the scrubbed gas to that of

for interference in monitor SO_2 measurements and correcting for meta-xylene interference may in practice correct for other aromatics as well). However, other volatile aromatic hydrocarbons may still interfere with the measurements [Advanced Pollution Instrumentation, ozone analyzer manual].

4.3.3.2.1 Results

The figures above show the monitor ozone concentration levels at Lille Valby, April - June, 1998. The monthly averages are given in Table 4.7.

4.3.4 DOAS versus Monitor measurements

DOAS data and quality control

The DOAS data used for the comparison of measurement methods are 30 minute OPSIS averages. As for NO_2, measurements with a corresponding light level below 15 % are excluded. The same discussion as given in section 4.2.3.1 on the reasons for this applies equally to the case of ozone measurements. Thus, the following quality control criteria are used:

$$\text{std.dev.} \geq 0 \qquad C_{DOAS} \geq -(2*\text{std.dev.}) \qquad \text{Light level} \geq 15\ \%$$

Measurements are excluded if they do not comply with all criteria. Plots of light level versus standard deviation and concentration versus standard deviation for the O_3 DOAS measurements April - September 1998, are given in Appendix B.2.

Monitor data

The monitor data used are 30 minute average values. For ease of calculation, the monitor ozone concentrations used are integer values. This is only acceptable because the purpose of this comparison of methods was only to look at the level of correlation between the methods.

Monthly averages

Table 4.7 The table shows the monthly average ozone concentrations at Lille Valby, 1998, as measured by the DOAS and monitor technique.

Month	DOAS O_3 - monthly averages (ppb)	DOAS O_3 Average light level (%)	Monitor O_3 - monthly averages (ppb)
April	30.4	30.2	30.7
May	35.97	30.3	38.4
June	32.2	28.0	35.0

The monitor monthly average ozone concentrations are higher than the DOAS ozone concentrations for all months. This is most pronounced for the months of May and June.

Interferences in monitor ozone measurements

As mentioned the ozone monitor eliminates interference from several compounds such as meta-xylene. However, other volatile aromatic hydrocarbons may interfere with the measurements due to their absorption in the UV region of the spectrum. Especially polycyclic aromatic hydrocarbons have highly structured absorption bands in

the UV region [F-Pitts & Pitts, 1986]. The presence of volatile aromatic hydrocarbons at the measurement site would influence on the monitor ozone measurements with a positive bias. Thus, in correspondance with the observed, resulting in higher ozone concentrations for the monitor technique.

4.3.4.1 Correlation between monitor and DOAS ozone

The correlation between the methods are shown below. Also shown are linear regression lines.

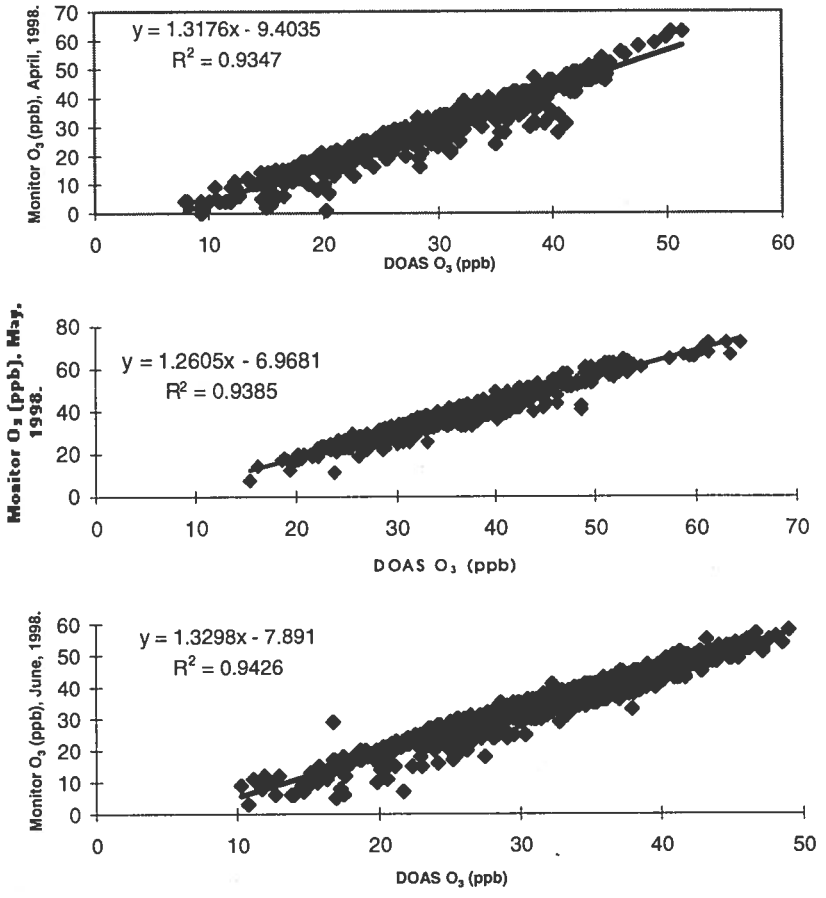

Figure 4.11 Monitor versus DOAS ozone measurements at Lille Valby, April-June, 1998.

Correlation between the methods

The correlation coefficients, R^2, between the methods improves slightly from April to June. However, throughout all months the linear regression lines crosses the x-axis, and thus the DOAS NO_2, not at the zero point but at 6 - 8 ppb. This suggests the existence of a zero point offset in the DOAS instrument. Performing a new reference calibration could show if this was the case.

Comparison with other studies

Virkkula also carried out comparisons between DOAS and monitor ozone data [Virkkula, A., 1996]. The DOAS system used was an OPSIS AR 500 system, similar to that used at Lille Valby. The path length of the DOAS system was 1021 m. and 28 m above the surface. The monitor used was a Dasibi 1008-AH ozone monitor. When plotting DOAS ozone concentrations against monitor ozone concentra-

tions an offset similar to that found in the Lille Valby comparison was found. Thus, the crossing of the regression line and the DOAS axis (in this case the y-axis) was at approximately 5 ppb. This is very similar to the offset found upon inspection of Figure 4.11 of the Lille Valby comparison. Virkkula mentiones zero-point calibration errors as the most likely reason for the large offset [Virkkula, A., 1996].

4.3.4.2 Analysis of discrepancies between the methods

Inspection of the data in tabular form suggests a relationship between the difference in ozone concentration, between the two methods, and the ozone concentration level. Thus, the difference between the methods are plotted as a function of DOAS ozone concentrations. The results are seen in the figures below.

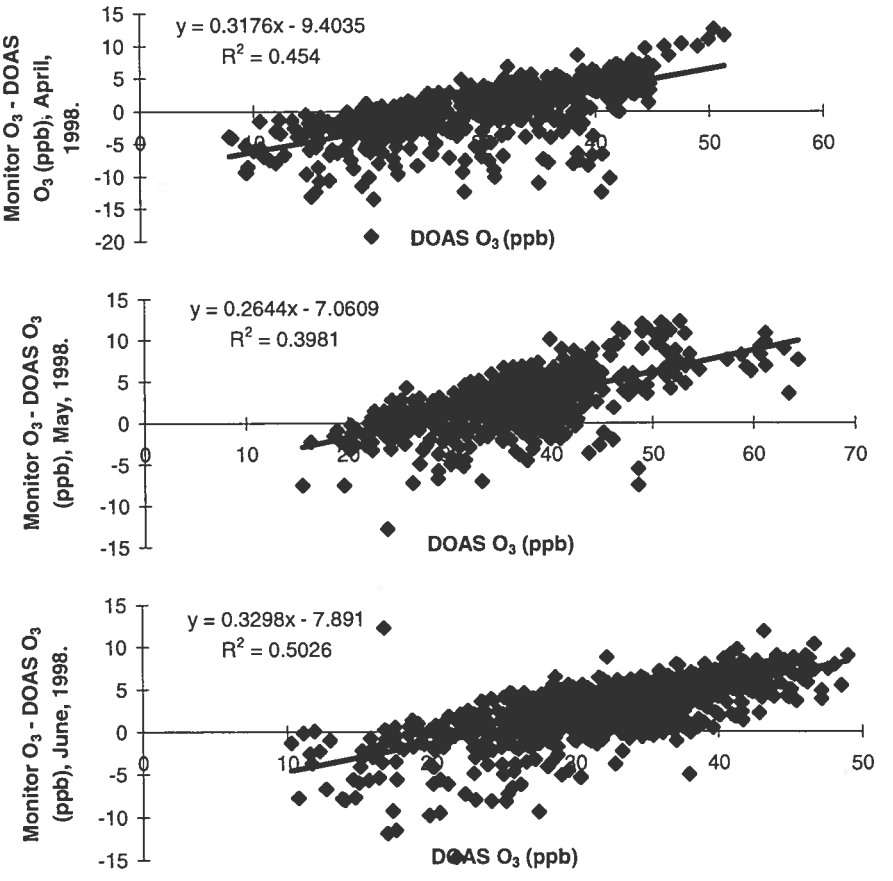

Figure 4.12 The difference in ppb between DOAS and monitor O_3 measurements versus DOAS O_3 at Lille Valby, April- June, 1998.

From Figure 4.12 it is seen that there is a clear linear correspondence between the difference of the methods and the ozone level. Large positive differences, that is when monitor O_3 is higher than DOAS O_3, are seen for high ozone levels. Correspondingly large negative differences are seen for low ozone levels. Above 40 ppb of ozone almost no negative differences are seen. Likewise, below 20 ppb of ozone only few positive differences occur.

Temperature dependency

The dependence of the difference between the two methods upon ozone concentration levels and the fact that no temperature correc-

tions are done on the DOAS measurements suggests a possible dependency of the difference upon temperature.

The results of plotting the difference between the methods (Monitor_ozone - DOAS_ozone) against temperature for the months May and June are given below.

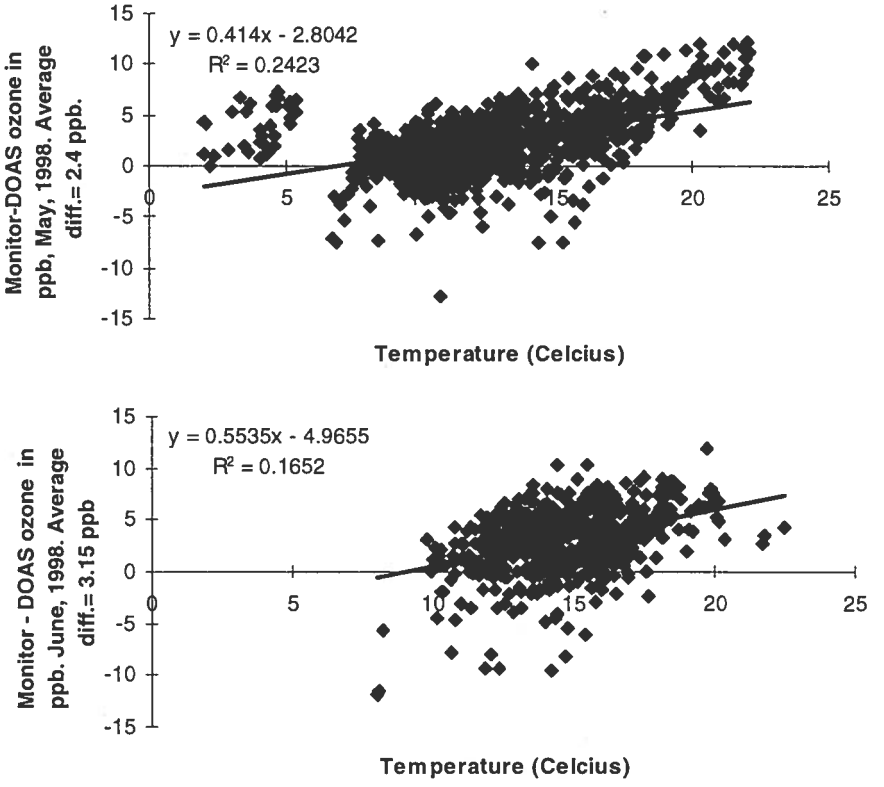

Figure 4.13 Monitor - DOAS ozone as a function of temperature at Lille Valby, May-June, 1998.

As suspected a linear dependence of the difference between the methods and the temperature is indicated. In May a small group of measurements, corresponding to temperatures below 7 degrees, stands out. The effect upon the correlation coefficient of removing these measurements is shown below. Also shown is the dependency of the measurement differences upon global radiation, wind direction and wind speed. The number of measurements for May and June are 985 (947, when excluding measurements at temperatures below 7 degrees) and 597 respectively.

No linear correlation

From figure 4.14 and 4.15 it can be seen that there is no correlation between the difference in ozone concentration of the two methods and wind speed. The same goes for wind direction and global radiation. However, some correlation with global radiation could be expected due to the connection between temperature and global radiation. This is reflected in the plot of May, 1998.

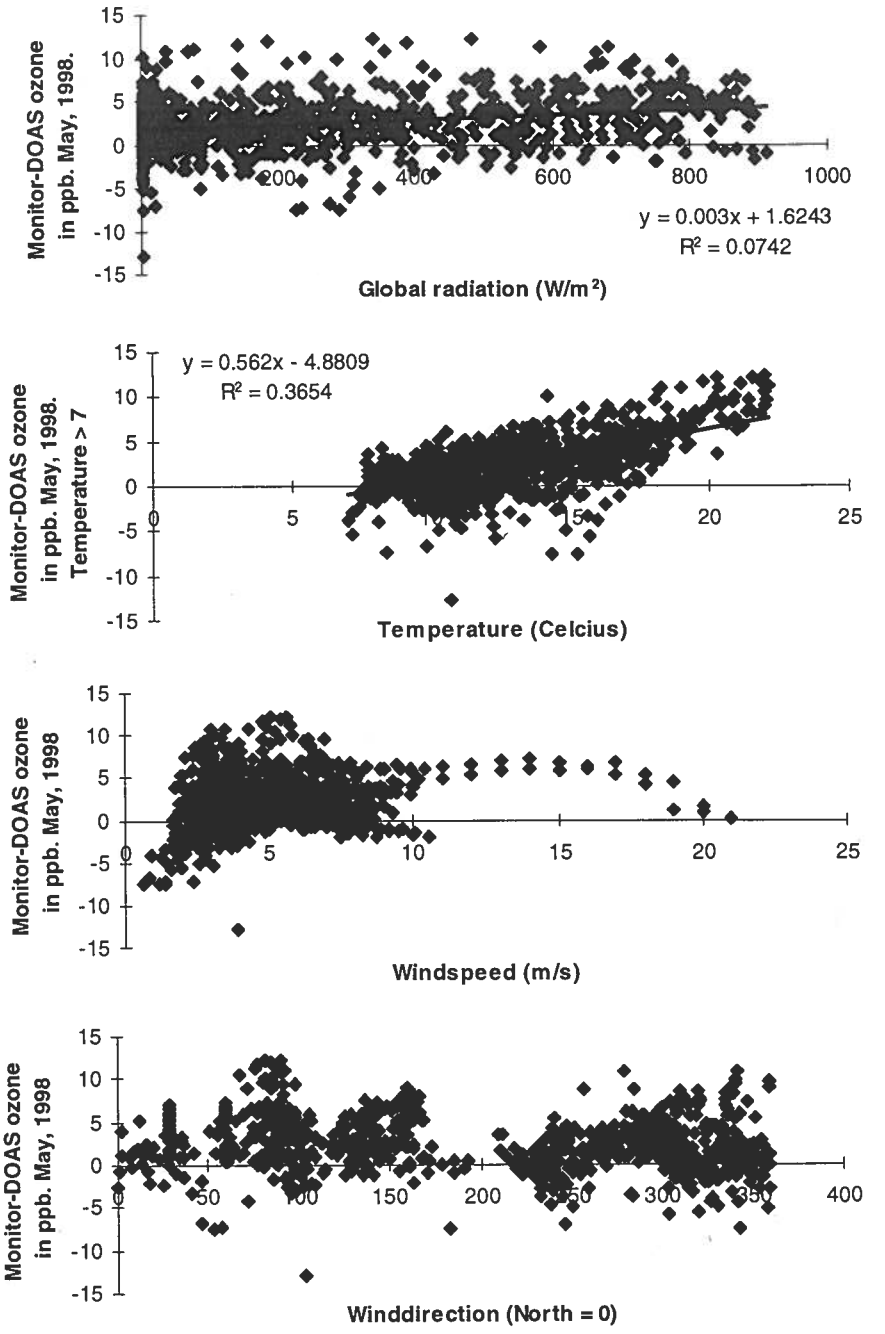

Figure 4.14 Monitor - DOAS ozone in ppb as a function of global radiation, wind speed, wind direction and for T > 7°C, May, 1998.

Effect of temperature on measurement discrepansies

The lack of temperature corrections for the DOAS measurements results in underestimated DOAS concentrations at temperatures above zero °C and overestimated concentrations below zero °C. This tendency is in accordance with the observed relationship between the difference, Monitor_ozone - DOAS_ozone, and temperature as was shown in Figure 4.13. However, the lack of temperature correction should not be able to account for the difference in measurements of up to 10 ppb.

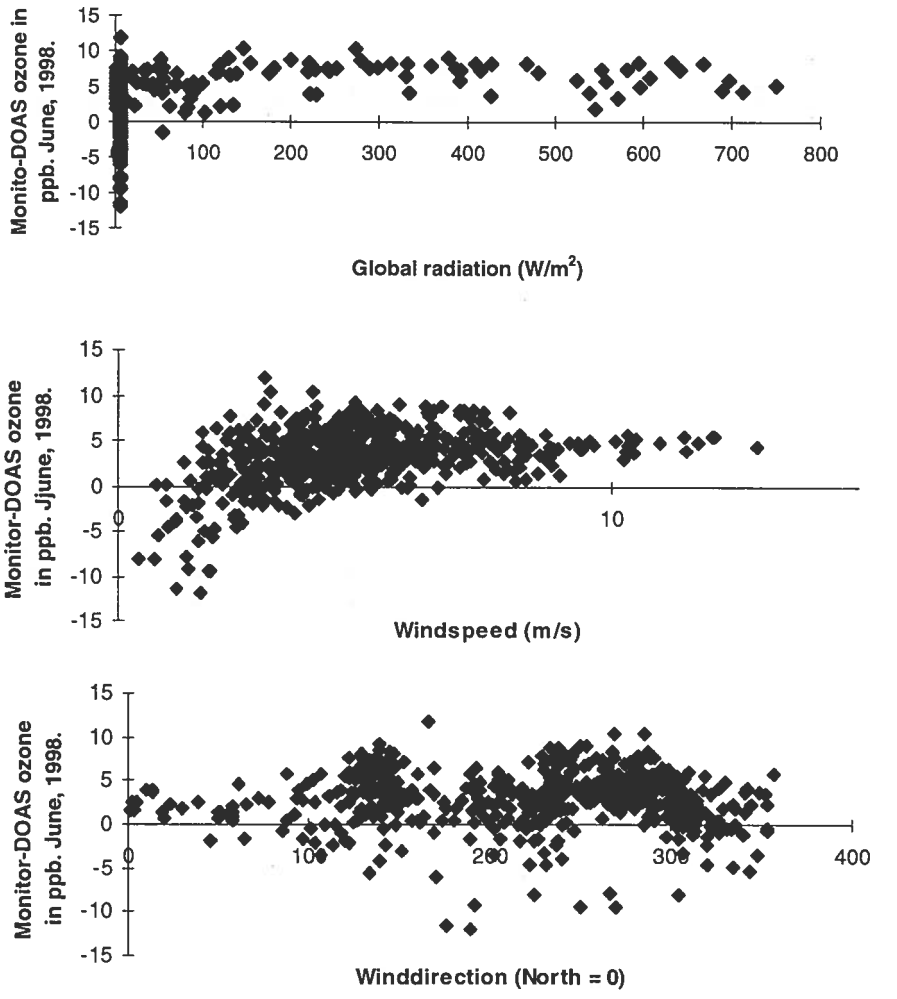

Figure 4.15 Monitor - DOAS ozone in ppb as a function of global radiation, wind speed and wind direction, June, 1998.

Temperature correction of DOAS data

The effect on the correlation between the DOAS and monitor ozone measurements of lacking temperature corrections on the DOAS data was tested by performing the correction on the existing data. This was done in the following way. First the DOAS ozone concentrations were converted back to micrograms/m^3. Then they were multiplied by the appropriate factor for converting from micrograms/m^3 to ppb at the temperature given by the meteorological data. The calculation of the conversion factors at different temperatures is described in section 3.6.2.1.

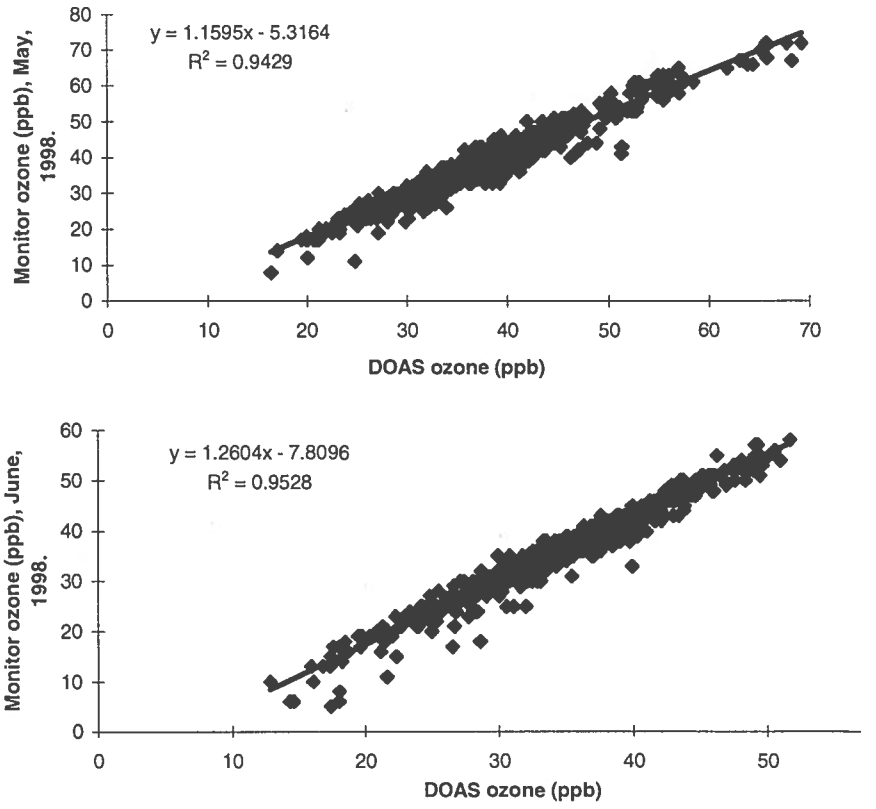

Figure 4.16 Monitor versus DOAS ozone data for Lille Valby, May-June, 1998. Note that the DOAS data are temperature corrected.

Effect of temperature corrected DOAS data

As can be seen from Figure 4.16 the temperature correction of the DOAS data resulted in a slight improvement of the correlation between the methods. The correlation coefficients, R^2, increased for both May and June and at the same time the slope decreased along with the negative y-axis offsets. However, there is still a large negative offset of 5 - 8 ppb on the y-axis. Thus, the lacking temperature correction of the DOAS data does not account for the discrepancies between the methods.

Comparison with other studies

Ziv and Iakovleva investigated the relationship between monitor and DOAS O_3 measurements at the HCØ (Copenhagen) monitoring station. They, as was observed in this study, observed a positive difference (monitor - DOAS ozone) for high temperatures and a negative difference for lower temperatures [Ziv, 1998]. They also found that for the yearly averages, the DOAS data were higher than the monitor data for the years 1994 - 1996, but negative for 1997 due to a large negative bias in September of 1997. However, for all years the DOAS measurements were found to be lower than the monitor measurements during April - July [Ziv, 1998]. This is in accordance with the measurements performed at Lille Valby, 1998, Table 4.7.

4.3.6 Conclusions

DOAS ozone measurements

Very few negative standard deviations and no negative concentrations are observed throughout the measurement period. Indicating that the evaluation of the spectra has converged properly.

Monitor/DOAS correlations

The correlation between the methods is slightly improved when the DOAS ozone measurements are temperature corrected. However, the temperature correction does not significantly improve the crossing of the linear regression lines on the y-axis at negative values of -5 - (-10) ppb.

Temperature corrections

Although the temperature correction of the DOAS data does not improve the correlation of the methods significantly it shows that temperature correction on the DOAS data should be performed.

Discrepancies between the methods

As was shown, the difference in ppb, between the methods depend on the ozone concentration. This and the fact that temperature correction of the DOAS data did not improve the correlation markedly, suggests that chemical reactions (as opposed to meteorological corrections or offset problems) may attribute to the discrepancy between the methods. Thus, possible interferences in the monitor ozone measurements should be looked into.

Higher monitor concentrations

In general the monitor ozone concentrations are higher than the corresponding DOAS ozone concentrations. This results in average monthly ozone concentrations being higher for monitor than DOAS data. As was shown, the lack of temperature correction on the DOAS data could not account for the extent of descrepancy observed.

DOAS replacing ozone monitors

Before DOAS ozone measurements can replace monitor ozone measurements, the discrepancies between the methods should be further investigated. Also the quality control of the DOAS data should be kept at a high level and temperature and pressure corrections should be performed.

4.4 HONO measurements at Lille Valby, 1998

4.4.1 Introduction

Motivation

The nitrous acid measurements at Lille Valby, 1998, were motivated by the wish to study the nitrogen chemistry related to the nitrate radical. Moreover nitrous acid is difficult to measure accurately and specifically using other measurement techniques due to the low concentrations found in the troposphere [F-Pitts and Pitts, 1986].

4.4.2 Measuring HONO by DOAS

Absorption in UV region

The absorption cross sections for nitrous acid in the UV region are sufficiently strong for its detection and measurement by the DOAS technique. The wavelength region employed by the DOAS technique is the 330 - 380 nm region [F.-Pitts and Pitts, 1986].

Absorption peaks

Especially the absorption peak at 365 nm is used in the measurement and detection of nitrous acid by the OPSIS DOAS systems [OPSIS, Sweden, 1995]. OPSIS do not supply information on the wavelength interval used.

Absorption cross sections

The absorption cross sections of nitrous acid (HONO) in the 330 - 380 nm region lies between 4.9 and a maximum of 23.6 * 10^{-19} cm^2 $molecule^{-1}$ at approximately 354 nm [Atkinson *et al.*, 1997].

Interference and spectral deconvolution

In this region of the spectrum absorption by NO_2 may interfere with the measurements. Thus a NO_2 reference spectrum is included in the deconvolution routine for nitrous acid measurements [OPSIS, Sweden, 1995].

4.4.3 The measurement campaign

Period of measurements

The measurement of HONO at Lille Valby was conducted April through September 1998. The DOAS instrument used is the one described in chapter 3. Meteorological data for the whole period are given in Appendix C.

Integration time

The integration time used in the HONO measurements was 1 minut at all times.

4.4.4 Results

The "raw" DOAS data, concentration and light level, are given in Appendix A.3.

4.4.6 Discussion

Quality control

The detection limit of HONO for the Lille Valby DOAS system of 0.33 ppb was calculated in chapter 3.5. This corresponds to 0.69 $\mu g/m^3$. Inspection of the "raw" data in Appendix A.3 shows that the concentration levels of HONO are close to zero throughout the whole measurement period. However some peaks of measurement values above 20 $\mu g/m^3$ do occur, especially in June. These peaks all coincide with very low light levels below 10 - 15 %. Thus, the peaks do not correspond to high concentrations of HONO but are mearly an example of the error in DOAS measurements when the light levels are too low.

Measuring close to the detection limit

A close inspection of the periods 2 - 6/6 and 2-5/7 gives clear examples of the consistency between light level and concentration levels when measuring close to the detection limit. Thus, from the figures in Appendix A.3, it is seen that the concentration level closely follows the light level, even at relatively high light levels. In the June episode the light level increases during daylight hours and decreases during the night. This is reflected in a corresponding variation in the concentration levels. In the case of the July episode the more constant light level is reflected in less fluctuation of the concentration level.

Comparison with other studies

In the remote troposphere the concentration of HONO is estimated to be < 30 ppt and in rural areas 0.03 - 0.8 ppb [F-Pitts and Pitts, 1986]. Perner and Platt measured HONO by DOAS at Julich in 1979. They were able to detect nitrous acid concentration levels of up to 0.8 ppb during early morning hours. Only in moderately polluted air, however [Perner *et al.*, 1979]. At Deuselbach, which is considered representative for European background air (in 1979) nitrous acid signals seemed to appear from the noise. However, the concentra-

tions could not have been above 0.05 - 0.1 ppb (the detection limit was 0.024 ppb) [Perner *et al.*, 1979]. Also in 1979 Platt and Perner measured HONO by DOAS at the Los Angeles air basin, Riverside, California. In this study they found concentrations up to 4.1 ppb (the detection limit was 0.28 ppb) [Platt *et al.*, 1980]. Platt *et al.* considers reaction 2.36 (chapter 2) and direct formation in combustion regions as the most likely sources of HONO [Platt *et al.*, 1980].

4.4.7 Conclusions

Concentration levels

The nitrous acid concentration levels were found to be below the detection limit of 0.33 ppb throughout the whole measurement period of May - September, 1998. This is in accordance with previous studies of nitrous acid concentration levels at background sites.

Peak concentrations

The unstable light level throughout the measurement period resulted in erroneous concentration peaks of above 20 $\mu g/m^3$ for light levels below 10 - 15 %.

4.5 Nitrate radical measurements at Lille Valby, 1998

4.5.1 Introduction

Motivation

So far, no measurements of the nitrate radical (NO_3) in Denmark has been published. The nitrate radical is an important night time oxidant in tropospheric chemistry. Thus, in understanding the full scope of tropospheric nitrogen chemistry the nitrate radical concentration levels, diurnal variations, lifetimes and production rates are important parameters.

4.5.2 Measuring NO_3 by DOAS

Absorption in the visible region of the spectrum

The nitrate radical has sufficiently strong absorption peaks in the visible region of the spectrum for its detection and measurement by the DOAS technique under atmospheric conditions. In particular one electronic transition in the red region of the spectrum results in two distinct absorption peaks at 662 nm (the 0-0 transition) and 623 nm (the first member of the progression) that are usually employed in the measurement of the radical [Wayne, R.P. *et al.*, 1991].

Absorption cross sections

The value of the absorption cross sections at the distinct peaks

$$\sigma_{623\,nm} = 2.1 * 10^{-17}\ cm^2\ molecule^{-1}$$

$$\sigma_{662\,nm} = 1.473 * 10^{-17}\ cm^2\ molecule^{-1}$$

are high enough to ensure low detection limits in ambient measurements [Atkinson *et al.*, 1997].

Uncertainties in determining σNO_3

Although absorption cross sections for the nitrate radical exist over a wide range of the spectrum the values are encumbered with some uncertainty. The uncertainty stems partly from the difficulties involved in determining the NO_3 concentration in the complex chemi-

cal reaction systems that result from the conditions under which the NO_3 is produced in the laboratory. Thus, an uncertainty in the estimated nitrate radical concentration results in corresponding uncertainties in the calculated absorption cross sections [Chapter 3, eq. 3.2]. The absorption cross section at 662 nm is uncertain within ± 10% [Wayne *et al.*,1991].

Temperature dependence of σNO_3

It is known that the nitrate radical absorption cross sections increases with decreasing temperature. However, the results from the temperature-dependence studies so far are not consistent [Wayne *et al.*, 1991]. Thus, the extent of the temperature dependence is not known, although upper limit ranges has been proposed [Wayne, R.P. *et al.*, 1991].

Effect of σNO_3 on NO_3 measurements

Uncertainties like the above are reflected as equivalent uncertainties in the nitrate radical concentration measurements. Thus, improved knowledge on the temperature dependence and exact values of the absorption cross sections would result in more reliable data of the nitrate radical concentration.

Type of absorption

Two possible sets of photodissociation products of the nitrate radical exists:

$$NO_3 + h\nu \rightarrow NO + O_2 \quad \text{(a)}$$

$$\rightarrow NO_2 + O\,(^3P) \quad \text{(b)}$$

The quantum yields of the reaction paths are not fully determined. However, in the wavelength interval from 450 to 700 nm reaction (b) seems to be favoured over (a) [F-Pitts & Pitts, 1986].

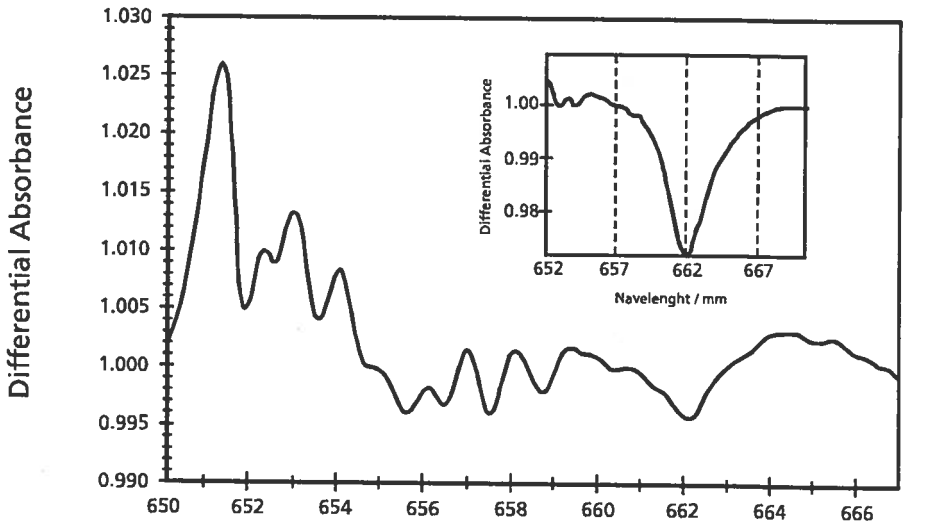

Figure 4.17 Differential absorption spectrum in the 650-667 nm region, showing structures from 650-660 due to the (311) vibrational band of atmospheric water vapor, and the NO_3 absorption centered at 662 nm ([NO_3] = 27.3 ppt). The inset shows a reference absorption spectrum of NO_3 at 662 nm [Plane *et al.*, 1992].

H_2O Interference

A prerequisite for correct measurement of concentrations by the DOAS technique is the ability to compensate for interfering species. In the case of the nitrate radical, the strong absorption of water vapor in the 640-670 nm region of the spectrum must be taken into account

absorption spectrum in the 650-667 nm region, showing structures due to water vapor and the nitrate radical.

Effect of interference

Clearly this interference needs to be removed from the spectrum in order to determine the nitrate radical concentration using the 662 nm absorption peak. If the interference is not removed however, the effect may be an underestimate of the nitrate radical concentration [Wayne, R.P. *et al.*, 1991]. This is due to the fact that some of the broad absorption caused by the H_2O band will be eliminated from the spectrum along with the other broadband absorptions. This results in a lower value of I_0' and thus, in the expression

$$A(i) = -\ln(I_0'/I) = N\sigma L \qquad (4.10)$$

the value of $\ln(I_0'/I) = A(i)$ will be lowered. This again results in an underestimate of the concentration (N) in the least-squares fitting procedure as can be seen from equation 3.3, chapter 3.

Daytime reference spectrum

Several approaches can be used to offset the interference from water vapor. Due to its rapid photolysis the nitrate radical can not exist during daylight hours. Thus, a nitrate radical spectrum taken a few hours after sunrise will not show any absorption due to nitrate radicals. However, the daytime reference spectrum will still show the absorption caused by H_2O in this region. Thus, by subtracting the daytime reference spectrum from the night time nitrate radical spectres the water vapor interference can be greatly diminished. A reference spectrum taken shortly after sunrise is preferred to one taken in the evening due to the closer resemblances in the morning and night time temperatures [Plane et al., 1991]. But as the water vapor content of the atmosphere varies greatly over the course of a day, even hours, this method is not entirely satisfactory.

H_2O reference spectrum

Another approach in eliminating water interference, is to include a reference spectrum of water in the general software deconvolution routine. This is the approach taken by the OPSIS DOAS system used at Lille Valby. Thus, by fitting the water reference spectrum to the absorption spectrum and subtracting it, the water interference is diminished. In this case however, the uncertainty in the calculated NO_3 concentration may be as high as 40% [Plane *et al.*, 1991].

Spectral deconvolution

In principle the nitrate radical could be measured as an absolute rather than differential optical absorption. As the nitrate radical is not present during daylight hours the subtraction of a daylight spectrum from a night time spectrum would give the absolute absorption of the radical. At least this would be the case if there were no other absorption or scattering effects that needed to be taken into account. Unfortunately this is not the case. Therefore the nitrate radical concentration is estimated using the same spectral deconvolution technique as for other atmospheric species. With the exception that a water reference spectrum is included in the deconvolution routine as explained above.

Quality control

The uncertainties involved in the measurement of the nitrate radical by the DOAS technique thus, falls in 3 groups:

1. The accuracy of the general spectral deconvolution procedure, as for other species.
2. Uncertainties in the determinations of σNO_3, as described above.
3. Water interference, as explained above.

4.5.3 The measurement campaign

Period of measurements

The measurement of the nitrate radical at Lille Valby was conducted April through September 1998. The DOAS instrument used is the one described in chapter 3. Meteorological data for the whole period are given in Appendix C.

Measurement time

The integration time used in the NO_3 measurements was 1 minut at all times.

Definition of night time

As the nitrate radical photolyses rapidly during daylight hours only night time measurements are of interest. Several approaches can be used to determine "night time" periods. In this study global radiation data was used to define night time periods when available. Unfortunately reliable global radiation data were only available during the first 2 months of measurements. Instead night time was simply defined as the time between 9 PM and 4 AM. This time interval roughly covers the "dark hours" in the Danish summer time.

4.5.4 Nitrate radical production rates

NO_3 precursors

The only important atmospheric source of the nitrate radical is the reaction of NO_2 with O_3:

$$NO_2 + O_3 \rightarrow NO_3 + O_2 \qquad (4.11)$$

Thus, the rate of, and extent to which the nitrate radical is formed in the atmosphere, is tightly connected with the concentration of its precursors NO_2 and O_3.

NO_3 production rates

The rate of formation of the nitrate radical can be found from the equation:

$$P_{NO3} = d[NO_3]/dt = k_{4.11}[NO_2][O_3] \qquad (4.12)$$

; where $k_{4.11} = 1.2 * 10^{-13} \exp(-2450/T)$ $cm^3 molecule^{-1} s^{-1}$.

At 298 K the value of $k_{4.11}$ is $3.2 * 10^{-17}$ [Atkinson *et al.*, 1997]. P_{NO3} is used in the remaining of this text as short for "nitrate radical production rate".

Nitrate radical production rates at Lille Valby '98

The nitrate radical production rates, P_{NO3}, at Lille Valby are calculated from the DOAS data in the following way. First the concentrations in $\mu g\ m^{-3}$ are converted to units of molecules cm^{-3}:

$$C_{\text{molecules cm-3}} = X\ \mu g\ m^{-3} * 2.46*10^{10}\ \text{molecules}\ cm^{-3}/(0.0409 * (MW)\mu g\ m^{-3})$$

An example calculation of P_{NO3} for the night of 4-5/6 1998, taking the concentrations at 01:30 AM which was 17.1 μgm^{-3} for NO_2 and 79.0 μgm^{-3} for O_3, gives:

$$P_{NO3} = k_x[NO_2][O_3]$$
$$= 3.2 * 10^{-17} \text{ molecules cm}^{-3}\text{s}^{-1} *$$
$$[17.1\ \mu\text{gm}^{-3} * 2.46*10^{10} \text{ molecules cm}^{-3}/0.0409 * 46\ \mu\text{gm}^{-3}] *$$
$$[79.0\ \mu\text{gm}^{-3} * 2.46*10^{10} \text{ molecules cm}^{-3}/0.0409 * 48\ \mu\text{gm}^{-3}]$$
$$= 7.1 * 10^{6} \text{ molecules cm}^{-3}\text{s}^{-1}.$$

The production rates are calculated using half hour averaged NO_2 and O_3 concentrations.

4.5.4.1 Results

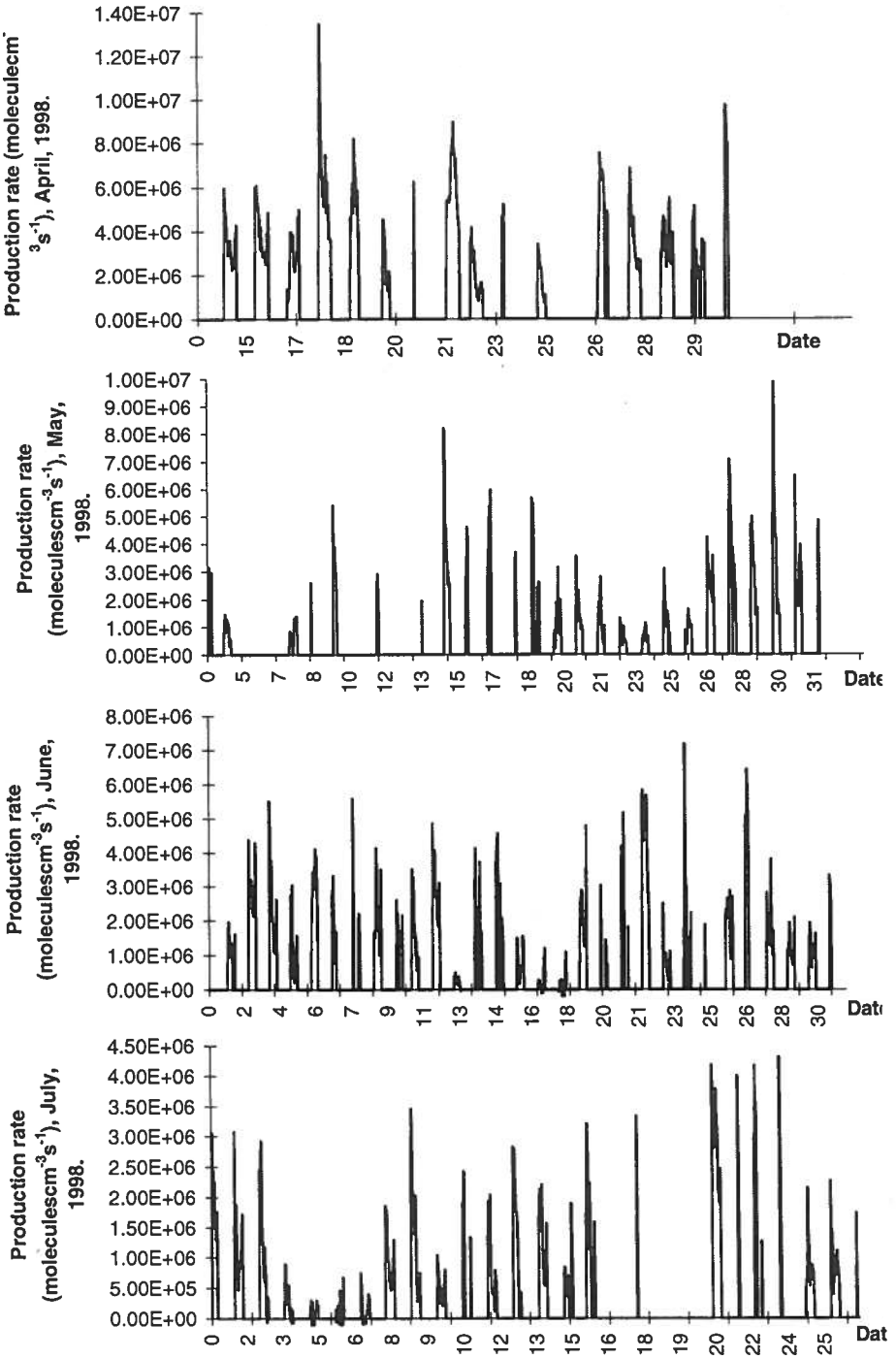

Figure 4.18 Nightly nitrate radical production rates at Lille Valby, April-July, 1998. Night time is defined as global radiation less than 2 W/m^2.

4.5.4.2 Discussion and comparisons

Lille Valby average production rates

The monthly average nitrate radical production rates at Lille Valby 1998 are given in Table 4.8 below. The calculations are made on half hour averages of the production rates.

Table 4.8 Average monthly nitrate radical production rates at Lille Valby 1998. Also given are monthly averages calculated by Ljungstrøm et. al for the years 1991-1992 [Ljungstrøm et. al, 1996].

Month	Lille Valby 1998 Average production rate in moleculescm^{-3}s^{-1}	Ljungstrøm et al. Lille Valby average production rates in moleculescm^{-3}s^{-1}
April	$4.04 * 10^6$	
May	$2.29 * 10^6$	$2.42 * 10^6$
June	$2.03 * 10^6$	
July	$1.22* 10^6$	$2.1 * 10^6$

A steady decrease in the average production rate is seen over the months April to July of 1998. The monthly average DOAS NO_2 concentrations for April, May and June, 1998, are 6.23, 2,81 and 2.95 ppb respectively. Thus, the decrease in nitrate radical production rates by a factor 2, can be explained by a decrease in NO_2 concentrations of almost the same factor. The monthly average DOAS ozone concentrations for April, May and June are 30.4, 35.9 and 32.2 ppb respectively. Thus, this could explain the average nitrate radical production rates in May being higher than those in June, although the average NO_2 concentration is lower for May.

Comparison with other studies

Ljungstrøm and Hallquist made similar calculations of the night time nitrate radical production rates at various locations in Scandinavia for the years 1991-1992 [Ljungstrøm *et al.*, 1996]. Lille Valby was one of these locations. The calculations were based on monitor rather than DOAS data. They found that the production rates at all locations reached the highest values during the spring and summer periods as opposed to the autumn and winter periods. For Lille Valby the calculated monthly average production rates for January, May, July and October were 1.17, 2.42, 2.1 ± 0.8 and 1.3 ± 0.2 respectively (all should be multiplied with 10^6 molecules cm^{-3}s^{-1}). This is in good agreement with the 1998 Lille Valby DOAS data as seen from Table 4.8. This goes for the magnitude of the production rates as well as for the decrease in these from May to July.

Monthly averages of same magnitude

The monthly average production rates from the various Scandinavian sites as calculated by Ljungstrøm and Hallquist are all of the same magnitude. Actually all monthly averages fall within the same range (0.71 - 5.1 * 10^6 moleculescm^{-3}s^{-1}), whether rural or urban sites, summer or winter periods are considered.

Seasonal averages

The lack of significant variations in the seasonal averages can be explained by the number of daylight hours in the seasons. Thus, in the spring and summer periods when production rates are high, the number of "dark hours" is low. In the winter the lower production rates are offset by the corresponding high number of "dark hours".

Urban and rural averages

Heintz et al. likewise calculated nitrate radical production rates from DOAS data in the order of $1*10^5$ molecules $cm^{-3}s^{-1}$ to $1*10^7$ molecules $cm^{-3}s^{-1}$ for The TOR station, Kap Arkona, 1993 - 1994 [Heintz *et al.*, 1996]. However, these data apparently also include daytime production rates which are obviously of little interest.

4.5.5 Nitrate radical concentration levels

Detection limits

The detection limit for measurement of the nitrate radical at Lille Valby was found to be 25 ppt. (See chapter 3).

4.5.5.1 Results

Measurement data

The "raw" DOAS NO_3 measurements from Lille Valby for the months May to September 1998 are given in Appendix A.4. For comparison raw data for May are shown along with data where measurements with a corresponding light levels below 5 % are excluded. From the raw data figure it can be seen that at zero light level the concentration drops to a default value of -1000 (and the standard deviation to a default value of 999). The main reason for the many sudden drops in light intensity is solar heating of the instrument as described in chapter 3.5. For the rest of the months only measurements with light levels above 5 % are shown. Notice that the erroneous "out of range" concentrations above 5 $\mu g/m^3$ coincide with very low light levels. As was the case for the HONO measurements.

4.5.5.2 Discussion and comparisons

Concentration levels below detection limit

As can be seen from Figure 4.19 below almost all of the measured nitrate radical concentrations are below $1 * 10^{-2}$ $\mu g\ m^{-3}$, which is equivalent to 3.6 ppt. This is far below the detection limit of 25 ppt. Also a large portion of the concentrations are negative. The standard deviations for all measurements are in the range of $7.4 * 10^{-4}$ to $4.4 * 10^{-3}$ $\mu g\ m^{-3}$ and thus, the many negative concentrations larger than two times the standard deviation indicates a serious error in the measurement, see chapter 3. What is seen in the figures should therefore not be taken as a measure of the nitrate radical concentration levels at Lille Valby. More likely what is seen is actually just "noise". Thus, the only conclusion that can be made on the nitrate radical levels at Lille Valby is that they are below the detection limit of 25 ppt and probably well below.

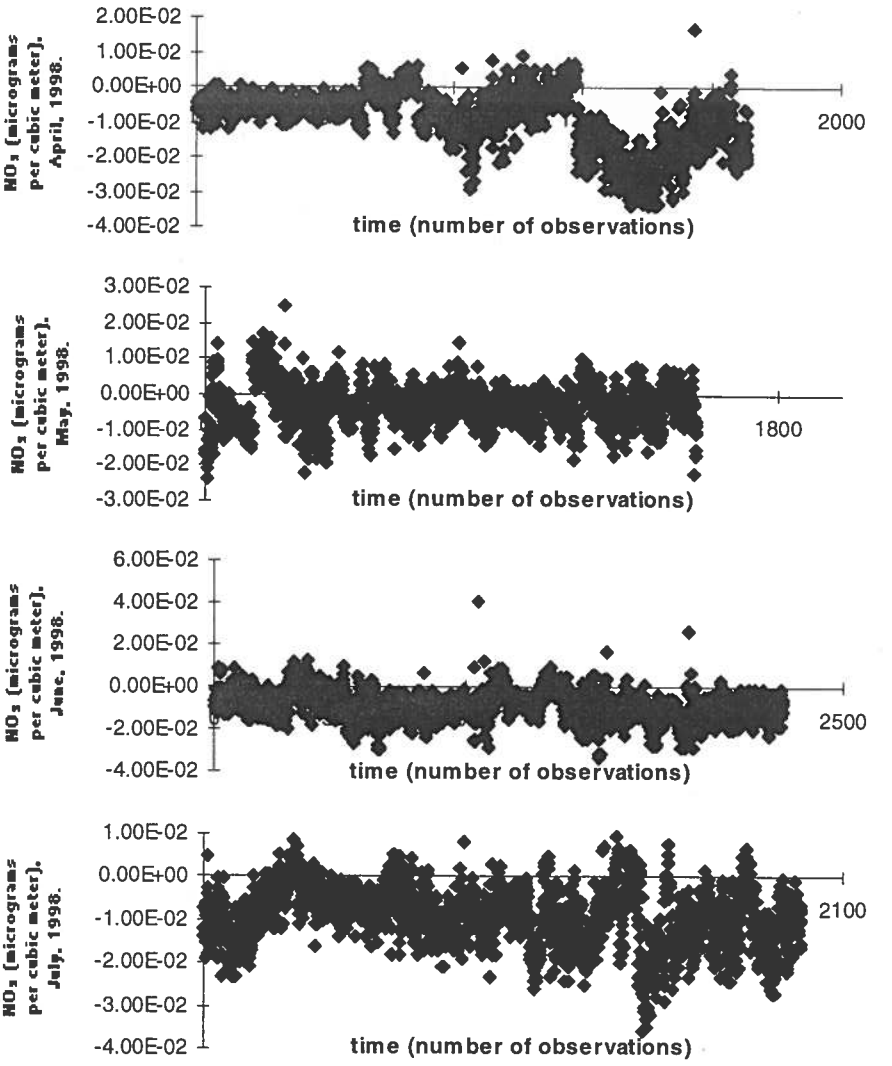

Figure 4.19 DOAS measurements of the nitrate radical at Lille Valby, 1998. The detection limit is 25 ppt = $7 * 10^{-2}$ micrograms/m^3.

Expected diurnal variations

The diurnal variation of NO_3 is expected to variate considerably from day to day, or more precise, from night to night. However, it would be expected that the concentration would increase some time after sunset and reach a peak concentration during the night. At dawn the concentration would then decrease again rapidly due to the photolysis of NO_3.

Diurnal variations at Lille Valby, 1998

However, as the nitrate radical concentrations are below detection limit the diurnal variations could not be established. As can be seen from the figures the diurnal variation is almost identical for the months May through July, 1998. The "peak" concentrations are around 10 AM. Again however, these variations are of no practical use.

Scandinavian measurement results

Some measurements have been made of the nitrate radical in Scandinavia. Platt *et al.* measured the nitrate radical by the DOAS technique in Deuselbach and Julich, 1980, using measurement path lengths of 4.8 and 3.5 kilometres respectively [Platt *et al.*, 1981]. At Julich, where measurements were conducted May through August the detection

limit was only exceeded on 5 nights, where concentrations up to 78 ppt was found. At Deuselbach measurements were made on April 11 to April 18, 1980. Here, on all but the first night, the nitrate radical concentrations were above detection limit of 6 ppt, and reached nightly peak concentrations of 40-280 ppt. Heintz and Platt measured the nitrate radical by the DOAS technique at a rural site in the Baltic Sea, Kap Arkona, in 1993-1994 [Heintz *et.al.*, 1996]. They used a measurement path length of 7 kilometres and thus, obtained a detection limit of ≤ 2 ppt. Out of a total of 225 measurement nights, on 206 nights the nitrate radical concentrations exceeded the detection limit. The average of these measurements was 7.8 ppt. The highest levels occurred in April, May and early June, reaching concentrations of nearly 100 ppt.

Likely DK nitrate radical levels

From the Lille Valby measurements, the described Scandinavian studies and model results (See chapter 5) the nitrate radical concentration level in Denmark under normal conditions are likely to be in the order of a few ppt. However, during summertime long range transport episodes of O_3 and NO_2 from central Europe, considerably higher levels should be expected. These episodes are facilitated by high pressure events, sunny weather and continued winds from the Southeast. The summer of 1998 was an (unusually) cold and rainy summer with no pronounced episodes of this kind.

4.5.6 Nitrate radical lifetimes

The nitrate radical lifetime

The lifetime of the nitrate radical can be found from the expression:

$$\tau NO_3 = [NO_3]/k_1[NO_2][O_3] \quad (4.13)$$

$$= [NO_3]/P_{NO3} \quad (4.14)$$

Again as the nitrate radical concentrations at Lille Valby 1998 were all below the detection limit of 25 ppt the actual nitrate radical concentrations are not available. However, a rough estimate of the lifetime span can be made using average night time NO_2 and O_3 concentrations and estimated NO_3 concentrations. Choosing the night of 4-5/6 1998, as in the example calculation of P_{NO3} above, with NO_2 and O_3 concentrations of 8.3 ppb and 37 ppb respectively, and estimating a nitrate radical concentration of 0.3 ppt, gives a nitrate radical lifetime of:

$$0.3 \text{ ppt} = 2.46 * 10^7 \text{ molecules cm}^{-3}/\text{ppt} * 0.3 \text{ ppt}$$
$$= 7.38 * 10^6 \text{ molecules cm}^{-3}$$

$$\tau_{NO3} = [NO_3] / P_{NO3}$$
$$= 7.38 * 10^6 \text{ molecules cm}^{-3} / 7.1 * 10^6 \text{ molecules cm}^{-3}\text{s}^{-1}$$
$$\approx 1 \text{ s.}$$

Estimated nitrate radical lifetime span

With the use of estimated nitrate radical concentrations the corresponding lifetimes can be calculated using the nitrate radical production rates and equation (4.14). This is done below for May - July 1998 in Figure 4.20. Two nitrate radical concentration estimates of 0.3 ppt and 10 ppt are used. Thus, for estimated nitrate radical concentrations of 0.3 ppt the lifetimes are in the range of 0-100 seconds. For

estimated nitrate radical concentrations of 10 ppt the lifetimes are in the range of 0-180 minutes. Note that as the nitrate radical concentration is constant the lifetimes increase with decreasing production rates. The lifetimes calculated in this way, are only indications of a possible lifetime span at Lille Valby, with the known production rates. Note that the general increase in lifetimes from May to July reflects a decrease in the production rates in the same period.

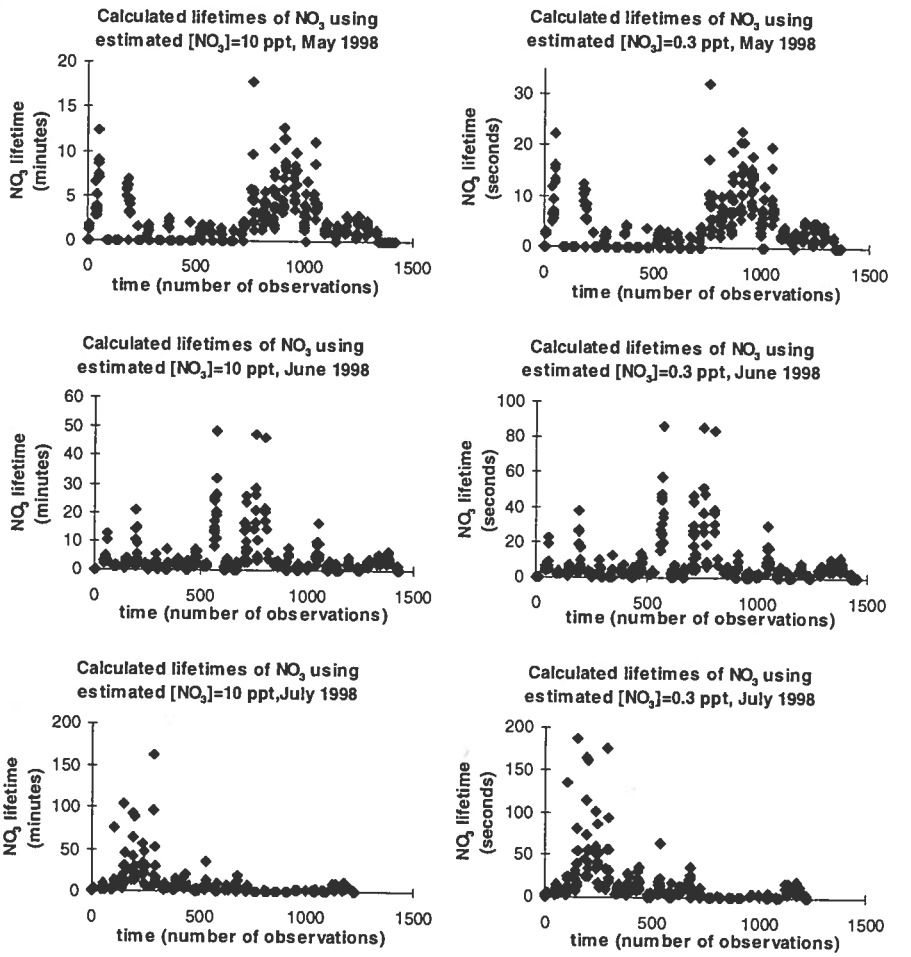

Figure 4.20 Estimated lifetimes ranges at Lille Valby, May - July, 1998.

Lifetimes from other studies

Heintz et al. measured NO_2, O_3 and NO_3 using DOAS at the TOR station Kap Arkona, 1993-1994. For these measurements the nitrate radical lifetimes spanned a range of 10-5600 seconds with an average life time of 250 seconds [Heintz et.al, 1996].

Dependence on relative humidity

Platt *et al.* found that the nitrate radical lifetimes for several sites in California, USA, was greatly dependent on the relative humidity. The longest lifetimes were found only at relative humidities below 50% [Platt *et al.*, 1984].

4.5.7 Nitrate radical loss mechanisms

Nitrate radical production rates

The nitrate radical production rates at Lille Valby are in the order of 2-6 * 10^6 molecules $cm^{-3} s^{-1}$. Thus, if there were no loss mechanisms for NO_3 the build-up of NO_3 over a seven hour period (9 PM to 4 AM) would be in the order of 2-6 ppb:

$(2 * 10^6$ moleculescm^{-3}s^{-1} $) * (7 * 3600)$ s $= 50.4 * 10^9$ moleculescm^{-3}
$= 2.05$ ppb

$(6 * 10^6$ moleculescm^{-3}s^{-1} $) * (7 * 3600)$ s $= 151.2 * 10^9$ moleculescm^{-3}
$= 6.15$ ppb

This is 2 orders of magnitude larger than the dection limit for the nitrate radical of 25 ppt. As the nitrate radical concentrations at Lille Valby were found to be below detection limits at all times, some appreciable loss mechanisms for the nitrate radical must be in operation

Modelled nitrate radical concentrations

The nitrate radical concentrations at Lille Valby as calculated by the ACDEP-model [Hertel, O., 1995] indicate an average night time nitrate radical concentration of 0.3 ppt (see chapter 5). Thus, this suggests that the nitrate radical removal rates at Lille Valby are of the same order of magnitude as the formation rates.

Radical concentrations versus formation rates

If the nitrate radical loss mechanism in operation were a simple first order reaction, a correlation between the radical concentration and the production rate would be expected [Platt *et al.*, 1994]. Platt & Heintz found however, that there were no correlation between formation rates of NO_3 and NO_3 concentrations [Platt *et al.*, 1994]. As the nitrate radical concentrations at Lille Valby, 1998, were all below the detection limit, a check of this kind could not be made.

Equilibrium with N_2O_5

Platt *et al.* found, in 1984, a dependence of nitrate radical lifetimes upon the relative humidity [Platt *et al.*, 1984]. Thus, at high relative humidities, above 50 %, the nitrate radical is effectively removed due to its equilibrium with N_2O_5 and the subsequent hydrolysis (heterogeneous) of N_2O_5. As the relative humidity in Denmark is usually high, this is a likely loss mechanism for nitrate radicals in Denmark. For comparison the mean relative humidity measured at Kastrup airport August - September 1997 was 74.3%. Also the equilibrium with N_2O_5 is shifted towards N_2O_5 with decreasing temperatures. Thus, the importance of N_2O_5 hydrolysis as a sink for NO_3, and NOx, increases with decreasing temperature.

Reaction with NO

As the NO at Lille Valby is predominantly emitted by daytime sources, mostly traffic, the reaction of NO_3 with NO is not likely to be an important loss mechanism for NO_3 at night time.

4.5.8 Conclusions

New calculation method

The measurements of the nitrate radical at Lille Valby, Sjælland, were originally motivated by the wish to study a new method for determining the nitrate radical concentration, using the DOAS technique. The purpose was to diminish the interference by water on nitrate radical measurements, to an extent much better, than previously done. However, this aim was not met because this would require spectra of the nitrate radical, that could not be obtained, due to the concentration level being below the detection limit.

NO_3 concentration levels at Lille Valby

The fact that all measurements of the nitrate radical at Lille Valby, 1998, was below the detection limit of 25 ppt, suggests that the nitrate radical concentration is generally low. The nitrate radical concentrations at Lille Valby as calculated by the ACDEP-model [Hertel

et al., 1993] indicates an average night time nitrate radical concentration of 0.3 ppt. Thus, the night-time nitrate radical concentrations at Lille Valby are likely to be in the order of a few ppt or less.

Lifetime of NO_3

The calculated lifetime span for NO_3, of a few seconds to 180 minutes, is a very rough estimate. In order to calculate the actual lifetime span of the nitrate radical at Lille Valby, the NO_3 concentration must be known.

Loss mechanisms for NO_3

The lack of NO_3 measurements above the detection limit makes it impossible to analyse the kind of loss mechanisms for NO_3 in operation at Lille Valby. However, the fast equilibrium with N_2O_5, and the high relative humidities, makes loss through N_2O_5 hydrolysis the most likely.

Importance of NO_3 chemistry at Lille Valby

The low concentration levels of NO_3 suggests that the nitrate radical chemistry is of minor importance at Lille Valby.

Winter time

However, it could be speculated that the nitrate radical chemistry would have an increased importance at wintertime due to the few daylight hours. Even at concentration levels of a few ppt. The importance of the nitrate radical as an atmospheric night time oxidant can be set in perspective by comparing the lifetime of a species with respect to the OH radical and NO_3 reactions respectively. This is done in section 2.1.4. Thus, for some species, oxidation by the nitrate radical may be of dominant importance even at NO_3 concentrations in the order of 10 ppt.

Summer time

The only periods in which elevated concentrations of the nitrate radical would be expected is during transport episodes of photochemical air pollution from central Europe, with high ozone concentration levels and a low $[NO]/[NO_2]$ ratio. Episodes of this kind occur predominantly during the spring and summer months [Granby, K., 1997].

Definition of night time

Data on the time of sunrise and sunset in the measurement period could, in retrospect, have been used for a more precise definition of the night time interval, when global radiation data were missing.

5 Modelling tropospheric chemistry

5.1 Introduction

Currently, mathematical models are widely used in atmospheric chemistry e.g. for interpretation of ambient measurements. Furthermore, atmospheric models are powerful tools in exploring the reaction mechanisms of the troposphere and in predicting future tendencies of pollution levels. Also they can be used for estimating the effects of various reduction policies and thus, help in choosing the most effectfull strategy. Transport-Chemistry models for the troposphere provide important inputs to global climate models, that are capable of computing possible future climatic scenarios and pollution concentration levels based on the current trends in emissions etc. This chapter gives a short introduction to the basics of models used in tropospheric modelling especially the ACDEP model used at the Danish National Environmental Research Institute (NERI).

5.2 Different types of models

Practical applications of tropospheric models are constrained by purpose of the application and in some cases as well on the computer available power. The basics of all models, however, are the chemical reactions and species chosen to simulate the chemical processes of the troposphere.

Representations of chemical reactions

Two different approaches, "lumping" and explicit representation, to the representation of the chemistry may be adapted. Combinations of the two are also possible. In the following the ACDEP model is briefly introduced. This model uses the Carbon Bond Mechanism IV, (CBM IV), a lumping technique, in implementing the tropospheric chemical reactions.

5.2.1 The ACDEP model

The Atmospheric Chemistry and Deposition model (ACDEP) is a variable scale Lagrangian trajectory model. From the receptor point trajectories are calculated, based on meteorological data, every 6 hours. The trajectories are calculated 96 hours back in time. Thus, the airparcels that reaches the receptor point (every 6 hours) have been underway for 96 hours in which they have been subjected to gaseous emissions, chemical transformations, vertical dispersion and dry- and wet deposition. The air parcel is represented as a vertical 1-D 10 layer column, extending from a height of 2 meters up to 2 kilometers [Hertel, O. *et al.*, 1995].

Horizontal transport

In the ACDEP model it is assumed that the wind speed and direction of the horizontal transport does not vary with height. Thus, the trajectories are calculated based on SIGMA-level 0.925 wind fields. That is the height above the ground that corresponds to a pressure of

0.925 that at the ground. Usually this is about 800 m above ground [Hertel, O. *et al*, 1995; Luftforurening].

Averaging of emissions

The emissions influencing on the air parcel along the trajectory are averaged over a square with sides that are 1/10 of the distance along the trajectory to the receptor point. This to some extent compensates for the simplification that the horizontal transport does not vary with height and the inaccuracy in computing the trajectories [Hertel, O., 1995].

Vertical dispersion, dry and wet deposition

The particular implementation of the vertical dispersion between the layers of the model and the dry- and wet deposition will not be described here. However, this is given by [Runge, E. *et al.*, 1997 and Hertel, O., 1995].

Chemical reactions

In the ACDEP model the description of the chemical reactions are based on the Carbon Bond Mechanism IV as discussed below.

5.2.1.1 The Carbon-Bond Mechanism (CBM-IV)

A chemical reaction scheme that has been used extensively over the past years in modelling tropospheric chemistry is the Carbon-Bond Mechanism (CBM-IV). The scheme was first presented in 1989, and is based on improvements on earlier reactions schemes. The ACDEP-model uses this model in a slightly modified version, including the reactions of HNO_4.

5.2.1.1.1 Condensation of reaction mechanisms

The Carbon-Bond Mechanism used in the ACDEP-model is a condensed version of an extented chemical reaction mechanism including 87 species and 204 reactions [Gery et al., 1989]. The condensation of the original scheme was performed using 4 different techniques:

1. Elimination of unimportant reactions and reaction-products.
2. Introduction of a universal peroxy-radical, for modelling all peroxy-radical reactions simultaneously.
3. Lumping (that is a grouping) of secondary reaction products. This was mainly done in order to simplify isoprene chemistry by replacing various reaction products by surrogate species already in the reaction scheme.
4. Mathematical and algebraic manipulations were performed in order to further reduce the number of reactions.

5.2.1.1.2 Carbon-Bond surrogate species

All inorganic and some organic species of special importance in tropospheric chemistry (formaldehyde, PAN, ethene and others) were represented explicitly.

Some organics however, were represented by surrogate compounds. Some of these groups are:

- PAR -representing single bonded one-carbon-atoms
- OLE -representing double-bonded two-carbon-atom
- ALD2 -representing a two-carbon CHO-group
- TOL -representing a seven-carbon (monoalkyl benzen species)

All species and reaction products in the scheme were replaced by equivalent combinations of these surrogate compounds. This procedure greatly reduces the amount of reactions necessary, as all further reactions can be simulated using the same set of equations, regardless of the sources of the participating species. Finally, to ensure that performance was not lost, the scheme was tested thoroughly before and after the condensation.

5.2.1.2 The ACDEP chemical reaction scheme

The chemical reaction scheme used in the ACDEP model consists of 35 species and 69 reactions. It is a modified version of the Carbon Bond Mechanism as described above. The modifications are [Hertel, O. *et al.*, 1993]:

- HNO_4 chemistry is included.
- Formation of organic nitrates is taken explicitly into account.
- NH_3 chemistry is included
- operators necessary for consistency of the EBI method (see below)

5.2.1.3 The EBI method

Chemical reactions as differential equations

The concentration of each species in the model can be represented as a differential equation of the form:

$$dc_i/dt = P_i - L_i c_i \qquad ; i = 1, ...nc \qquad (1)$$

; where c_i is the concentration of species i, P_i is the chemical production (including emission) of species i, L_i is the loss (chemical and deposition) of species i and nc is the number of species in the reaction mechanism. Thus, in order to calculate the concentration of all species in every time step when running the model a set of differential equations needs to be solved. Several approaches exist. The one described below is the EBI method [Hertel, O. *et al.*, 1993]used in the ACDEP model.

The EBI numerical method

The numerical method used in the ACDEP model is the EBI (Euler Backward Iterative). The method is based on the backward Euler approximation of equation (1):

$$c_i^{n+1} = c_i^n + P_i^{n+1} \Delta t - L_i^{n+1} \Delta t c_i^{n+1} \qquad (2)$$

; where Δt is the time step used. This linear equation ensures that the chemical mass balance is preserved. Equation 2 can be rearranged to give:

$$c_i^{n+1} = c_i^n + P_i^{n+1} \Delta t / (1 + L_i^{n+1} \Delta t) \qquad (3)$$

from which the concentration of species i can be found. As the concentration of species i may depend on the concentration of other species through the production and loss terms in equation 3 the concentration of all species is a set of coupled differential equations.

Solution of the equations in a straight forward manner, that is simply applying a numerical iterative method by calculating the production and loss terms using the concentrations from the previous time step does not apply. The reason for this is that a large number of iterations would be needed for convergence and in the case of strong couplings between species the method may not converge [Hertel, O., 1995]. Thus, for groups of species that are strongly coupled, explicit solutions are introduced. An example of a strongly coupled system that is solved explicitly is that of NO_3 and N_2O_5. In this case the set of equations that needs to be solved is:

$$[NO_3] = [NO_3]_0 + P'_{15}\Delta t + r_{15,16}\Delta t[N_2O_5] - L_{15}\Delta t[NO_3] \quad (4)$$

$$[N_2O_5] = [N_2O_5]_0 + r_{16,15}\Delta t[NO_3] - L_{16}\Delta t[N_2O_5] \quad (5)$$

; where $[X]_0$ is the concentration of species X from the previous time step, $P'_{15}\Delta t$ is production of NO_3 other than from the equilibrium with N_2O_5, $r_{15,16}\Delta t[N_2O_5]$ is the production of NO_3 from the equilibrium with N_2O_5 and $L_{15}\Delta t[NO_3]$ is the total loss of NO_3 in that time step. The concentration of NO_3 and N_2O_5 is found from the solutions to equations, 3 and 4:

$$[NO_3] = \frac{(1+L_{16}\Delta t)([NO3]_0 + P'_{15}\Delta t) + r_{15,16}\Delta t[N_2O_5]_0}{(1+L_{15}\Delta t)(1+L_{16}\Delta t) - r_{15,16}\Delta t\, r_{16,15}\Delta t} \quad (6)$$

$$[N_2O_5] = \frac{(1+L_{15}\Delta t)[N_2O_5]_0 + r_{16,15}\Delta t[NO3]_0 P'_{15}\Delta t}{(1+L_{15}\Delta t)(1+L_{16}\Delta t) - r_{15,16}\Delta t\, r_{16,15}\Delta t} \quad (7)$$

Similar explicit solutions are found for the system including NO, NO_2, O_3 and $O(^3P)$, the system consisting of OH, HO_2, HNO_2 and HNO_4 and the system of C_2O_3 and PAN. Explicit solutions to these systems can be found in Hertel *et al*, 1993.

The concentrations of the remaining species are calculated using equation 3.

Criteria for convergence of the method

The convergence criteria applied for concentrations solved by equation 3 is:

$$| c_{old} - c_{new} | \leq A\,(c_{old} + c_{new}) \quad (8)$$

; where c_{old} is the concentration as calculated in the previous time step and c_{new} is the concentration as calculated in the current time step. A is the prescribed accuracy (relative error), that varies for different species. This criteria is tested for all compounds and the iteration is proceeded until convergence has been reached for all compounds [Hertel, O. *et al.*, 1993].

5.2.2 The Leeds model

The lumping of species used in chemical reaction schemes has been used extensively. One of the advantages of using lumping in chemical reaction schemes is the reduction in the number of reactions required. Thus, the time for computation of each iterative step is

kept at a reasonable level. This was particularly important in the past decades where computational power was both expensive and limited by the current state of computer technology. The computational power is still a limiting factor in the atmospheric models used today. Up to 90 % of the computation time in typical transport-chemistry models is spent on solving the chemistry part of the model. However, computational power increased markedly in the 90's which has allowed for still more complex and demanding atmospheric models.

5.2.2.1 Explicit chemical reaction schemes

An example of an attempt to create an explicit reaction scheme for modelling tropospheric chemistry is the Master Chemical Mechanism (MCM) from the Department of the Environment (DoE) at the University of Leeds. The DoE has developed explicit chemical mechanisms for use in photochemical trajectory models. In particular the chemistry of various volatile organic compounds (VOC) has been implemented. These are now used within the EMEP (European monitoring and evaluation programme) to quantify the potential of each VOC for photochemical ozone production [Derwent *et al.*, 1996].

In describing the degradation of more than 120 VOC's the MCM uses a reaction scheme containing over 2400 chemical species and over 7100 chemical reactions. [Derwent *et al.*, 1998].

Disadvantages of explicit mechanisms

One of the major disadvantages of explicit chemical mechanisms like the MCM, is clearly the very large number of reactions included. Also a significant amount of computational power is needed for running an explicit mechanism like the MCM.

Comparison with non explicit mechanisms

Thus, while earlier only the inorganic chemistry was treated in an explicit manner in chemical reaction schemes used in tropospheric modelling, the tendency is towards including still more explicit reactions for organic species. However, as is the case with the MCM chemical reaction scheme, some mechanisms are still needed for reducing the total number of reactions whilst maintaining the essential features of the chemistry [Jenkin *et al.*, 1997].

5.3 Modelling nitrate radical chemistry

As mentioned in section 4.5 the nightly nitrate radical concentrations at Lille Valby was measured April through September 1998. The detection limit for the measurements of NO_3 was 25 ppt. However, during the entire period of measurements the concentrations did not exceed this limit.

5.3.1 Nitrate radical concentrations

Thus, for comparison the nitrate radical concentrations at Lille Valby have been calculated by the ACDEP model. As the meteorological data for 1998 were not available at the time of the calculations, data from 1997 were used. The nightly nitrate radical concentrations shown in Figure 5.1 are for the trajectories arriving at the Lille Valby

station at midnight. The modelled nitrate radical concentrations are shown in Figure 5.1.

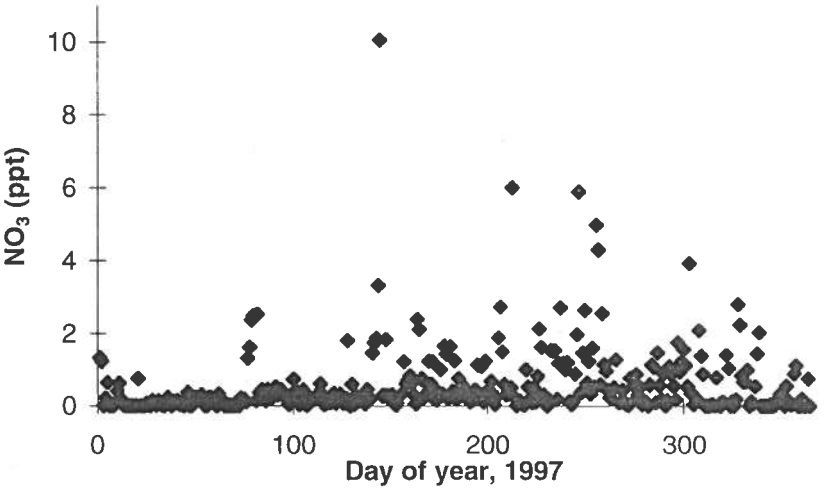

Figure 5.1 Night-time (Midnight) nitrate radical concentrations, 1997, calculated by the ACDEP model.

Average nitrate radical concentrations

The average nitrate radical concentration for 1997 is 0.33 ppt. Although, meteorological data for 1997 was used instead of data for 1998, this should not alter the level of the nitrate radical concentrations markedly. Thus, the low average nitrate radical concentration cannot be explained by the fact that the meteorology data used were from 1997.

Comparison with DOAS measurements

The DOAS measurements of NO_3 did not exceed the detection limit of 25 ppt throughout the measurement period of April - September, 1998. This in accordance with the calculated yearly night-time NO_3 concentrations of 0.33 ppt suggests that the nitrate radical concentrations at Lille Valby are in the order of a few ppt. This was concluded in section 4.5. Thus, the ACDEP model calculations suggests that in order to measure the nitrate radical at Lille Valby, the detection limit should be lowered considerably to at least a few ppt.

5.3.2 Nitrate radical production rates

Modelled production rates

For comparison with DOAS measurements the modelled nitrate radical production rates at Lille Valby 1997 were calculated. The calculations are based on the trajectories arriving at the Lille Valby station at midnight, as for the nitrate radical concentrations. The nitrate radical production rate is found as:

$$d[NO_3]/dt = k\,[NO_2][O_3]$$

;where $k = 1.2 * 10^{-13} \exp(-2450/T)$ $cm^3 molecule^{-1} s^{-1}$ and k is for the reaction of NO_2 with O_3 to produce NO_3 [De more et. al, 1997]. Figure 5.2 below shows the calculated production rates for 1997.

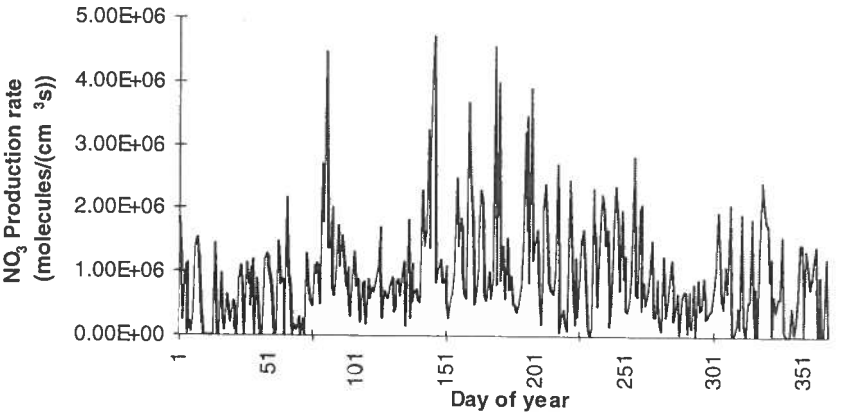

Figure 5.2 Nitrate radical production rates calculated from ACDEP model data, 1997. The calculations are for the trajectories arriving at Lille Valby at midnight.

Figure 5.2 shows that the highest production rates occur in the spring and summer periods.

Comparison with DOAS production rates

The monthly averaged production rates, calculated from the ACDEP model data for April, May, June and July, 1997, are given below in Table 5.1 For comparison the production rates for 1998, calculated from the DOAS data is included.

Table 5.1 Nitrate radical production rates at Lille Valby. 1997 ACDEP model data and 1998 DOAS data.

Month	DOAS data Lille Valby 1998 Average production rate moleculescm^{-3}s^{-1}	ACDEP Model Lille Valby 1997 Average production rate moleculescm^{-3}s^{-1}
April	$4.04 * 10^6$	$8.5 * 10^5$
May	$2.29 * 10^6$	$1.29 * 10^6$
June	$2.03 * 10^6$	$1.54 * 10^6$
July	$1.22 * 10^6$	$1.28 * 10^6$

Model/DOAS production rates

From Table 5.1 it is seen that the production rates calculated from the DOAS and ACDEP model data respectively are of the same magnitude. Also the same decrease in production rates is observed for both data sets. However, for the month of April, the DOAS and ACDEP calculated production rates differ by a factor of 5. Clearly, the best correspondence is that for July. Also, the nitrate radical production rates calculated by the ACDEP model are in the same range as those found by Ljungstrøm *et al.*, Table 4.9.

5.4 Diurnal variations in HNO_3 production

In order to compare the importance of night-time production of HNO_3, at a NO_3 concentration level of 0.33 ppt, relative to the day-time source of HNO_3, these were calculated using ACDEP data.

Night-time production of HNO_3

The equilibrium between N_2O_5, NO_3 and NO_2 and the hydrolysis of N_2O_5 to produce HNO_3 constitutes a night-time source of nitric acid. This night-time source of HNO_3 thus depends on the nitrate radical concentration level. At a NO_3 concentration level of 0.33 ppt, the calculated production rates of HNO_3 through the hydrolysis reaction is given in Figure 5.3 The yearly averaged production rates for the night-time HNO_3 production is $1.4 * 10^{-2}$ ppt/s.

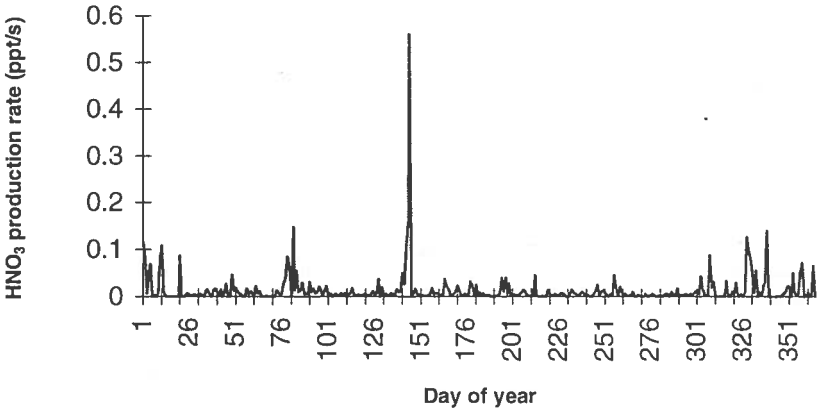

Figure 5.3 Night-time HNO_3 production rates calculated from ACDEP data. The reaction rate used is from the ACDEP model and is $0.4750 * 10^{-3}$ s^{-1} [Hertel, O., 1995].

Day-time production of HNO_3

At day-time the most important HNO_3 formation reaction is that of OH with NO_2. The calculated production rates of HNO_3 for the day-time reaction is given in Figure 5.4. The average yearly production rate is $2.08 * 10^4$ ppt/s.

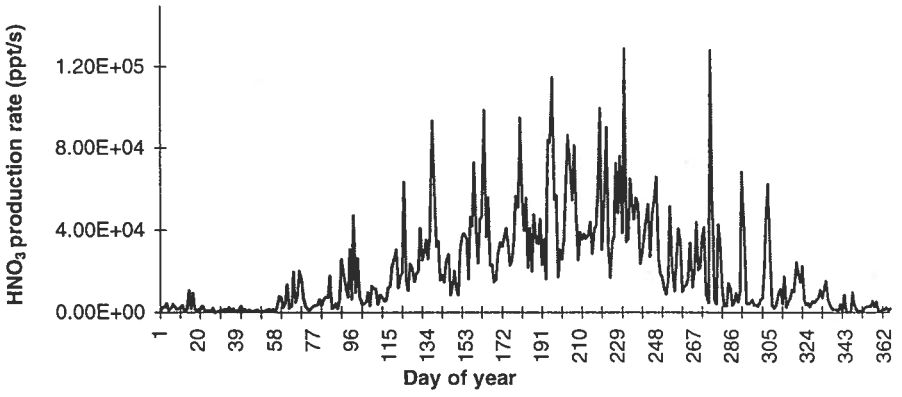

Figure 5.4 Day-time HNO_3 production rates calculated from ACDEP data. The reaction rate used is from the ACDEP model and is $0.2717 ppb^{-1}s^{-1}$ [Hertel, O. *et al*, 1995].

Day- and night-time HNO_3 production

The day-time HNO_3 production of $2.08 * 10^4$ ppt/s, totally dominates the overall HNO_3 production rate at a nitrate radical concentration level of 0.33 ppt. At this nitrate radical concentration level the average night-time HNO_3 production rate is only $1.4 * 10^{-2}$ ppt/s. Wayne *et al.* states that the daytime production of HNO_3 from the reaction of OH + NO_2 matches the yearly-averaged yield of nitric acid

from NO_3 and N_2O_5 in certain parts of the Northern hemisphere [Wayne *et al.*, 1991]. Thus, this seems not to be the case at Lille Valby.

NOx turnover

Thus, at nitrate radical levels of a few ppt or less, as assumed for Lille Valby, the NOx turnover is not markedly enhanced by night-time loss of HNO_3 through N_2O_5 hydrolysis.

5.5 Conclusions

Lille Valby nitrate radical concentration level

The observed and modelled nitrate radical concentrations at Lille Valby both show very low levels - in the order of a few ppt or less. The low levels could be due to the NO levels in the model being too high for a background like Lille Valby. However, the emissions are graduated in the model, so that only 1/3 occur during night-time.

Nitrate radical production rates

The peak nitrate radical production rates are in the order of 10^{6} molecules/(cm^3s), for the ACDEP model results as well as for the production rates calculated from the DOAS data.

Diurnal variation in HNO_3 production rate

The day-time HNO_3 production rate of 2.08 * 10^4 ppt/s, dominates the overall HNO_3 production rate at a nitrate radical concentration level of 0.33 ppt.

NOx turnover

Thus, this suggests that the NOx turnover at Lille Valby is not enhanced by night-time NO_3 chemistry (at NO_3 concentration levels of 0.33 ppt), especially the heterogeneous removal of N_2O_5, believed to be the dominant loss process at Lille Valby as concluded in chapter 4.5.

6 Implementation of a chemical reaction scheme

6.1 Introduction

The chemical reaction scheme which is currently being used in the ACDEP model is a modified version of the lumped mechanism CBM IV. In order to introduce a new explicit chemical reaction scheme into the ACDEP model a new chemical reaction scheme is implemented in a simple box-model. Explicit reaction schemes have the advantage of being easier to update, than lumped reaction schemes like the CBM-IV. Test and update of the reaction scheme can then be performed in the box-model, before the new reaction scheme is finally implemented in the ACDEP model.

6.2 Implementation and update of a new chemical reaction scheme

A routine for solving a new chemical reaction scheme was constructed for future use in the ACDEP-model. The reaction scheme was developed at the University of Bergen for modelling chemical processes in the troposphere [Strand and Hov, 1994]. It is the intention to further modify the reaction scheme by improving specific parts. These parts include heterogeneous chemistry, dry-deposition, nitrate radical chemistry, isoprene chemistry and more. Thus, the modification and update of the chemical reaction scheme, UiB (University in Bergen), includes:

1. Update of reaction rates.
2. Division of reactions into heterogeneous and homogeneous modules.
3. Division into groups of S-chemistry, N-chemistry, photolysis reactions etc.
4. Exclusion of obsolete reactions.
5. Addition of reactions based on:
   - implementation of heterogeneous module.
   - new reaction mechanisms not previously included.
   - implementation of specific modules dedicated to describe chemistry of particular interest (NO_3, isopren etc.).
6. Documentation of the above steps.
7. Verification of the resulting chemical reaction scheme.
8. Implementation and verification of the scheme in the ACDEP model.

6.2.1 The UiB chemical reaction scheme

A major motivation for using condensed reaction schemes like the Carbon-Bond Mechanism in early transport-chemistry models of complex chemistry was the limited computing capacity of the current

computers. However, the continuous increase in computational power allows the use of still more complex reaction schemes, in which practically all species are represented explicitly.

6.2.2 Differences from the Carbon-Bond Mechanism (CBM-IV)

In the new chemical reaction scheme, UiB, all species are represented explicitly. The scheme includes 116 reactions involving 52 species. In contrast with the CBM-IV all reactions of organics are treated explicitly. In the CBM-IV the oxidation of NO to NO_2 by peroxy radicals was represented by a single universal peroxy radical. In the new scheme several specific NO-peroxy radical reactions are listed.

The species concentrations are calculated using the iterative procedure called the Euler Backward Iterative (EBI) as previously described in chapter 5. If a group of species interact strongly with each other, extremely small time steps are needed in order to ensure convergence. In order to avoid this, the concentrations of strongly coupled species are calculated by solving the system describing the interactions. The groups that are in this way solved semi-explicitly are

- NO, NO_2, O_3 and O (^3P)
- PAN and CH_3COO_2
- NO_3 and N_2O_5
- OH, HO_2, HNO_2 and HNO_4
- NH_3, HNO_3 and NH_4NO_3

The solutions are found by solving systems like those in equation (5.4) and (5.5). The remaining concentrations are found using equation (5.3).

6.2.3 Update of reaction rates.

In order to ensure that the reaction rates used in the chemical reaction scheme are consistent with the current knowledge, they have to be updated on a regular basis. For the reactions given below, the reaction rates have in this way been updated compared with Asbjørn and Hov (1994). The updating of reaction rates is only in the start phase. However, some examples of reaction rates that should be updated are given below.

The reaction:

$$NO + HO_2 \rightarrow NO_2 + OH$$

in the UiB reaction scheme had the reaction rate:

$3.7 * 10^{-12} * \exp (250/ T(n))$ (molecules $cm^{-3} s^{-1}$)[DeMore *et al.*, 1992].

Should be updated to:

$3.5 * 10^{-12} * \exp(250/T(n))$ (molecules $cm^{-3} s^{-1}$)[DeMore *et al.*, 1997].

The reaction:

$$OH + NO_2 + M \rightarrow HNO_3$$

in the UiB reaction scheme has the reaction rate:

k_0^{300}	k_∞^{300}	F_c
2.6E-30(T(n)/300)**(-3.2) * M(n)*	*2.4E-11* (T(n)/300) **(-1.3)*	*0.6*

[DeMore *et al.*, 1992].

Should be updated to:

k_0^{300}	-n	k_∞^{300}	-m	F_c
2.5 ± 0.1 E-30	-4.4 ± 0.3	1.6 ± 0.2 E-11	-1.7 ± 0.2	0.6

[DeMore *et al.*, 1997].

The reaction:

$$2\,NO_3 \rightarrow 2\,NO_2 + O_2$$

in the UiB reaction scheme had has the reaction rate $2.7 * 10^{-16}$ [Wayne, 1991]. Should be replaced by $2.3 * 10^{-16}$ [DeMore *et al.*, 1997].

All reactions in the UiB mechanism should be checked in this way.

6.2.4 Division into groups

In order to obtain a better overview of the reaction scheme the reactions were divided into groups. More groups will be added as the work progresses, depending on fields of interest etc. At present groups of reactions of N-chemistry, S-chemistry, peroxyradicals and photolysis reactions exist. Thus, these groups of reactions can be updated and modified separately. The species in the various groups are:

Nitrogen Species: *NO, NO_2, NO_3, N_2O_5, HNO_3, HNO_4, HONO*

Sulfur Species: *SO_2, Sulphate*

Peroxyradicals: *CH_3O_2, $C_2H_5O_2$, sec$C_4H_9O_2$, $CH_3COCHO_2CH_3$, $CH_2O_2CH_2OH$, $CH_3CHO_2CH_2OH$, $OXYLOHO_2$, $MemalO_2$, $OxylO_2$, $IsopO_2$, $MVKO_2$*

Heterogeneous and homogeneous reactions

One of the aims of the chemical reaction scheme update is to get a clear separation of homogeneous and heterogeneous reactions. This is done in order to be able to treat the heterogeneous chemistry far better in the resulting chemical reaction scheme than in that used today. As an example, the separation of reactions relating to nitrogen chemistry is shown below.

Table 6.1 Reactions of nitrogen species in the UiB shemical reaction scheme, divided into homogeneous and heterogeneous reactions.

Homogeneous Nitrogen Reactions	
Reactants	Products
$O(^3P)$+ NO	> NO_2
O_3 + NO	> NO_2
O_3 + NO_2	> NO_3
NO + NO_3	> 2 NO_2
NO + HO_2	> NO_2
NO_2 + NO_3	> NO + NO_2
NO_2 + NO_3	> N_2O_5
NO_2 + OH	> HNO_3
2 NO_3	> 2 NO_2
NO_3 + H_2O_2	> HO_2 + HNO_3
N_2O_5	> NO_2 + NO_3
NO_2 + HO_2	> HNO_4
HNO_4	> NO_2 + HO_2
OH + HNO_4	> NO_2
OH + HNO_3	> NO_3
HONO + OH	> NO_2 + H_2O
NO + OH	> HONO
Heterogeneous nitrogen reactions	
N_2O_5 + H_2O	> 2 HNO_3
HONO + HONO	> NO + NO_2 + H_2O
NO + NO_2 + H_2O	> HONO + HONO

6.2.5 Exclusion of obsolete reactions

The reaction in the UiB mechanism:

$$O(^3P) + NO \xrightarrow{M} NO_2 \qquad (1)$$

has no practical importance in tropspheric chemistry compared with the reaction:

$$O_2 + O(^3P) \xrightarrow{M} O_3 \qquad (2)$$

as the ratio $k_1[NO]/k_2[O_2]$ is $2 * 10^{-6}$ as calculated below.

$$k_1 = d[NO_2]/dt = k_1[NO][O(^3P)]$$

$$k_2 = d[O_3]/dt = k_2[O_2][O(^3P)]$$

$$\Rightarrow k_1/k_2 = k_1[NO]/k_2[O_2]$$

If the concentration of NO is 10 ppt = $2.46 * 10^8$ molecules cm^{-3} and the concentration of O_2 is $0.157 * 2.65 * 10^{19}$ molecules cm^{-3} = $4.16 * 10^{18}$ (The pressure at 2000 m is reduced to 0.785 % of the ground pressure. The density of atmospheric air is $2.65 * 10^{19}$ molecules cm^{-3}. The temperature at 2000 m is 275 K).

$k_{0,1}^{300} = 9 * 10^{-32}$, n = 1.5
$k_{0,1}^{275} = k_{0,1}^{300}(275/300)^{-n} = 1.025 * 10^{-31}$

$k_{\infty,1}^{300} = 3.0$, n = 0
$k_{\infty,1}^{275} = k_{\infty,1}^{300}(275/300)^{-n} = 3.0 * 10^{-11}$

; where $k_{0,1}^{300}$ is the low pressure limit for reaction (1) and $k_{\infty,1}^{300}$ is the high pressure limit for reaction (1) [DeMore *et al.*, 1997].

$$k_1^{2000m} = \frac{k_0(T)[M]\ k_\infty(T)[M]}{k_0(T)[M] + k_\infty(T)[M]} F_c^{\left(\frac{1}{1+\log_{10}(k_0(T)[M]/k_\infty(T)[M])^2}\right)}$$

; where $F_c = 0.6$ and using M = 0.785 instead of $4.16 * 10^{18}$ molecules cm^{-3} as only the ratio is important gives:

$k_1^{2000m} = 2.3 * 10^{-29}$

;likewise using $k_{0,2}^{300} = 6.0 * 10^{-34}$, n = 2.3 (No k_∞ was given for reaction (2) [DeMore *et al.*, 1997])

$k_2(M,T) = k_1^{2000m} = 7.3 * 10^{-34}$

Thus,

$k_1[NO]/k_2[O_2] =$
$(2.31 * 10^{-29} * (2.46 * 10^8/2.65 * 10^{19})/(7.3 * 10^{-34} * 0.157)$
$= 2 * 10^{-6}$

Hence reaction 1 is of insignificant importance relative to reaction 2 and can be excluded from the UiB reaction scheme.

6.2.6 Addition of reactions

Including reactions of HONO

The UiB reaction mechanism does not include HONO as a species, or any of its reactions. To compensate for this HONO was introduced as species nr. 52 and 4 reactions were included. These are given below.

$HONO + HONO \rightarrow NO + NO_2 + H_2O$
$NO + NO_2 + H_2O \rightarrow HONO + HONO$
$HONO + OH \rightarrow NO_2 + H_2O$
$NO + OH \rightarrow HONO$

Further reactions can be added in order to study specific parts of the chemistry, such as isoprene chemistry, or nitrate radical chemistry, more thoroughly.

6.3 Implementation of the UiB chemical reaction scheme

The UiB chemical reaction scheme was implemented in an existing simple box-model. Thus, the new chemical reaction scheme can be thoroughly tested before it is implemented in the ACDEP model.

Input to the box-model

The start time of simulation (month, day, hour), time step interval (in seconds) and the number of time steps to be performed must be supplied to the box-model. Thus, for 1500 time steps of 100 seconds each, the simulation will run for 41.66 hours.

Emissions input parameters

The emissions and initial concentrations of the various species must be supplied. The following emission estimates were used for simulating Danish background conditions, like Lille Valby.

$$E\_NOx = 1.4 * 10^6 \text{ ton } NO_2/km^2/y$$
$$E\_SOx = 0.71 * 10^6 \text{ ton } SO_2\text{-}S/km^2/y$$
$$E\_VOC = 1.4 * 10^7 \text{ ton } CH/km^2/y$$

Meteorological input parameters

The cloudiness (cloud cover in per cent), relative humidity, temperature and water vapor content must be specified as well.

6.4 Modelling N_2O_5 chemistry

Because the nitrate radical is in rapid equilibrium with N_2O_5, the heterogeneous formation of nitric acid from N_2O_5 (g) and H_2O(l), constitutes an important sink for the nitrate radical (and NOx). The hydrolysis reaction:

$$N_2O_5\,(g) + H_2O\,(l) \rightarrow 2\,HNO_3\,(aq) \qquad (6.1)$$

is the most important loss mechanism for the nitrate radical at Lille Valby (section 4.5). Thus, the effect of the rate of heterogeneous removal of N_2O_5 on the nitrate radical concentration level was studied, using the simple box-model described above.

Heterogeneous loss of N_2O_5 by a box model

In order to investigate the effect of the rate of heterogeneous removal of N_2O_5 on the nitrate radical concentration level the reaction rate of the heterogeneous removal of N_2O_5 was changed in the Box-model, and the subsequent change in the nitrate radical concentration level observed. As can be seen from Figure 6.1 below, changing the heterogeneous loss rate of N_2O_5 has a pronounced effect on the nitrate radical concentration levels.

Nitrate radical dependence on N_2O_5 loss

As can be seen from Figure 6.1, a 1.order loss rate for N_2O_5 of $2 * 10^{-10}$ s^{-1} results in a nitrate radical concentration of 7.3 ppt. Loss rates of $2 * 10^{-9}$ and $2 * 10^{-6}$ s^{-1} results in concentrations of 3.7 ppt and 2.0 ppt respectively. Further increasing the loss rate did not result in a pronounced reduction of the nitrate radical concentration level. The homogeneous loss rate used was the upper limit rate of $1.3 * 10^{-21}$ cm^3 $molecule^{-1}s^{-1}$ [F.-Pitts and Pitts, 1986]. Thus, the nitrate radical concentration is greatly dependent on the heterogeneous rate of N_2O_5 loss.

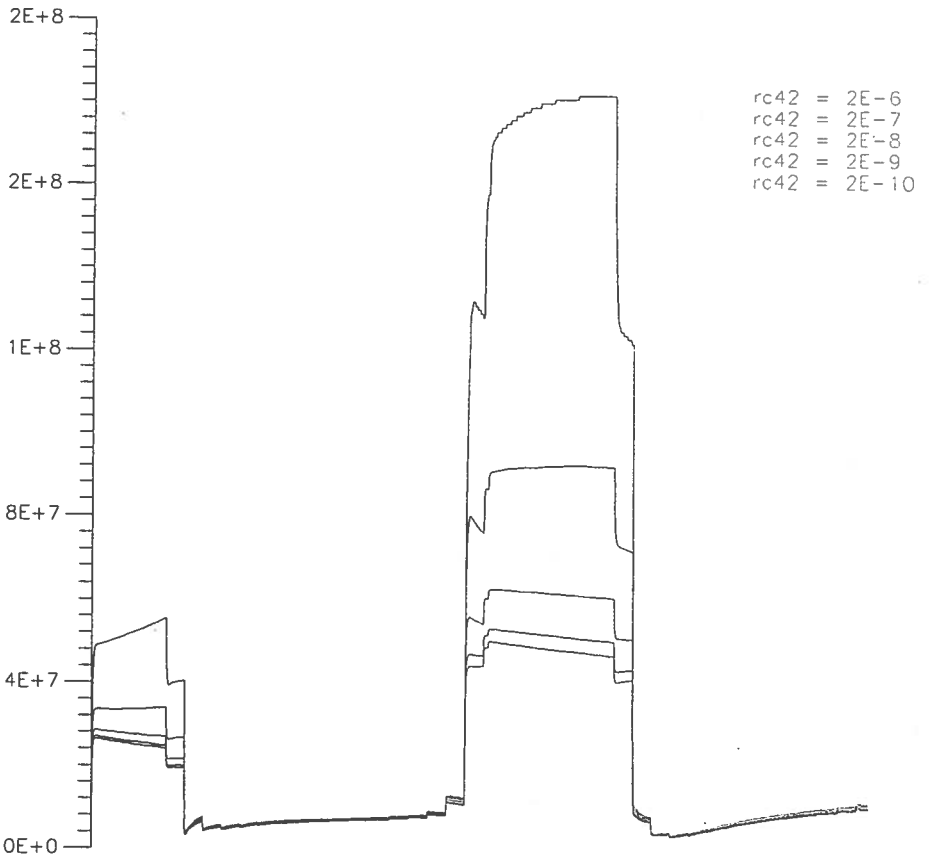

Figure 6.1 The nitrate radical concentration level at varying reaction rates of heterogeneous loss of N_2O_5. The nitrate radical concentration are in molecules/cm^3. The reaction rates are in s^{-1}. The initial concentrations of N_2O_5, NO_3, NO_2, NO and O_3 were 0, 0, 10, 0.5 and 40 ppb respectively.

6.5 Verification of the model

Before the new chemical reaction scheme is adapted for use in the ACDEP model it should be thoroughly tested and verified. This can be done either by comparison of product simulations with environmental chamber data or by incorporating the chemical reaction scheme into an already verified tropospheric model for comparison with atmospheric measurement data [Jenkin *et al.*, 1997].

6.6 Conclusions

The new chemical reaction scheme

The work of updating and modifying the UiB chemical reaction scheme for future implementation in the ACDEP model has only just been initiated.

Heterogeneous loss of N_2O_5

Changing the heterogeneous loss rate of N_2O_5 has a pronounced effect on the box-model nitrate radical concentration levels.

7 Conclusion

The DOAS technique

The DOAS technique offers a reliable, accurate and specific measurement of tropospheric species, with great time resolution, provided that maintenance of the instrument and quality control of the measurement data is kept at a high level. Also, temperature and pressure corrections of the DOAS data should be performed. However, in the case of NO_3 measurements, the interference from H_2O needs to be eliminated properly. In general, uncertainties in the absorption cross sections, and unaccounted for interfering species, will result in errors in the DOAS measurements.

The OPSIS DOAS system

It would be desirable if OPSIS supplied more information on the evaluation of spectra and the wavelength regions used. Also, an improved, user friendly software interface, is highly recommended.

DOAS replacing monitors

Before DOAS instruments can replace monitor measurements, results of the two measurement methods should be compared and discrepancies between the methods should be investigated and understood. On this basis it must be decided, if DOAS measurements can replace the monitor techniques.

NO_2 DOAS measurements

The NO_2 calibration of the DOAS instrument showed that the DOAS technique is capable of measuring NO_2 with the desired accuracy. However, the Lille Valby NO_2 measurements also show that in order to ensure quality measurements, maintenance, such as regular reference calibration, and quality control of the data must be kept at a high level. In particular, a more stable light level is desirable.

DOAS/monitor NO_2 correlation

The analysis of the correlation between the DOAS and monitor NO_2 measurement methods does reveal discrepancies between the two methods. Except for April, 1998, the monthly average NO_2 concentrations are higher for the monitor, than for the DOAS. The dependence of correlation's, between the DOAS and monitor measurement methods, upon ozone concentration levels, supports the theory, that discrepancies lies partly in the amount of gaseous nitrogen species other than NO_2, that are reduced in the NOx monitor. The study of Ziv and Iakovleva shows that the discrepancy between the methods is dependent on temperature. This should be further investigated by comparing monitor data with temperature corrected DOAS data.

DOAS replacing NO_2 monitors

DOAS measurements could effectively replace monitor NO_2 measurements if the data quality control and instrument maintenance is kept at a high level, and temperature and pressure corrections are performed.

O_3 DOAS measurements

Very few negative standard deviations and no negative concentrations are observed throughout the measurement period. Indicating that the evaluation of the O_3 spectra has converged properly.

DOAS/monitor O_3 correlation

In general the monitor ozone concentrations are higher than the corresponding DOAS ozone concentrations. This results in average monthly ozone concentrations being higher for monitor than DOAS

data. The correlation between the methods is slightly improved when the DOAS ozone measurements are temperature corrected, but could not account for the extent of descrepancy observed.

DOAS replacing O_3 monitors

The analysis of the correlation between the DOAS and monitor O_3 measurements methods reveals discrepancies between the two that are not fully understood. Before DOAS ozone measurements can replace monitor ozone measurements, the discrepancies between the methods should be further investigated. Also, temperature and pressure corrections of the DOAS data should be performed.

Nitrate radical DOAS measurements

The measurements of the nitrate radical at Lille Valby, were originally motivated by the wish to study a new method for determining the nitrate radical concentration, using the DOAS technique. However, this could not be done as the concentration level of NO_3 was below the detection limit.

NO_3 concentration levels at Lille Valby

The fact that all measurements of the nitrate radical at Lille Valby, 1998, was below the detection limit of 25 ppt, suggests that the nitrate radical concentration is low. Calculations of the nitrate radical concentrations at Lille Valby by the ACDEP-model, indicates an average night time nitrate radical concentration of 0.33 ppt. Thus, the night-time nitrate radical concentrations at Lille Valby are likely to be in the order of a few ppt or less. The lifetime and loss mechanisms of the nitrate radical could not be calculated, due to the concentration level below the detection limit. Production rate calculations showed that some loss mechanism must be in operation. However the loss mechanism could not be studied due to the concentrations being below the detection limit.

Elevated nitrate radical concentrations

Elevated concentrations of the nitrate radical would be expected only during transport episodes of photochemical air pollution from central Europe, with high ozone concentration levels and a low $[NO]/[NO_2]$ ratio.

HONO measurements

The nitrous acid concentration levels were found to be below the detection limit of 0.33 ppb. This is in accordance with other studies of the background level.

Modelling studies

ACDEP model calculations predicts a nitrate radical concentration level at Lille Valby of 0.33 ppt. The nitrate radical production rates calculated form ACDEP model NO_2 and O_3 data, were of the same magnitude as those calculated using DOAS NO_2 and O_3 data. The HNO_3 production rates calculated from ACDEP model data suggests that the night-time HNO_3 production, via N_2O_5 hydrolysis, is of minor importance in NOx turnover at Lille Valby, compared to the daytime production via the OH, NO_2 reaction. Finally, the heterogeneous removal rate of N_2O_5 via hydrolysis, was shown to influence on the nitrate radical concentration level as expected.

Future suggestions

In order to study the nitrogen chemistry at Lille Valby, in particular the nitrate radical and nitrous acid, the detection limit of the DOAS system should be greatly reduced. This could be achieved by a longer path length.

Acknowledgements

I would like to acknowledge the following persons:

My supervisors, Henrik Skov, National Environmental Research Institute and Torben Stroyer Hansen, Department of Chemistry, University of Odense, for advise and feedback. Ole Hertel for supervision on the modelling part and for use of the ACDEP data. NERI for use of the Lille Valby DOAS instrument, computers etc. Everybody at ATMI. Poul Hummelshøj (Risø) for meteorology data from the RIMI-project. NMR for financial support. Christian Lohse for financial support. Carsten Stenholt for speeding up things. Lillian, Lars and Poul for always feeling welcome in their home. H.H. Hoff for acknowledgement. My family for financial support. Klaus for financial support and nerd-assistance. Ib for everything.

References

Advanced pollution Instrumentation, Inc.6565 Nancy Ridge Drive, San Diego, CA. 92121 - 2251

Alexis, N., Tarlo, S.M. and Silverman, F. 1994. Effects of ozone in human studies. In Environmental Oxidants, Volume 28 in the Wiley series Advances in Environmental Science and Technology, John Wiley & Sons, Inc., US.

Allegrini, I., febo, A., Giliberti, C. and Giusto, M. 1996. Measurement of photochemical pollution in the urban environment of Rome by means of a proper cpmbination of DOAS and atmospheric stability monitor. OPSIS, RAP-85. OPSIS AB, Furulund.

Ammann, M., Kalberer, M., Jost, D.T., Tobler, L., Rossler, E., Piguet, D., Gaggeler, H.W. and Baltensperger, U. 1998. Nature, Vol. 395.

Atkinson, R., Winer, A.M. and Pitts, J. N. JR. 1996. Estimation of night-time N_2O_5 concentrations from ambient NO_2 and NO_3 radical concentrations and the role of N_2O_5 in night-time chemistry. Atmospheric Environment. Vol. 20, No. 2, pp. 331-339.

Atkinson, R., Baulch, D.L., Cox, R.A., Hampson Jr, J.F., Kerr and Troe, J. 1992. Evaluated kinetic and photochemical data for atmospheric chemistry: Supplement IV. In J. Phys. Ref. Data, Vol. 21, No. 6, 1992.

Atkinson, R., Baulch, D.L., Cox, R.A., Hampson Jr, J.F., Kerr, J.A., Rossi, M.J. and Troe, J. 1997. Evaluated kinetic, photochemical and heterogeneous data for atmospheric chemistry: Supplement V. In J. Phys. Ref. Data, Vol. 26, No. 3, 1997.

Atkinson, R., Baulch, D.L., Cox, R.A., Hampson Jr, J.F., Kerr, J.A., Rossi, M.J. and Troe, J. 1997. Evaluated kinetic, photochemical and heterogeneous data for atmospheric chemistry: Supplement VI. In J. Phys. Ref. Data, Vol. 26, No. 6, 1997.

Axelsson, H., Edner, H., Galle, B., Ragnarson, P. and Rudin, M. 1990. Differential optical absorption spectroscopy (DOAS) measurements of ozone in the 280-290 nm wavelength region. Applied Spectroscopy, Vol. 44, No. 10.

Behnke, W., Kruger, H.-U., Scheer, V., Zetzsch, C. 1991. Formation of atomic Cl from sea spray via photolysis of nitryl chloride: Determination of the sticking coefficient of N_2O_5 on NaCl aerosol. J. Aerosol Sci., Vol. 22, Suppl. 1, pp. S609-S612.

Camy-Peyret, C. et al. 1996. Intercomparison of instruments for tropospheric measurements using differential optical absorption spectroscopy. Journal of Atmospheric Chemistry, 23: 51-80.

Crutzen, P.J., Lawrence, M.G. and Poschl, U. 1999. On the background photochemistry of tropospheric ozone. Tellus (1999), 51 A-B, 123-146. Munksgaard, Denmark, 1999.

DeMore, W.B., Molina, M.J., Sander, S.P., Golden, D.M., Hampson, R.F., Kurylo, M.J., Howard, C.J. and Ravishankara, A.R. 1987. Chemical kinetics and photochemical data for use in stratospheric modeling. Evaluation Number 8. NASA, jet propulsion Laboratory, Pasadena, US.

Derwent, R.G., Jenkin, M.E. 1991. Hydrocarbons and the long-range transport of ozone and PAN across Europe. Atmospheric Environment. Vol. 25A, No. 8, pp. 1661-1678.

Derwent, R.G., Jenkin, M.E. and Saunders, S.M. 1996. Photochemical ozone creation potentials for a large number of reactive hydrocarbons under European conditions. Atmospheric Environment. Vol. 30, No. 2, pp. 181-199.

Derwent, R.G., Jenkin, M.E., Saunders, S.M. and Pilling, M.J. 1998. Photochemical ozone creation potentials for organic compounds in northwest Europe calculated with a master chemical mechanism. Atmospheric Enivronment, Vol. 32, No. 14/15, pp. 2429-2441.

Dongfen, G., m.fl. 1995. "First-order sensitivity and uncertainty analysis for a regional-scale gas-phase chemical mechanism".

Dongfen, G., m.fl. (96). "Global uncertainty analysis of a regional-scale gas-phase chemical mechanism".

Fenger, J. 1997. En atmosfære med voksende problemer... Historien om luftforurening. TEMA-rapport fra DMU nr. 11/1997. National Environmental Research Institute, Roskilde, DK.

Fenter, F.F., Caloz, F. and Rossi, M.J. 1996. Heterogeneous kinetics of N_2O_5 uptake on salt, with a systematic study of the role of surface presentation (for N_2O_5 and HNO_3). J. Phys. Chem., Vol. 100, No. 3.

Finlayson-Pitts, B.J. and Pitts, J.N. 1986. Atmospheric chemistry: Fundamentals and experimental techniques. John Wiley & Sons, New York, US.

Flatøy, F., Hov, Ø., Smit, H. 1995. Three-dimensional model studies of exchange processes of ozone in the troposphere over Europe. Journal of of geophysical research, Vol. 100, No. D6, pp. 11465-11481.

Gard, E.E., Kleeman, M.J., Gross, D.S., Hughes, L.S., Allen, J.O., Morrical, B.D., Fergenson, D.P, Dienes, T., Galli, M.E., Johnson, R.J., Cass, G.R., Prather, K.A. 1998. Direct observation of heterogeneous chemistry in the atmosphere. Science, Vol. 179.

Graedel, T.E. and Crutzen, P.J. 1993. Atmospheric change: An earth system perspective. W.H. Freeman and Co., New York, US.

Galle, B., Axelsson, H., Bergqvist, B., Eilard, A., Mellqvist J. and Zetterberg, L. 1997. Development of DOAS for atmospheric trace species

monitoring. Instrument development for atmospheric research and monitoring, Eurotrac, Vol. 8, Lidar profiling, DOAS and tunable diode laser spectroscopy. Springer-Verlag Berlin Heidelberg, Germany.

Gao, D., Stockwell, W.R., Milford, J.B. 1995. First-order sensitivity and uncertainty analysis for a regional-scale gas-phase chemical mechanism. Journal of Geophysical Research, Vol. 100, No. D11, pp. 23,153-23,166.

Gao, D., Stockwell, W.R., Milford, J.B. 1996. Global uncertainty analysis of a regional-scale gas-phase chemical mechanism. Journal of Geophysical Research, Vol. 101, No. C4, pp. 9107-9119.

Gery, M.W., Whitten, G.Z., Killus, J.P. and Dodge, M.C. 1989. A photochemical kinetics mechanism for urban and regional scale computer modeling. Journal of geophysical research, Vol. 94, No. D10.

Granby, K. 1997. Tropospheric measurements of photochemical products. PhD Thesis. National Environmental Research Institute, Roskilde, Denmark, 133 pp.

Heintz, F., Platt, U., Flentje, H., Dubois, R. 1996. Long-term observation of nitrate radicals at the Tor station, Kap Arkona (Rugen). Journal of geophysical research, Vol. 101, No. D17, pp. 22891-22910, october 20, 1996.

Hertel, O., Berkowicz, R., Christensen, J. and Hov,Ø. 1993. Test of two numerical schemes for use in atmospheric transport-chemistry models. Atmospheric Environment Vol 27A, No. 16, pp. 2591-2611.

Hertel, O., Skov, H., Ellermann, T., 1996. Aerosol contribution to Nitrogen deposition to Danish waters 1989-95. Poster in the proceedings of NOSA/NORSAC Symposium 1996 (Ed. Poul Hummelshøj), Elsingore, Denmark, Nov. 15-17 1996. Risø-R-934 (EN). pp 102-104.

Hertel, O. 1995. Transformation and deposition of sulphur and nitrogen compounds in the marine boundary layer. Dr. Scient thesis. National Environmental Research Institute, Roskilde, Denmark. 215 pp.

Hertel, O. 1995. Luftforurening. Kompendium om parametrisering af kemiske reaktioner i atmosfæren. Kemisk Institut, Københavns Universitet, s.71.

Hertel, O., Christensen, J., Runge, E.H., Asman, W. A. H., Berkowicz, R., Hovmand M. and Hov, Ø. Development and testing of a new variable scale air pollution model - ACDEP, Atmospheric Environment Vol. 29. No 11., 1995.

Hertel, O. and Skov, H. 1996. Evaluation of the aerosol contribution to the nitrogen load to Danish waters 1989-94. J. Aerosol Sci., Vol. 27, suppl. 1, pp. S59-S60.

Hjorth, J., Lohse, C., Nielsen, C.J., Skov, H. and restelli, G. 1990. Products and mechanisms of the gas-phase reactions between NO_x and a series of alkenes. The journal of physical chemistry, Vol. 94, No. 19.

Hjorth, J., Notholt, J., Restelli, G. 1992. A spectroscopic study of the equilibrium $NO_2 + NO_3 + M \leftrightarrow N_2O_5 + M$ and the kinetics of the $O_3/N_2O_5/NO_3/NO_2$/air system. International Journal of chemical kinetics, Vol. 24, 51-65.

Holten-Andersen, J., Christensen, N., Kristiansen, L.W., Kristensen, P. and Emborg, L. 1997. The state of the environment in Denmark, 1997. NERI, Technical report No. 243. National Environmental Research Institute, Roskilde, Denmark.

Jenkin, M.E., Saunders, S.M. and Pilling, M.J. 1997. The tropospheric degradation of volatile organic compounds: A protocol for mechanism development. *Atmospheric Environment* Vol 31, No. 1, pp. 81-104.

Jensen, N.R., Hjorth, J., Lohse, C., Skov, H. and Restelli, G. 1991. Products and mechanism of the reaction between NO_3 and dimethylsulphide in air. Atmospheric environment Vol. 25A, No. 9.

Kuhn, M., P.J.H. Builtjes, m. fl. 1998. Intercomparison of the gas-phase chemistry in several chemistry and transport models. Atm. Env. Vol. 32, No. 4, pp. 693-709.

Lelieveld, J. and Crytzen, P.J. 1991. The role of clouds in tropospheric photochemistry. Journal of Atmospheric Chemistry 12: 229-267.

Ljungstrom E. and Hallquist, M. 1996. Nitrate radical formation rates in scandinavia. Atmospheric Environment Vol. 30, No. 16, pp. 2925-2932.

Manahan, S.E. 1994. Environmental chemistry. Lewis Publishers. CRC Press, Inc. US.

Miller, J.C. and Miller, J.N. 1993. Statistics for analytical chemistry, third edition. Ellis Horwood and Prentice Hall, GB.

Mustafa, M.G. 1994. Health effects and toxicology of ozone and nitrogen dioxide. In Environmental Oxidants, Volume 28 in the Wiley series Advances in Environmental Science and Technology, John Wiley & Sons, Inc., US.

Nielsen, T., Hertel, O., Christensen, C. S., Egeløv, A., Granby, K., Hansen, A. B., Platz, J., and Skov, H., 1996. Comparison of field measurements and a trajectory model. Poster in proceedings of NOSA/NORSAC Symposium 1996 (Ed. Poul Hummelshøj), Elsingore, Denmark, Nov. 15-17 1996. Risø-R-934 (EN). pp 121-123.

Notholt, J., Hjorth, J. and Raes, F. Formation of HNO_2 on aerosol surfaces during foggy periods in the presence of NO and NO_2. 1992. Atmospheric Environment, Vol. 26A, No. 2, pp. 211-217.

Noxon, J.F., Norton, R.B. and Henderson, W.R. 1978. Observation of atmospheric NO_3. Geophysical research letters, Vol. 5, No. 8, 1978.

OPSIS, 1995. Software manual. OPSIS AB, Furulund, may 1995.

OPSIS, 1996. Quality Assurance and Quality Control using Opsis analysers for air quality monitoring. OPSIS AB, Furulund, september 1996.

Palmgren, F., Ruwim, B., Jensen, S.S. and Kåre, K. 1997. Luftkvalitet i danske byer. TEMA-rapport fra DMU, nr. 16/1997. Danmarks Miljøundersøgelser, Roskilde, Denmark.

Perner, D. and Platt, U. 1979. detection of nitrous acid in the atmosphere by differential optical absorption. Geophysical Research Letters, Vol. 6, No. 12.

Pitts Jr., J.N., Finlayson-Pitts, B.J., Winer, A.M. 1977. New insights into old problems on chemical transformations in photochemical smog are provided by tunable lasers and long path FT-IR spectrometers. Env. Science & Technology, pp. 568-573.

Plane, J.M.C., Nien, C. 1991. A study of nighttime NO3 chemistry by differential optical absorption spectroscopy. SPIE Vol. 1433.

Plane, J.M.C., Nien, C. 1992. Differential optical absorption spectrometer for measuring atmospheric trace gases. Rev. Sci. Instrum. 63 (3), march.

Platt, U., Perner, D. and Patz, H.W. 1979. Simultaneous measurement of atmospheric CH_2O, O_3 and NO_2 by differential optical absorption. Journ. of geo.phys. res., Vol. 84, No. C10.

Platt, U., Perner, D. 1980. Direct measurements of atmospheric CH_2O, HNO_2, O_3, NO_2 and SO_2 by differential optical absorption in the near UV. Journal of geophysical res., Vol. 85, No. C12.

Platt, U., Perner, D., G.W. Harris, M. Winer, J.N. Pitts Jr. 1980. Observations of nitrous acid in urban atmosphere by differential optical absorption. Nature Vol. 285, pp. 312-314, 29 may.

Platt, U., Perner D., Winer, A. M., Harris, G. W. and Pitts Jr., J. N. 1980. Detection of NO_3 in the polluted troposphere by differential optical absorption. Geophysical research letters.

Platt, U., Perner, D., Schrøder, J., Kessler, C. and Toennissen, A. 1981. The diurnal variation of NO_3. Journal of geophysical research, Vol. 86, No. C12.

Platt, U. F., Winer , A. M., Biermann, H. W., Atkinson, R. and Pitts Jr., J. N. 1984. Measurement of nitrate radical concentrations in continental air. Environ. Sci. Technol., Vol. 18, No.5.

Platt, U., LeBras, G., Poulet, G., Burrows, J.P. and Moortgat, G. 1990. Peroxy radicals from night-time reaction of NO_3 with organic compounds. Nature, Vol. 348.

Platt, U. and Heintz, F. 1994. Nitrate radicals in tropospheric chemistry. Israel Journal of Chemistry, Vol. 34, pp.289-300.

Pommereau, J., F. Goutail, P. Laville and M. Nunes-Pinharanda. 1997. Development of a long path UV-visible spectrometer for atmospheric composition monitoring. In instrument development for atmospheric research and monitoring, Eurotrac, Vol. 8. Lidar profiling, DOAS and tunable diode laser spectroscopy. Springer-Verlag Berlin Heidelberg, Germany.

Rudich, Y., Talukdar, R.K. and Ravishankara, A.R. 1998. Multiphase chemistry of NO_3 in the remote troposphere. Journal of geophysical research, Vol. 103, No. D13, pp. 16,133-16,143.

Runge, E., Hertel, O., Sørensen J.H. et al. 1997. Modelling the atmospheric nitrogen deposition to Løgstør Bredning. Model results for the periodds april 17 to 30 and august 7 to 19 1995. NERI Technical report No. 195. National Environmental Research Institute, Roskilde, Denmark.

Simonaitis, R., Meagher, J.F. and Bailey, E.M. 1997. Evaluation of the condensed carbon bond (CB-IV) machanism against smog chamber data at low VOC and NOx concentrations.

Skov, H., Egeløv, A. H., Granby, K. and Nielsen T. 1997. Relationships between ozone and other photochemical products at Ll. Valby, Denmark. Atm. Env. Vol. 31, No. 5, pp.685-691.

Smith, N., J.M.C. Plane, C. Nien, P.A. Solomon. 1995. Nighttime radical chemistry in the San Joaquin valley. Atm. Env. Vol 29, pp. 2887-2897.

Smith, N., H. Coe, B. Allan and J. Plane. 1997. Differential optical studies at East Anglia. Instrument development for atmospheric research and monitoring, Eurotrac, Vol. 8. Lidar profiling, DOAS and tunable diode laser spectroscopy. Springer-Verlag Berlin Heidelberg, Germany.

Sorteberg A., Hov Ø., Solberg S. m.fl. 1998. Gaseous and particulate oxidized and reduced nitrogen species in the atmospheric boundary layer in Scandinavia in spring. Journal of Atmospheric Chemistry 30: 241-271.

Stockwell, W. R., Middleton, P., Chang, J. S. 1990. The second generation acid deposition model chemical mechanism for regional air quality modeling. Journal of geophysical research, vol. 95, No. D10.

Strand, A. and Hov, Ø. 1994. A two-dimensional global study of tropospheric ozone production. J.Geophys.Res. Vol. 99, pp. 22,877-22,895.

Strand, A. and Hov, Ø. 1995. The impact of man-made and naturel Nox emissions on upper tropospheric ozone: A two-dimensional model study. Atmospheric Environment, Vol. 30, No. 8, pp. 1291-1303.

Stutz, J. and U. Platt. 1997. A new generation of DOAS instruments. Instrument development for atmospheric research and monitoring,

Eurotrac, Vol. 8, Lidar profiling, DOAS and tunable diode laser spectroscopy. Springer-Verlag Berlin Heidelberg, Germany.

Thomas, K., Volz-Thomas, A., Mihelcic, D., Smit, H.G.J., Kley, D. 1998. On the exchange of NO_3 radicals wtih aqueous solution: solubility and sticking coefficient. Journal of Atmospheric Chemistry, 29: 17-43.

Vignati,E., Hertel, O., 1996. Modelling Atmospheric Nitrogen Deposition to Sea. A newly initiated study of the influence of aerosols and heterogeneous chemistry. Poster in the proceedings of NOSA/NORSAC Symposium 1996 (Ed. Poul Hummelshøj), Helsingør, Denmark, Nov. 15-17 1996. Risø-R-934 (EN). pp 140-142.

Vignati, E., de Leeuw, G., Hertel, O., and Berkowicz, R., 1996. Analysis of Aerosol measurements from the Vindeby Experiment. Poster of the European Aerosol Conference, Delft, 9-12 Sep 1996. J. Aeros. Sci., 27(suppl. 1), pp s109-s110.

Virkkula, A. 1996. Performance of a differential optical absorption spectrometer for surface O_3 measurements in the Finnish arctic. OPSIS RAP-87. Atmospheric environment, Vol. 31, No. 4, pp 545-555.

Wayne, R.P., Barnes, I., Biggs, P., Burrows, J.P., Canosa-Mas, C.E., Hjorth, J., Le Bras, G., Moortgat, G.K., Perner, D., Poulet, G., Restelli, G. and Sidebottom, H. 1991. The nitrate radical: physics, chemistry, and the atmosphere. Atmospheric Environment, Vol. 25A, No. 1.

Zetzsch, C. and Behnke, W. 1992. Heterogeneous photochemical sources of atomic Cl in the troposphere. Ber. Bunsenges. Phys. Chem., No. 3.

Ziv, A. and Iakovleva, E. 1998. Monitoring and analysis of air pollution in St. Petersburg. Second milestone report. National Environmental Research Institute, Roskilde, Denmark.

Appendix A.1

Lille Valby DOAS measurements

NO_2

This appendix gives the results of the Lille Valby NO_2 DOAS measurements. Pages 118 through 123 gives the concentration level in micrograms per cubicmeter, light level and standard deviation in micrograms per cubicmeter, for April - September, 1998. Measurements with corresponding light levels below 15 % have been excluded. Pages 124 through 128 gives the May - September, 1998, NO_2 measurement data, when measurements with corresponding light levels below 5 % are excluded.

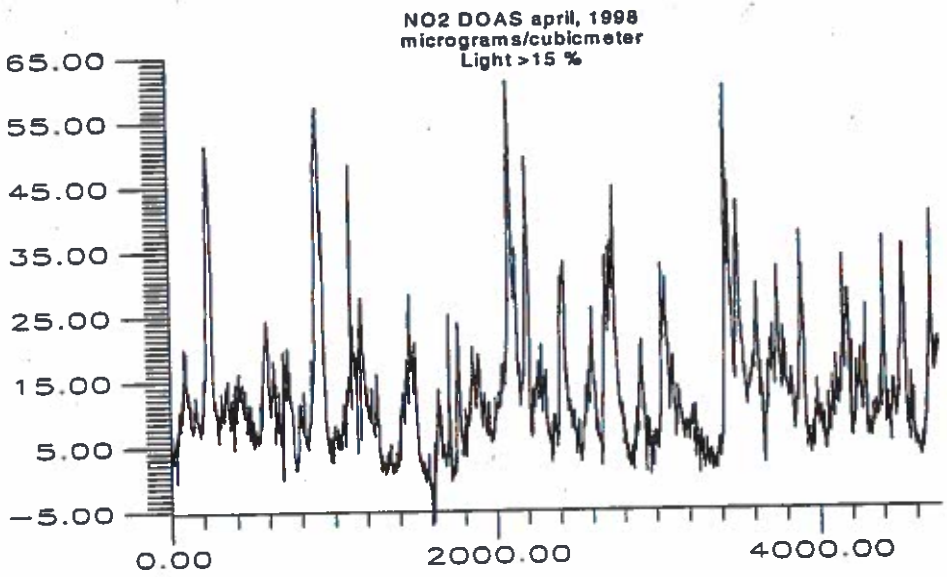
NO2 DOAS april, 1998
micrograms/cubicmeter
Light >15 %
65.00
55.00
45.00
35.00
25.00
15.00
5.00
-5.00
0.00
2000.00
4000.00

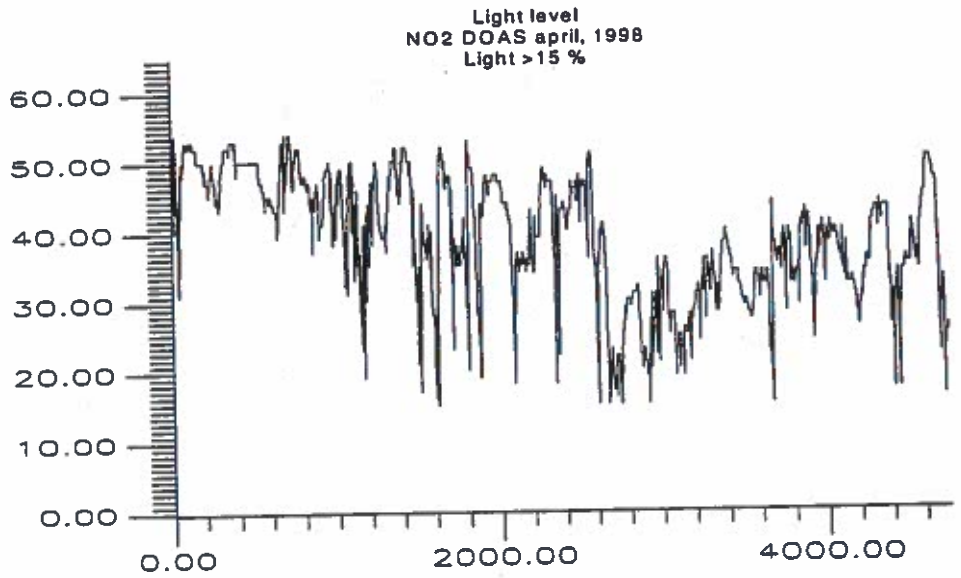
Light level
NO2 DOAS april, 1998
Light >15 %
60.00
50.00
40.00
30.00
20.00
10.00
0.00
0.00
2000.00
4000.00

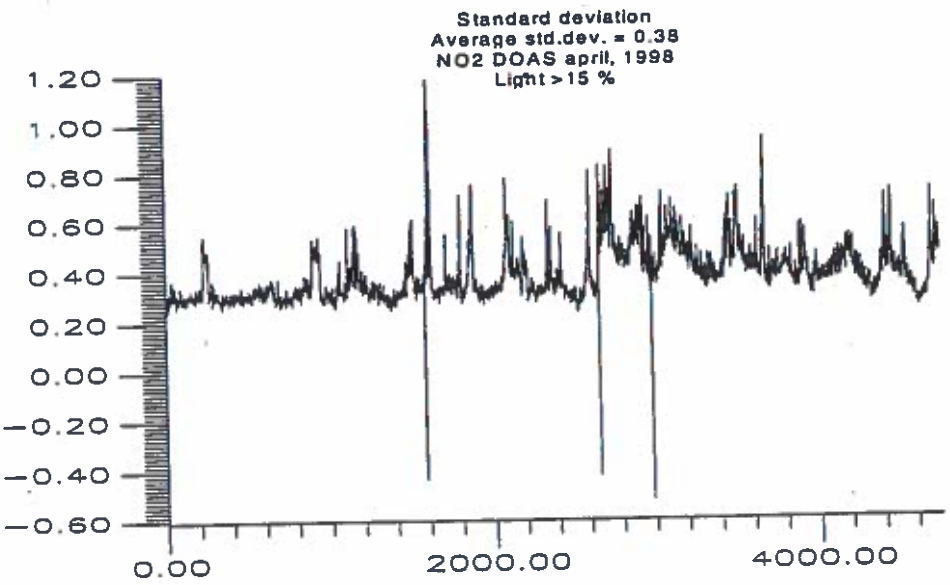
Standard deviation
Average std.dev. = 0.38
NO2 DOAS april, 1998
Light >15 %
1.20
1.00
0.80
0.60
0.40
0.20
0.00
-0.20
-0.40
-0.60
0.00
2000.00
4000.00

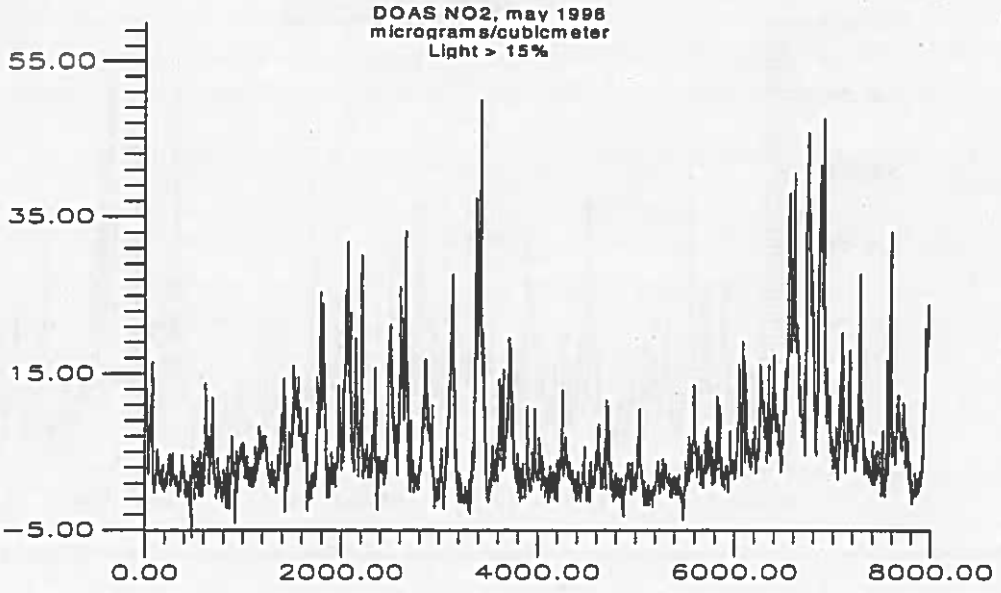
DOAS NO2, may 1998
micrograms/cubicmeter
Light > 15%
55.00
35.00
15.00
-5.00
0.00
2000.00
4000.00
6000.00
8000.00

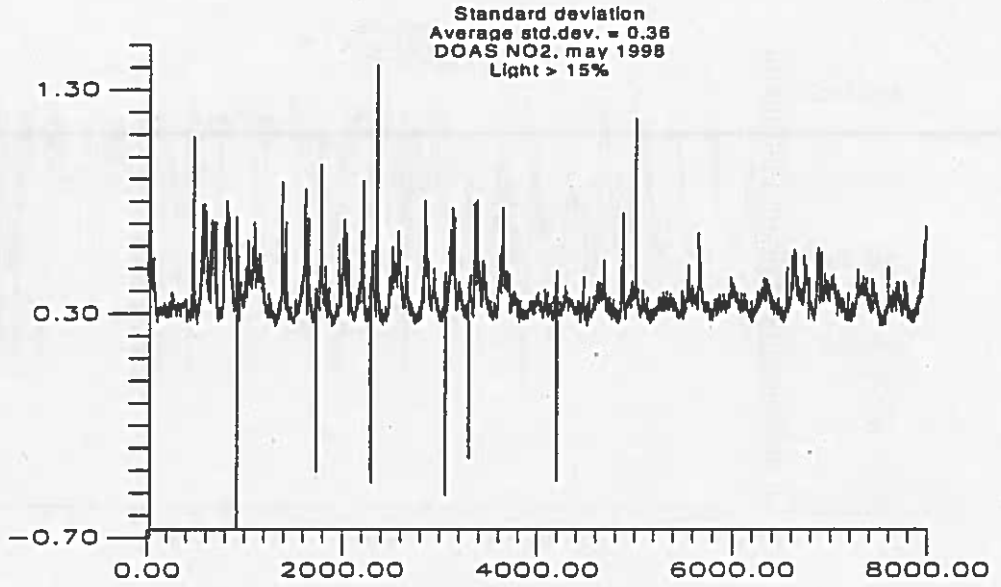
Standard deviation
Average std.dev. = 0.36
DOAS NO2, may 1998
Light > 15%
1.30
0.30
-0.70
0.00
2000.00
4000.00
6000.00
8000.00

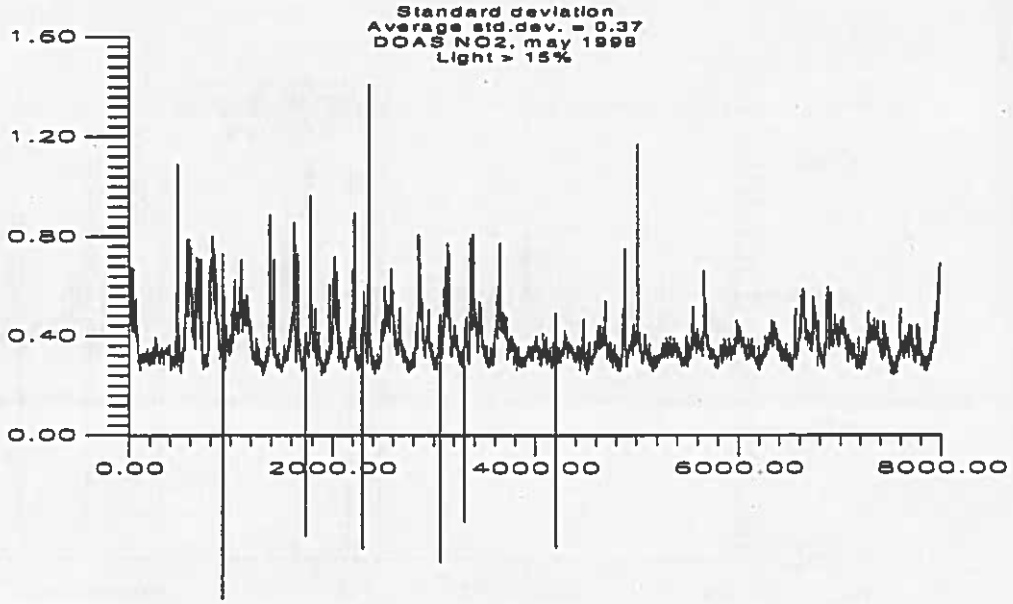
Standard deviation
Average std.dev. = 0.37
DOAS NO2, may 1998
Light > 15%
1.60
1.20
0.80
0.40
0.00
0.00
2000.00
4000.00
6000.00
8000.00

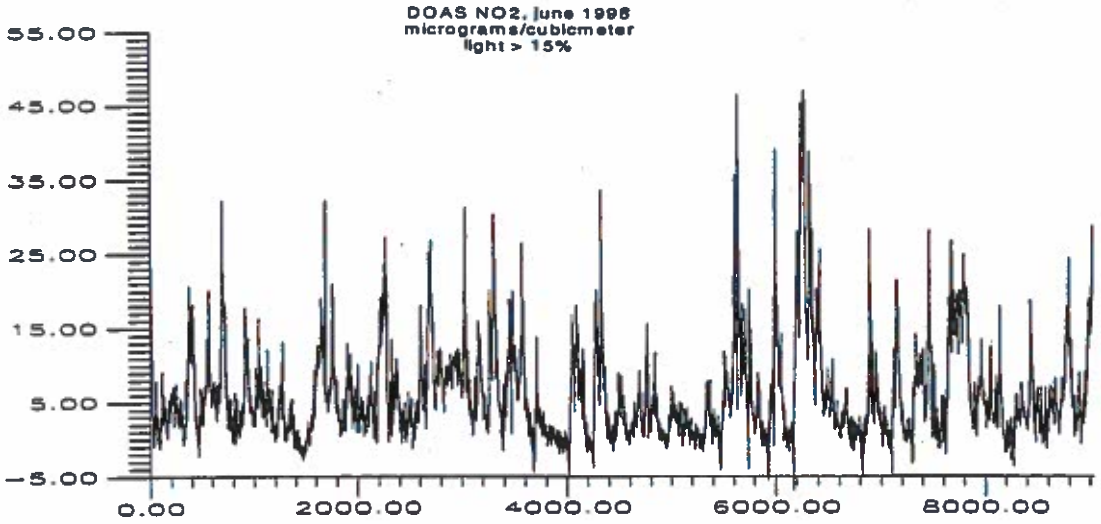
DOAS NO2, june 1998
micrograms/cubicmeter
light > 15%
55.00
45.00
35.00
25.00
15.00
5.00
-5.00
0.00
2000.00
4000.00
6000.00
8000.00

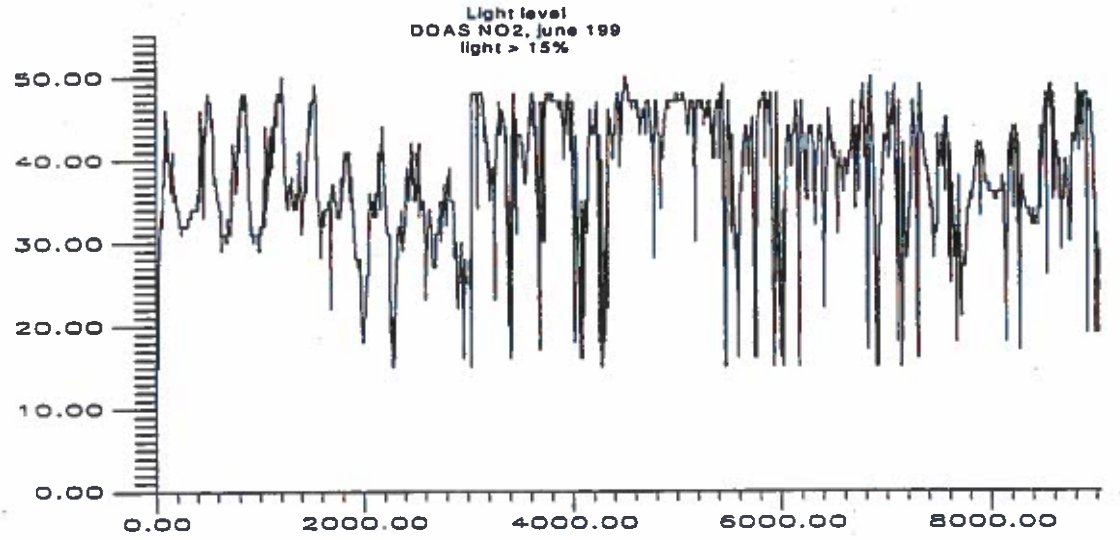
Light level
DOAS NO2, june 199
light > 15%
50.00
40.00
30.00
20.00
10.00
0.00
0.00
2000.00
4000.00
6000.00
8000.00

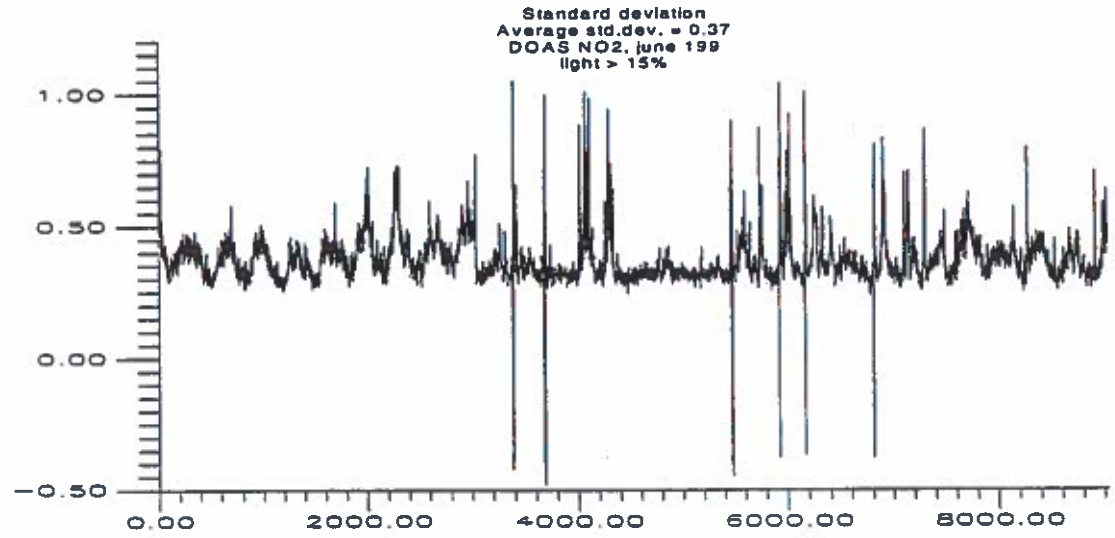
Standard deviation
Average std.dev. = 0.37
DOAS NO2, june 199
light > 15%
1.00
0.50
0.00
-0.50
0.00
2000.00
4000.00
6000.00
8000.00

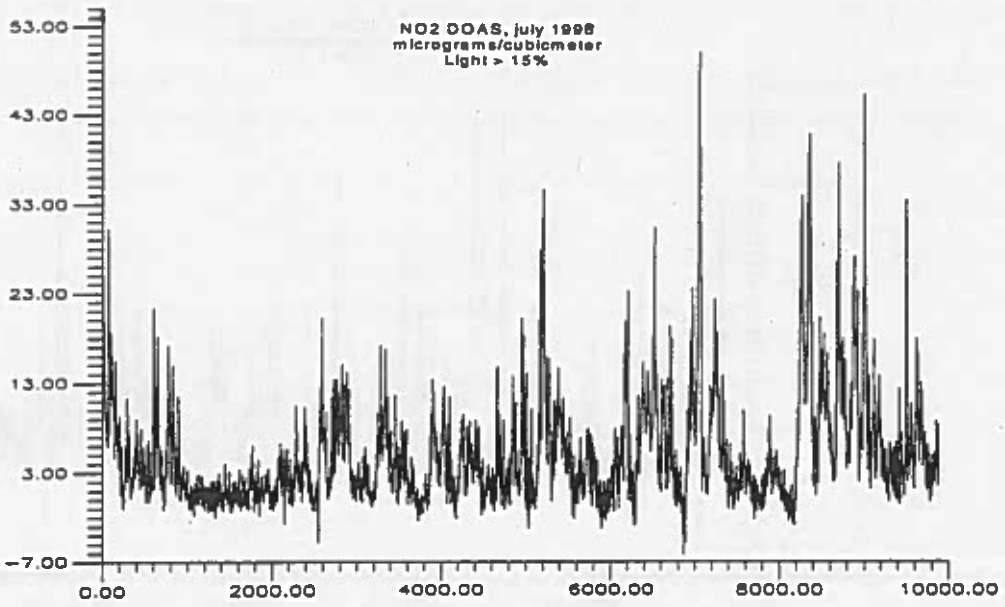
NO2 DOAS, july 1998
micrograms/cubicmeter
Light > 15%
53.00
43.00
33.00
23.00
13.00
3.00
-7.00
0.00
2000.00
4000.00
6000.00
8000.00
10000.00

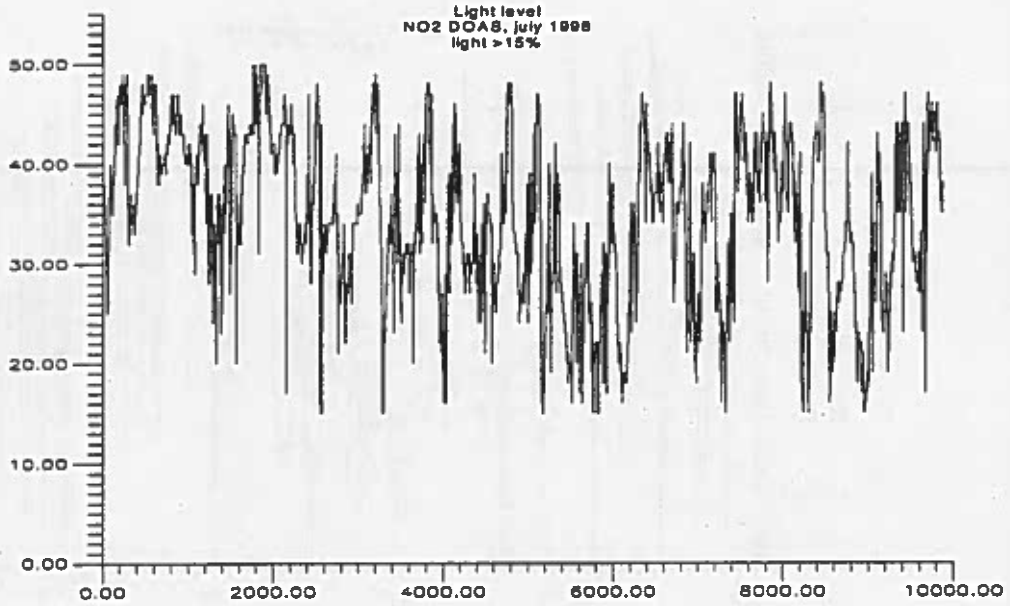
Light level
NO2 DOAS, july 1998
light >15%
50.00
40.00
30.00
20.00
10.00
0.00
0.00
2000.00
4000.00
6000.00
8000.00
10000.00

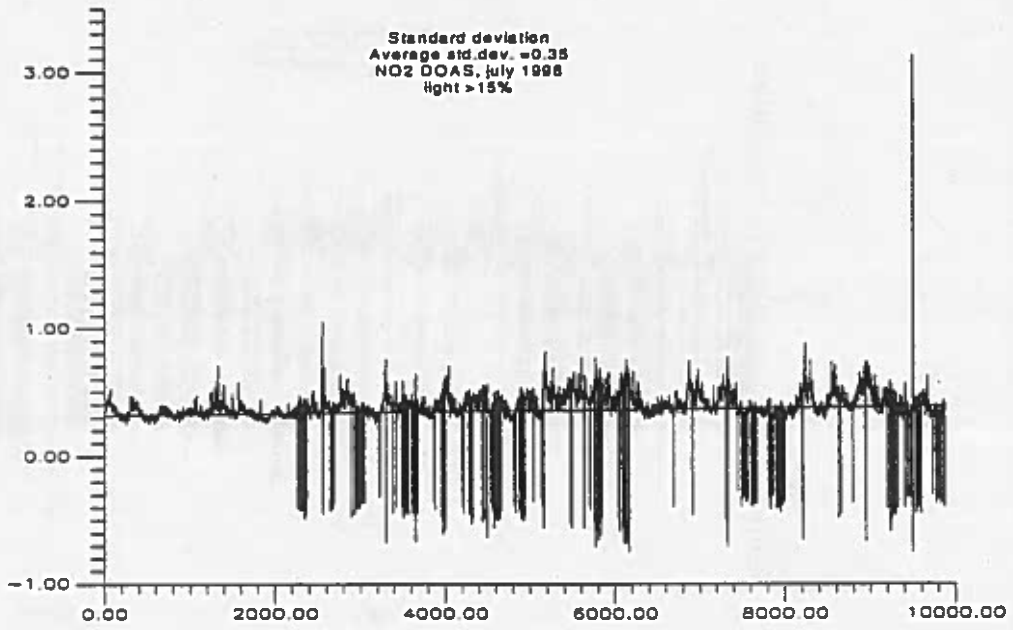
Standard deviation
Average std.dev. =0.35
NO2 DOAS, july 1998
light >15%
3.00
2.00
1.00
0.00
-1.00
0.00
2000.00
4000.00
6000.00
8000.00
10000.00

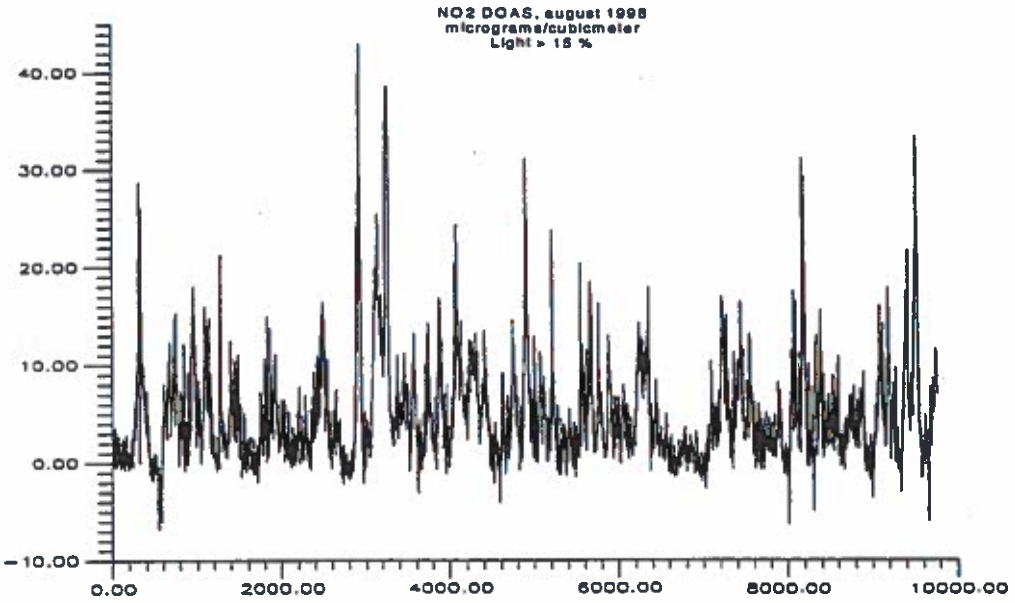
NO2 DOAS, august 1998
micrograms/cubicmeter
Light > 15 %
40.00
30.00
20.00
10.00
0.00
-10.00
0.00
2000.00
4000.00
6000.00
8000.00
10000.00

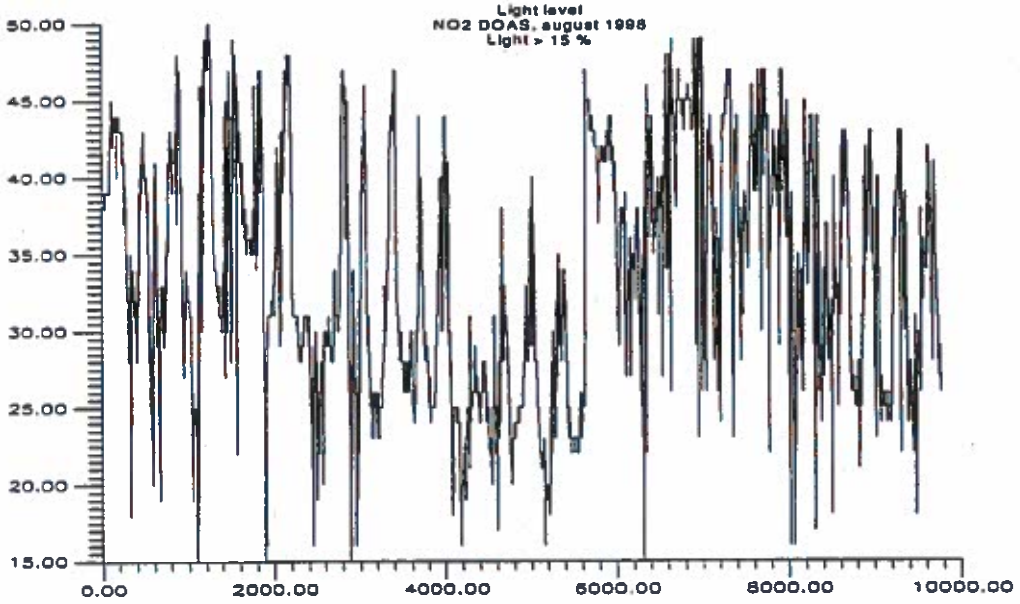
Light level
NO2 DOAS, august 1998
Light > 15 %
50.00
45.00
40.00
35.00
30.00
25.00
20.00
15.00
0.00
2000.00
4000.00
6000.00
8000.00
10000.00

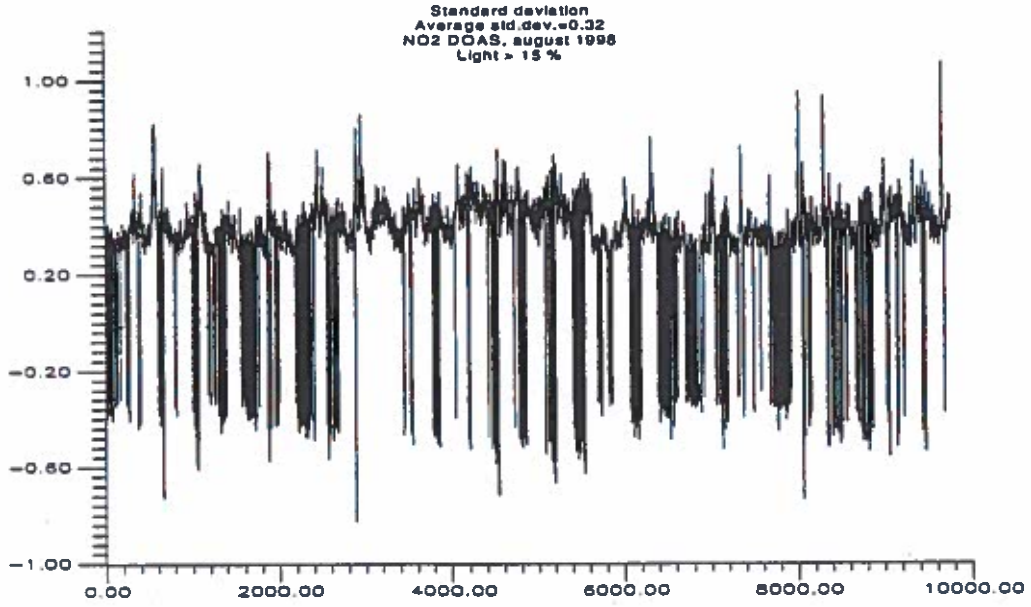
Standard deviation
Average std.dev.=0.32
NO2 DOAS, august 1998
Light > 15 %
1.00
0.60
0.20
-0.20
-0.60
-1.00
0.00
2000.00
4000.00
6000.00
8000.00
10000.00

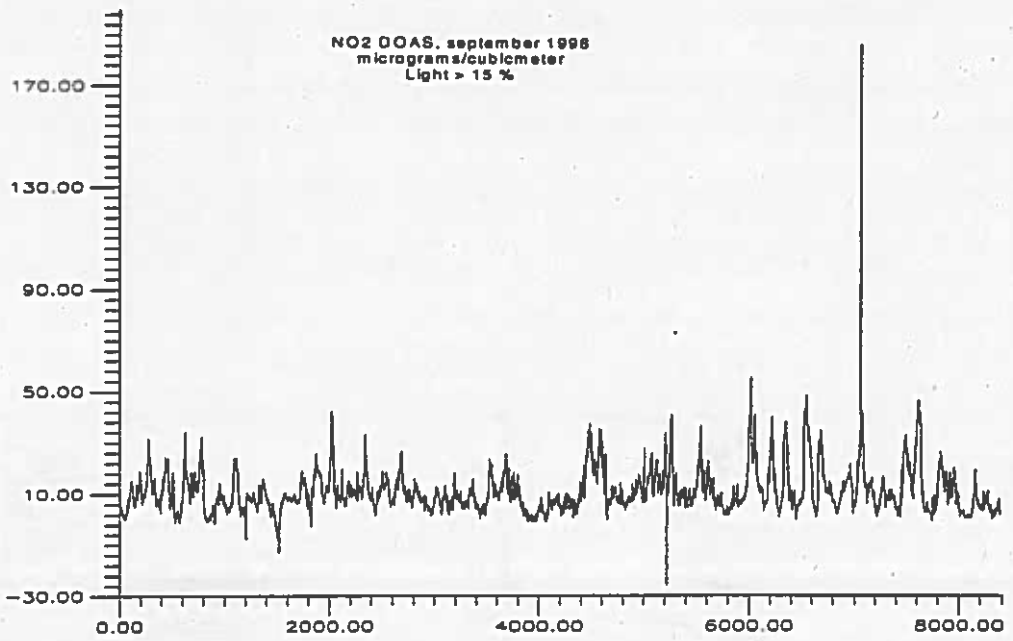
NO2 DOAS, september 1998
micrograms/cubicmeter
Light > 15 %
170.00
130.00
90.00
50.00
10.00
-30.00
0.00
2000.00
4000.00
6000.00
8000.00

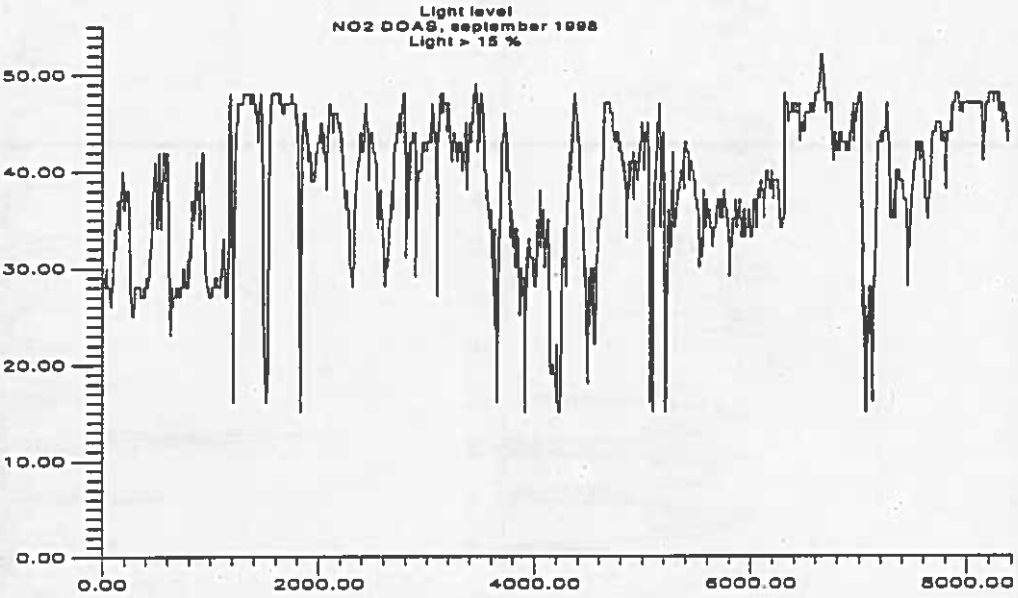
Light level
NO2 DOAS, september 1998
Light > 15 %
50.00
40.00
30.00
20.00
10.00
0.00
0.00
2000.00
4000.00
6000.00
8000.00

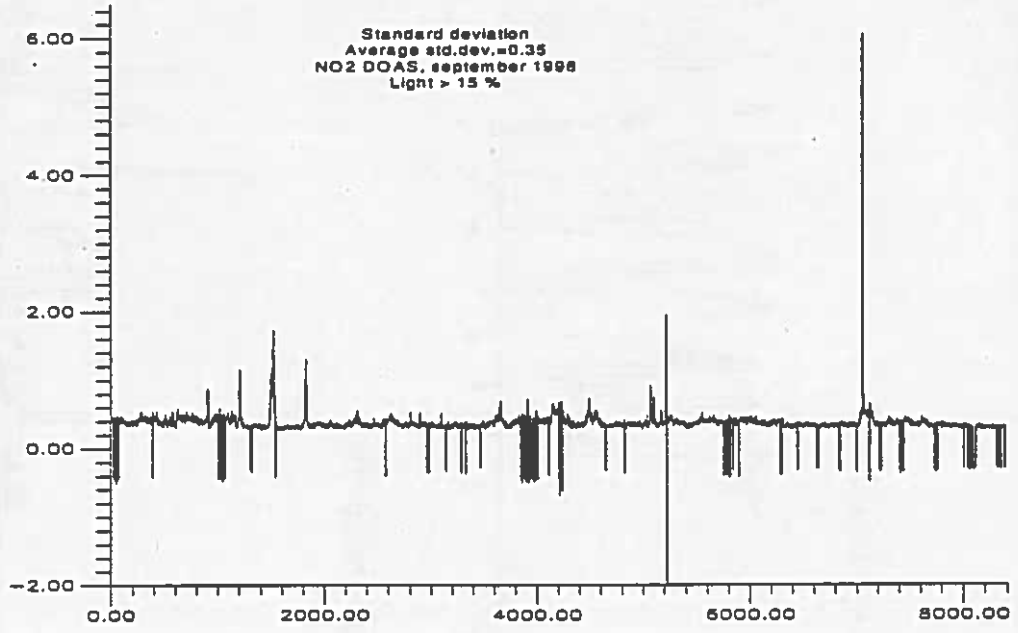
Standard deviation
Average std.dev.=0.35
NO2 DOAS, september 1998
Light > 15 %
6.00
4.00
2.00
0.00
-2.00
0.00
2000.00
4000.00
6000.00
8000.00

2090 Lille Valby Minutmiddelværdier for 19980501-19980531

Nulpunktskorrigerede data

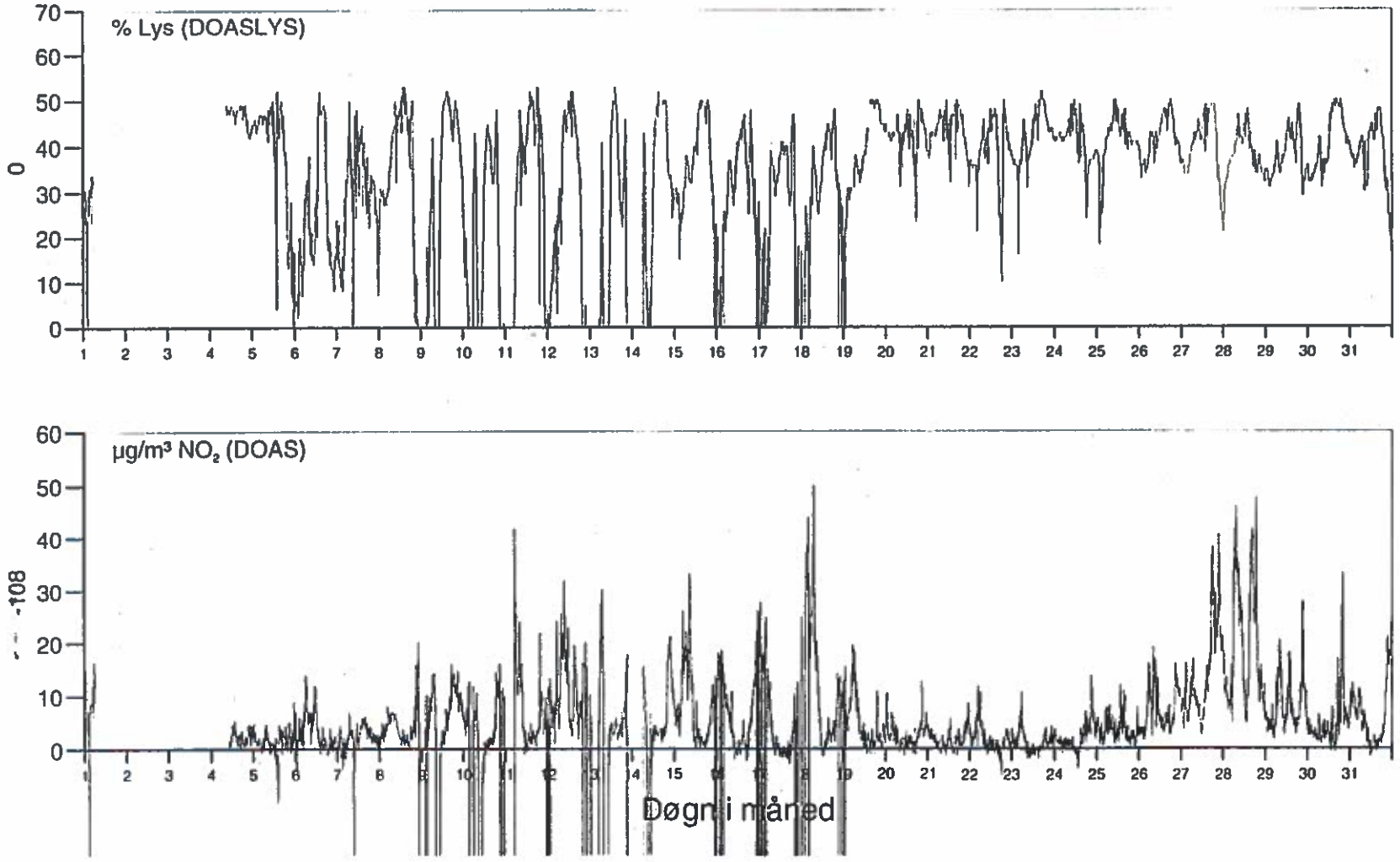

19990420

2090 Lille Valby Minutmiddelværdier for 19980601-19980630

Nulpunktskorrigerede data

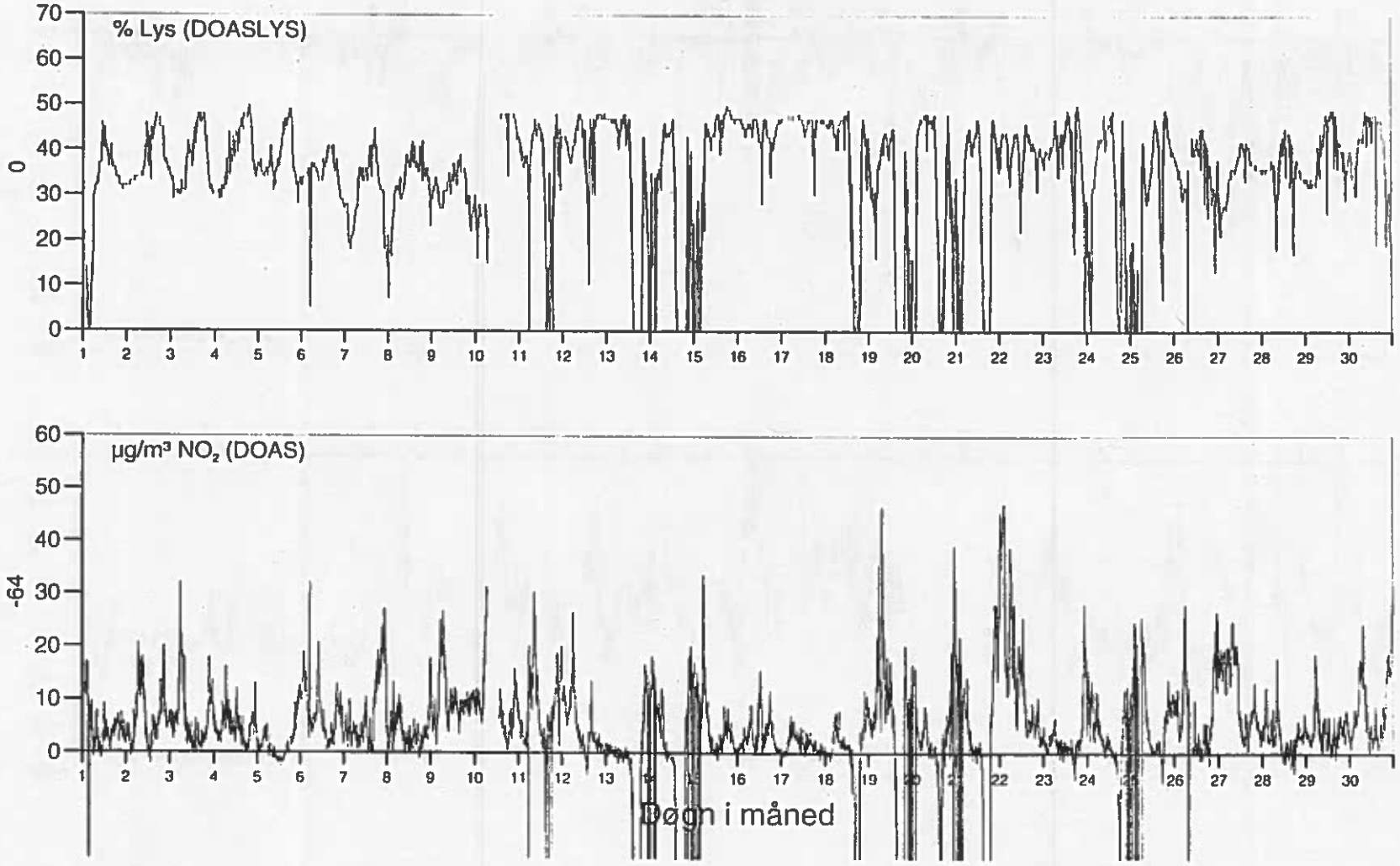

19990420

2090 Lille Valby Minutmiddelværdier for 19980701-19980731

Nulpunktskorrigerede data

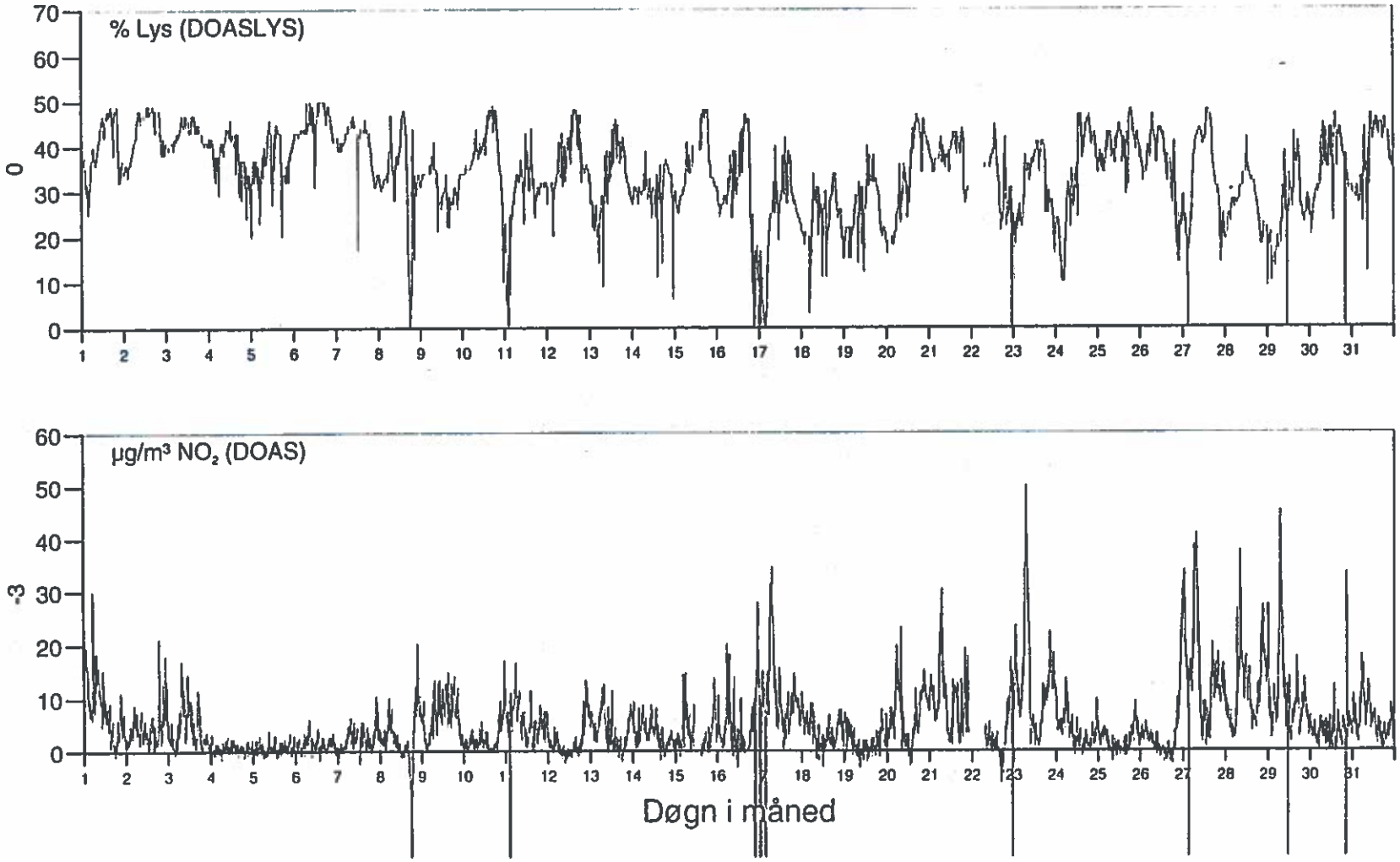

19990420

2090 Lille Valby Minutmiddelværdier for 19980801-19980831

Nulpunktskorrigerede data

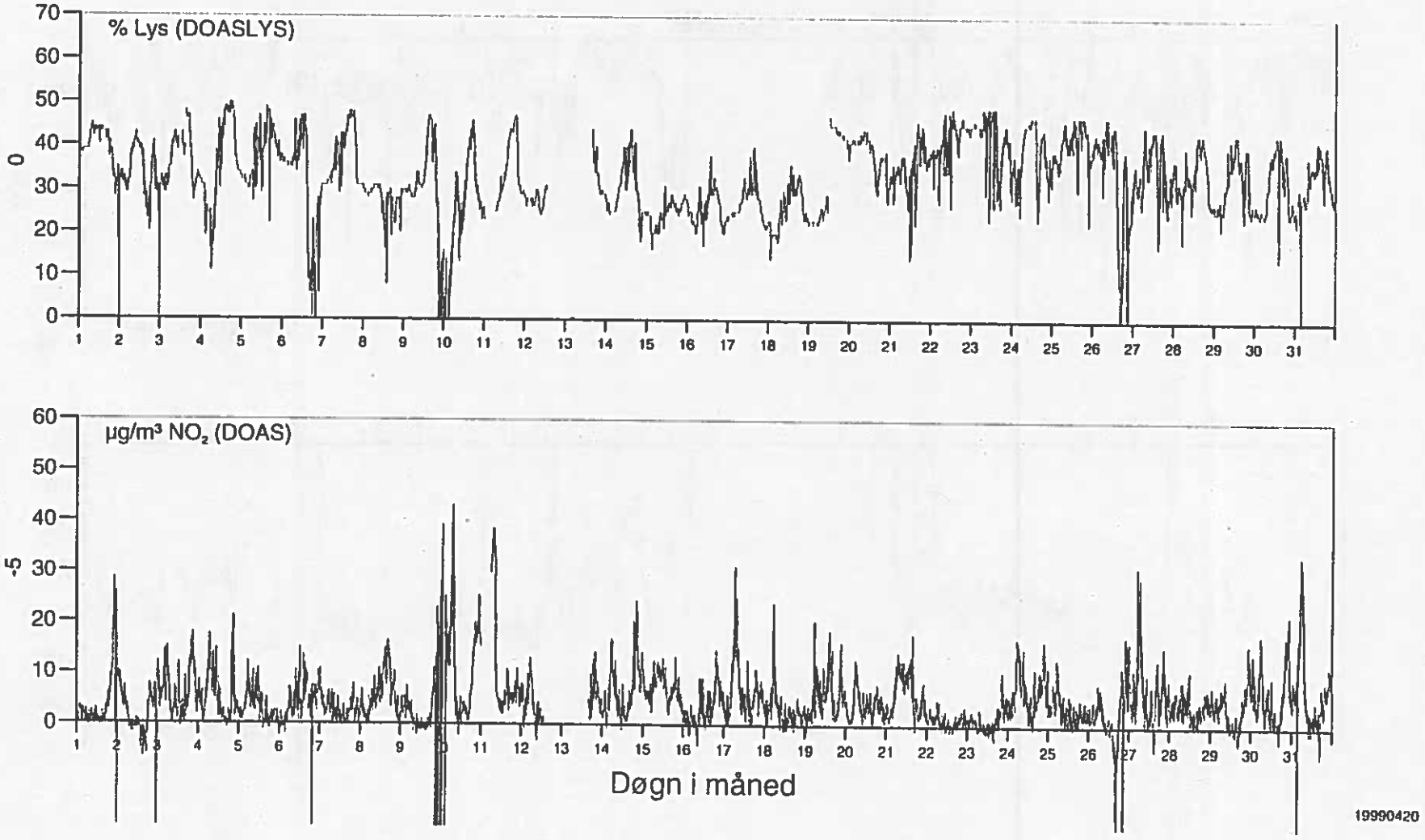

19990420

2090 Lille Valby Minutmiddelværdier for 19980901-19980930

Nulpunktskorrigerede data

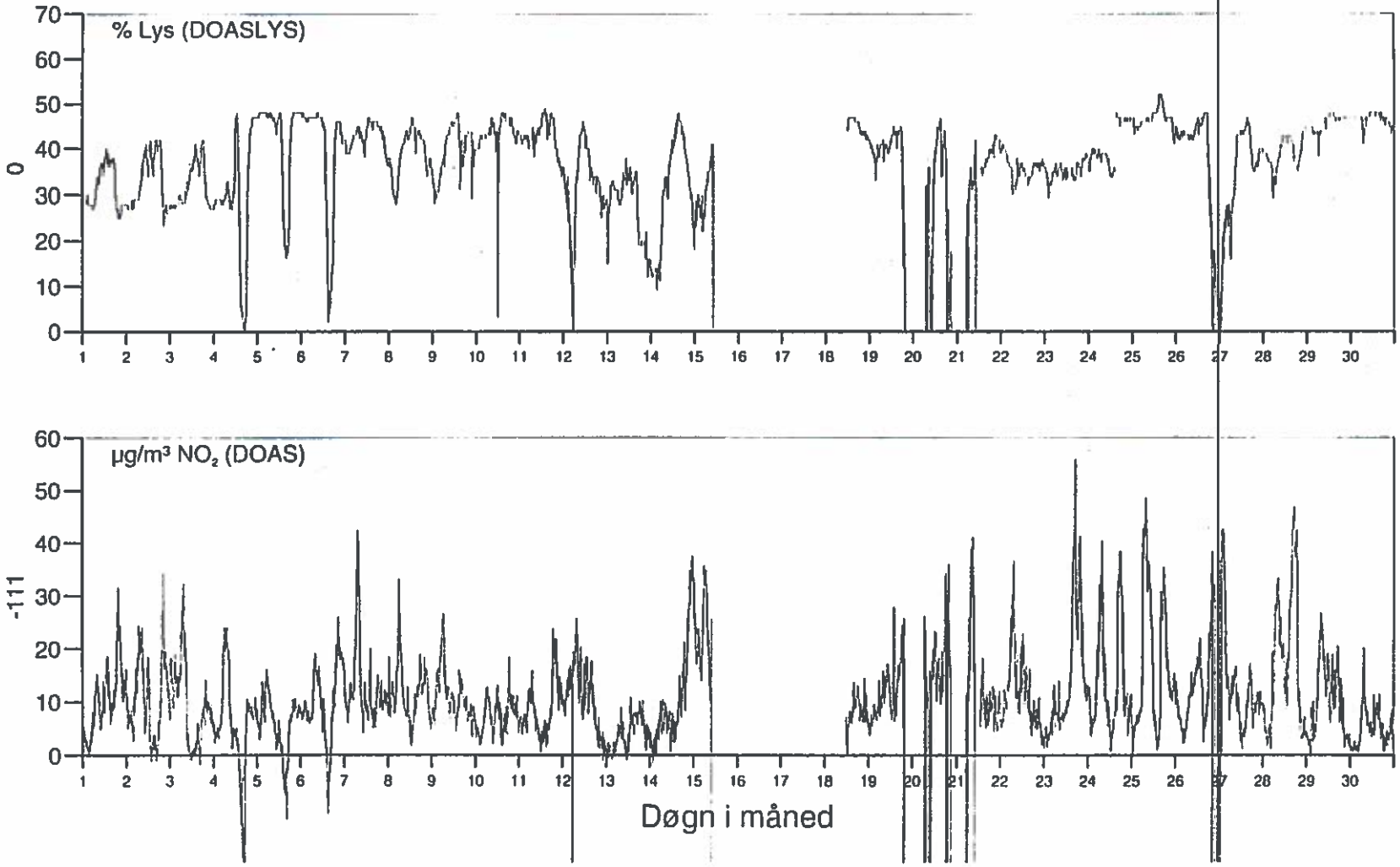

19990420

Appendix A.2

Lille Valby DOAS measurements

O_3

This appendix gives the results of the Lille Valby O_3 DOAS measurements. Pages 130 through 134 gives the May - September, 1998, O_3 measurement data, where measurements with a corresponding light level below 5 % have been excluded.

2090 Lille Valby Minutmiddelværdier for 19980501-19980531

Nulpunktskorrigerede data

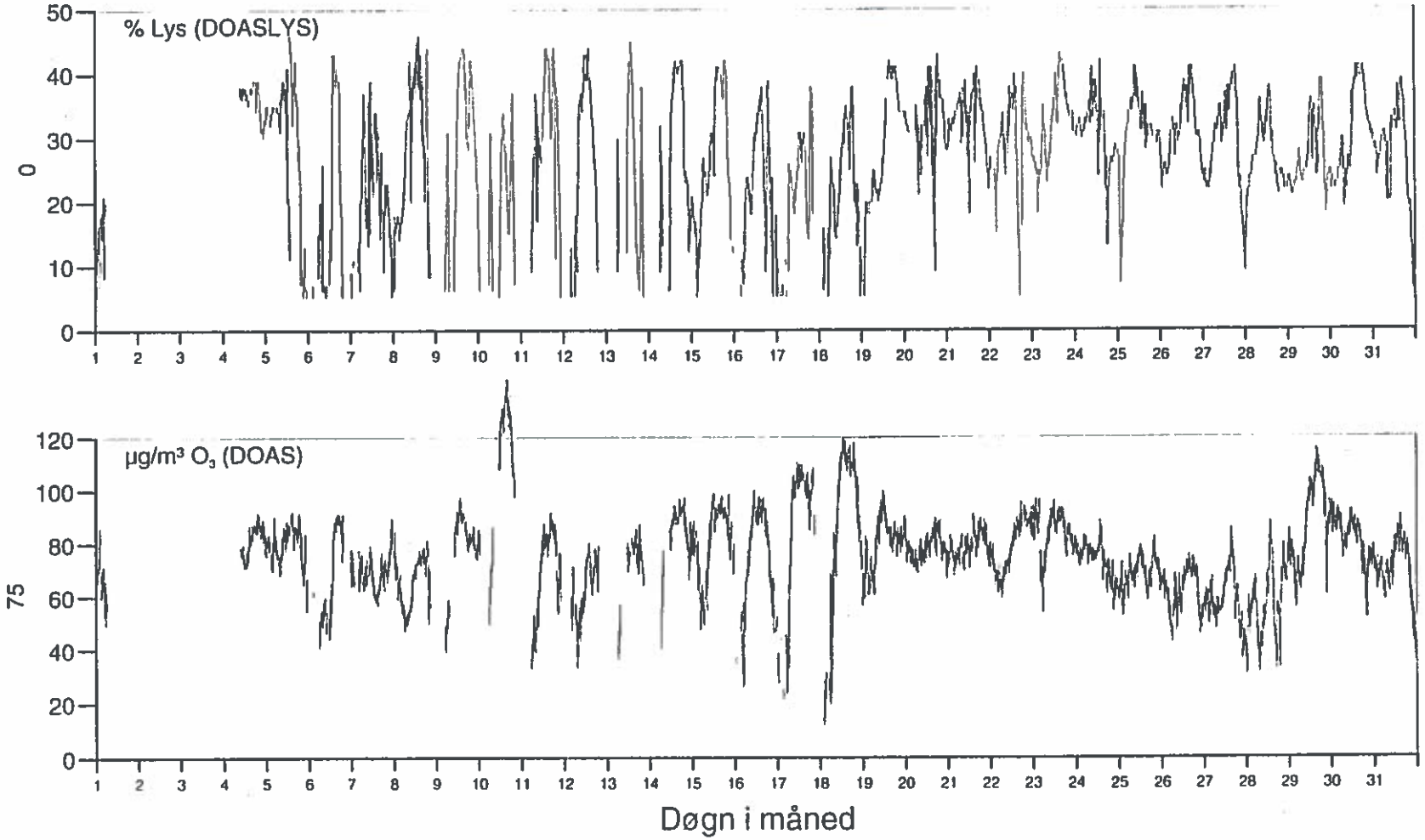

19990423

2090 Lille Valby Minutmiddelværdier for 19980601-19980630

Nulpunktskorrigerede data

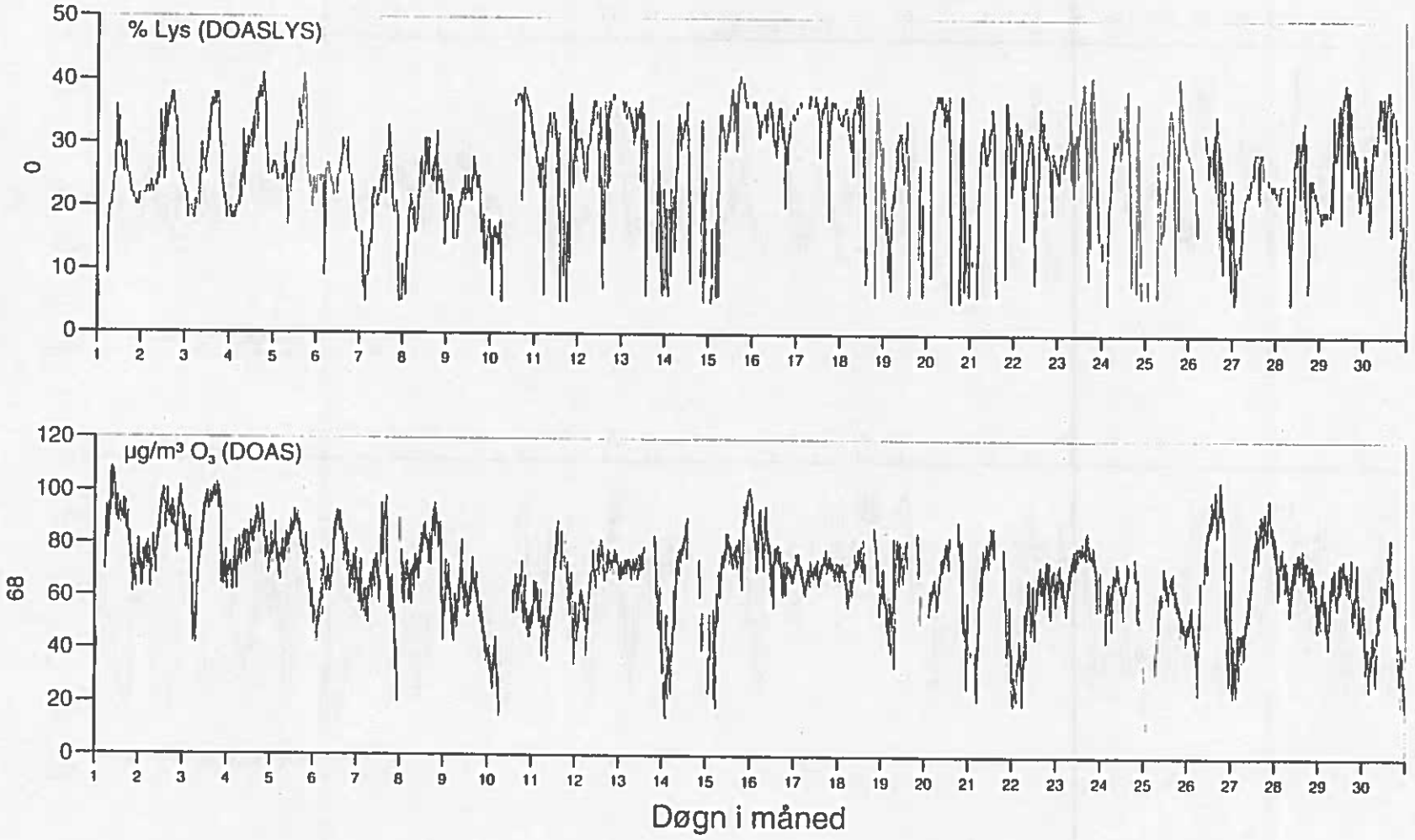

19990423

2090 Lille Valby Minutmiddelværdier for 19980701-19980731

Nulpunktskorrigerede data

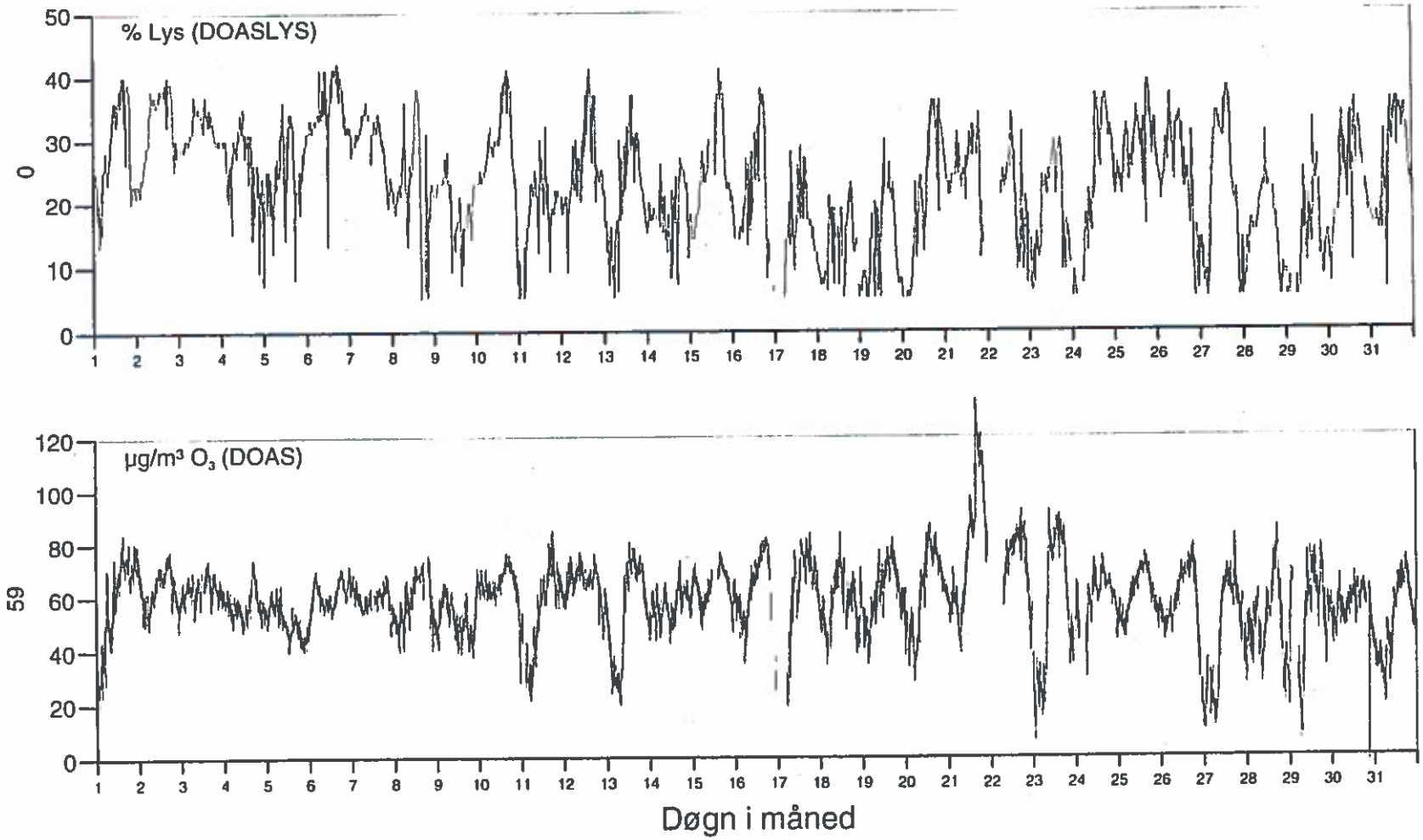

19990423

2090 Lille Valby Minutmiddelværdier for 19980801-19980831

Nulpunktskorrigerede data

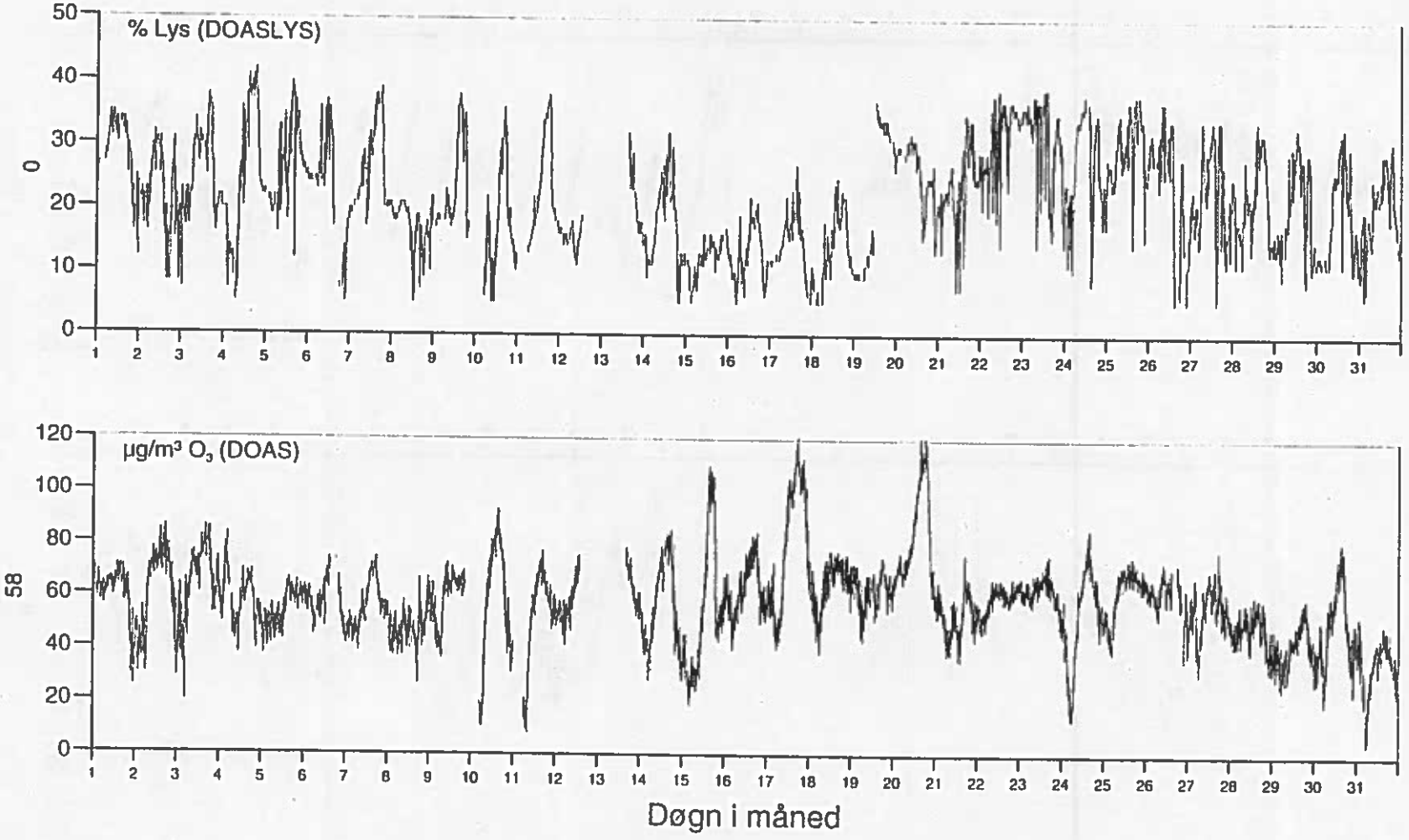

19990423

2090 Lille Valby Minutmiddelværdier for 19980901-19980930

Nulpunktskorrigerede data

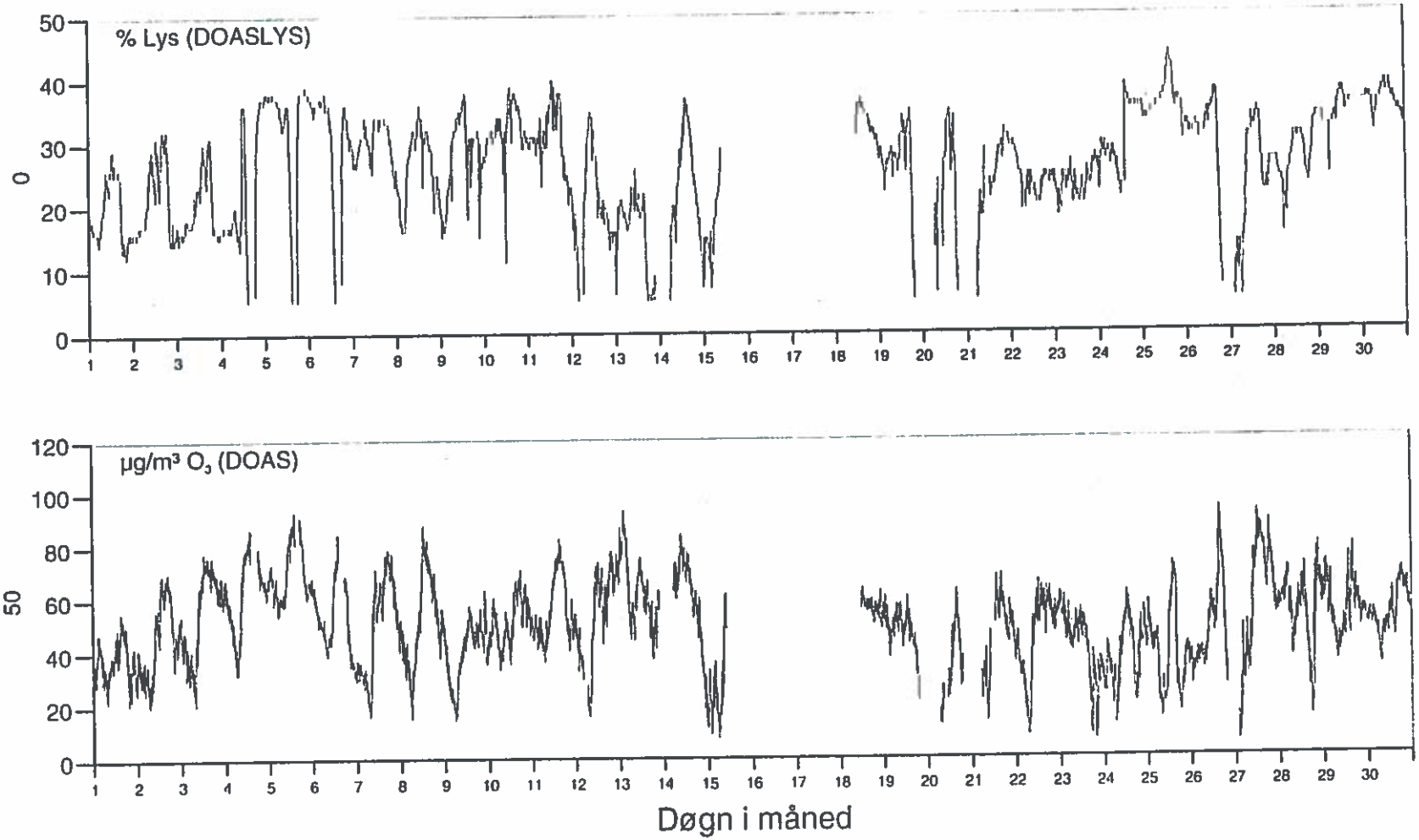

19990423

Appendix A.3

Lille Valby DOAS measurements

HONO

This appendix gives the results of the Lille Valby HONO DOAS measurements. Pages 136 - 137 shows concentration level and light level for selected periods, see chapter 4.4. Pages 138 though 142 gives the May - September, 1998, HONO measurement data, where measurements with corresponding light levels below 5 % have been excluded.

2090 Lille Valby Minutmiddelværdier for 19980602-19980606

Nulpunktskorrigerede data

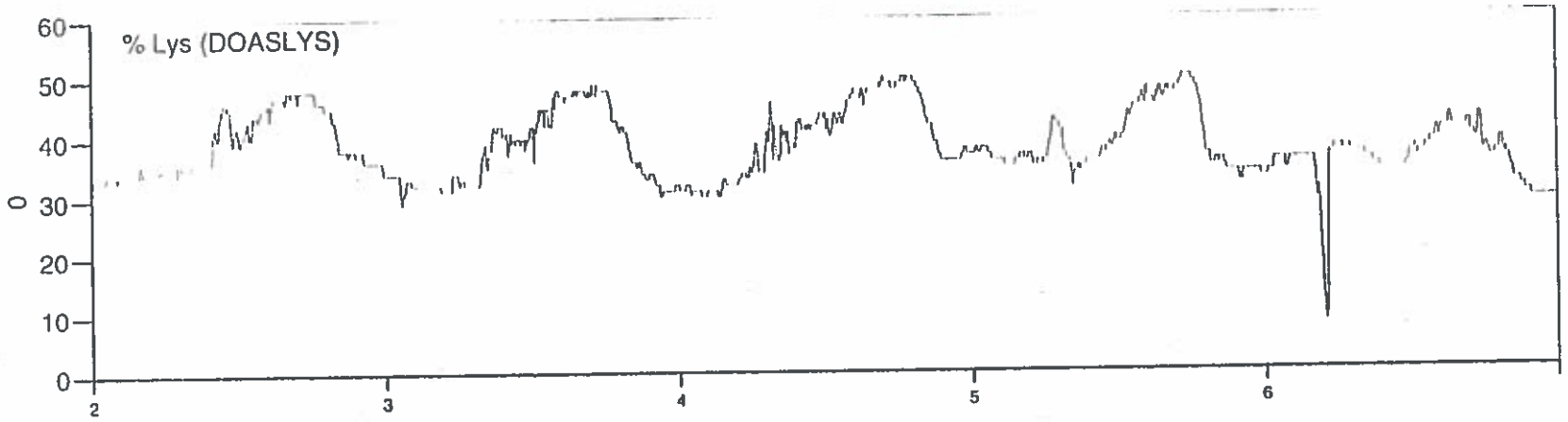

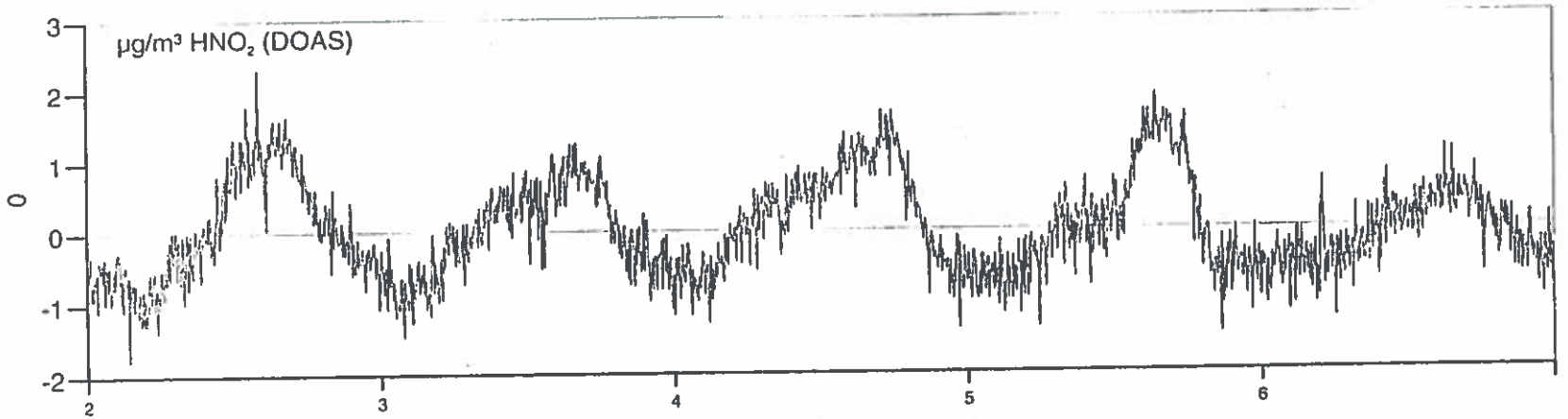

Døgn i måned

19990423

2090 Lille Valby Minutmiddelværdier for 19980702-19980705

Nulpunktskorrigerede data

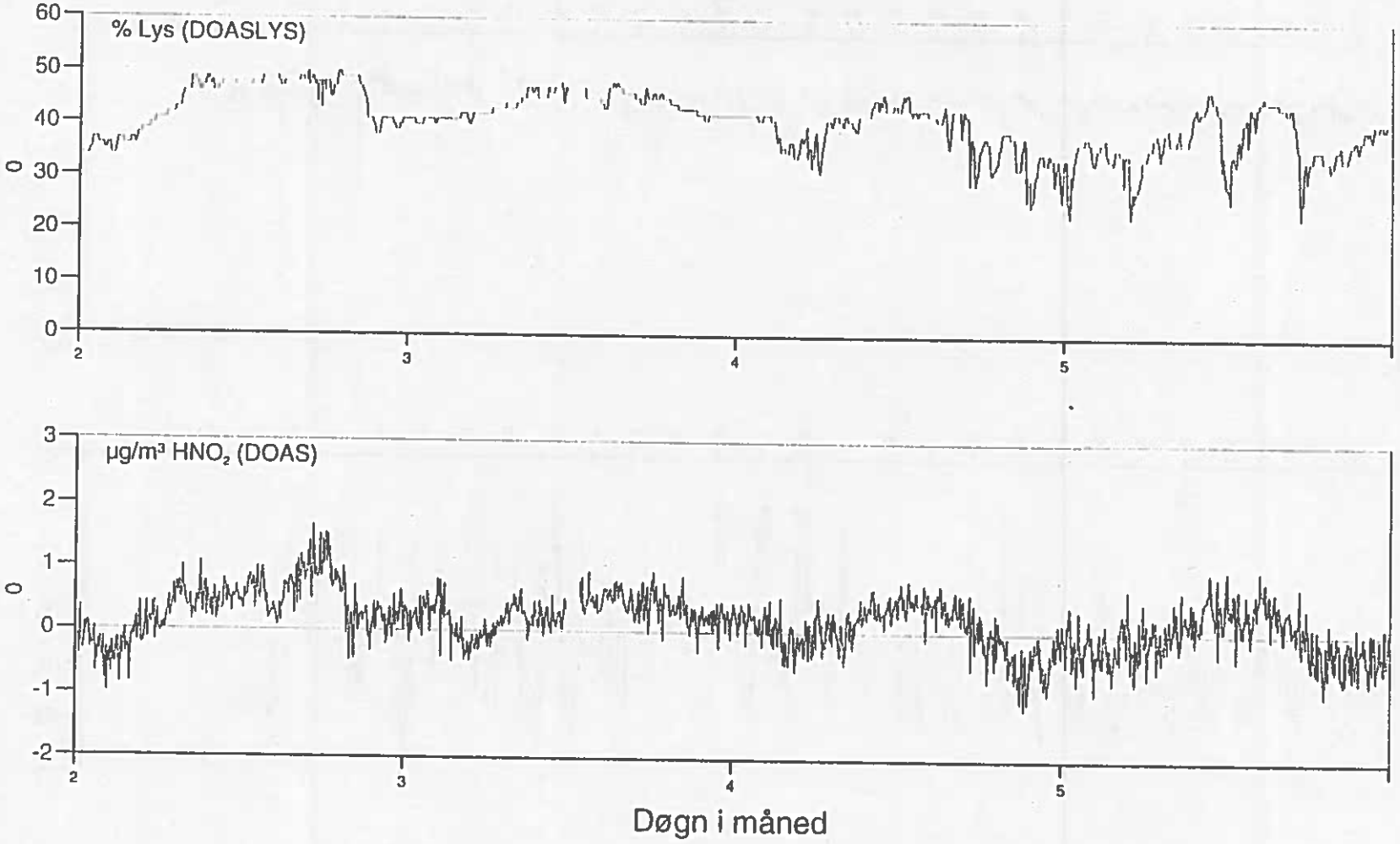

19990423

2090 Lille Valby Minutmiddelværdier for 19980501-19980531

Nulpunktskorrigerede data

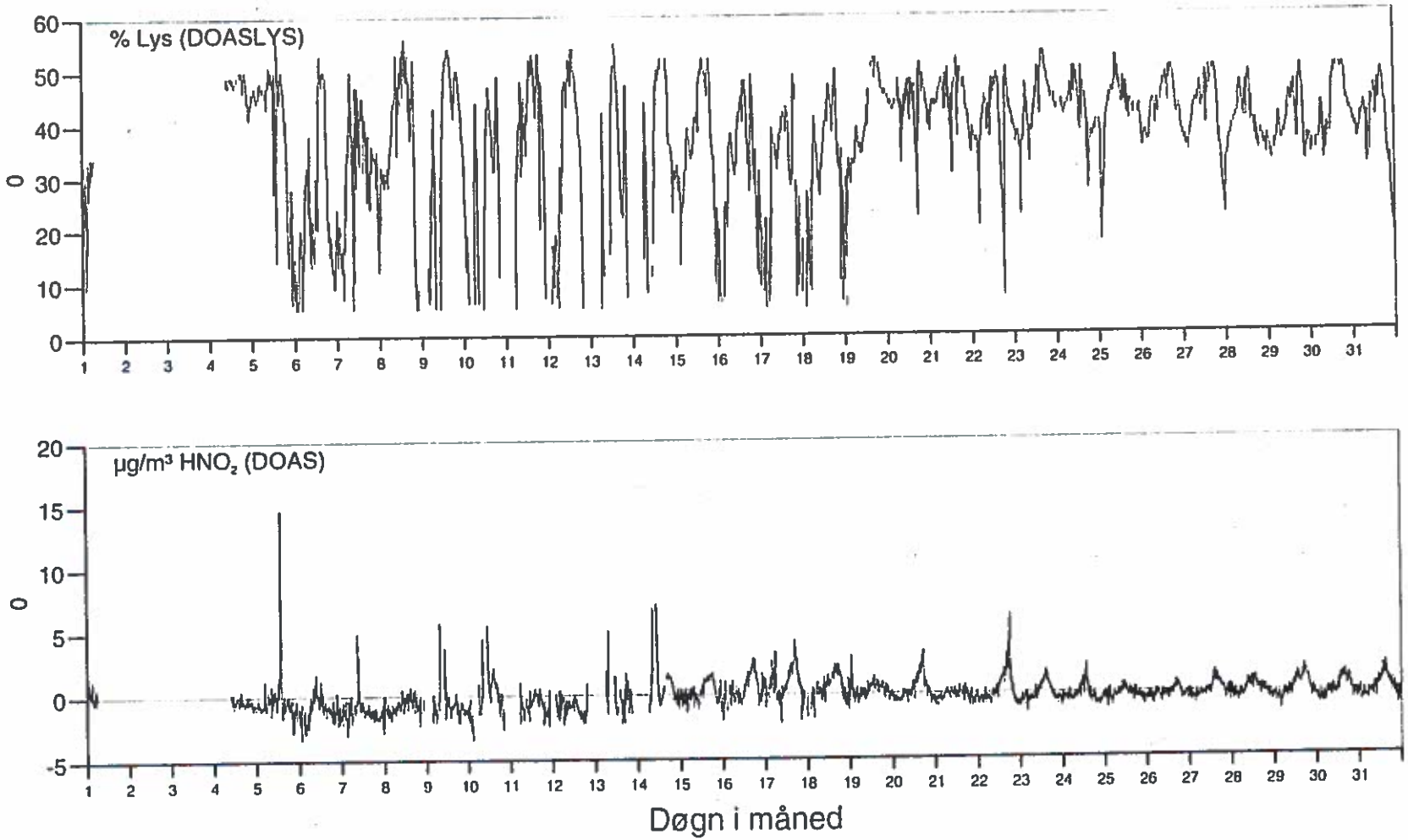

19990423

2090 Lille Valby Minutmiddelværdier for 19980601-19980630

Nulpunktskorrigerede data

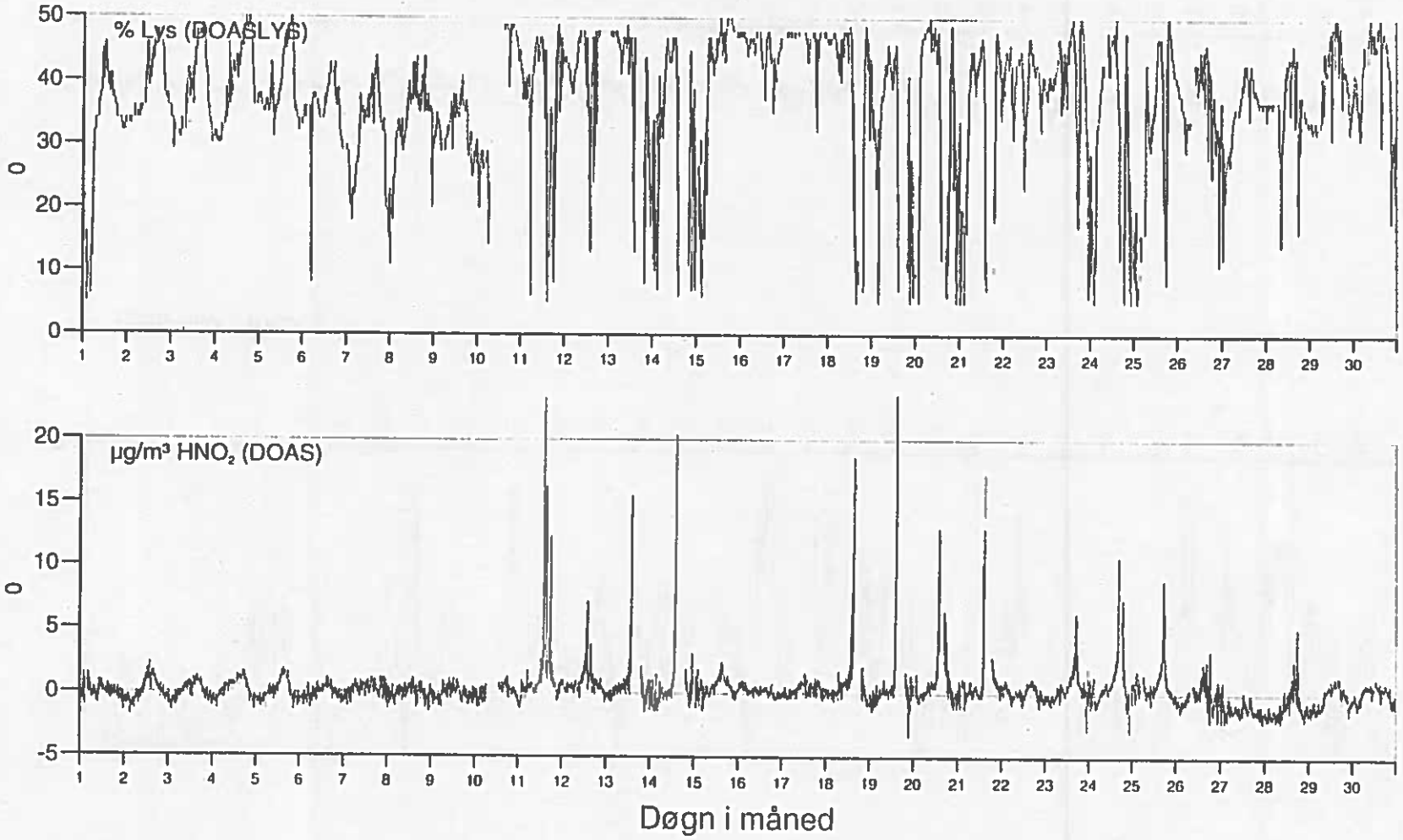

19990423

2090 Lille Valby Minutmiddelværdier for 19980701-19980731

Nulpunktskorrigerede data

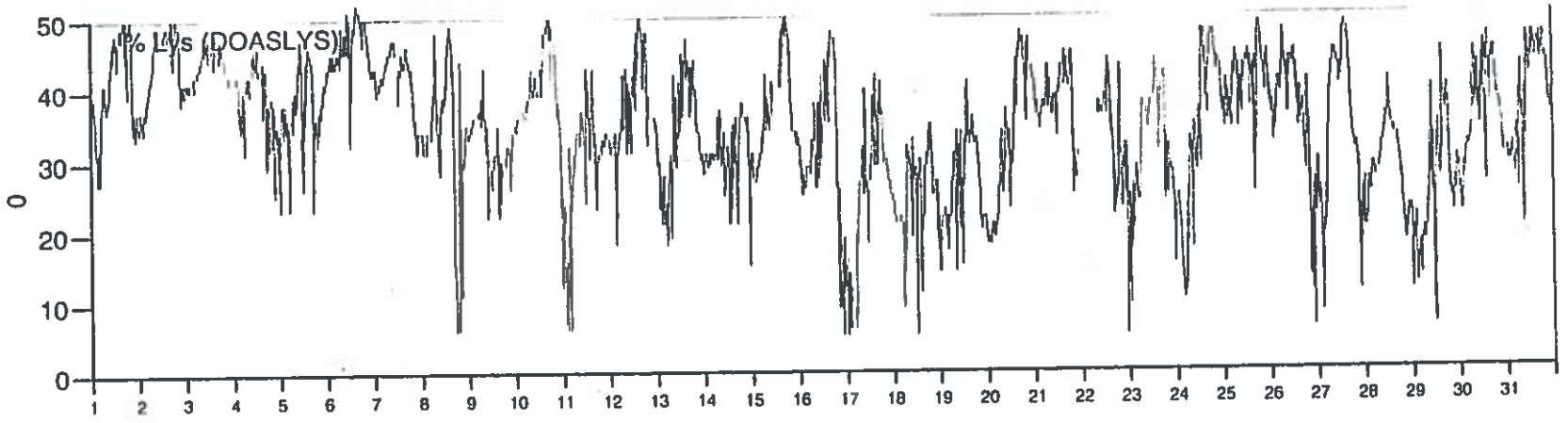

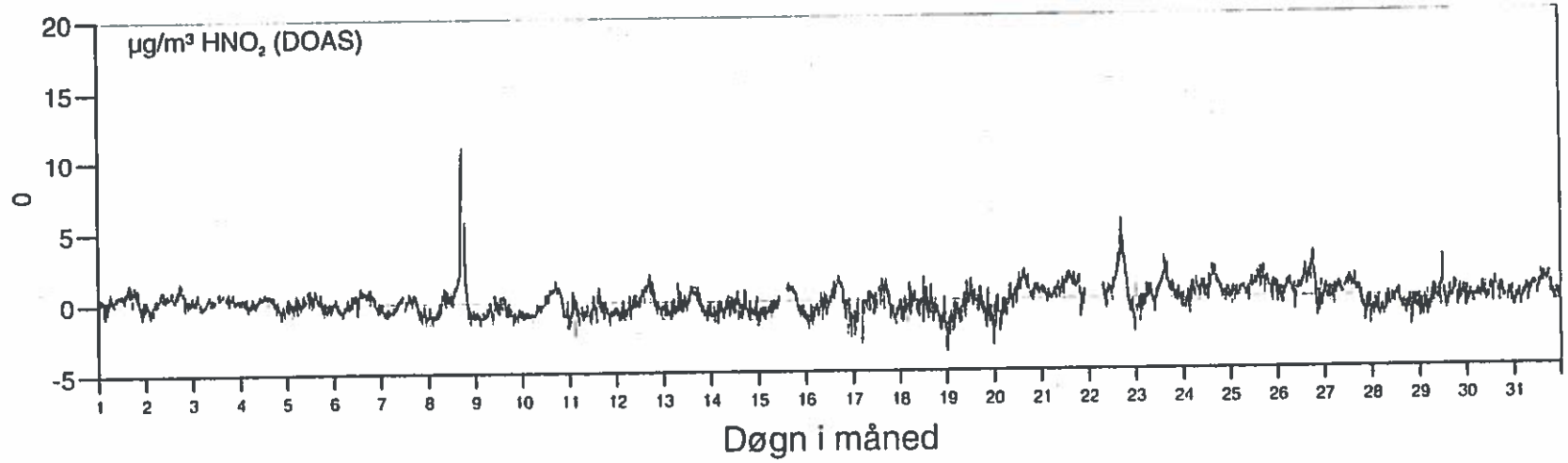

19990423

2090 Lille Valby Minutmiddelværdier for 19980801-19980831

Nulpunktskorrigerede data

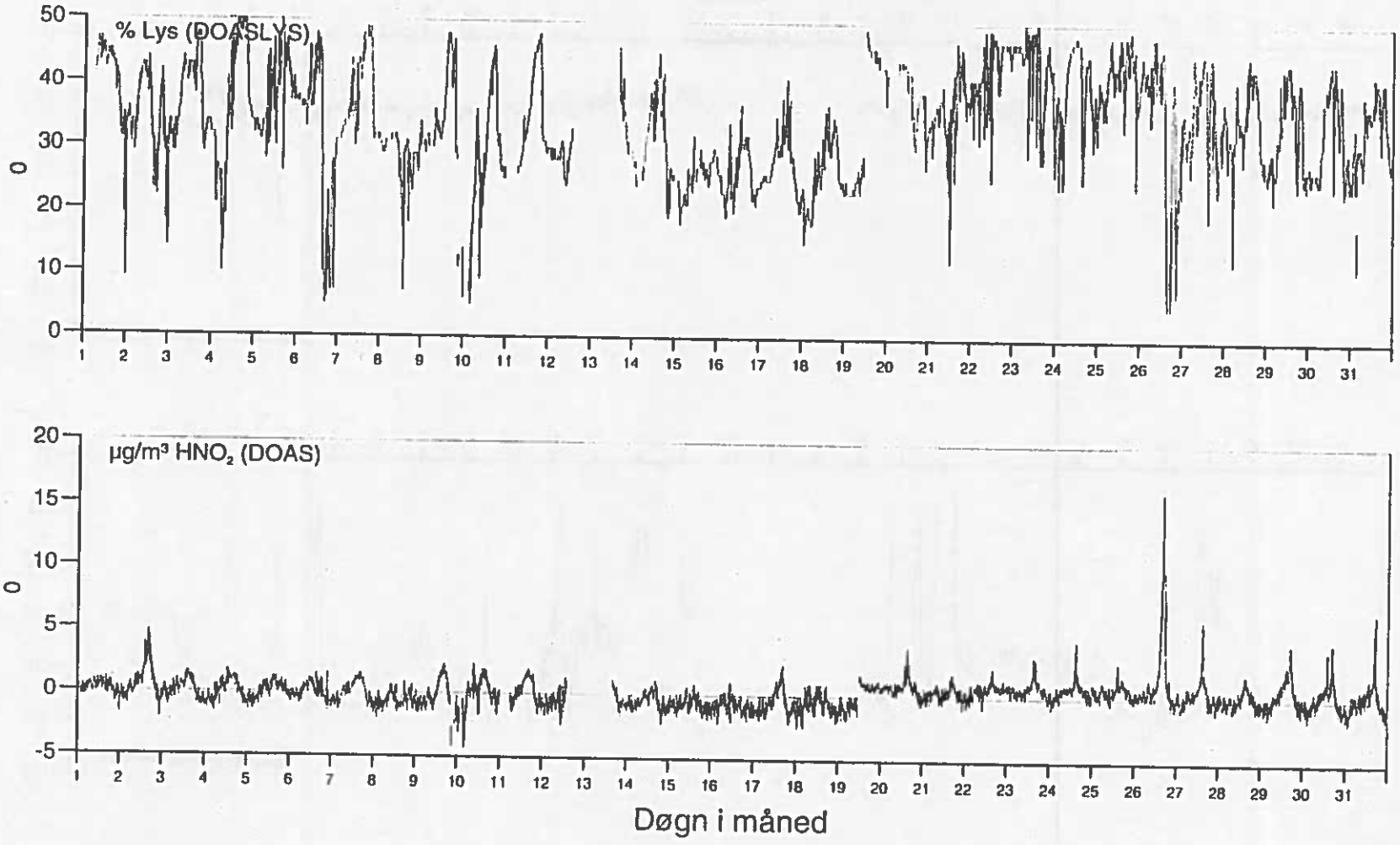

19990423

2090 Lille Valby Minutmiddelværdier for 19980901-19980930

Nulpunktskorrigerede data

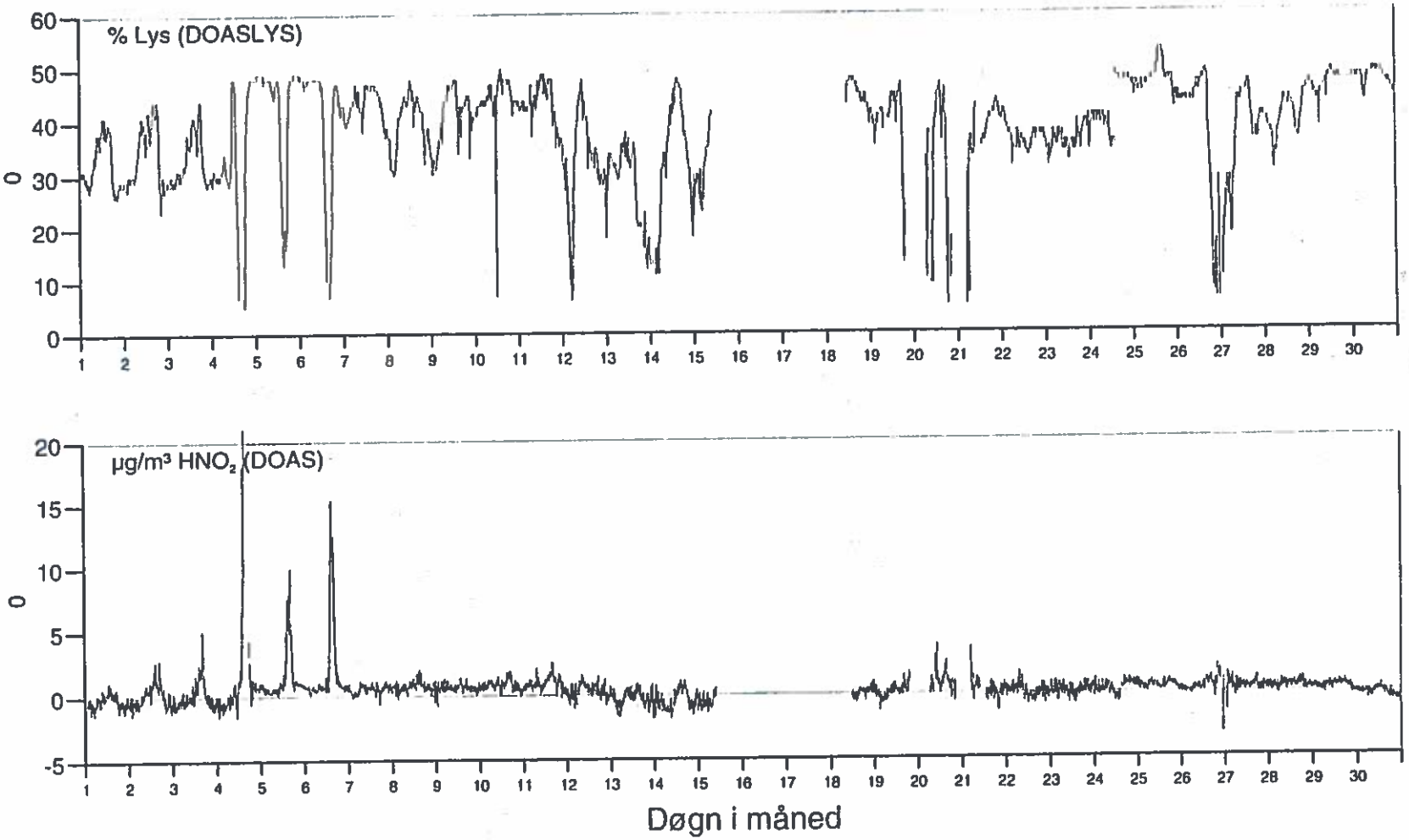

19990423

Appendix A.4

Lille Valby DOAS measurements

NO_3

This appendix gives the results of the Lille Valby NO_3 DOAS measurements. Page 144 shows the concentration level and light level of the "raw" data for May, 1998. Pages 145 through 149 gives the May - September, 1998, NO_3 measurement data, when light levels below 5 % have been excluded.

2090 Lille Valby Minutmiddelværdier for 19980501-19980531

Rå data

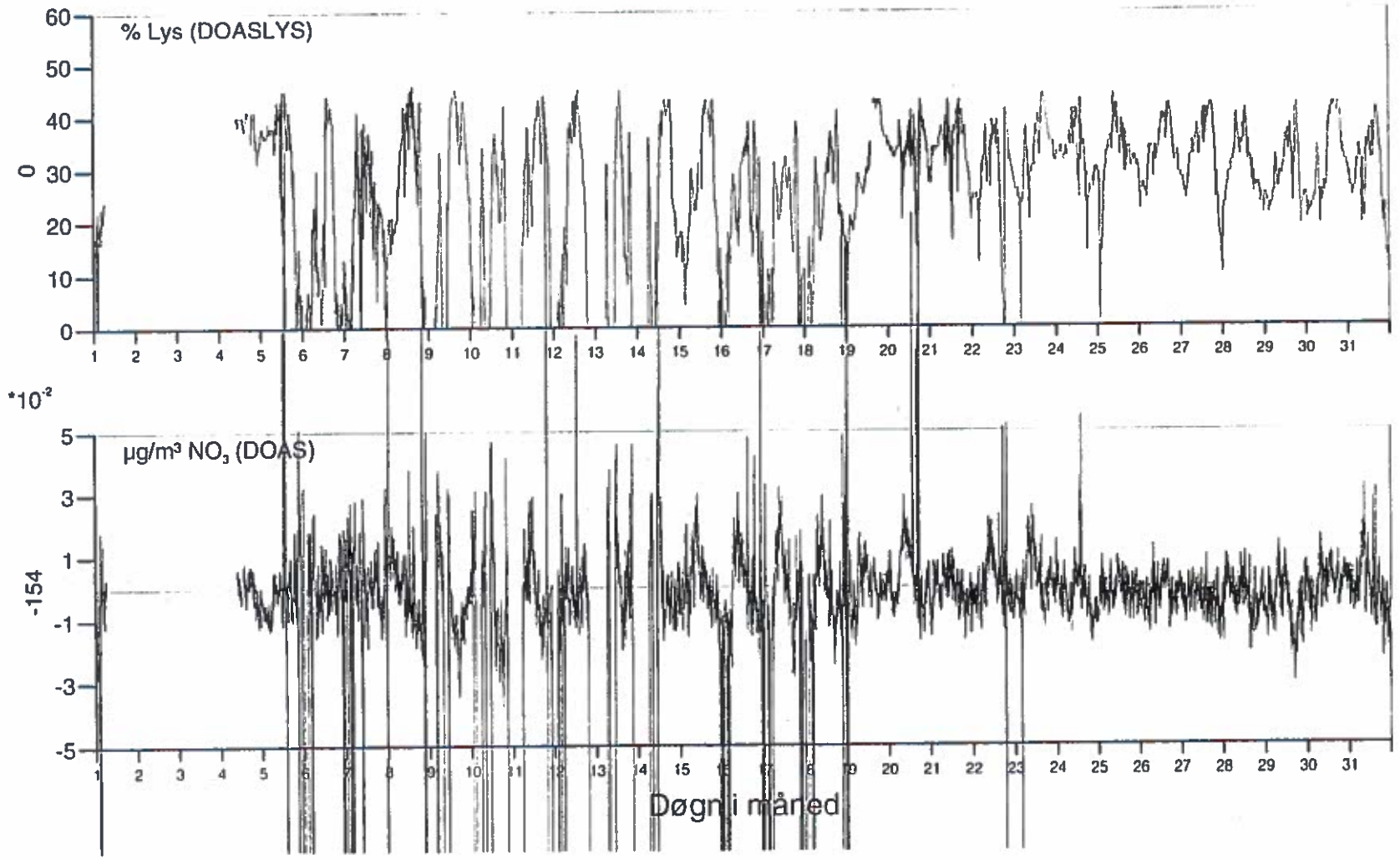

19990515

2090 Lille Valby Minutmiddelværdier for 19980501-19980531

Nulpunktskorrigerede data

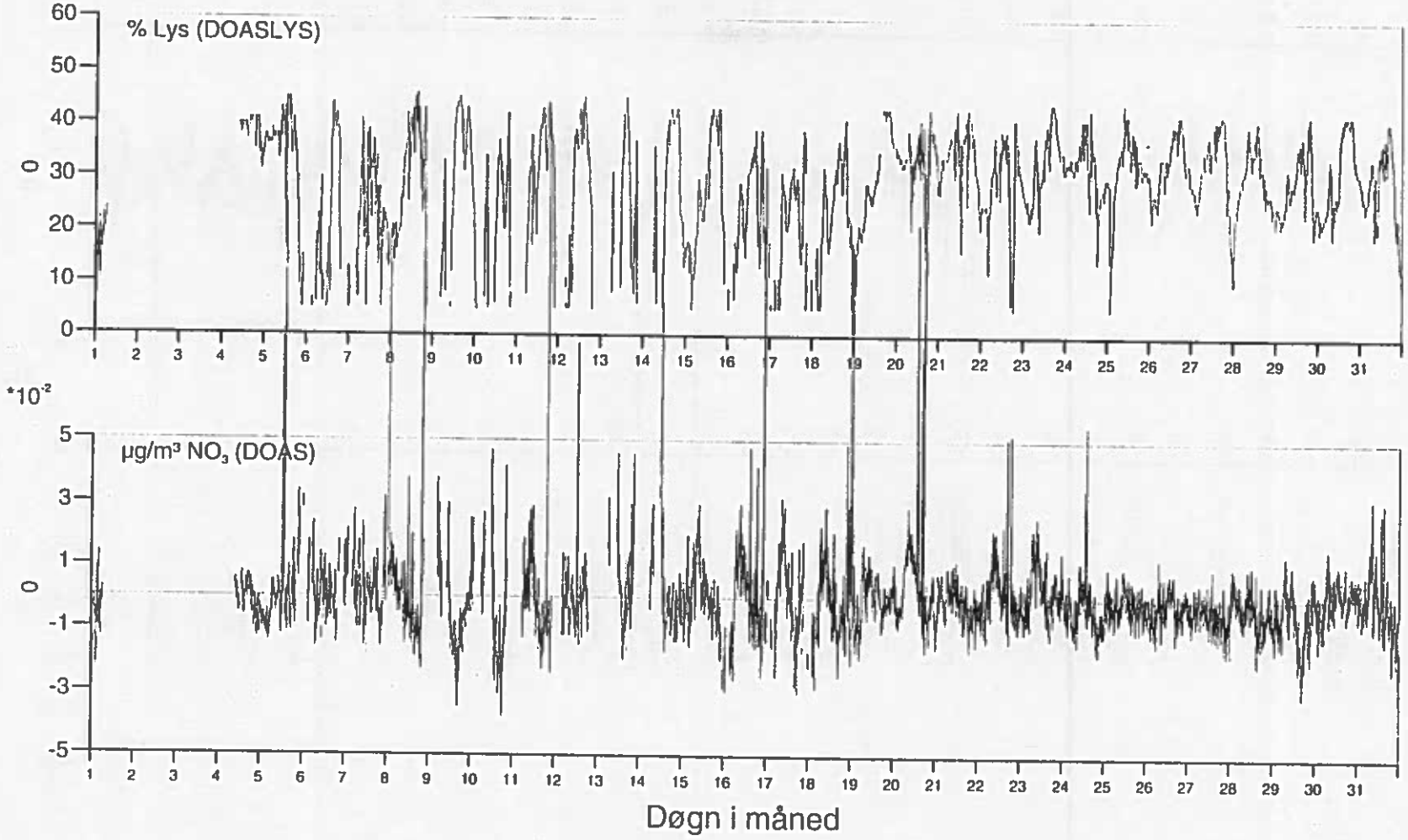

19990515

2090 Lille Valby Minutmiddelværdier for 19980601-19980630

Nulpunktskorrigerede data

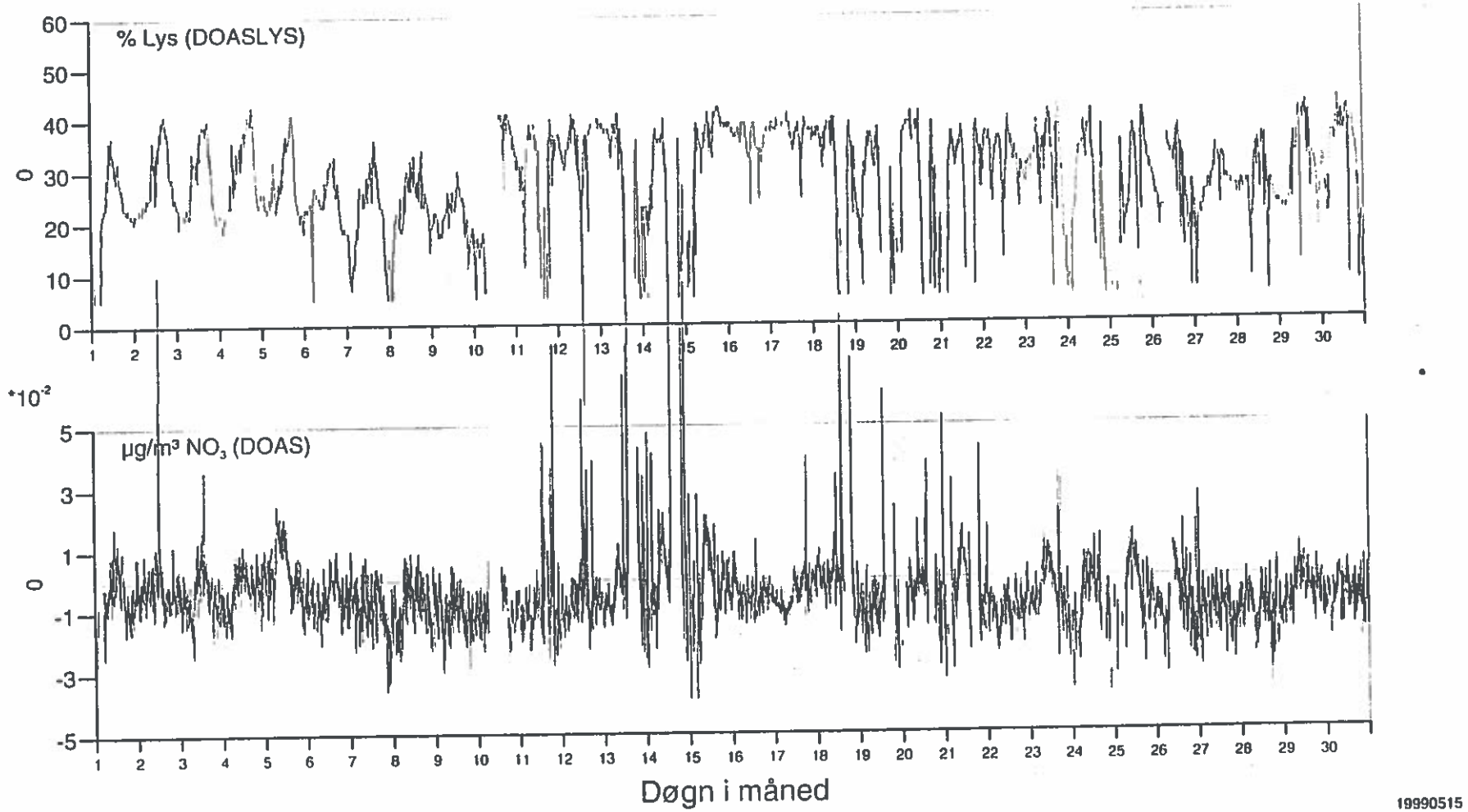

19990515

2090 Lille Valby Minutmiddelværdier for 19980801-19980831

Nulpunktskorrigerede data

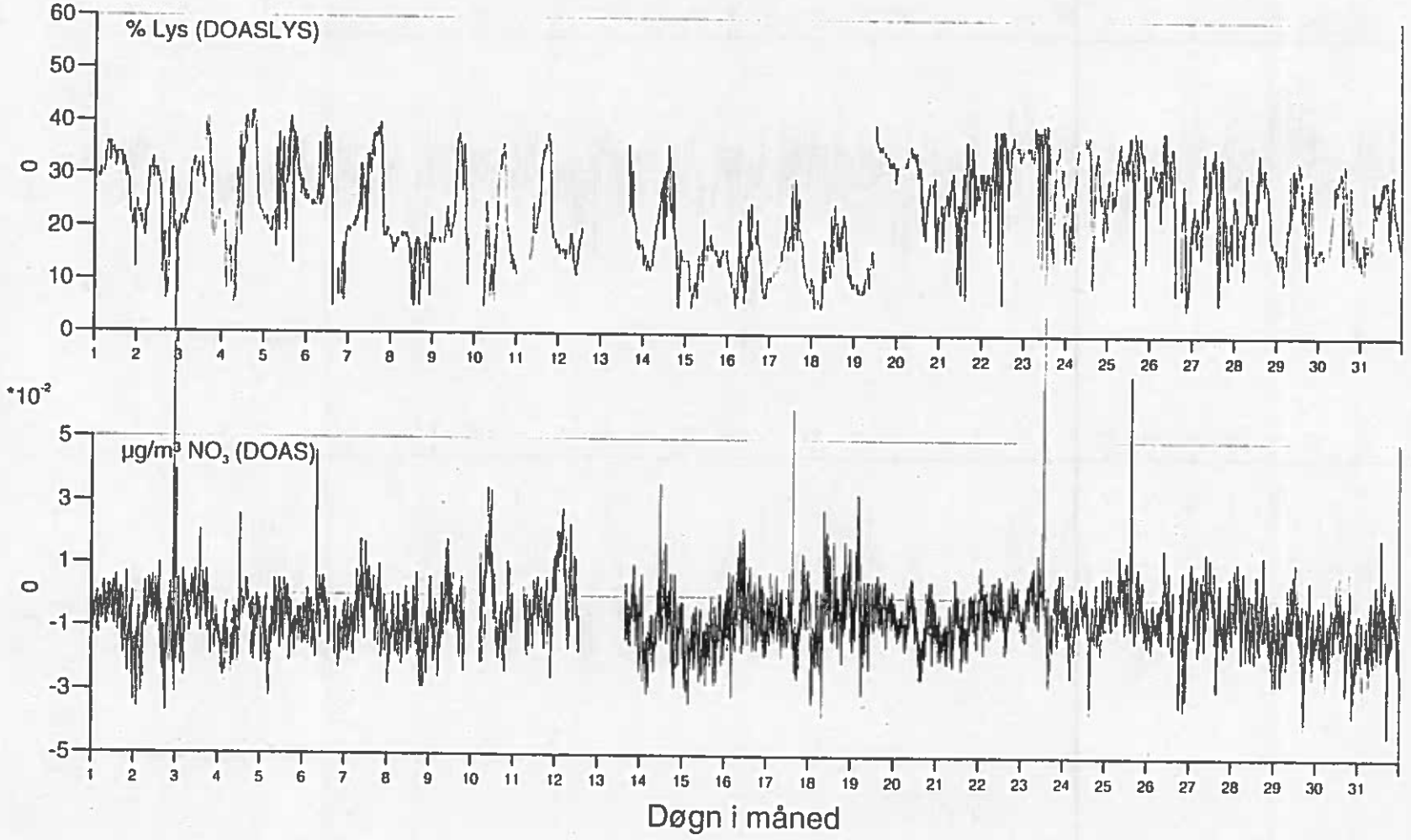

19990515

2090 Lille Valby Minutmiddelværdier for 19980701-19980731

Nulpunktskorrigerede data

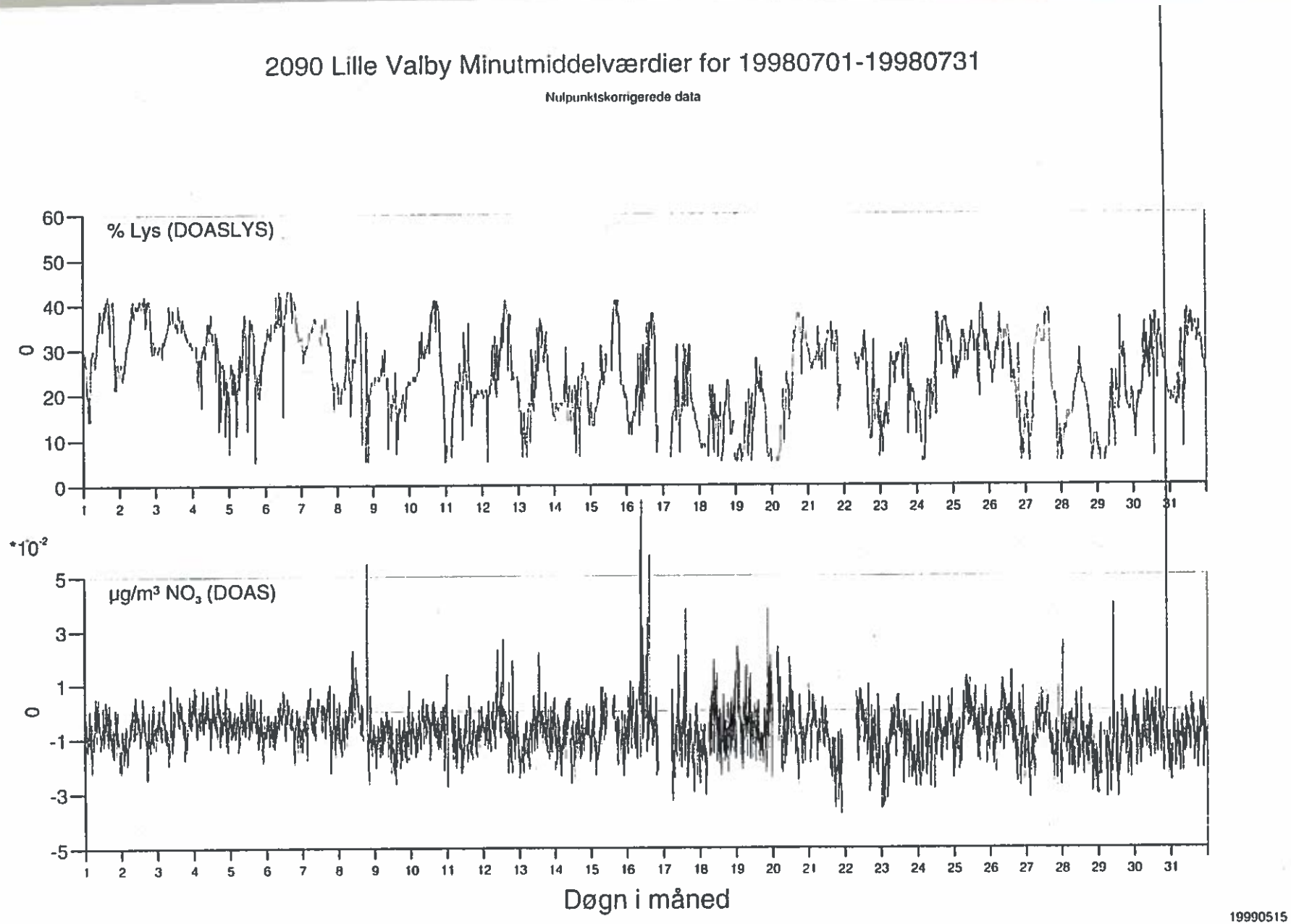

19990515

2090 Lille Valby Minutmiddelværdier for 19980901-19980930

Nulpunktskorrigerede data

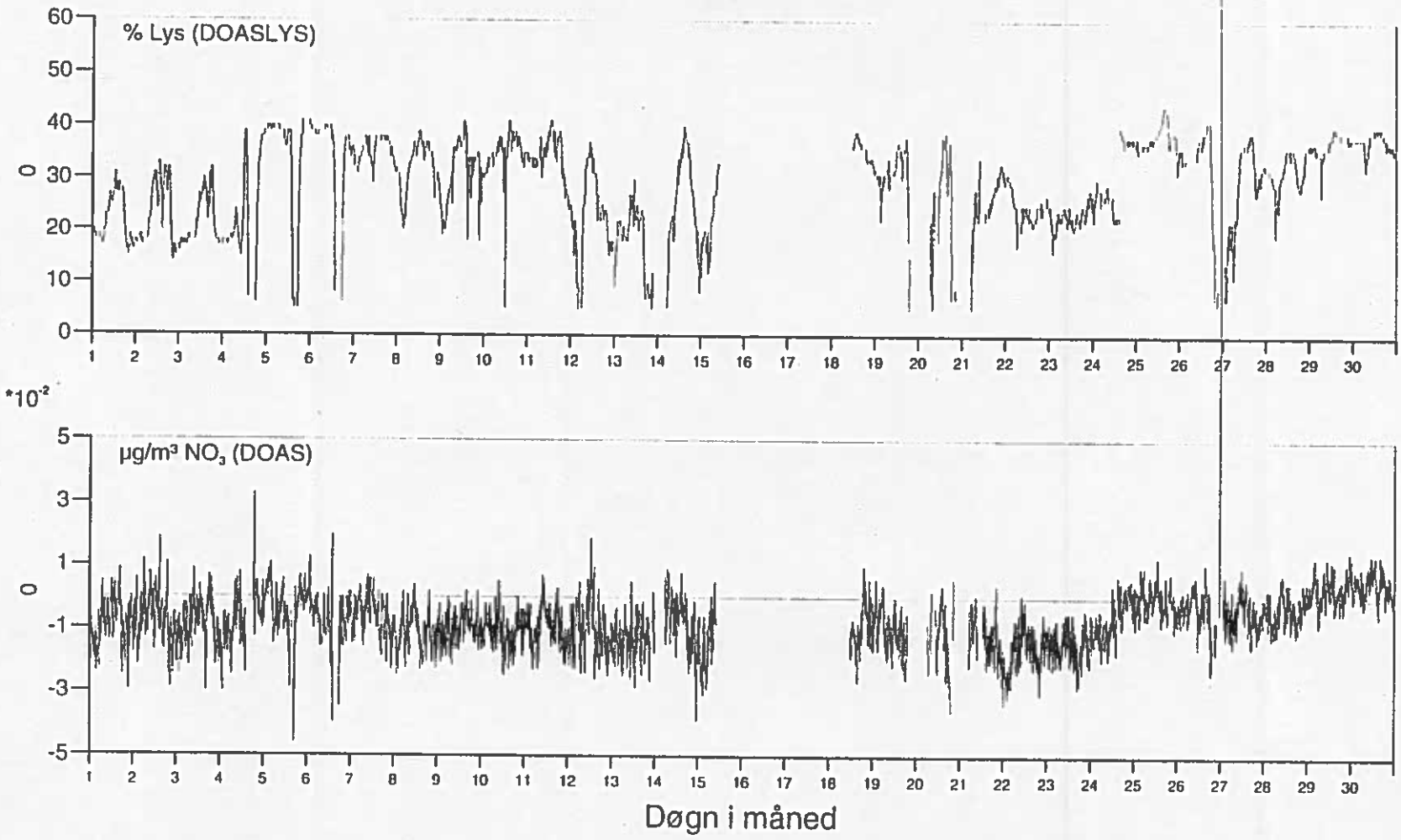

19990515

Appendix B.1

DOAS Quality Control

NO_2

This appendix shows plots of light level versus std.dev. and concentration versus std.dev. for the Lille Valby NO_2 DOAS measurements, April - September, 1998. The plots can be used in quality control of the DOAS data as described in chapter 3.6.

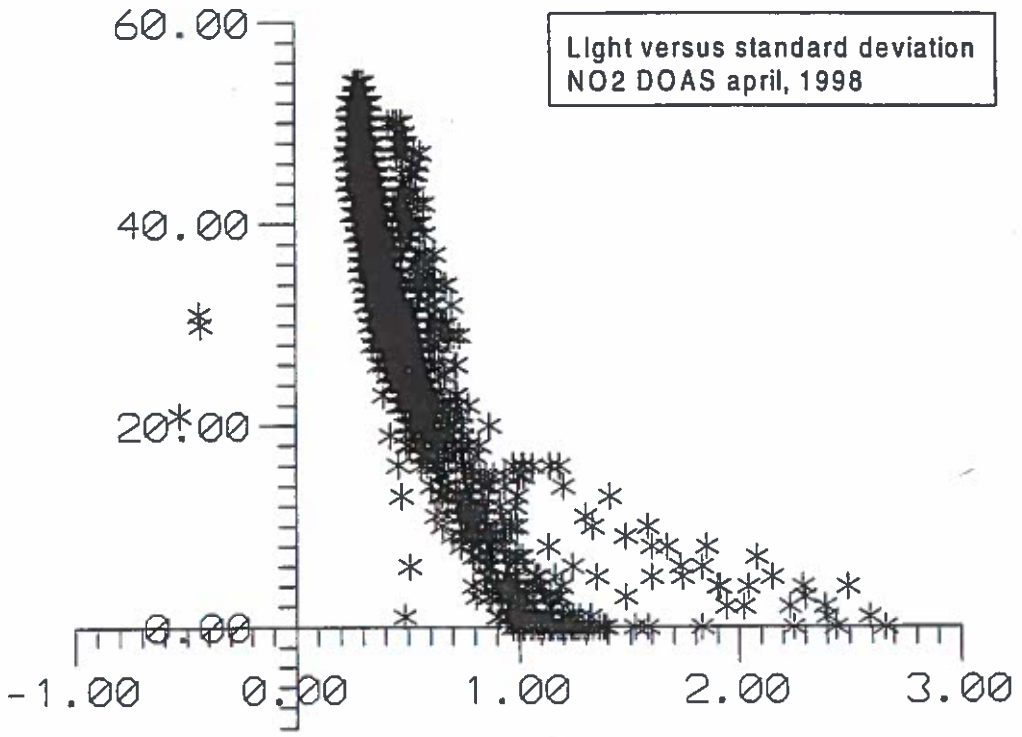
Light versus standard deviation
NO2 DOAS april, 1998
60.00
40.00
20.00
0.00
-1.00
0.00
1.00
2.00
3.00

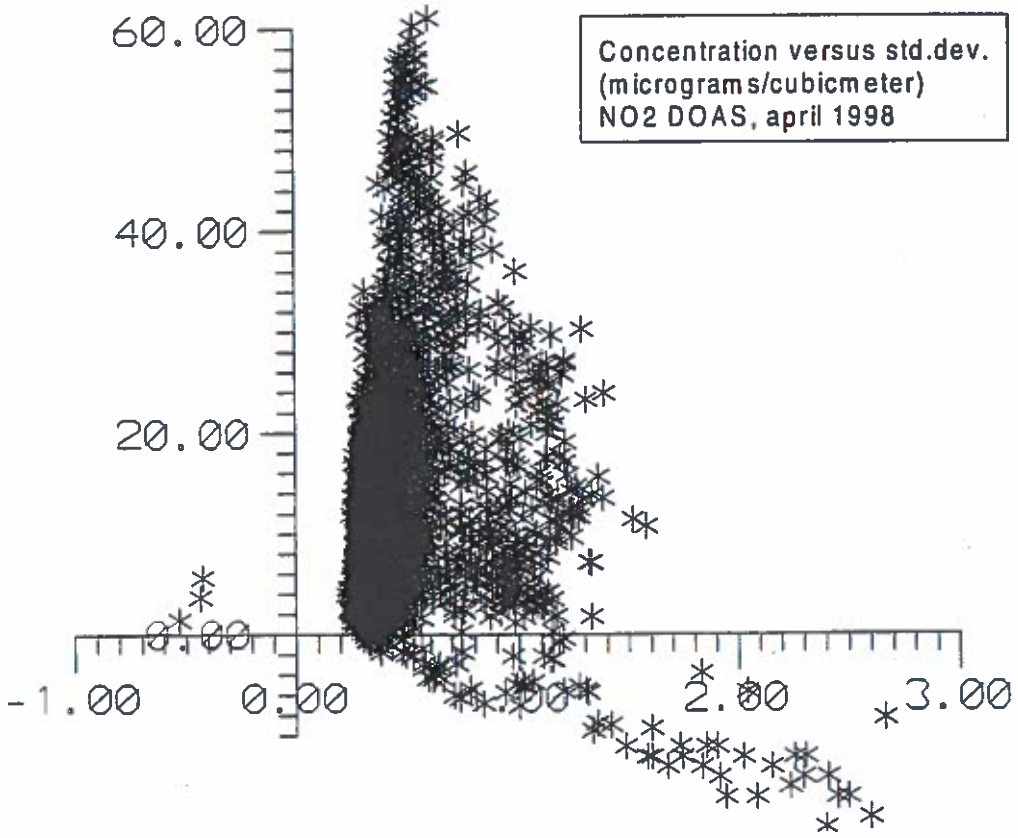
Concentration versus std.dev.
(micrograms/cubicmeter)
NO2 DOAS, april 1998
60.00
40.00
20.00
0.00
-1.00
0.00
2.00
3.00

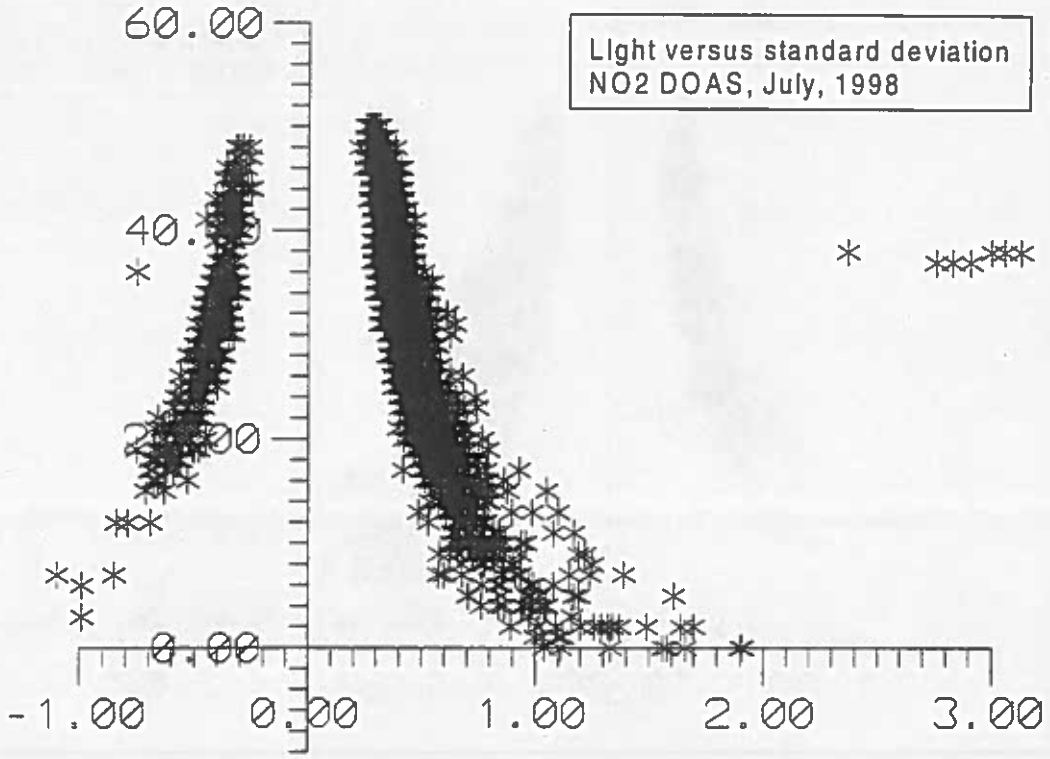
Light versus standard deviation
NO2 DOAS, July, 1998
60.00
40.00
20.00
0.00
-1.00
0.00
1.00
2.00
3.00

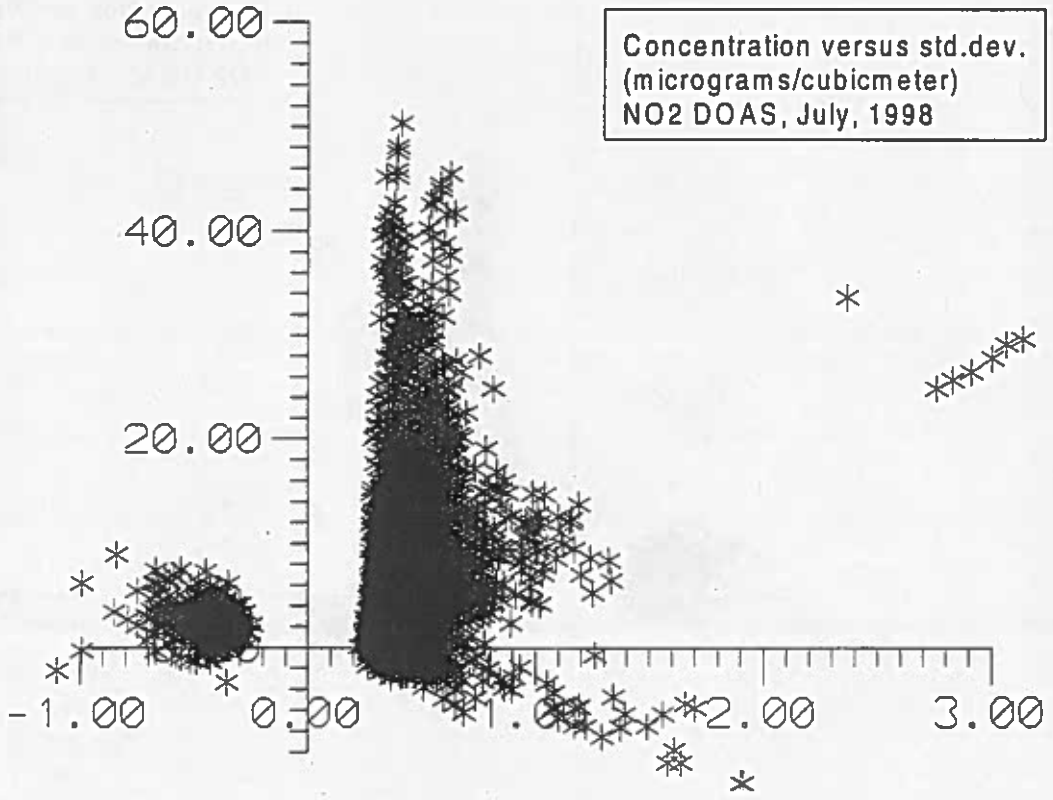
Concentration versus std.dev.
(micrograms/cubicmeter)
NO2 DOAS, July, 1998
60.00
40.00
20.00
-1.00
0.00
1.00
2.00
3.00

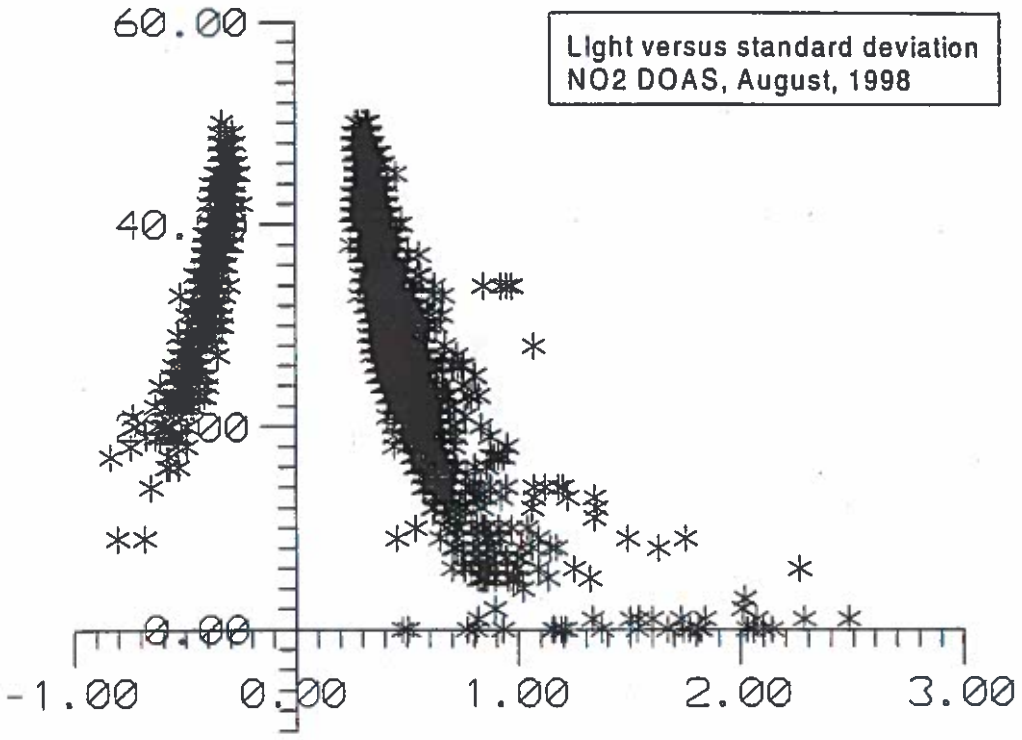
Light versus standard deviation
NO2 DOAS, August, 1998
60.00
40.00
0.00
-1.00
0.00
1.00
2.00
3.00

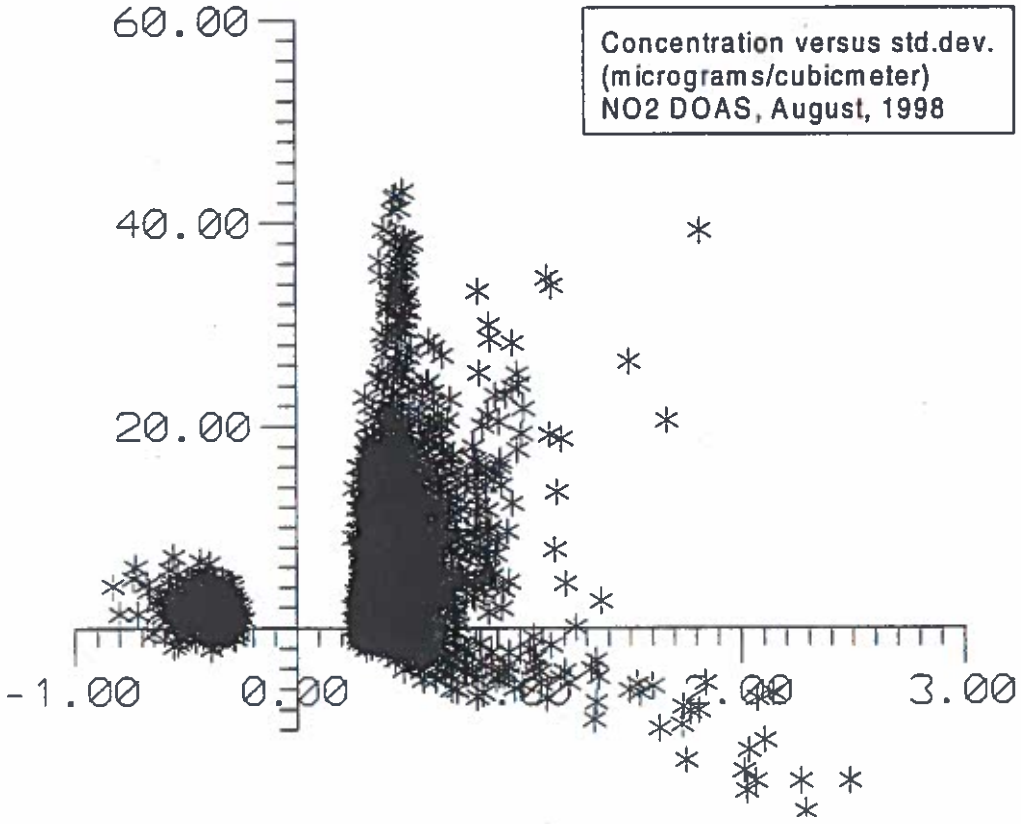
Concentration versus std.dev.
(micrograms/cubicmeter)
NO2 DOAS, August, 1998
60.00
40.00
20.00
-1.00
0.00
3.00

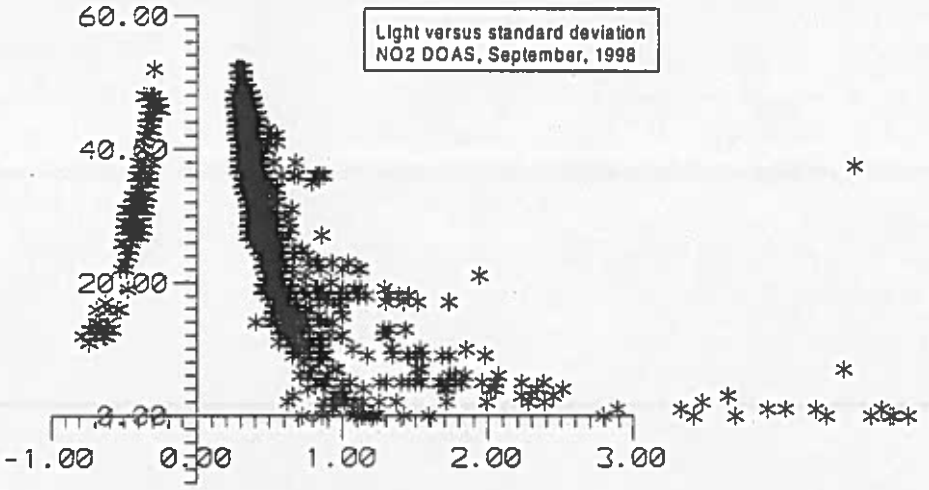
Light versus standard deviation
NO2 DOAS, September, 1998
60.00
40.00
20.00
0.00
-1.00
0.00
1.00
2.00
3.00

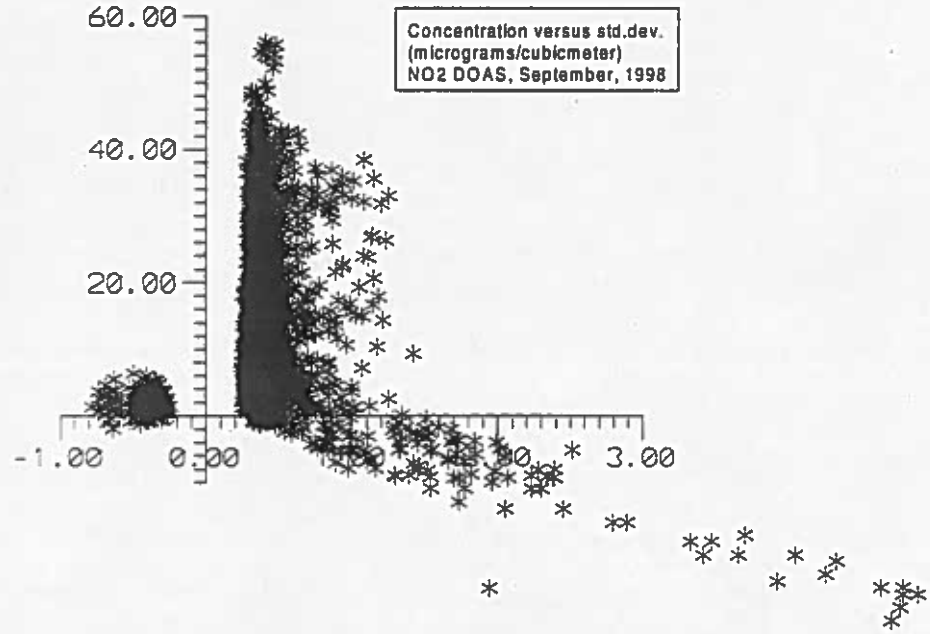
Concentration versus std.dev.
(micrograms/cubicmeter)
NO2 DOAS, September, 1998
60.00
40.00
20.00
-1.00
0.00
3.00

Appendix B.2

DOAS Quality Control

O_3

This appendix shows plots of light level versus std.dev. and concentration versus std.dev. for the Lille Valby O_3 DOAS measurements, April - September, 1998. The plots can be used in quality control of the DOAS data as described in chapter 3.6.

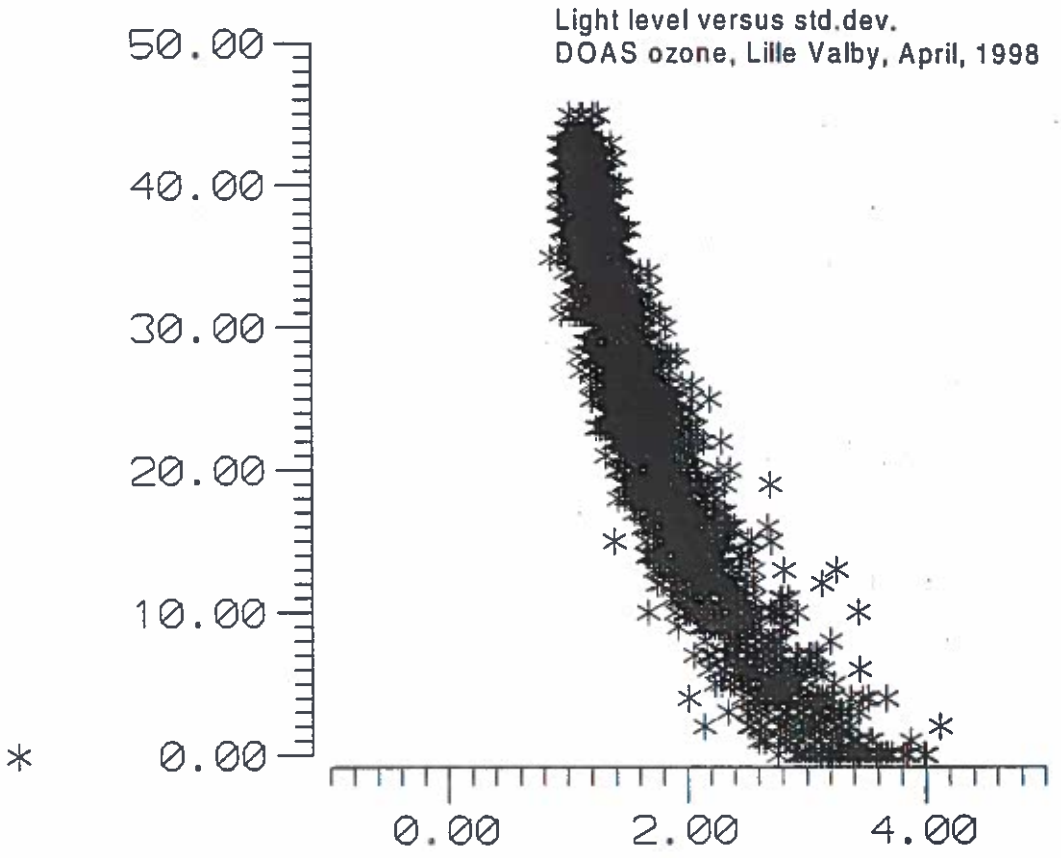
Light level versus std.dev.
DOAS ozone, Lille Valby, April, 1998
50.00
40.00
30.00
20.00
10.00
0.00
0.00
2.00
4.00

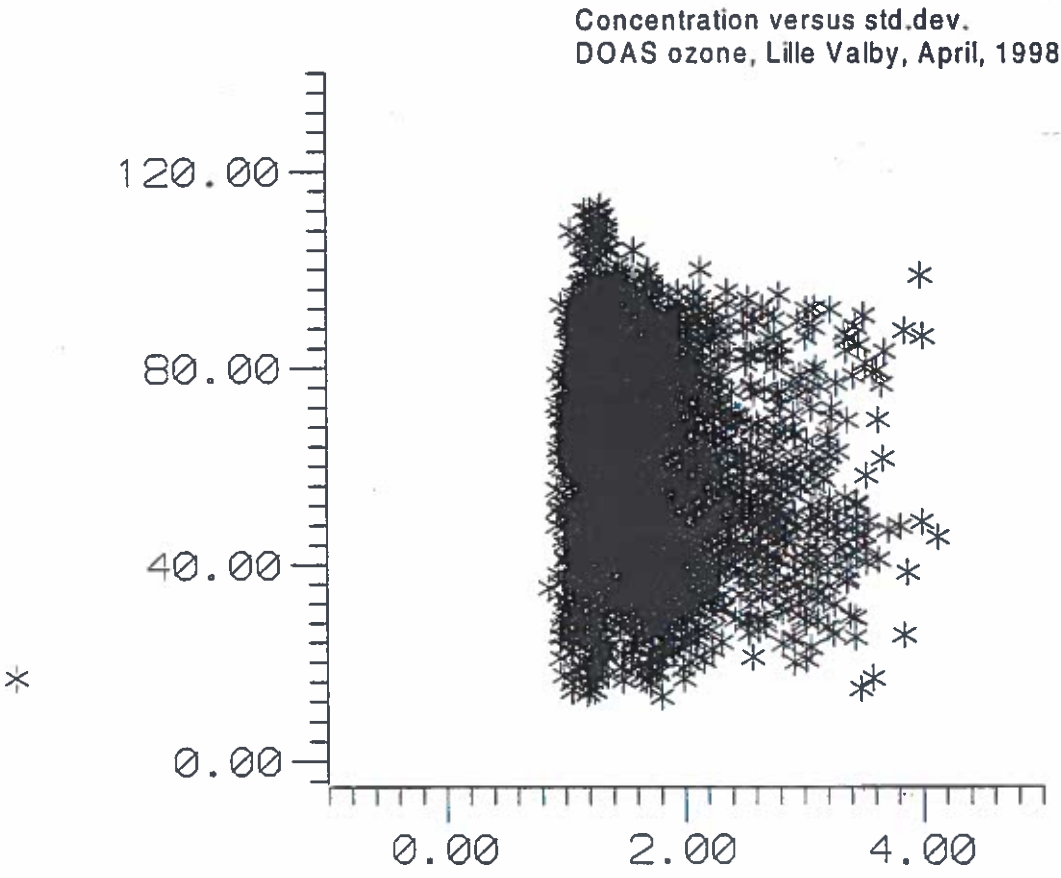
Concentration versus std.dev.
DOAS ozone, Lille Valby, April, 1998
120.00
80.00
40.00
0.00
0.00
2.00
4.00

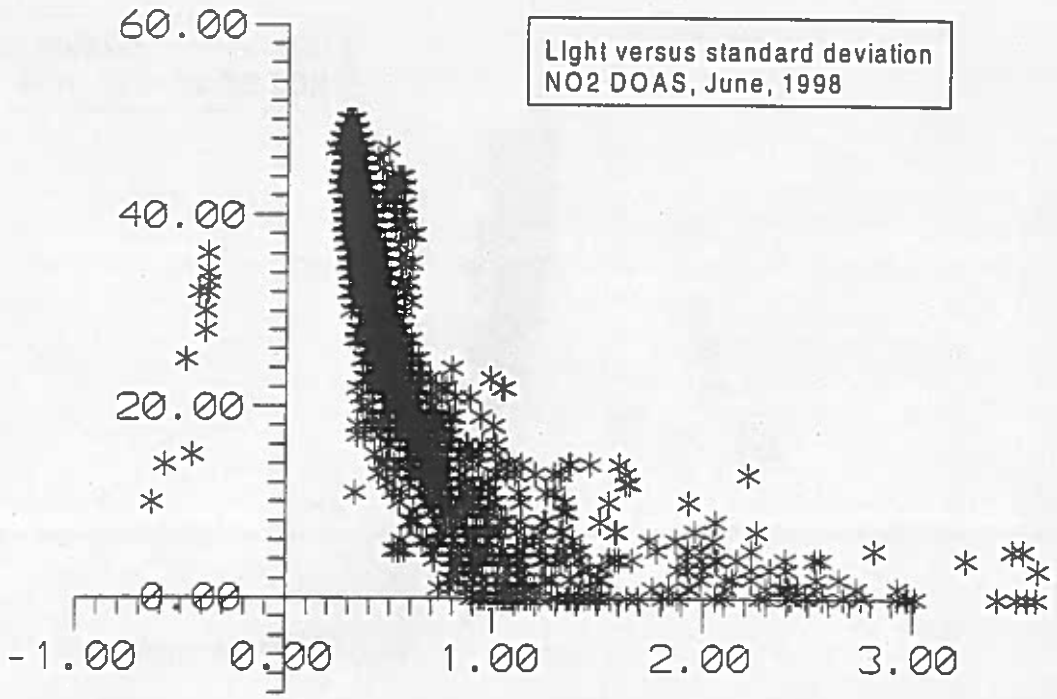
LIght versus standard deviation
NO2 DOAS, June, 1998
60.00
40.00
20.00
0.00
-1.00
0.00
1.00
2.00
3.00

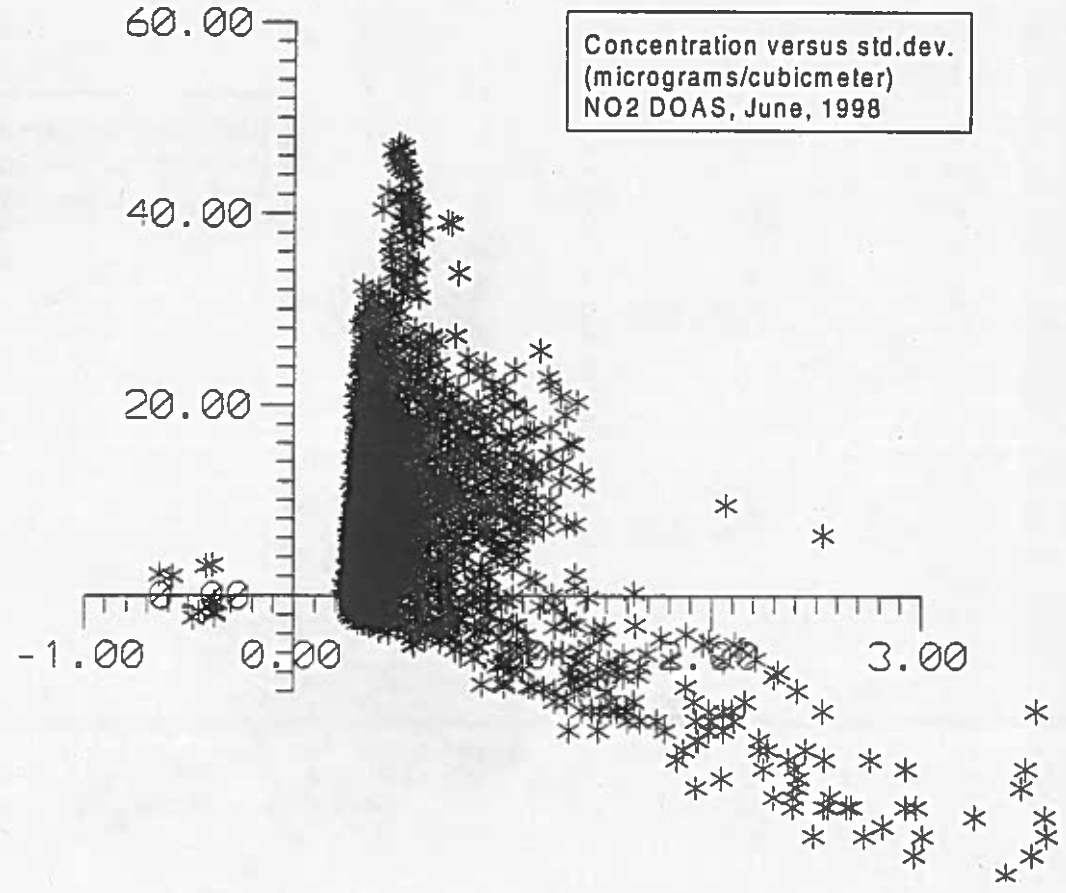
Concentration versus std.dev.
(micrograms/cubicmeter)
NO2 DOAS, June, 1998
60.00
40.00
20.00
0.00
-1.00
0.00
3.00

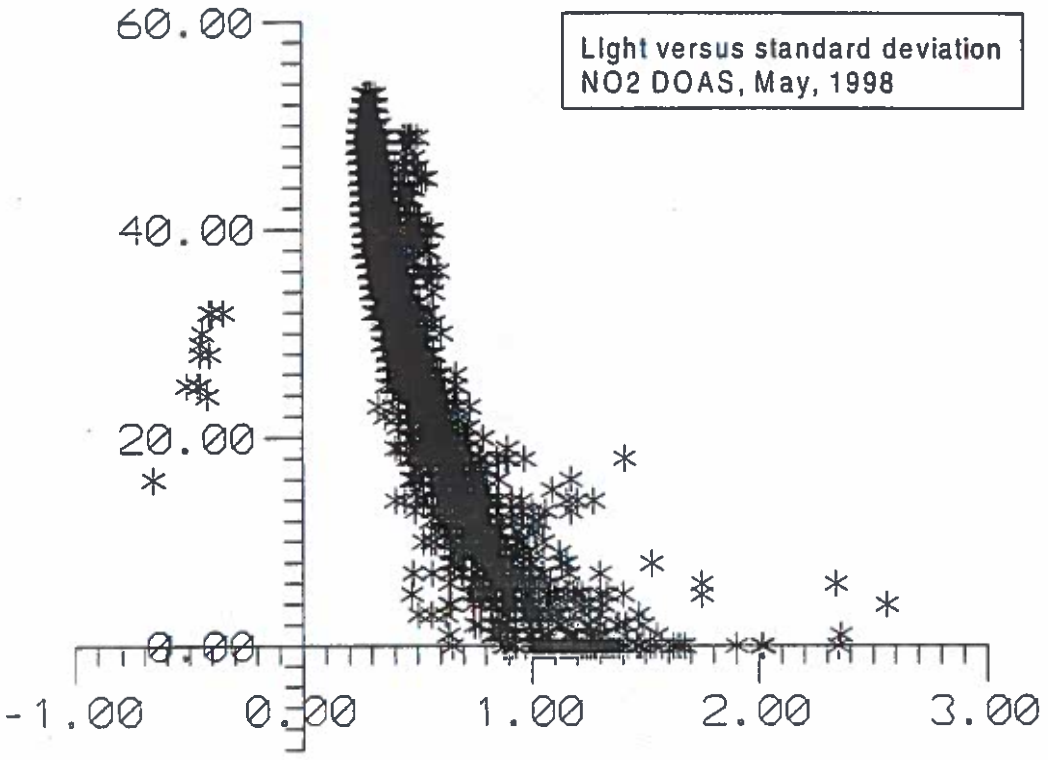
Light versus standard deviation
NO2 DOAS, May, 1998
60.00
40.00
20.00
0.00
-1.00
0.00
1.00
2.00
3.00

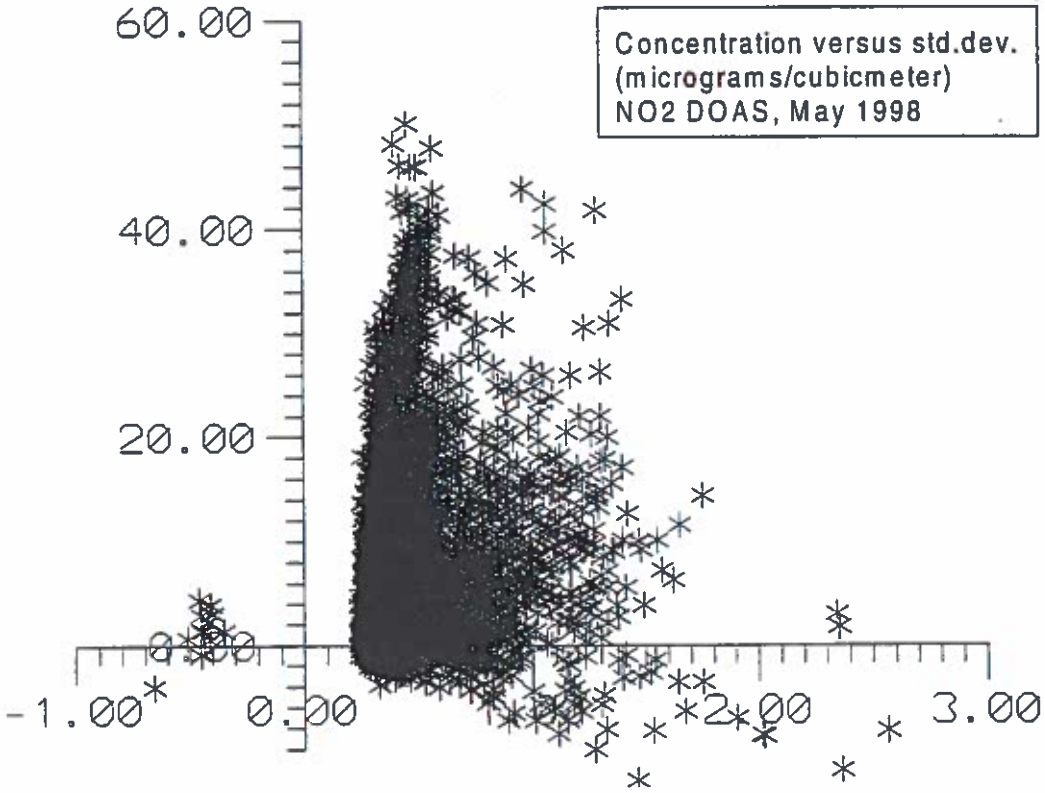
Concentration versus std.dev.
(micrograms/cubicmeter)
NO2 DOAS, May 1998
60.00
40.00
20.00
0.00
-1.00
0.00
2.00
3.00

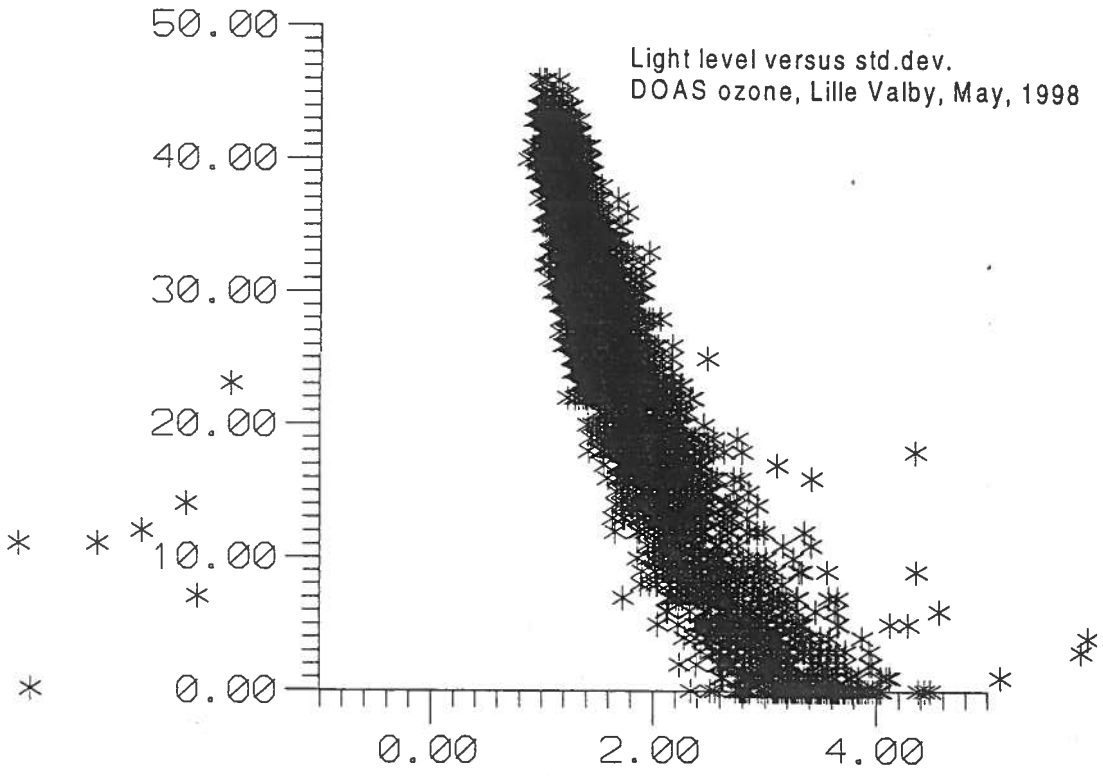
Light level versus std.dev.
DOAS ozone, Lille Valby, May, 1998
50.00
40.00
30.00
20.00
10.00
0.00
0.00
2.00
4.00

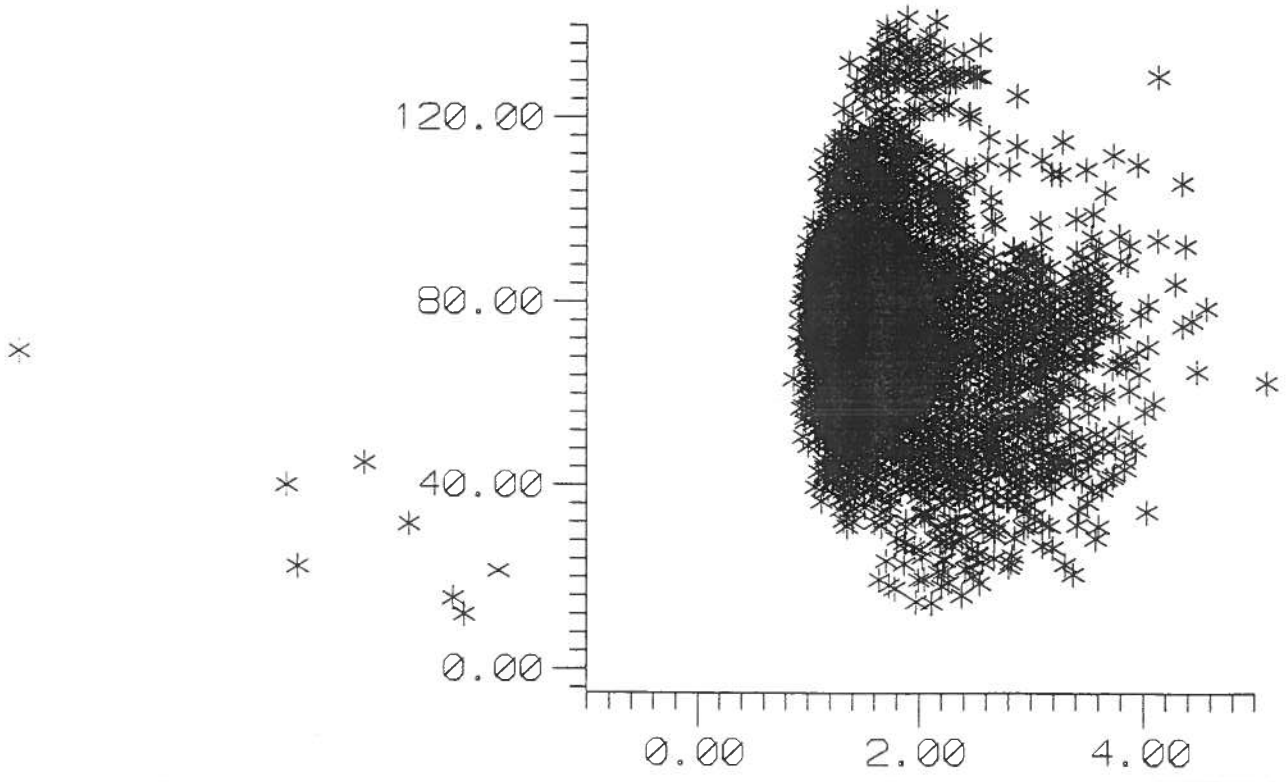
Concentration versus std.dev.
DOAS ozone, Lille Valby, May, 1998
120.00
80.00
40.00
0.00
0.00
2.00
4.00

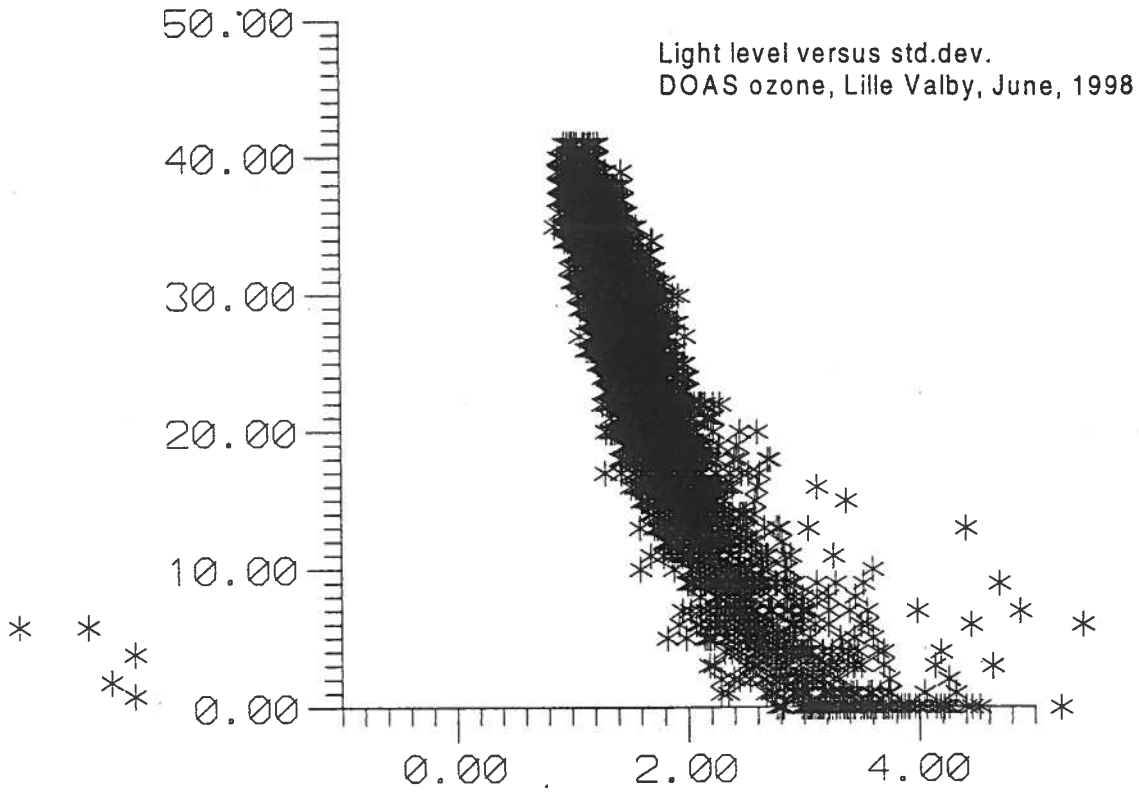
Light level versus std.dev.
DOAS ozone, Lille Valby, June, 1998
50.00
40.00
30.00
20.00
10.00
0.00
0.00
2.00
4.00

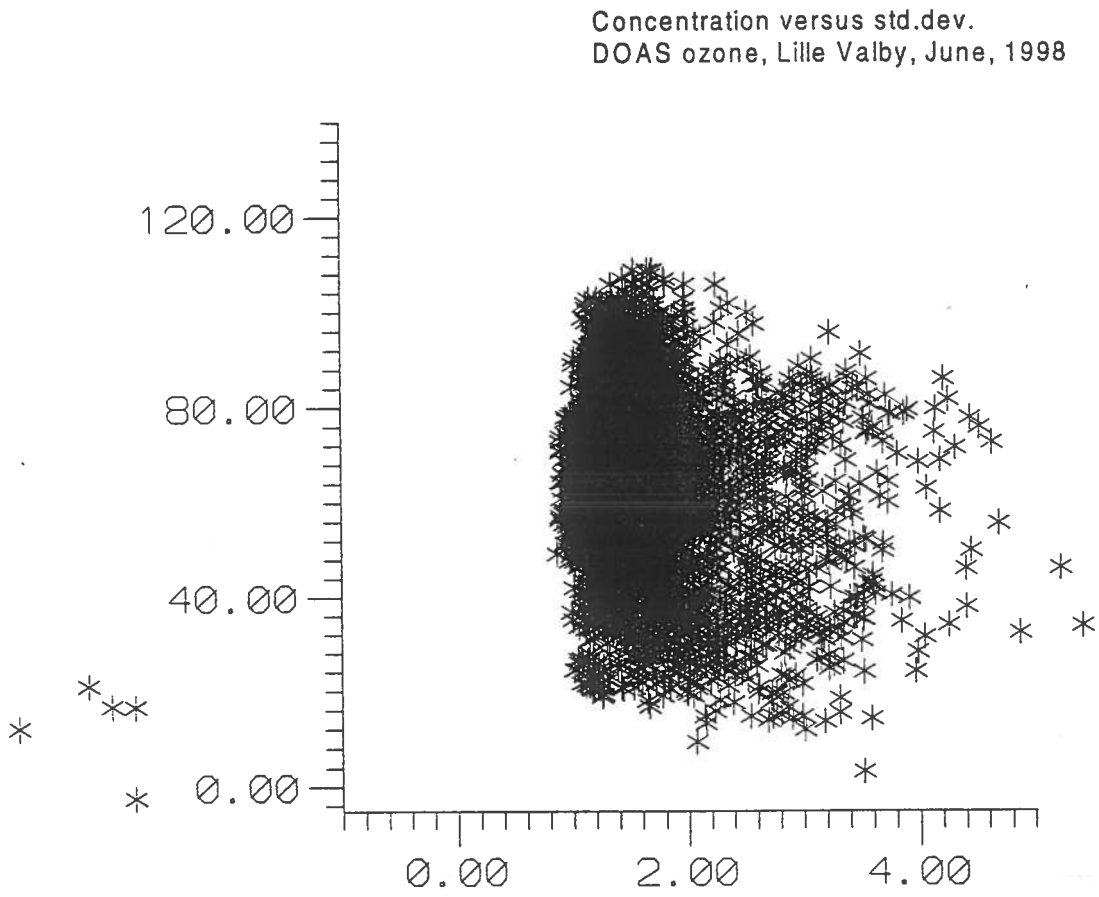
Concentration versus std.dev.
DOAS ozone, Lille Valby, June, 1998
120.00
80.00
40.00
0.00
0.00
2.00
4.00

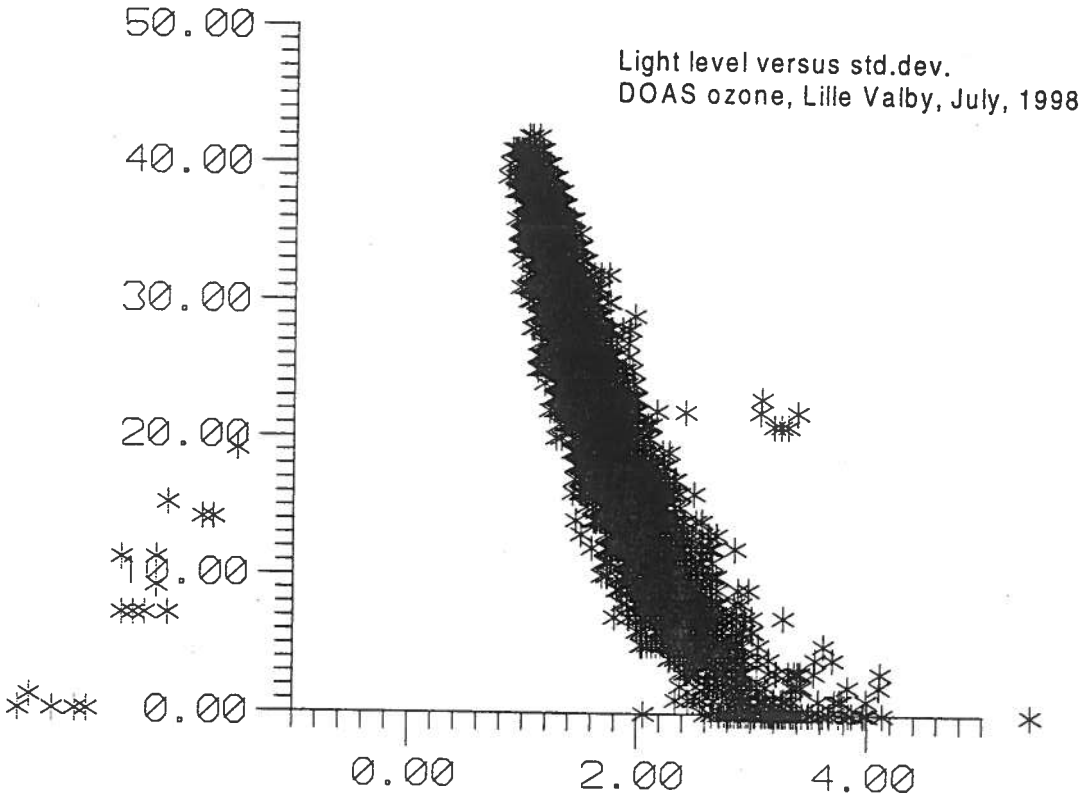
Light level versus std.dev.
DOAS ozone, Lille Valby, July, 1998
50.00
40.00
30.00
20.00
10.00
0.00
0.00
2.00
4.00

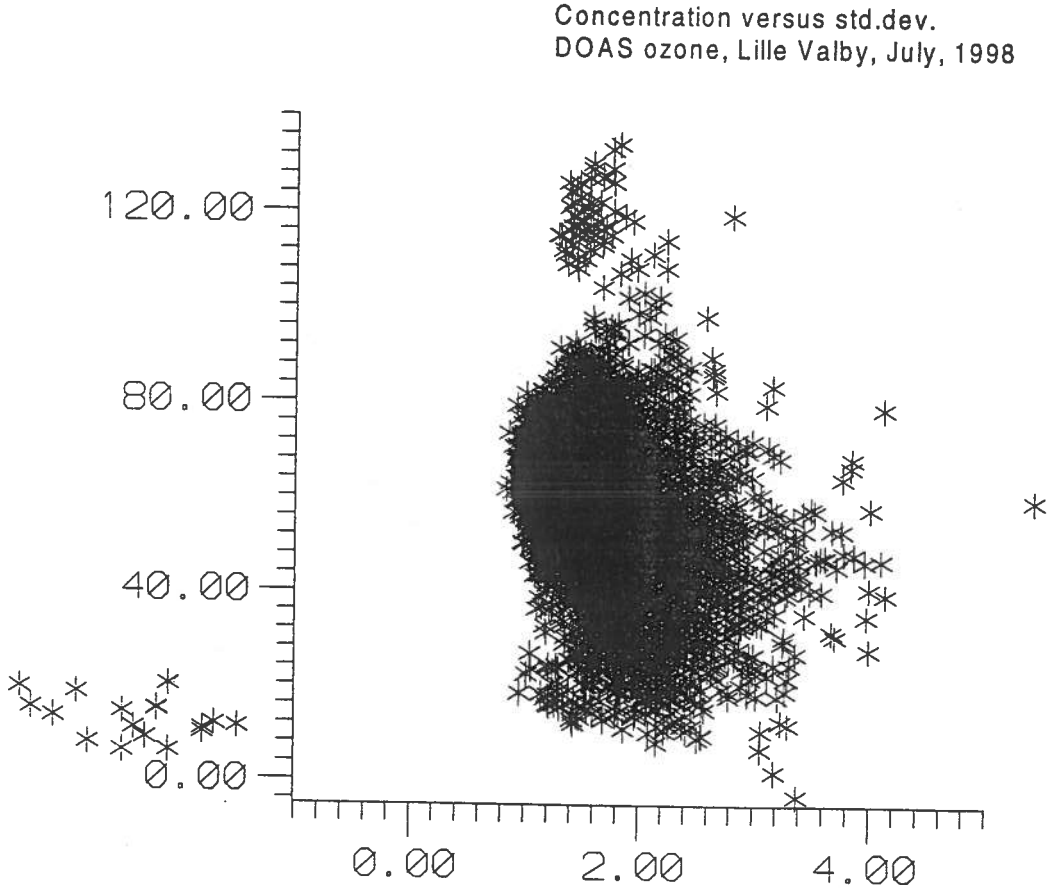
Concentration versus std.dev.
DOAS ozone, Lille Valby, July, 1998
120.00
80.00
40.00
0.00
0.00
2.00
4.00

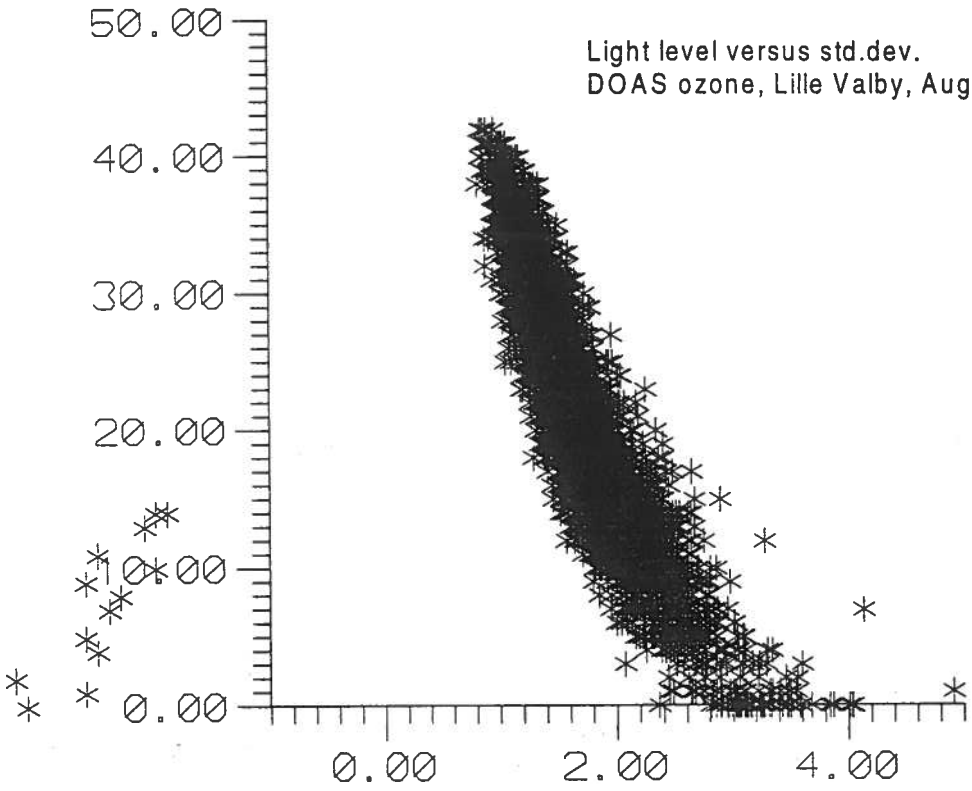
Light level versus std.dev.
DOAS ozone, Lille Valby, August, 1998
50.00
40.00
30.00
20.00
10.00
0.00
0.00
2.00
4.00

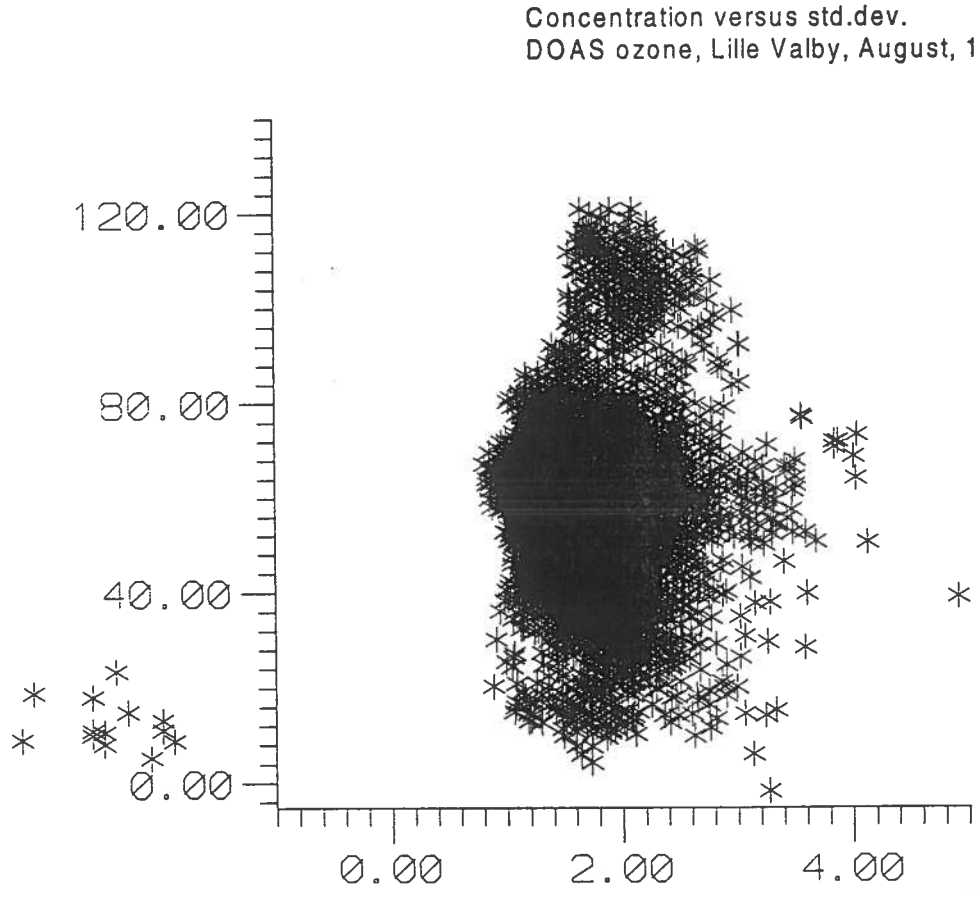
Concentration versus std.dev.
DOAS ozone, Lille Valby, August, 1998
120.00
80.00
40.00
0.00
0.00
2.00
4.00

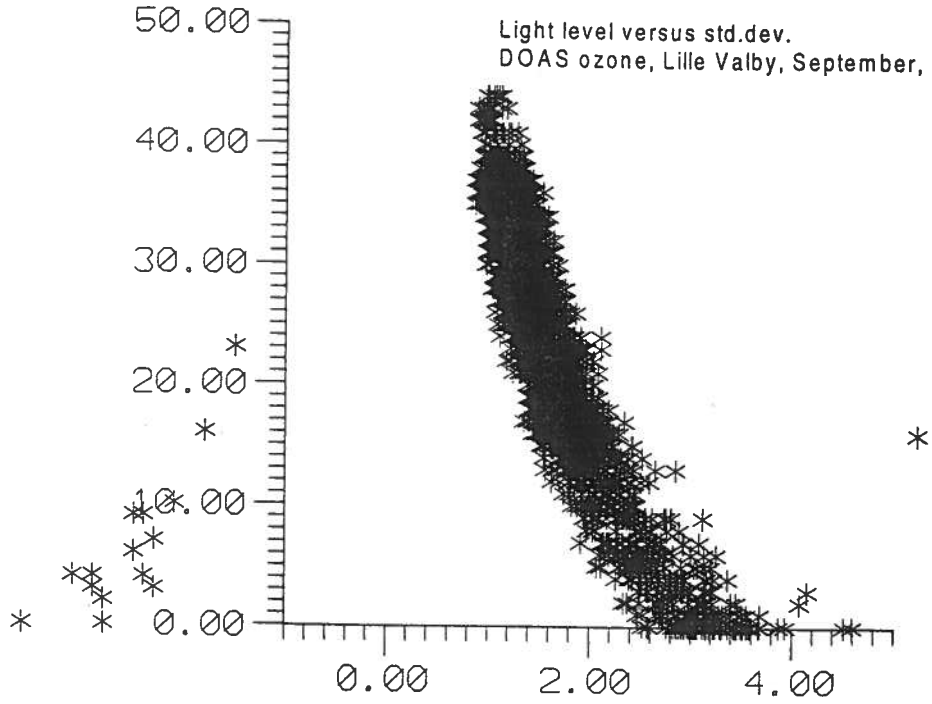
Light level versus std.dev.
DOAS ozone, Lille Valby, September, 1998
50.00
40.00
30.00
20.00
10.00
0.00
0.00
2.00
4.00

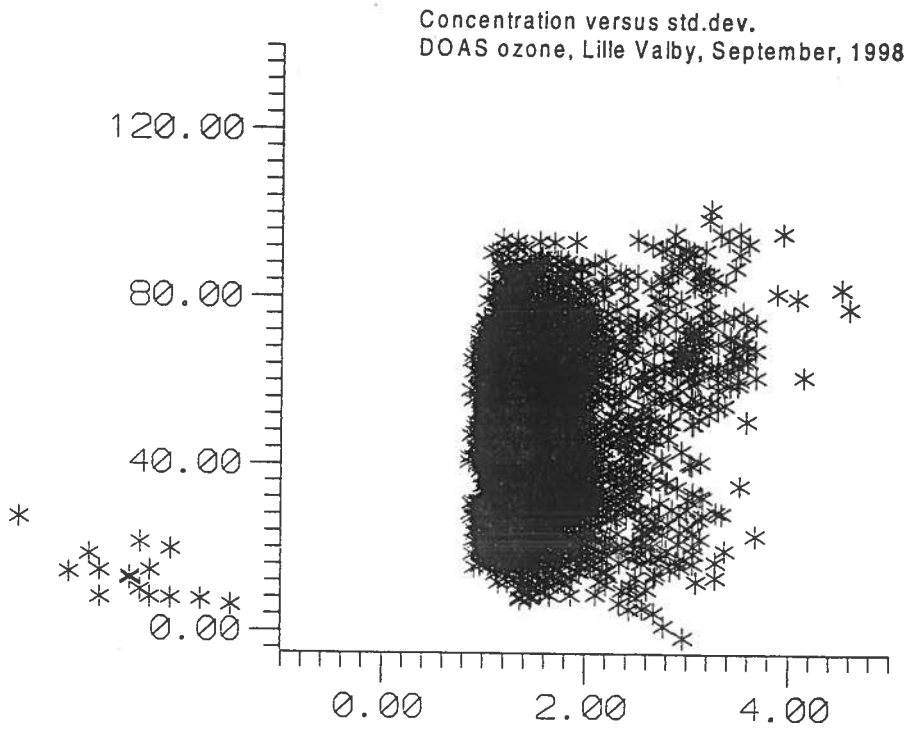
Concentration versus std.dev.
DOAS ozone, Lille Valby, September, 1998
120.00
80.00
40.00
0.00
0.00
2.00
4.00

Appendix C

Lille Valby Meteorological Data April - September 1998

- RIMI (Risoe Integrated Environmental Project) data

This appendix gives the meteorological data used together with the Lille Valby DOAS measurements, April - September, 1998.

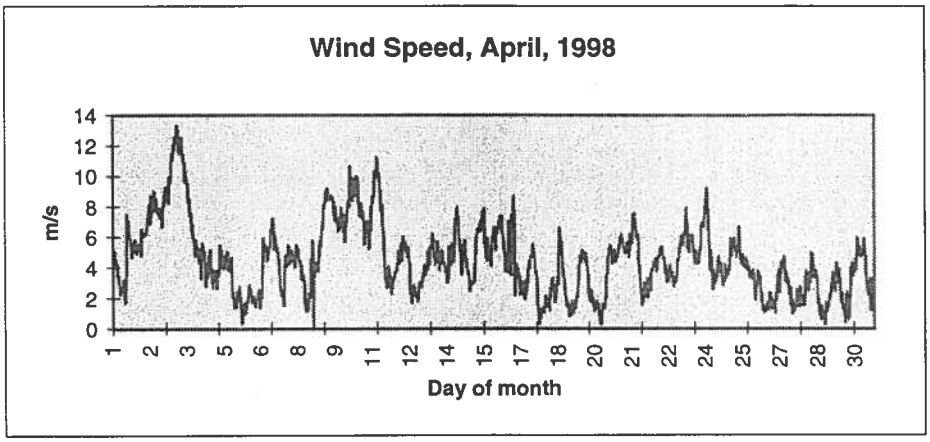
Wind Speed, April, 1998
m/s
0
2
4
6
8
10
12
14
1 2 3 5 6 8 9 11 12 14 15 17 18 20 21 22 24 25 27 28 30
Day of month

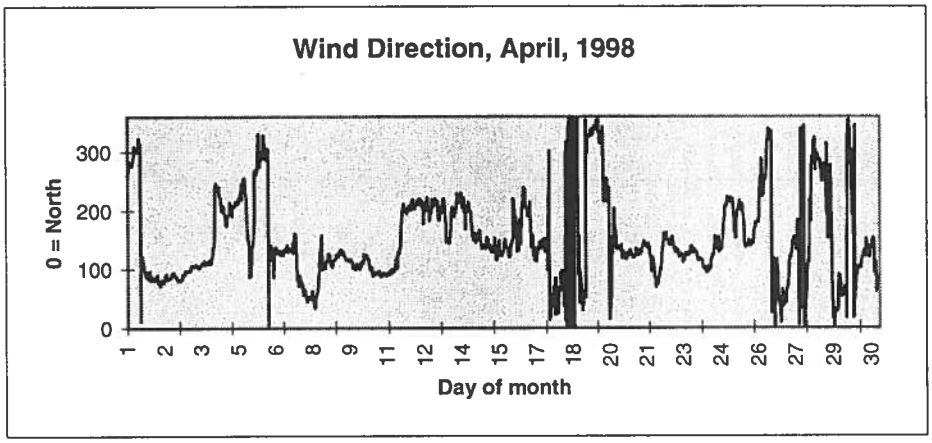
Wind Direction, April, 1998
0 = North
0
100
200
300
1 2 3 5 6 8 9 11 12 14 15 17 18 20 21 23 24 26 27 29 30
Day of month

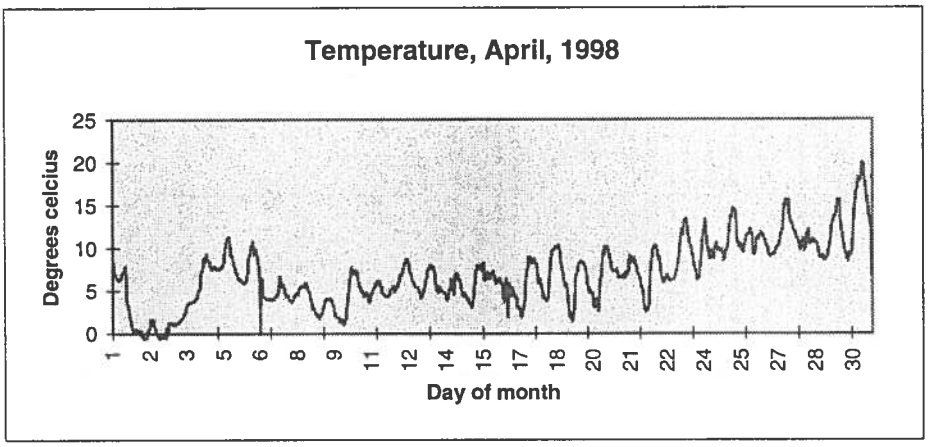
Temperature, April, 1998
Degrees celcius
0
5
10
15
20
25
1 2 3 5 6 8 9 11 12 14 15 17 18 20 21 22 24 25 27 28 30
Day of month

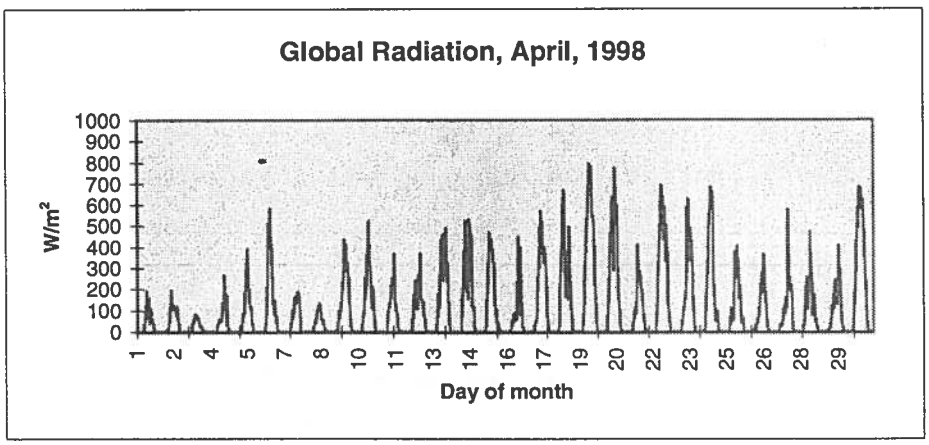
Global Radiation, April, 1998
W/m²
0
100
200
300
400
500
600
700
800
900
1000
1 2 4 5 7 8 10 11 13 14 16 17 19 20 22 23 25 26 28 29
Day of month

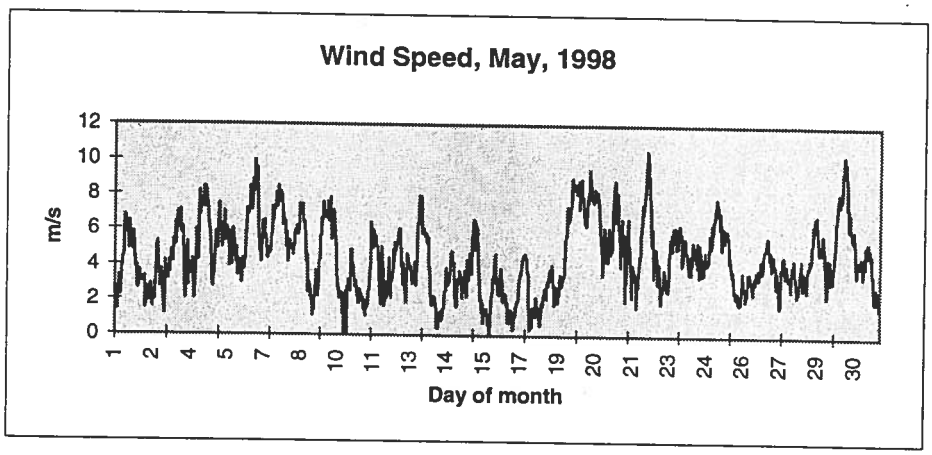
Wind Speed, May, 1998
m/s
0
2
4
6
8
10
12
1 2 4 5 7 8 10 11 13 14 15 17 19 20 21 23 24 26 27 29 30
Day of month

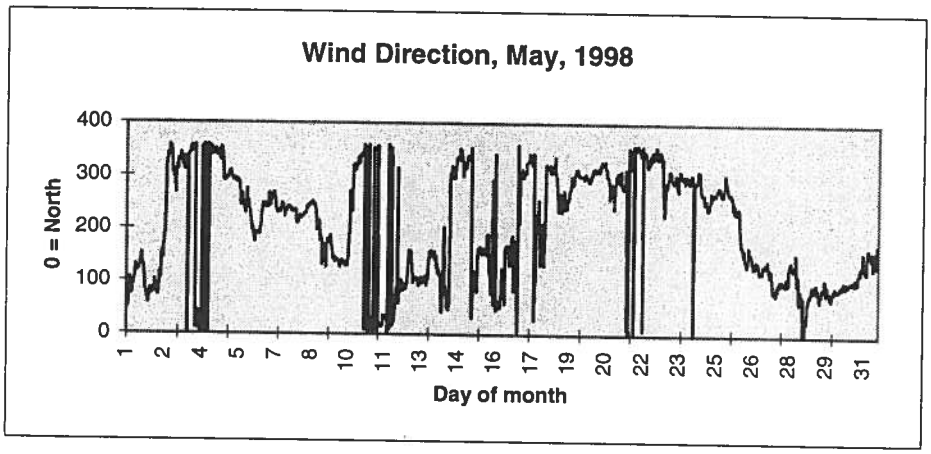
Wind Direction, May, 1998
0 = North
0
100
200
300
400
1 2 4 5 7 8 10 11 13 14 16 17 19 20 22 23 25 26 28 29 31
Day of month

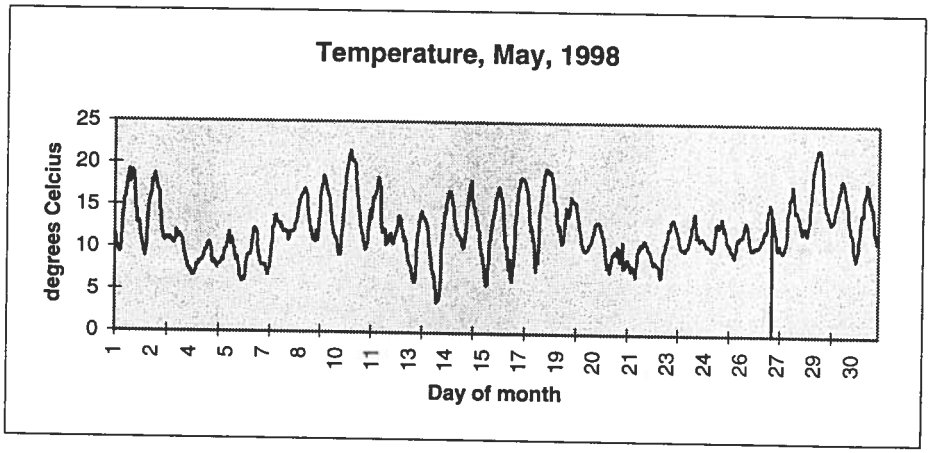
Temperature, May, 1998
degrees Celcius
0
5
10
15
20
25
1 2 4 5 7 8 10 11 13 14 15 17 19 20 21 23 24 26 27 29 30
Day of month

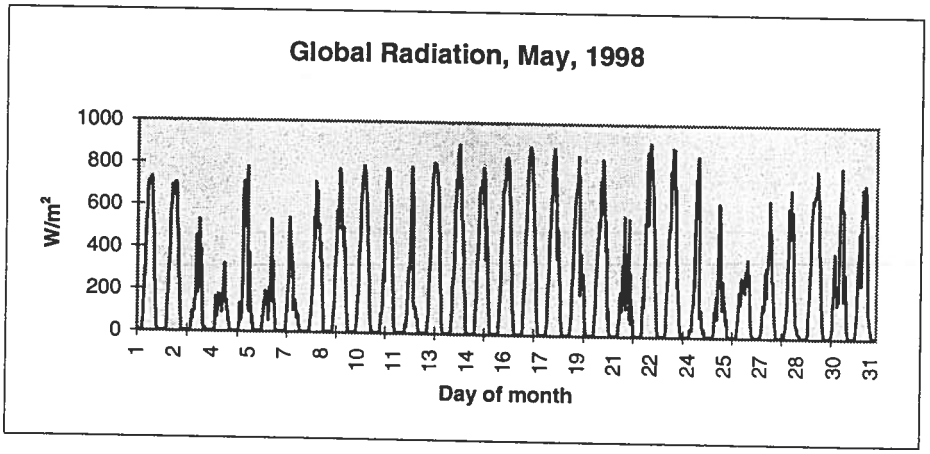
Global Radiation, May, 1998
W/m²
0
200
400
600
800
1000
1 2 4 5 7 8 10 11 13 14 16 17 19 21 22 24 25 27 28 30 31
Day of month

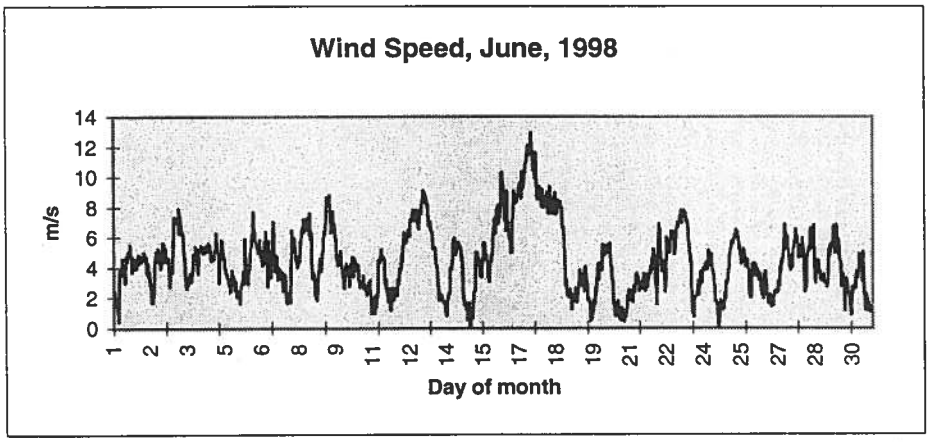
Wind Speed, June, 1998
m/s
0
2
4
6
8
10
12
14
1 2 3 5 6 8 9 11 12 14 15 17 18 19 21 22 24 25 27 28 30
Day of month

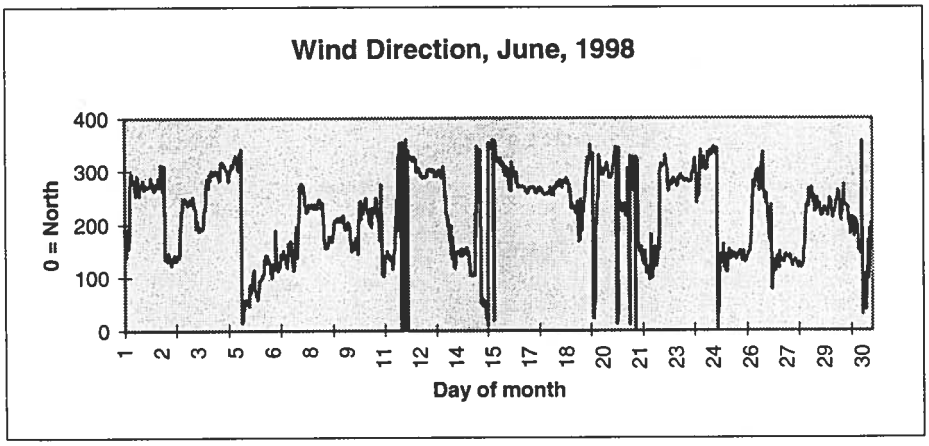
Wind Direction, June, 1998
0 = North
0
100
200
300
400
1 2 3 5 6 8 9 11 12 14 15 17 18 20 21 23 24 26 27 29 30
Day of month

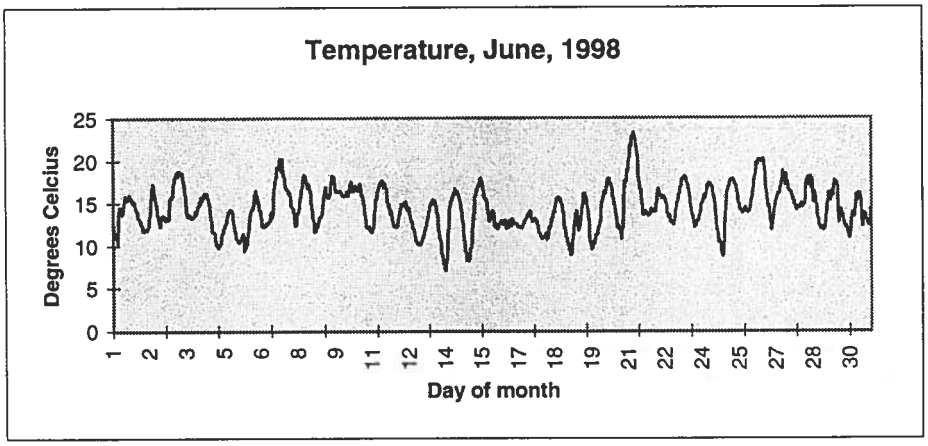
Temperature, June, 1998
Degrees Celcius
0
5
10
15
20
25
1 2 3 5 6 8 9 11 12 14 15 17 18 19 21 22 24 25 27 28 30
Day of month

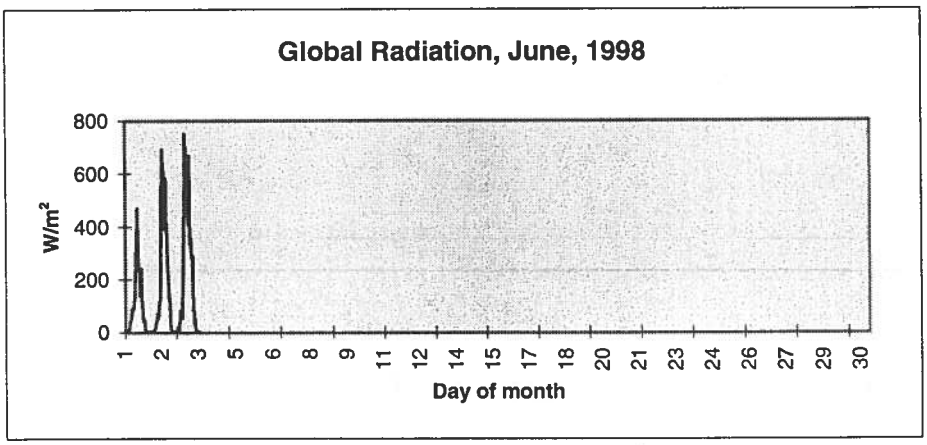
Global Radiation, June, 1998
W/m²
0
200
400
600
800
1 2 3 5 6 8 9 11 12 14 15 17 18 20 21 23 24 26 27 29 30
Day of month

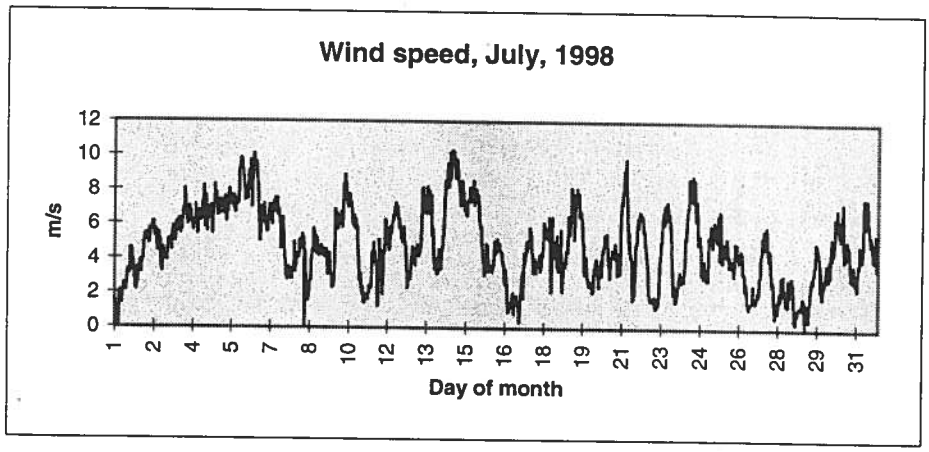
Wind speed, July, 1998
m/s
0
2
4
6
8
10
12
1 2 4 5 7 8 10 12 13 15 16 18 19 21 23 24 26 28 29 31
Day of month

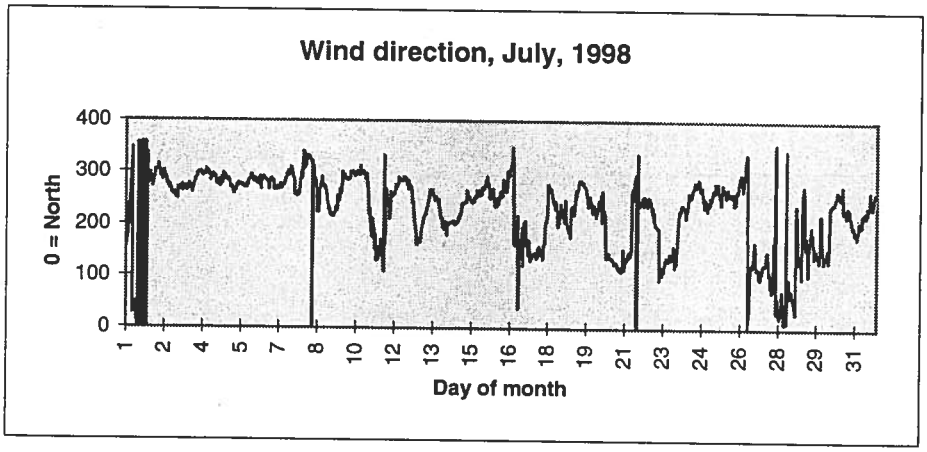
Wind direction, July, 1998
0 = North
0
100
200
300
400
1 2 4 5 7 8 10 12 13 15 16 18 19 21 23 24 26 28 29 31
Day of month

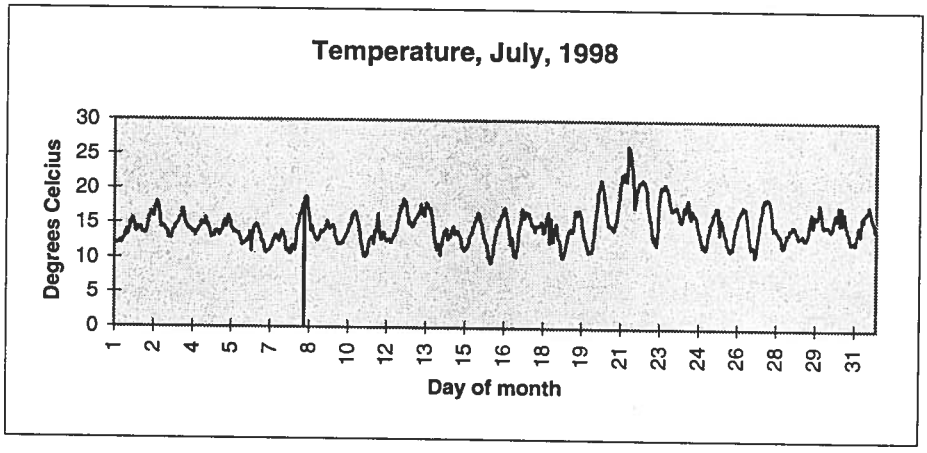
Temperature, July, 1998
Degrees Celcius
0
5
10
15
20
25
30
1 2 4 5 7 8 10 12 13 15 16 18 19 21 23 24 26 28 29 31
Day of month

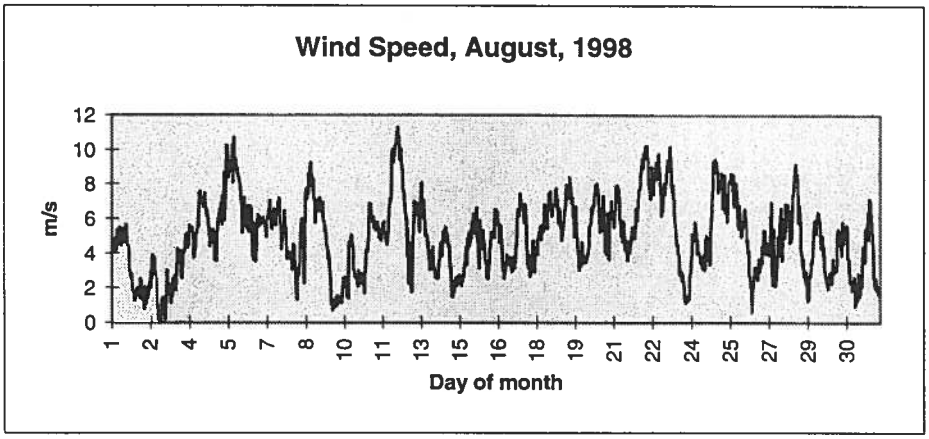
Wind Speed, August, 1998
m/s
12
10
8
6
4
2
0
1 2 4 5 7 8 10 11 13 15 16 18 19 21 22 24 25 27 29 30
Day of month

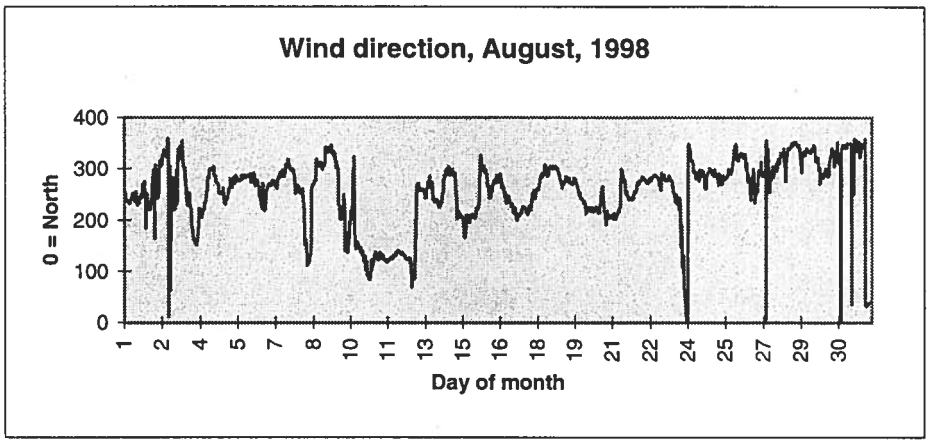
Wind direction, August, 1998
0 = North
400
300
200
100
0
1 2 4 5 7 8 10 11 13 15 16 18 19 21 22 24 25 27 29 30
Day of month

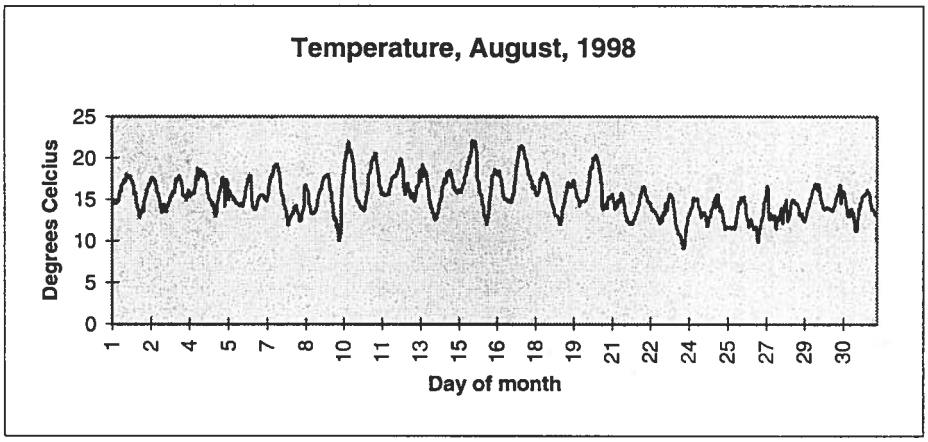
Temperature, August, 1998
Degrees Celcius
25
20
15
10
5
0
1 2 4 5 7 8 10 11 13 15 16 18 19 21 22 24 25 27 29 30
Day of month

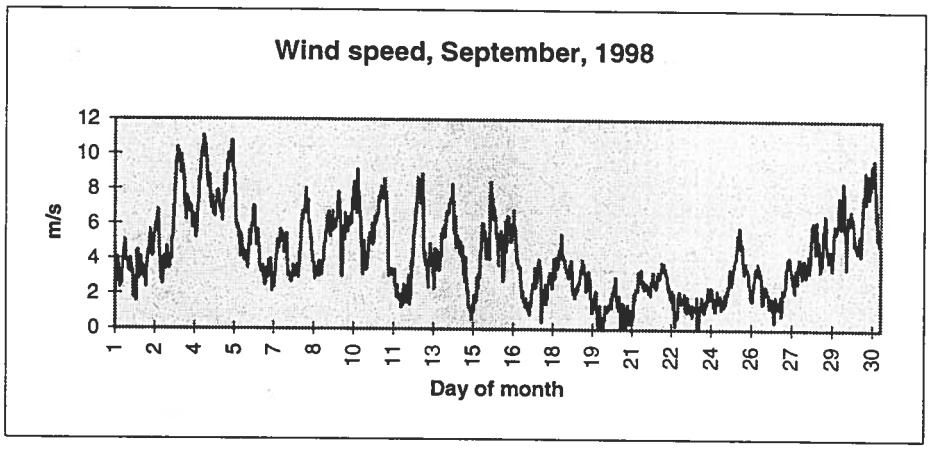
Wind speed, September, 1998
m/s
0
2
4
6
8
10
12
1 2 4 5 7 8 10 11 13 15 16 18 19 21 22 24 26 27 29 30
Day of month

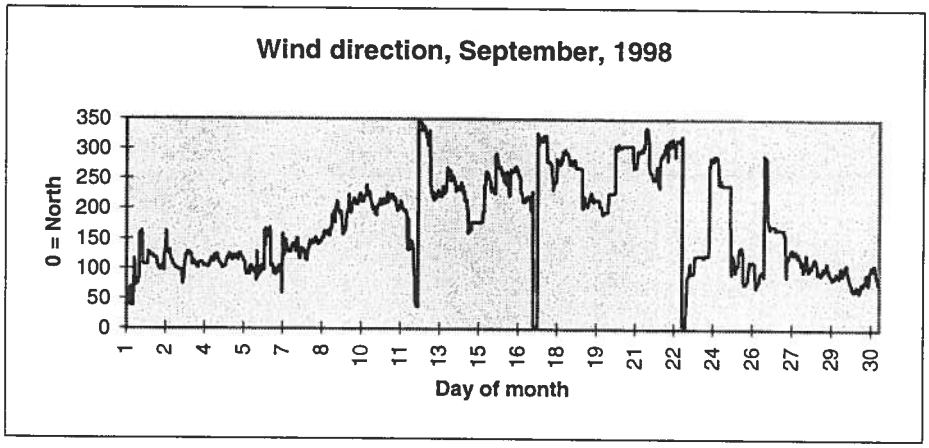
Wind direction, September, 1998
0 = North
0
50
100
150
200
250
300
350
1 2 4 5 7 8 10 11 13 15 16 18 19 21 22 24 26 27 29 30
Day of month

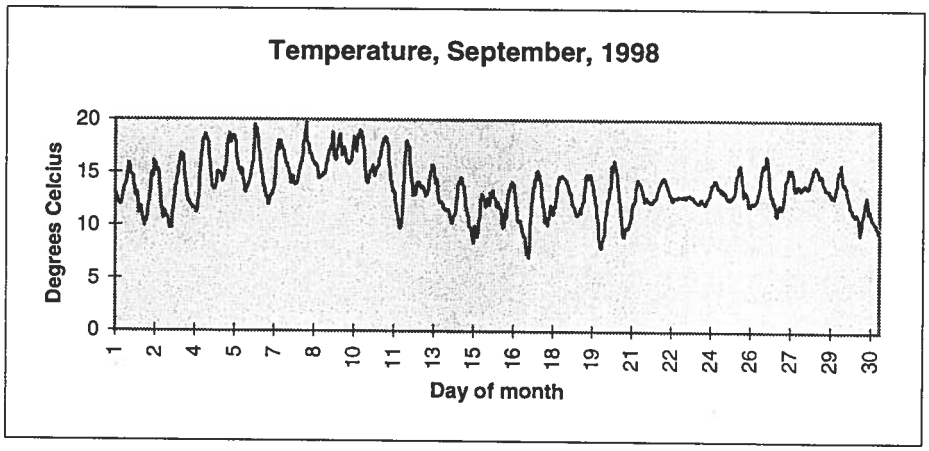
Temperature, September, 1998
Degrees Celcius
0
5
10
15
20
1 2 4 5 7 8 10 11 13 15 16 18 19 21 22 24 26 27 29 30
Day of month

Appendix D

DOAS NO_2 Calibration Results

On page 176 the results of the DOAS NO_2 calibration described in chapter 3.7 is given in tabular form. Page 177 shows the calibration curves for the mass flow controllers used in the calibration.

Calibration with delution system

Cc=961ppb

		Reading 1		Reading 2		Reading 3		Reading 4		Reading 5		Mean value		Calculated
	% NO2	An.resp.Y	St.dev	An.resp.Y	St.dev	An.resp.Y	St.dev	An.resp.Y	St.dev	An.resp.Y	St.dev	An.resp.Y	St.dev	value
L1	50	240.4	0.5	240.5	0.5	240.7	0.5	240.3	0.5	240.5	0.5	240.48	0.5	238.4241
0.09924	25	121.1	0.3	121.1	0.3	121.8	0.3	121.6	0.6	121	0.3	121.32	0.36	119.2121
	12.5	63	0.2	63	0.2	62.9	0.2	62.9	0.2	63	0.2	62.96	0.2	59.60603
	Mean											141.5867	0.35333	
	50	338.8	0.7	339.6	0.7	340.1	0.7	340	0.7	339.7	0.7	339.64	0.7	334.5722
L1+L2	25	170.9	0.4	171.1	0.4	171.3	0.3	171.1	0.4	171.3	0.4	171.14	0.38	167.2861
0.13926	12.5	87.8	0.3	87.9	0.3	88.6	0.3	88.4	0.3	87.9	0.3	88.12	0.3	83.64304
	6.25	47.5	0.2	47.6	0.2	47.2	0.2	47.1	0.2	47	0.2	47.28	0.2	41.82152
	Mean											161.545	0.395	
	50	370.1	0.8	369.7	0.8	369.9	0.8	370.1	0.8	369.9	0.8	369.94	0.8	359.0296
L1+L2+L3	25	186.4	0.4	185.9	0.4	185.9	0.4	185.6	0.4	185.9	0.4	185.94	0.4	179.5148
0.14944	12.5	96.1	0.3	95.9	0.3	96	0.3	95.9	0.3	96.2	0.3	96.02	0.3	89.7574
	6.25	50.1	0.2	50.3	0.2	50.5	0.2	50.4	0.2	50.5	0.2	50.36	0.2	44.8787
	Mean											175.565	0.425	
	50	266.6	0.5	266.7	0.5	266.1	0.5	265.9	0.5	266.3	0.5	266.32	0.5	262.8816
L1+L3	25	133.2	0.3	133.8	0.3	133.7	0.3	133.6	0.3	133.5	0.3	133.56	0.3	131.4408
0.10942	12.5	68.8	0.2	69.1	0.2	68.8	0.2	69.1	0.2	69	0.2	68.96	0.2	65.72039
	Mean											156.28	0.33333	
	50	24.9	0.1	25.2	0.1	24.5	0.1	24.7	0.2	24.6	0.2	24.78	0.14	24.45745
L3	25	12.1	0.1	11.9	0.1	12.1	0.1	12.1	0.2	12.3	0.2	12.1	0.14	12.22873
0.01018	12.5	6.3	0.2	6.6	0.1	6.6	0.1	6.5	0.1	6.4	0.1	6.48	0.12	6.114363
	Mean											14.45333	0.13333	
	50	122.7	0.3	122.5	0.3	122.8	0.3	122.5	0.3	122.4	0.3	122.58	0.3	120.6055
L3+L2	25	61.6	0.2	61.4	0.2	61.4	0.2	61.9	0.2	61.8	0.2	61.62	0.2	60.30275
0.0502	12.5	31.9	0.2	32.1	0.2	32	0.1	32	0.1	32	0.2	32	0.16	30.15138
	Mean											72.06667	0.22	
	50	97.8	0.3	97.8	0.3	97.6	0.3	96.6	0.3	97.4	0.3	97.44	0.3	96.14805
L2	25	49.6	0.2	49.8	0.2	50.2	0.2	49.8	0.2	50.5	0.2	49.98	0.2	48.07403
0.04002	12.5	25.5	0.1	25.5	0.1	25.4	0.2	25.7	0.2	25.6	0.1	25.54	0.14	24.03701
	Mean											57.65333	0.21333	

Calibration curves for the mass flow controllers used in NO_2 calibration